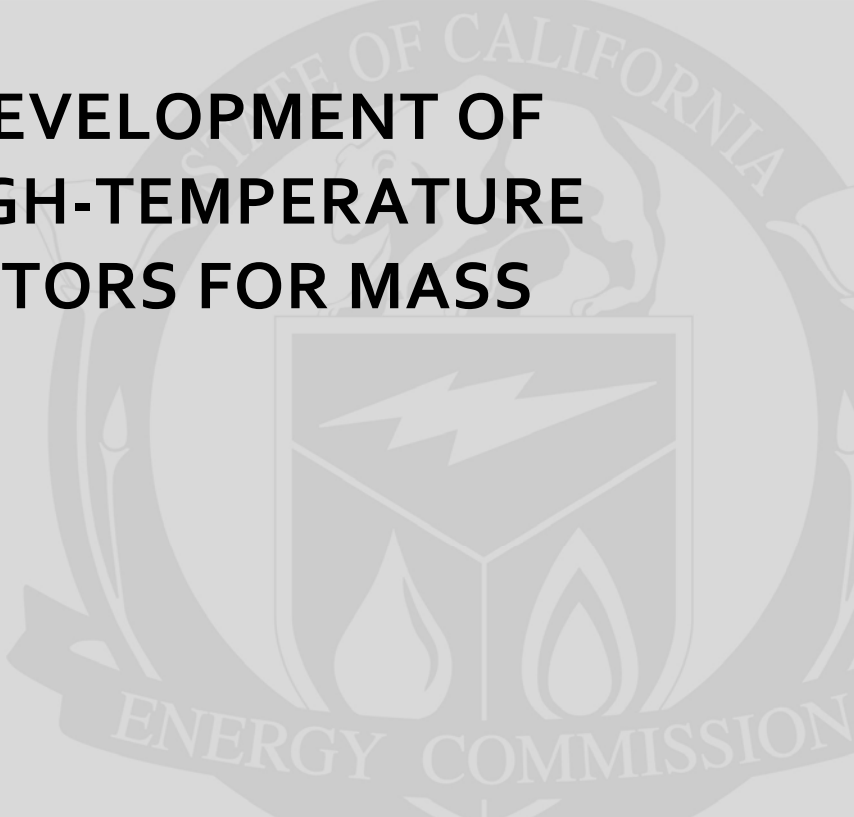


**Public Interest Energy Research (PIER) Program
FINAL PROJECT REPORT**

**DESIGN AND DEVELOPMENT OF
LOW-COST, HIGH-TEMPERATURE
SOLAR COLLECTORS FOR MASS
PRODUCTION**



Prepared for: California Energy Commission
Prepared by: The Regents of the University of California

MAY 2012
CEC-500-2012-050

Prepared by:

Primary Author(s):
Roland Winston

University of California, Merced
Merced, CA 95243

Contract Number: 500-05-021



Prepared for:

California Energy Commission

Michael Lozano
Contract Manager

Virginia Lew
Office Manager
Energy Efficiency Research Office

Laurie ten Hope
Deputy Director
RESEARCH AND DEVELOPMENT DIVISION

Robert P. Oglesby
Executive Director

DISCLAIMER

This report was prepared as the result of work sponsored by the California Energy Commission. It does not necessarily represent the views of the Energy Commission, its employees or the State of California. The Energy Commission, the State of California, its employees, contractors and subcontractors make no warrant, express or implied, and assume no legal liability for the information in this report; nor does any party represent that the uses of this information will not infringe upon privately owned rights. This report has not been approved or disapproved by the California Energy Commission nor has the California Energy Commission passed upon the accuracy or adequacy of the information in this report.

Acknowledgements

This work was supported by the California Energy Commission's Public Interest Energy Research Program, Sol Focus, and the United Technologies Research Center). Authors acknowledge the guidance and assistance given by Heater Poiry, Steve Horne, Gary Conley, Randy Gee, Mary-Jane Hale, and Guenter Fischer of Sol Focus

Project team members included: Alfonso Tovar, Jesus Cisneros, Kevin Balkoski, Alexander Ritschel, Gerardo Diaz, Roland Winston- University of California, Merced and Randy Gee, Mary-Jane Hale and Guenter Fischer of Sol Focus.

Please site this report as follows:

Winston, R. 2011. *Design and Development of Low-Cost, High-Temperature Solar Collectors for Mass Production*. California Energy Commission Public Interest Energy Research Program Report: CEC-500-2012-050.

Preface

The Public Interest Energy Research (PIER) Program supports public interest energy research and development that will help improve the quality of life in California by bringing environmentally safe, affordable, and reliable energy services and products to the marketplace.

The PIER Program, managed by the California Energy Commission (Energy Commission), conducts public interest research, development, and demonstration (RD&D) projects to benefit California.

The PIER Program strives to conduct the most promising public interest energy research by partnering with RD&D entities, including individuals, businesses, utilities, and public or private research institutions.

PIER funding efforts are focused on the following RD&D program areas:

- Buildings End-Use Energy Efficiency
- Energy Innovations Small Grants
- Energy Related Environmental Research
- Energy Systems Integration
- Environmentally Preferred Advanced Generation
- Industrial/Agricultural/Water End Use Energy Efficiency
- Renewable Energy Technologies
- Transportation

Design and Development of Low-Cost, High-Temperature Solar Collector For Mass Production is the final report for the project (Contract Number 500-05-021) conducted by the staff of the University of California Merced. The information from this project contributes to PIER's Industrial/Agricultural/Water End-Use Energy Efficiency and Renewable Energy Programs.

For more information about the PIER Program, please visit the Energy Commission's website at www.energy.ca.gov/pier or contact the Energy Commission at 916-327-1551.

Table of Contents

Acknowledgements	i
Preface.....	ii
Table of Contents	iii
List of Tables.....	ix
Executive Summary	1
1.0 Introduction	8
2.0 Project Outcomes.....	10
2.1. Task 2.0	10
2.1.1. Introduction.....	10
2.1.2. Applications	10
2.2. Task 3.0	26
2.2.1. Technical System Architectures for Application of Solar Heat.....	26
2.2.2. Safety Considerations for XCPC Applications	53
2.3. Task 4.0	55
2.4. Task 5	66
2.5. Task 6	95
2.6. Task 7	110
2.7. Task 8	121
2.8. Task 9	123
2.9. Task 10	144
2.10. Task 11	155
2.11. Task 12	163
2.12. Task 13	169
2.13. Task 14	170
2.14. Task 15	171
2.15. Task 16	179
2.15.1. Tested Collectors.....	179
2.15.2. Test Protocol.....	179
2.15.3. Description of Test Loop	181
2.15.4. Instrumentation	183
2.15.5. Test Results of “Metal absorber with glass-to-metal seal – North-South orientation”	183
2.15.6. Test Results of “Metal absorber with glass-to-metal seal – East-West orientation”	189
2.15.7. Discussion.....	193
2.16. Task 17	198
2.17. Task 18	201
2.18. Task 19	207
2.18.1. Tested Collectors.....	208
2.18.2. Collector Thermal Efficiency: Method 1.....	208
2.18.3. Collector Thermal Efficiency: Method 2.....	209

2.18.4.	Temperature dependence of collector efficiency	209
2.18.5.	Description of Test Loop	210
2.18.6.	Instrumentation	212
2.18.7.	Test Results of “U-Tube with Alanod Reflectors in North-South orientation”	212
2.18.8.	Test Results of “U-Tube with Alanod Reflectors in East-West orientation” 216	
2.18.9.	Test Results of “X-Tube with Alanod Reflectors in East-West orientation” 219	
2.18.10.	Test Results of “U-Tube with Reflectech Reflectors in North-South orientation”	223
2.18.11.	Test Results of “U-Tube with Reflectech Reflectors in East-West orientation”	228
2.18.12.	Summary of Results	231
2.18.13.	Discussion.....	232
3.0	Conclusions and Recommendations	260

List of Figures

Figure 1. An Early XCPC Prototype at UC Merced	2
Photo Credit: The Regents of the University of California	2
Figure 2. The 10kW SolFocus Test Loop at NASA/Ames	2
Photo credit: The Regents of the University of California	2
Figure 3. The 10kW B2U Prototype at GTI.....	3
Photo credit: The Regents of the University of California	3
Figure 4. Parallel Reflectors with Evacuated Glass Tubes	4
Photo credit: The Regents of the University of California	4
Source: The Regents of the University of California.....	5
Figure 5. XCPC Thermal Efficiency at Various Temperatures	6
Source: The Regents of the University of California.....	6
Figure 6. Evolution of absorption chiller technology over the years.....	11
Source: The Regents of the University of California.....	11
Figure 7. Broad's Double-Effect Absorption Chiller	13
Source: The Regents of the University of California.....	13
Source: The Regents of the University of California.....	13
Figure 8. Schematic of a typical adsorption chiller configuration.....	15
Source: The Regents of the University of California.....	15
Figure 9. Solid (a) and liquid (b) desiccant technologies ²	16
Source: The Regents of the University of California.....	16
Figure 10. Vapor compression Figure 11. Organic rankine cycle.....	18
Figure 12. Vacuum distillation system ¹⁰	22

Figure 13. Solar Thermal Driven Single Effect Chilling System.....	27
Source: The Regents of University of California	27
Figure 14. Carrier 16JB single effect LiBr absorption chiller	28
Figure 15. Diagram of a solar thermal driven double effect absorption chiller: using hot oil	29
Figure 16. DN and 16 DE double effect chiller made by Carrier.....	30
Figure 17. Diagram of a solar thermal driven double effect absorption chiller: using steam	32
Figure 18. Diagram of a solar thermal driven triple effect absorption chiller	34
Figure 19. Trane and York triple effect chillers	35
Figure 20. Diagram of a solar thermal driven combined heating and cooling.....	37
Figure 21. Solar ORC conceptual system architecture	39
Figure 22. UTC Power PureCycle™ product	39
Figure 23. System parasitic power for single effect chillers	43
Figure 24. System reliability block diagram.....	44
Figure 25. System parasitic power for double effect chillers	46
Figure 26. System Parasitic Electric Consumption Sensitivity at full load	47
Figure 27. Reliability block diagram XCPC driven double effect chillers.....	48
Figure 28. On board parasitics for chillers.....	49
Figure 29. Reliability block diagram XCPC driven double effect chillers.....	50
Figure 30. Reliability block diagram XCPC driven ORC	52
Figure 32: Top view and cross section view of XCPC concept #1 (drawing is not to scale).....	64
Figure 36. Projected XCPC Efficiency v Temperature	67
Figure 37. All-glass dewars – direct flow and all-glass dewar filled with thermal fluid - indirect flow	68
Figure 38. Variation of selective coating absorptance with incidence angle	69
Figure 39. Shape of XCPC reflector for all-glass dewars.....	70
Figure 40. Incidence Angle Modifier (IAM) for 58mm OD dewars.....	70
Figure 41. Incidence Angle Modifier (IAM) for design using absorber with glass-to-metal seal.....	71
Figure 42. Sketch of all-glass dewar tube (cross-section)	72
Figure 43. Sketch of all-glass dewar tube (side cross-section)	73
Figure 44. Metal absorber with glass-to-metal seal.....	73
Figure 46 & 47. Transversal section and schematic of heat fluxes	78
Figure 48. Corning Pyrex 7740 Transmittance curve	79
Figure 49.....	79
Figure 50. Heat fluxes at glass interface	80
Figure 51. Heat fluxes at absorber interface.....	81
Figure 52. Heat fluxes at absorber / heat exchanger	81
Figure 53. Thermal Circuit.....	83
Figure 53. Output temperature of fluid when irradiation is kept constant and while fluid input temperature varies according to table 1	85

Figure 54. Differences in Temperature: Absorber – Input and Output - Input.....	86
Figure 55. Output temperature of fluid when input temperature is kept constant at $T_{in}=400$ K.....	87
Figure 56. Differences in Temperature: Absorber – Input and Output - Input.....	87
Figure 57. Output temperature of fluid when input temperature is kept constant at $T_{in}=473$ K.....	88
Figure 58. Output temperature of fluid when input temperature is kept constant at $T_{in}=473$ K.....	89
Figure 59. Differences in Temperature: Absorber – Input and Output – Input.....	89
Figure 60. Spectral reflectance of Alnanod Reflective Surfaces.....	96
Figure 61: Measuring radius Figure 62: Reflectivity measurements of Alnanod.....	97
Figure 63. Corning Pyrez 7740 Transmittance.....	98
Figure 64. Perkin-Elmer spectrophotometer Figure 65. Perkin-Elmer spectrophotometer.....	99
Figure 66. Borosilicate Glass Tube Transmittance.....	99
Figure 68. Expected absorptance of selective coating as a function of incidence angle.....	102
Figure 69: Measured absorptance of selective coating as a function of incidence angle.....	102
Figure 70. Beijing Eurocon Heat Pipe Geometry and Characteristics.....	105
Figure 71. Manifold and Heat Pipe Arrangement.....	109
Figure 72. Direct Flow All Glass Dewar.....	111
Figure 73. Ray Traces over the Design Acceptance Angle.....	112
Figure 74. Horizontal Dewar Reflector Dimensions.....	113
Figure 75. Direct Flow Dewar Efficiency.....	114
Figure 76. Vertical Dewar Reflector Dimensions.....	115
Figure 77. Indirect Flow Dewar.....	116
Figure 78. Expected Performance for Indirect Flow Dewar.....	117
Figure 79. Metal Absorber Tube (Counter Flow).....	118
Figure 80. Horizontal Metal Absorber Tube Reflector Dimensions.....	119
Figure 81 Performance predictions for three types of selective absorbers.....	120
Figure 82. Various collector efficiency equation coefficients.....	121
Figure 83 Solar thermal energy output (assuming 50% efficiency) for a 991 m ² collector for a two day period June 2-3.....	124
Figure 84. DOE-2 output for four building types in Los Angeles.....	125
Figure 85. Absorption chiller COP as a function of the cooling water inlet temperature.....	126
Figure 86. Los Angeles retail store cooling load and solar heat profiles.....	127
Figure 87. Typical 48-hour solar, cooling and electricity profiles of Los Angeles 120 ft ² retail.....	128
Figure 88. Annual profile of cooling generation compared with the cooling demand.....	128
Figure 89. A 3-day profile of cooling generation compared with the cooling demand.....	129
Figure 90. Solar cooling ratio for the four buildings in the four cities.....	129
Figure 91. Solar utilization ratio for the four buildings in the four cities.....	130
Figure 92. Solar cooling capacity statistics.....	130
Figure 93. Solar cooling capacity statistics.....	131
Figure 94. Payback of the solar cooling system in Los Angeles.....	132

Figure 95. Diagram of solar driven ORC.....	133
Figure 96. Los Angeles ORC power generation and solar heat profiles	134
Figure 97. Typical 48-hour solar heat and electricity generation profiles in Los Angeles.....	135
Figure 98. Total solar heat and power generation in four cities.....	135
Figure 99. ORC operation statistics	136
Figure 100. Solar driven ORC electricity savings	137
Figure 101. XCPC driven ORC payback as a function of ORC and solar collector costs.....	137
Figure 102. Payback of solar driven cooling system at different cities.....	138
Figure 103. Payback of solar driven cooling system with different chiller capacity	139
Figure 104. Horizontal Glass to Metal Tube Efficiency	146
Figure 105. Horizontal Dewar Efficiency	147
Figure 107. Transmittance by Wavelength.....	148
Figure 108. Metal Absorber Collector with AR	149
Figure 109. Direct Flow Dewar with AR	149
Figure 110. Spectral Reflectance.....	150
Figure 111. Metal Absorber with Reflectec	151
Figure 112. Direct Flow with Reflectec	151
Figure 113. Metal Absorber Design.....	152
Figure 114. Metal Absorber Thickness.....	153
Figure 115 Metal Absorber with AR and Reflectec.....	154
Figure 116. Direct Flow Tube with AR and Reflectec	155
Figure 117. All glass dewar: direct flow Figure 118. Metal absorber with glass-to-metal seal	157
Figure 119. Direct Flow Dewar	158
Figure 120. Metal Absorber	159
Figure 121. Annular Performance in a Diffused Environment.....	160
Figure 122. Annular Performance in a Direct Solar Environment	160
Figure 123. Schematic of XCPC Design	164
Figure 124. Cross section of absorber tube.....	164
Figure 125. Evacuated glass tube with metal absorber (all units in mm)	166
Figure 126. Manifold for North-South orientation [all units in mm].....	167
Figure 126b: Manifold for East-West orientation [all units in mm].....	167
Figure 127b. Cross section of reflector for East-West orientation	168
Figure 128. End view (upper drawing) and length view (three lower drawings) of frame for XCPC system in North-South orientation.....	169
Figure 129. Expected Optical Efficiency and Incidence Angle Modifier for East-West orientation.....	170
Figure 130. Expected thermal efficiency of XCPC.....	171
Figure 131. Schematic of Test Facility	173
Figure 132. Collector time constant.....	175
Figure 133. Example of a collector efficiency vs. temperature curve.....	178

Figure 134. Schematic of Test Facility	182
Figure 135. North-South Counterflow with Alanod Effective Reduced Efficiency Curve.....	185
Figure 136. North-South Counterflow with Alanod Effective Standardized Efficiency Curve.....	185
Figure137. North-South Counterflow with Alanod Direct Reduced Efficiency Curve	186
Figure138. North-South Counterflow with Alanod Direct Standardized Efficiency Curve	187
Figure 139. North-South Counterflow with Alanod: IAM Chart.....	188
Figure 140. North-South Counterflow Time Constant Plot	189
Figure 141. East-West Counterflow with Alanod Effective Reduced Efficiency Curve	191
Figure 142. East-West Counterflow with Alanod Effective Standardized Efficiency Curve	191
Figure 143. East-West Counterflow with Alanod Direct Reduced Efficiency Curve	192
Figure 144. East-West Counterflow with Alanod Direct Standardized Efficiency Curve	192
Figure 145. North-South Counterflow with Alanod: Measured vs. Model.....	193
Figure 146 East-West Counterflow with Alanod: Measured vs. Model.....	195
Figure 147. Counterflow Efficiencies: North-South vs. East-West.....	196
Figure 148. Shows the comparison between expectations from modeling with achieved test results.	199
Figure 149. Comparison of measured and modeled collector efficiency	199
Figure150. Schematic of absorber tube used in tested XCPC	200
Figure 151. Schematic of Test Facility	202
Figure 152. Collector time constant.....	204
Figure 153. Example of a collector efficiency vs. temperature curve.....	207
Figure 154. Schematic of Test Facility	211
Figure 155. North-South U-Tube with Alanod Effective Reduced Efficiency Curve.....	214
Figure 156. North-South U-Tube with Alanod Effective Standardized Efficiency Curve.....	214
Figure 157. North-South U-Tube with Alanod Direct Reduced Efficiency Curve	215
Figure 158. North-South U-Tube with Alanod Direct Standardized Efficiency Curve	215
Figure 159. East-West U-Tube with Alanod Effective Reduced Efficiency Curve.....	217
Figure 160. East-West U-Tube with Alanod Effective Standardized Efficiency Curve	218
Figure 161. East-West U-Tube with Alanod Direct Reduced Efficiency Curve	218
Figure 162. East-West U-Tube with Alanod Direct Standardized Efficiency Curve	219
Figure 163. East-West X-Tube with Alanod Effective Reduced Efficiency Curve.....	221
Figure 164 East-West X-Tube with Alanod Effective Standardized Efficiency Curve.....	221
Figure 165. East-West X-Tube with Alanod Direct Reduced Efficiency Curve.....	222
Figure 166. East-West X-Tube with Alanod Direct Standardized Efficiency Curve	222
Figure 167. North-South U-Tube with Reflectech Effective Reduced Efficiency Curve	224
Figure 168 North-South U-Tube with Reflectech Effective Standardized Efficiency Curve	225
Figure 169. North-South U-Tube with Reflectech Direct Reduced Efficiency Curve.....	225
Figure 170. North-South U-Tube with Reflectech Direct Standardized Efficiency Curve.....	226
Figure 171. North-South U-Tube with Reflectech stagnation test results.....	227

Figure 172. East-West U-Tube with Reflectech Effective Reduced Efficiency Curve.....	229
Figure 173 East-West U-Tube with Reflectech Effective Standardized Efficiency Curve.....	229
Figure 175. East-West U-Tube with Reflectech Direct Reduced Efficiency Curve	230
Figure 175 East-West U-Tube with Reflectech Direct Standardized Efficiency Curve	230
Figure 176. East-West U-Tube with Reflectech: IAM Chart.....	231
Figure 177. North-South Collector Efficiency (Effective)	233
Figure 178. North-South Collector Efficiency (DNI).....	233
Figure 179. East-West Collector Efficiency (Effective).....	235
Figure 180. East-West Collector Efficiency (DNI)	235
Figure 181 U-Tube Collector Efficiency (Effective).....	236
Figure 182. East-West Collector Efficiency (DNI)	237
Figure 183 Collector Efficiency (Effective)	238
Figure 184. Collector Efficiency (DNI).....	239

List of Tables

Table 1. Comparison of the XCPC System to Other Solar Thermal Systems	4
Table 2. Absorption Chillers, Generator Temperatures and COPs.....	13
Table 3. Decision matrix for technology down selection.....	25
Table 4. Major design specifications for solar thermal driven single effect absorption chillers	27
Table 5. Major design specifications for oil driven solar thermal double effect absorption chillers.....	30
Table 6. Major design specifications for oil driven solar thermal double effect absorption chillers.....	33
Table 7. Major design specifications for oil driven solar thermal triple effect absorption chillers.....	35
Table 8. Heating mode design specifications for an oil driven solar chilling/heating system	37
Table 9. Major design specifications for XCPC driven ORC cycle.....	40
Table 10. Equipment cost estimates (less collector, storage tank and front end collector to tank piping).....	53
Table 11. Comparison of Features	64
Table 12. Variation of output temperature of fluid when irradiation is kept constant at $G_c = 326.7 \text{ W}$	85
Table 13. Variation of output temperature of fluid when the input temperature is kept constant at $T_{in}=400 \text{ K}$	86
Table 14. Variation of output temperature of fluid when the input temperature is kept constant at $T_{in}=473 \text{ K}$	88

Table 15. Heat Pipe Heat Transport Limitations	106
Table 16. Estimated Heat Transport Limits.....	108
Table 17. Condenser Side Heat Transfer Estimates.....	110
Table 18. Cost comparison of XCPC design concepts in high volume production (10,000 tubes).....	123
Table 19. System specifications for solar cooling system	127
Table 20. Detailed analysis results for 120k ft ² retail store with solar cooling	131
Table 21. System specifications for solar power generation system with ORC	134
Table 22. Detailed analysis results with solar ORC.....	136
Table 23. Modeling of solar driven cooling for a 80k sq ft supermarket.....	141
Table 24. Modeling of solar driven cooling for a 120k sq ft retail store	142
Table 25. Modeling of solar driven cooling for a 270k sq ft hospital.....	142
Table 26. Modeling of solar driven cooling for a 270k sq ft hotel	143
Table 27. Selective Foil Properties	145
Table 28. Cermet Properties.....	145
Table 29. All Glass Dewar Advanced Cermet Coatings.....	146
Table 30. Component Improvement Summary	155
Table 31. Cost Comparison of XCPX Design Concepts in High Volume Production (10,000 tubes).....	161
Table 32. Down-Select Matrix.....	163
Table 33. Summary expectations table.....	171
Table 34. Collector Description of North-South Counterflow with Alanod Collector....	183
Table 35. Performance Characteristics of North-South Counterflow with Alanod Collector	184
Table 36. Description of East-West Counterflow with Alanod Collector	189
Table 37. Performance Characteristics of East-West Counterflow with Alanod Collector	190
Table 38. Comparison of the North-South and East-West Counterflow with Alanod collectors.....	195
Table 39. Collector Description of North-South U-Tube with Alanod Collector.....	212
Table 40. Performance Characteristics of North-South U-Tube with Alanod Collector.	213
Table 41. Description of East-West U-Tube with Alanod Collector	216
Table 42. Performance Characteristics of East-West U-Tube with Alanod Collector	217
Table 43. Description of East-West Counterflow with Alanod Collector	219
Table 44. Performance Characteristics of East-West X-Tube with Alanod Collector.....	220
Table 45. Description of North-South U-Tube with Reflectech Collector.....	223
Table 46. Performance Characteristics of North-South U-Tube with Reflectech Collector	224
Table 47. Stagnation test conditions for North-South U-Tube with Reflectech	226

Table 48. Description of East-West U-Tube with Reflectech Collector.....228
 Table 49. Performance Characteristics of East-West U-Tube with Reflectech Collector.228
 Table 50. Performance Summary of All Collectors Based on Effective Irradiation.....232
 Table 51. Performance Summary of All Collectors Based on Direct Normal Irradiation232

Abstract

This report describes the design and development a of low-cost, high-temperature solar thermal collector system for mass production with SolFocus, Inc. The external compound parabolic concentrator can be readily manufactured at a cost of \$15 to \$18 per square foot, and has an efficiency of 50 percent at a temperature of 400°F.

During this project, a total of seven different external compound parabolic concentrator configurations were created and tested at the University of California, Merced. After improving the reflector technology and incorporating a new evacuated thermal absorber design, a prototype was constructed and tested. After further improvements and adjustments, a 10 kilowatt prototype was manufactured and tested by SolFocus at the NASA Ames Research Center in California. This prototype has been in operation since the spring of 2008.

The project demonstrates a significant advance in solar thermal technology, with potential practical applications in the areas of solar heating, cooling, power generation, and desalination. External compound parabolic concentrator based systems could potentially replace natural gas driven systems, leading to a more conservative use of natural resources and a reduction in atmospheric pollutants including methane and carbon dioxide. As a result of this research, a new startup company, B2U Solar, was launched from SolFocus to commercialize the external compound parabolic concentrator technology. B2U Solar is developing applications in three areas with immediate potential, including: heating ventilation, and air conditioning, which employs double-effect absorption cooling; industrial/commercial boiler or oil heater augmentation; and process heat.

Keywords: Solar thermal collector, external compound parabolic concentrator XCPC, reflector, solar heating, cooling, power generation, desalination, atmospheric pollutants, B2U, HVAC

Executive Summary

Introduction

Commercial solar thermal collectors ~~at a distributed scale~~ are predominantly flat plates that do not have the ~~high temperature~~ capability to provide process heat, power double effect absorption chillers, or produce electric power at high temperatures. A more cost effective solar thermal collector capable of producing heat at a temperature of approximately 400°F is needed for industries.

The discovery and development of non-imaging optics has enabled non-tracking (fixed) concentrating solar collectors generating heat up to 600°F. In March 2002, Bergquam Energy Systems completed a project to design and optimize solar absorption chillers. This project, funded by Public Interest Energy Research program-Renewables Program (contract number 500-02-035), was the first demonstration ~~worldwide~~ showing that a double effect absorption chiller can be powered by a solar thermal system, based on non-imaging optics for the concentration of sunlight. Several overseas companies ~~overseas~~ took up this technology concept and developed similar products to be commercialized. However, most of these products are, ~~in most cases,~~ not cost-competitive and ~~not or~~ geared to California's climate requirements.

This report describes the design and development of a ~~of~~ low-cost, high-temperature solar thermal collector system for mass production. Working with corporate participants, SolFocus and United Technologies Research Center, the research team at the University of California, Merced ~~has~~ developed an innovative non-tracking system, consisting of a series of stationary evacuated solar thermal absorbers paired with external non-imaging reflectors. Called an external compound parabolic concentrator, this system is able to operate with a solar thermal efficiency of 50% at a temperature of 400°F. The external compound parabolic concentrator can be readily manufactured at a cost of \$15 - \$18 per square foot.

During the course of this project, a total of seven different external compound parabolic concentrator configurations were tested, and an initial external compound parabolic concentrator prototype was created and tested at UC Merced (Figure 1). After improving the reflector technology and incorporating a new evacuated thermal absorber design, an improved prototype was constructed and tested. The East-West collector with U-Tubes and Reflectech reflectors performed the best out of ~~our the~~ tests, with roughly 47 percent efficiency at 200°C. After further improvements and adjustments, a 10 kW prototype was manufactured by SolFocus and tested at the NASA/Ames facility (Figure 2). This prototype has been in operation since the spring of 2008.



Figure 1. An Early XPCP Prototype at UC Merced
Photo Credit: The Regents of the University of California



Figure 2. The 10kW SolFocus Test Loop at NASA/Ames
Photo credit: The Regents of the University of California

The external compound parabolic concentrator can replace natural gas used for heat and space cooling with solar energy, leading to a more cost effective use of natural resources and decreased air emissions. Given that conventional flat plate collectors, and even the Winston-Series Compound Parabolic Collector manufactured by Solargenix Energy, cannot operate with a positive efficiency at temperatures above 250°F, this project represents a major advance in practical solar heating, cooling and power generation.

The success of this project has also stimulated the creation of a new company called B2U Solar. B2U Solar was recently spun out of SolFocus to commercialize the external compound parabolic concentrator technology. The company is already focusing its commercial efforts on immediate high potential areas, including: heating, ventilating, and cooling employing double-effect absorption cooling; industrial/commercial boiler or oil heater augmentation; and process heat. A new prototype has been manufactured and installed by B2U at the Gas Technology Institute (GTI) in Chicago.



Figure 3. The 10kW B2U Prototype at GTI

Photo credit: The Regents of the University of California

Currently, UC Merced researchers are collaborating with industry on another high impact area for this technology. Evaluations are under way that could lead a new UC Merced research partnership focused on harnessing solar thermal energy for water desalination projects in California's Central Valley and beyond.

Technical Description

The external compound parabolic concentrator consists of a series of stationary evacuated solar thermal absorbers paired with external non-imaging reflectors. The design consists of a set of parallel cylindrical absorbers, each of them placed in the center of an evacuated glass tube. Each absorber is thermally connected to a manifold using a U tube. Each glass tube is surrounded by a non-imaging reflector made of Alanod aluminum. The basic design is shown in Figures 4.



Figure 4. Parallel Reflectors with Evacuated Glass Tubes

Photo credit: The Regents of the University of California

The advantage of using integrated heat pipes for the external compound parabolic concentrator is that the connection does not require plumbing since there is no exchange of fluid. This simplifies the installation, facilitates tube replacement and enhances the reliability. The external compound parabolic concentrator design allows for low-cost mass production, because all components are currently mass produced and available at very low prices. When compared to existing system designs (see Table 1), the external compound parabolic concentrator system represents a major advance in the field of low-cost high temperature solar thermal collectors

Table 1. Comparison of the external compound parabolic concentrator system to other solar thermal systems

<i>Technological concept</i>	<i>Pros</i>	<i>Cons</i>
<i>Flat plate collector</i>	<i>Stationary</i>	<i>Limited to temperatures well below 200°F</i>
<i>Parabolic Trough</i>	<i>Can operate up to 600°F</i>	<i>Tracking required</i>

<i>Technological concept</i>	<i>Pros</i>	<i>Cons</i>
<i>Integrated Compound Parabolic Concentrator (ICPC)</i>	<ul style="list-style-type: none"> - <i>No tracking required</i> - <i>Can operate up to 500°F</i> 	<i>Expensive</i>
<i>External Compound Parabolic Concentrator (XCPC)</i> <i>[our approach]</i>	<ul style="list-style-type: none"> - <i>No tracking required</i> - <i>Amenable to low cost mass production (\$15 - \$18 psf)</i> 	<i>Limited to temperatures up to 450°F</i>

Source: The Regents of the University of California

Project Objective and Outcome

UC Merced’s objective for this project was to develop and demonstrate a new concentrating solar thermal collector system that is able to operate with a system efficiency of at least 50 percent at a temperature of 400°F, and to reduce the cost of a 400°F-capable distributed-scale solar thermal collector systems by 50 percent from the current \$30 per square foot to \$15 per square foot.

Working with corporate participants SolFocus and United Technologies Research Center, the research team at the University of California, Merced has developed an innovative non-tracking system consisting of a series of stationary evacuated solar thermal absorbers paired with external non-imaging reflectors. Called an external compound parabolic concentrator, this system is able to operate at or near a solar thermal efficiency of 50% at a temperature of 400°F (see Figure 5).

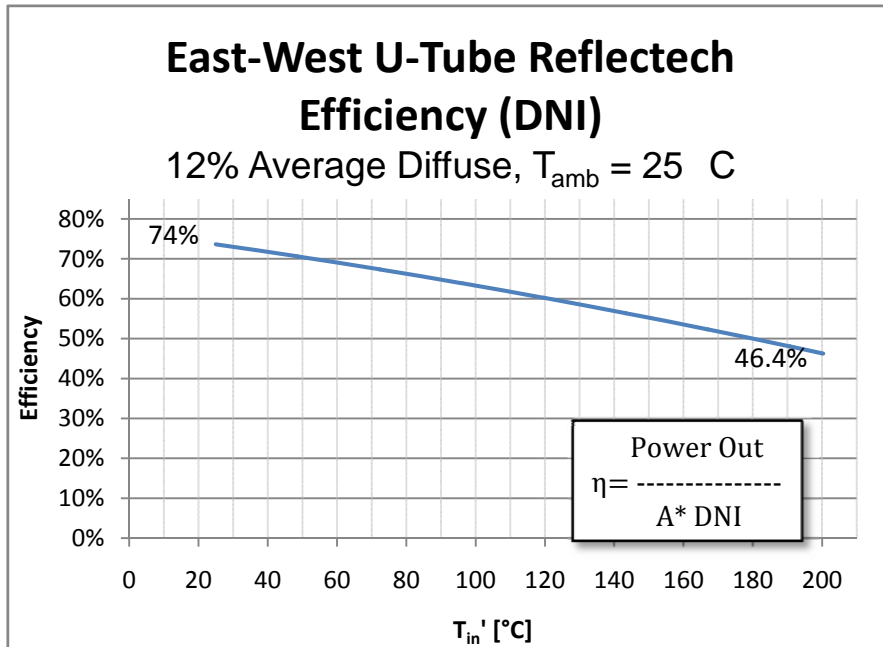


Figure 5. XCPC Thermal Efficiency at Various Temperatures

Source: The Regents of the University of California

Based on information provided by B2U (a new California Corporation created for the sole purpose of commercializing the technology), the cost to manufacture that was developed under this contract is within \$15 - \$18 per square foot.

Conclusion

This project met its stated objectives and was completed within budget. The design is both thermally efficient and affordable to manufacture. The project partner SolFocus has already spun off a new company called B2U to commercialize this technology in numerous high-impact areas.

Using private funding, UC Merced researchers are now building a “solar cooling” prototype at UC Merced to showcase this technology, and new applications for this technology are being explored.

Benefits to California

The use of the innovative concentrating solar thermal system will provide the following public benefits to California:

- Environmental value
- Natural gas displacement
- Electric peak demand reduction
- Transmission and Distribution grid relief
- Job creation in the renewable energy industry

1.0 Introduction

This project demonstrates the effects of the design and configuration change in an evacuated tube based solar thermal collector utilizing non-tracking compound parabolic concentrators. High temperature operation (400° F) was achieved with acceptable optical and overall efficiencies.

Design enhancements in the evacuated tube assemblies focused primarily on the flow paths to optimize heat transfer and flow rates. Three designs were evaluated in east-west (horizontal) and north-south (vertical) configurations.

Compound parabolic concentrators were designed with a wide acceptance angle to facilitate use without the need of a tracking mechanism. Alanod and Reflectech were used to line the concentrators. Each were evaluated separately to ascertain their respective impacts on optical and overall system performance.

A 10 kW prototype system was built and evaluated by SolFocus, Inc. The system performed well; however, the optimum configuration was dependent on the desired operating temperature.

2.0 Project Outcomes

2.1. Task 2.0

2.1.1. Introduction

This report summarizes the findings of a broad survey conducted by the United Technologies Research Center (UTRC) with the objective of identifying promising applications for the external compound parabolic concentrator (XCPC) solar heat collector technology being developed by UC Merced and SolFocus. The survey focused on identifying applications that could operate on waste or solar generated heat in the temperature range of 200° F to 500° F. This represents the potential upper and lower bounds for working fluid from the solar thermal collectors. The applications surveyed can be qualified into four broader categories:

- a) Heat driven cooling/heating technology
- b) Heat driven electric power generation technology
- c) Heat driven water treatment technology
- d) Heat driven industrial processes

The identified applications in each of these categories were evaluated based on the following evaluation criteria:

- 1) **Technical feasibility and viability** – Related to the ease with which the application could be integrated with the XCPC collector and the overall effectiveness of the application
- 2) **Economic competitiveness** – Related to the envisioned cost of the integrated system against other alternatives
- 3) **Market potential** – Related to the target markets that might be serviced by the envisioned product and its relative competitiveness in those markets
- 4) **Time to commercialization** – Related to the time it would take to commercialize the integrated system
- 5) **Other considerations** – Related to the institutional and legal barriers that might hinder commercialization of the envisioned system

2.1.2. Applications

The applications were ranked based on qualitative assessments in each of the evaluation criteria. Based on these assessments two technologies were selected for further study (see Task 3 reports). These include:

- a) Solar driven cooling/heating using absorption chillers (single, double and triple effect)
- b) Solar driven organic Rankine cycle (ORC) for electrical power generation

Heat driven cooling/heating technologies

Thermal energy captured in the working fluid that circulates through the XCPC collectors can be used in conjunction with various thermally activated cooling technologies (TAT)¹ to produce chilled water that can be used in cooling and refrigeration applications.

Alternatively, the thermal energy can be used to remove humidity from the air which is desirable in comfort and food storage applications. There are three major types of TAT cooling technologies that could work with the XCPC collectors. These include: absorption chillers, adsorption chillers and desiccant systems.

Some of the absorption chillers offered in the market today can operate in both heating and cooling mode. It may be possible to recover some additional heat (for space heating) from the XCPC working fluid that exits the chiller, but it is likely that such an alteration might adversely impact the collector efficiency.

Absorption chillers technology basics

The Department of Energy – Distributed Energy Program, has a very detailed description on the technology basics of absorption chillers. Figure 6 below shows a timeline for the evolution of absorption chiller technology over the years.

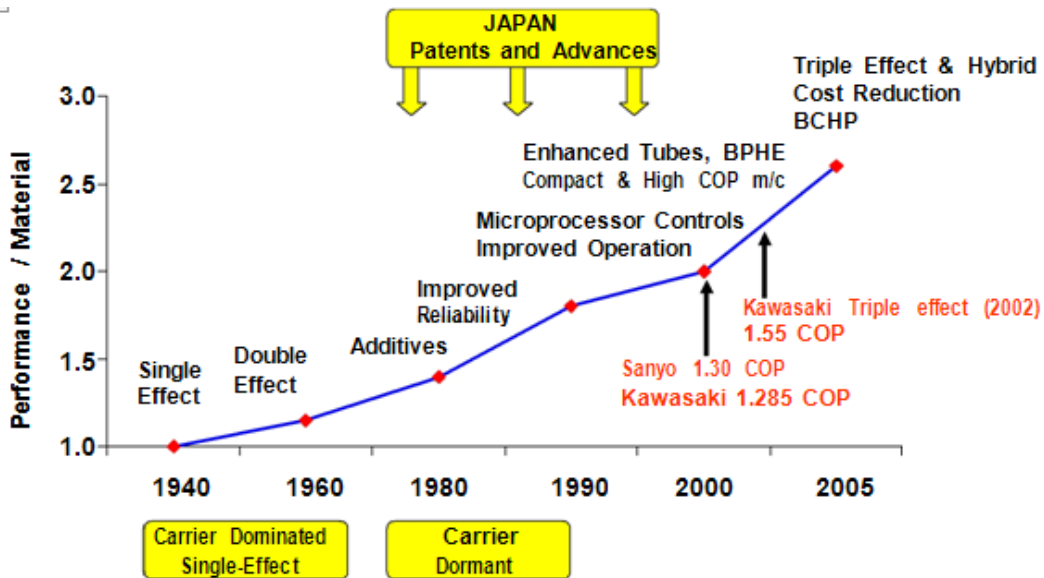


Figure 6. Evolution of absorption chiller technology over the years

Source: The Regents of the University of California

Briefly, the absorption chiller uses a thermal method for compressing the refrigerant vapor compared to the mechanical method (compressors) used in most electric vapor compression

(VC) chillers. The equipment typically uses a working fluid pair such as ammonia-water or lithium bromide-water and the amount of cooling provided can range from a few refrigerant tons for residential applications to more than one thousand tons for commercial applications. The ammonia-water pair has been in limited usage for several years due to the toxicity issues associated with ammonia. In current lithium bromide – water based chillers, water is the refrigerant and aqueous lithium bromide is the absorbent. Water in vapor phase exiting the evaporator is absorbed by the lithium bromide solution in the absorber and this solution is pumped to the generator where heat is used to remove the water from the lithium bromide solution which is subsequently pumped back to the absorber. Several designs use natural gas or other fuel driven methods to provide heat to the generator. Thermal energy obtained from industrial waste heat sources, solar etc. could be used as an alternative method for heating the generator stage. This can provide added benefits of reduced emissions and minimize energy costs (less fuel consumed). The performance metric for cooling cycles is the coefficient of performance (COP) and enhancing the amount of water produced using the refrigerant vapor from a high stage generator can enhance performance of the absorption chiller. Absorption chillers are thereby offered as single effect, double effect and triple effect chillers with the key distinction among the three technologies being the number of generators used in the chiller and the temperatures at which they operate. Figure 7, shows a schematic of BROAD's double effect absorption chiller where the heat is generated by burning natural gas.

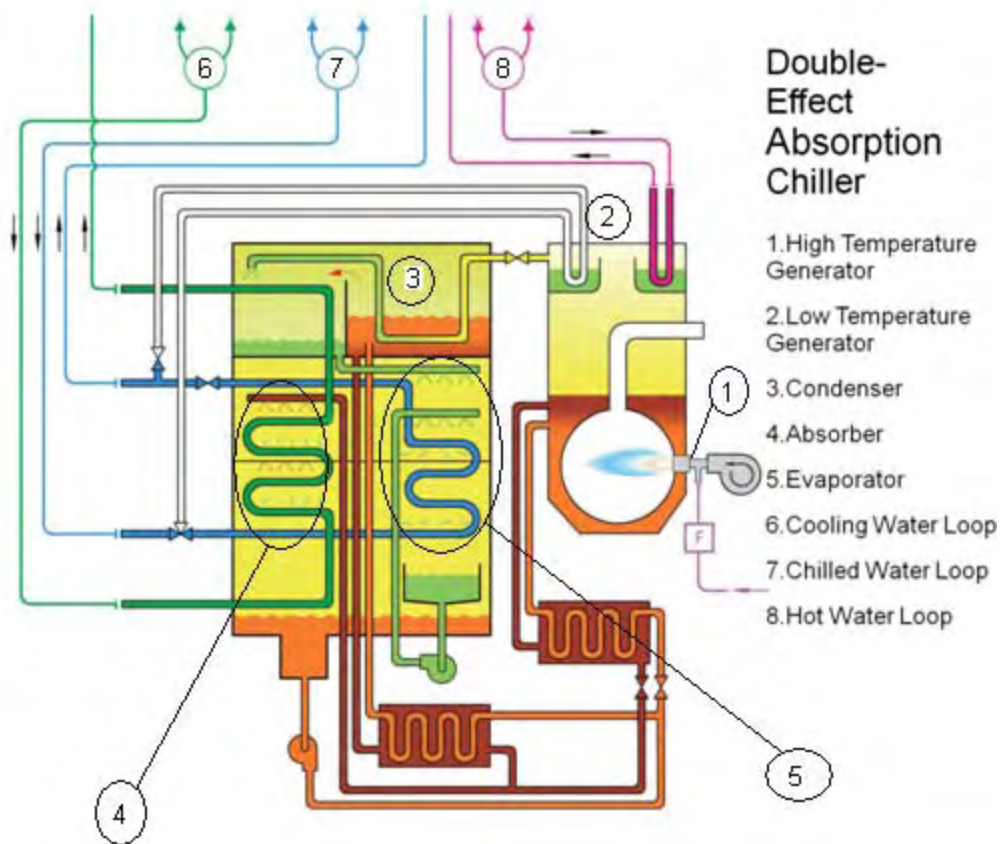


Figure 7. Broad's Double-Effect Absorption Chiller

Source: The Regents of the University of California

Table 2 ,summarizes the generator temperatures and associated COPs typical for the three types of absorption chiller technologies

Table 2. Absorption Chillers, Generator Temperatures and COPs

Chiller type	Temperature range	COP range
Single effect	> 185 F	0.5-0.75
Double effect	> 285 F	1.1-1.4
Triple effect	> 350 F	1.5-1.8

Source: The Regents of the University of California

Technology Evaluation

Technical feasibility and viability

Absorption chillers have been successfully demonstrated for several integrated applications with waste heat. Solar driven absorption chillers were demonstrated by

Carrier in the 1970s and additional demonstration work has been performed by Broad and other major heating, ventilating, and cooling (HVAC) companies as well. All the work done so far suggests a high degree of technical feasibility for a XCPC driven absorption chiller.

Economic competitiveness

Economic competitiveness for the integrated XCPC with the absorption chiller system largely depends upon the ability of the XCPC to hit cost targets of <\$100/m². In doing so, the operational expenditures for the system are comparable to absorption chillers operating on natural gas (~4 cents/kWh). Rising fuel costs further enhance the attractiveness of the absorption chiller option.

Market potential

Absorption chillers in the US market compete with electrically driven vapor compression chillers and cheap electricity prices have prevented their mass adoption in this market. The VC systems have COP's in the range of: 3-4. This implies that the higher the COP of the thermal activated technology (TAT) chiller, the greater the chance it has of capturing the market share, particularly when consumer electricity prices are on the rise especially in California.

Time to commercialization

Single and double effect chillers have been available in the commercial space for several years, and Kawasaki has recently introduced triple effect chillers in the Asian market. This implies that successful commercial development of the XCPC in two years could lead to integrated chiller product offerings within five years.

Other considerations

Potential legal and institutional barriers for an integrated XCPC-chiller product will depend primarily on the type of working fluid used in the XCPC and the ability to safely install the collectors and transport this fluid to the chiller. Corrosion issues and refrigerant leaks are the main concerns for absorption chiller systems from a legal and institutional perspective and technology maturity coupled with market adoption dictates how these barriers are overcome. The chiller systems themselves are commercial products and there should be no major institutional barriers for single and double effect chillers. Triple effect chillers on the other hand might require additional qualification before they can penetrate the US market primarily because of the lower technology maturity of these systems.

Adsorption chillers technology basics

Adsorption chillers^{3,4} have been considered as alternatives for absorption chillers because of their lower operating temperatures and potential advantages such as no corrosion issues,

no hazardous leaks etc. (primarily associated with lithium bromide solutions in absorption chillers). A typical working pair in the adsorption chiller is water (refrigerant) and silica gel (adsorbent). In this system there are two adsorbent beds that alternate between a generation stage and an adsorption stage. The generation stage requires heat and this heat can be provided by various renewable and non-renewable sources. The heat source temperatures for these systems can be in the 120° F to 200° F range (lower limit of the XCPC) and their COPs are usually lower than single effect absorption chillers (close to 0.6). Figure D, shows a schematic of an adsorption chiller cycle.

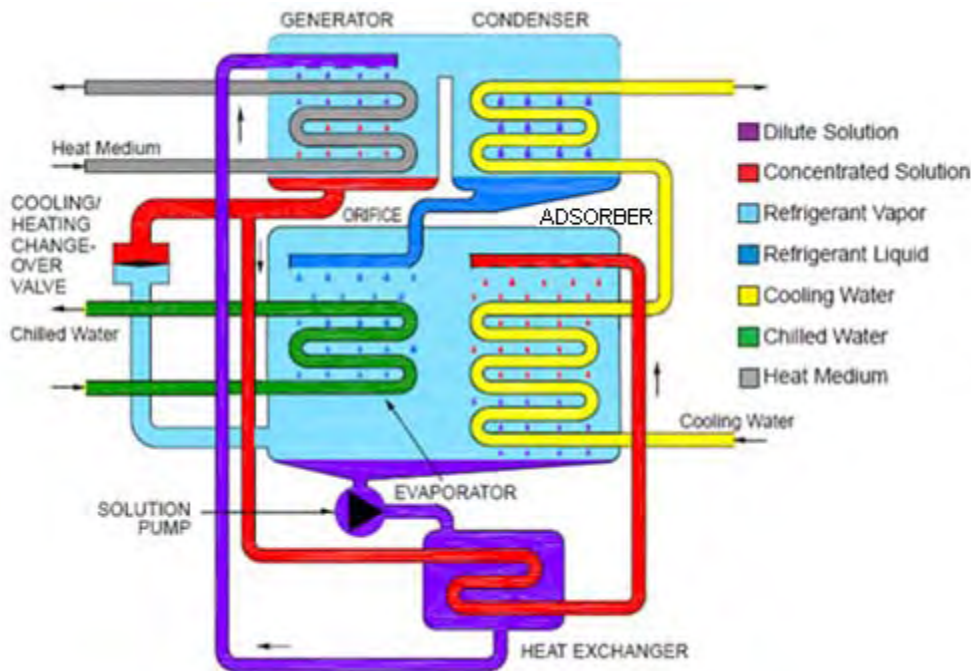


Figure 8. Schematic of a typical adsorption chiller configuration

Source: The Regents of the University of California

Technology Evaluation

Technical feasibility and viability

Adsorption chillers are present in the Japanese market today and HIJC USA Inc. in the United States is marketing a Japanese product. Integration of this device with the XCPC while feasible may not necessarily be the best use of the high quality heat that is obtained from the XCPC.

Economic competitiveness

Adsorption chillers at a COP of 0.6 could compete favorably with single effect chillers from

a cost and reliability perspective. Double effect machines with higher COPs (more cooling capacity per unit of thermal energy input) are economically more competitive than current adsorption chillers.

Market potential

Adsorption chillers could compete well as cooling technology offered in markets where low grade waste heat (<200 F) is readily available. The low COP of these devices makes their ability to displace vapor compression chillers even more difficult than double effect absorption chillers.

Time to commercialization

Adsorption chillers are available in the market today and while an XCPC integrated adsorption chiller could be commercialized, the current technology with its lower temperature of operation is not the ideal fit for the XCPC collector. Future generation adsorption chillers with higher COPs and higher temperature operations could be better fits; however, no such device is available commercially.

Other considerations

There seem to be no major legal or institutional barriers that might prevent the current water-silica gel based adsorption chillers from entering the market. Attempts to improve the COP might require moving to refrigerants such as ammonia and this may introduce barriers primarily due to concerns about toxicity of the refrigerant.

Desiccant cooling technology basics

Desiccant cooling² is a popular method for humidity control and the basic principle for this technology is the use of a sorbent material to remove moisture from an air stream. The sorbent material can be solid (silica gel, alumina etc.) or liquids (lithium chloride, glycol etc.). Thermal energy is used to regenerate the sorbent material and waste heat or solar could be one of the sources of this thermal energy. Several companies including Carrier, Munters, AIL Research etc. to name a few offer desiccant based humidity control products.

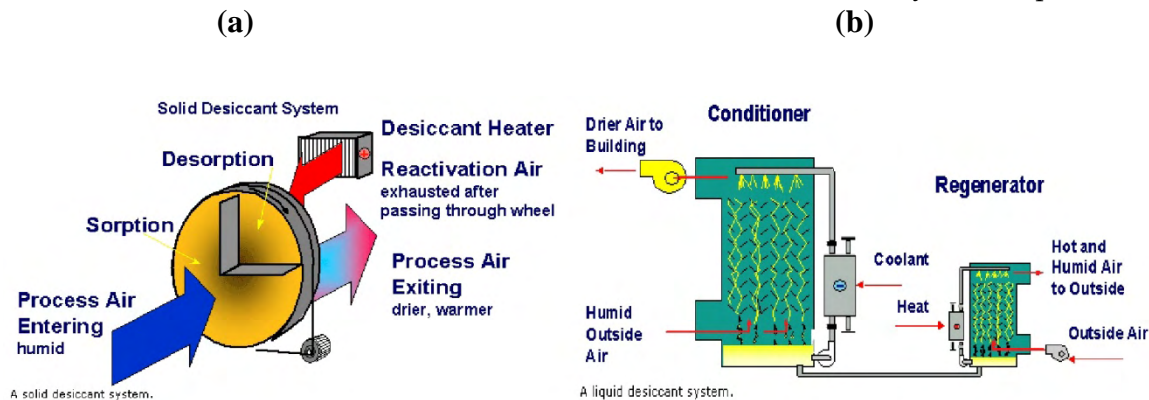


Figure 9. Solid (a) and liquid (b) desiccant technologies²

Source: The Regents of the University of California

Technology Evaluation

Technical feasibility and viability

Most of the desiccant systems can operate with low quality waste heat (as low as 150° F) and while it is technically feasible to interface this with the XCPC, this particular application may not be the best use of the high quality thermal energy obtained from the collectors.

Economic competitiveness

The desiccant systems can be expensive products and the economic competitiveness of an integrated system will primarily depend on making the collector prices competitive with the current method used for regenerating the sorbent material. Since the quality of heat required to regenerate sorbent materials in desiccant systems is quite low, there are cheaper off the shelf low temperature thermal collectors that may be a better choice for an integrated solution.

Market potential

Market potential for desiccant based dehumidifiers was projected to be \$300 M in North America in 2006⁶. The market share for solar driven desiccant dehumidifiers is not significant and it is unclear if the XCPC would offer any benefit in terms of penetrating into this market.

Time to commercialization

Several desiccant cooling system products exist today and it is conceivable that any potential solar integrated desiccant product can be developed in a span of 1-2 years.

Other considerations

Solid desiccant systems are the most prevalent in the market today; and, there are almost no legal or institutional barriers preventing the adoption of this technology. However, working fluid in the solar collector, and the need to pump corrosive fluids in liquid desiccant systems could be of concern from an institutional stand point.

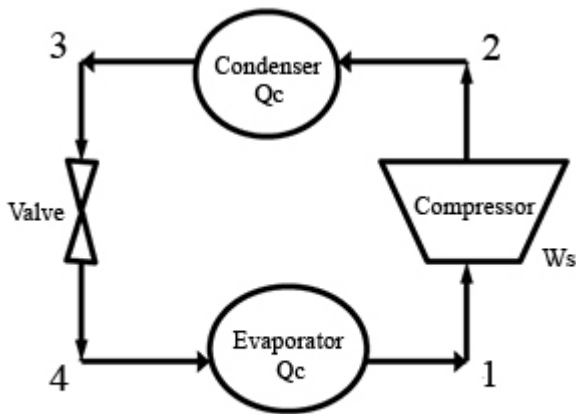
Heat driven electrical power generation

Currently, one of the more popular methods for converting solar energy to electrical energy in the distributed power generation market is photovoltaic technology. Solar thermal based power generation cycles have been demonstrated for utility scale applications. Creating a distributed solar thermal electrical generation product that could compete by offering lower leveled cost of electricity than PV could provide a path to capture a share of the growing \$11 B/yr solar electricity generation market. There are three types of distributed generation products that could be compatible with the XCPC. These include:

- a) ORC based products
- b) Steam cycle based products
- c) Stirling cycle based products.

Organic Rankine Cycle based products technology basics

The Organic Rankine Cycle (ORC), in simple terms, is a vapor compression cycle that is operated in reverse. Figures 10 and 11, are a schematic representation of an ORC compared to a traditional VC refrigeration cycle. The motor and the compressor used to compress the refrigerant are replaced by a turbine and a generator. The overall efficiency is sensitive to (among other factors) the type of refrigerant used in the system. The key interface between XCPC collector working fluid and the ORC would be the evaporator/boiler heat exchanger. This heat exchanger would have to be appropriately designed based on the working fluid that is finally selected for the collector. Companies such as ORMAT, UTC Power etc. currently offer ORC products that could be readily interfaced with the XCPC.



The Vapor Compression Cycle

Figure 10. Vapor compression

Source: The Regents of University of California

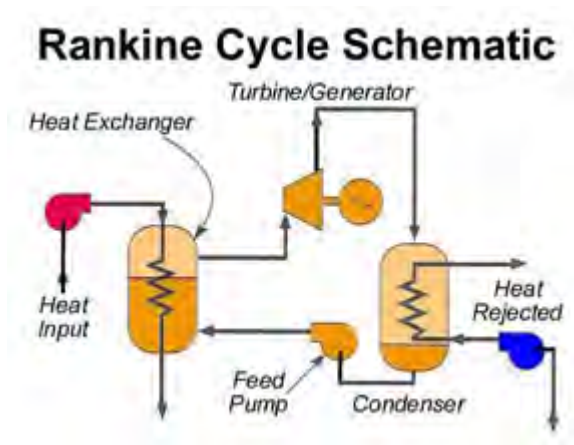


Figure 11. Organic rankine cycle

Source: The Regents of University of California

Technology Evaluation

Technical feasibility and viability

There are a couple of commercialized ORC products including the PureCycle™ from UTC Power that could use heat provided by XCPC collectors to produce power for distributed applications. The temperature from the XCPC is within the desired range required for operation of this product (demonstrated for temperatures as low as 200 °F). One of the important elements that may need to be redesigned for an integrated system is the supervisory control to enable seamless performance under transient solar insolation conditions.

Economic competitiveness

The PureCycle™ product in volume would cost in the neighborhood of \$1/W and this coupled with low cost XCPC would offer customers a solar based electrical power generation solution that is about half the cost of conventional photovoltaic (PV) today. The key advantage of the integrated product is that the components that comprise the core power generating system exist as virtual commodities in volume production today.

Market potential

A distributed solar-ORC product would compete in the space occupied by conventional PV today. Initial markets would likely include big box retail stores, supermarkets etc. that are projected to be in the \$4 B range by 2010 (based on projections from the PV industry).

Time to commercialization

The current PureCycle™ product can operate at temperatures up to 300 °F and the integrated product with an XCPC operating at this temperature could be offered within a five year time frame. There might be the possibility of altering refrigerants so that the cycle operates at higher temperatures and higher efficiencies. These systems might take well over five years to develop.

Other considerations

Currently there are no major legal or institutional barriers envisioned for an integrated product given that the ORC is a commercial offering. Changing regulations on refrigerant usage could become a major consideration especially when designs need to be improved from an efficiency standpoint. The system will require compliance with electrical codes and standards should it become a grid tied product.

Steam Cycle Based products

Technology basics

Steam cycles work on the operating principle of feeding high pressure steam into rotating turbomachinery that converts the mechanical energy to electrical energy using a motor. Utility scale solar thermal energy driven steam cycles⁸ have been demonstrated as part of the DOE-Solar Energy Technologies Program (SETP). Recently Carrier⁹ has introduced a micro-steam generator product that is targeted towards the distributed generation market and this product may be an ideal integration candidate if the XCPC heat is used to create high pressure, wet steam.

Technology evaluation

Technology feasibility and viability

The technology in theory should be feasible and viable but there may be some redesign required for the generator during transient operation (periodic dip in solar insolation and/or **working fluid flow rate temperatures**). **Efficiency would be low in this system because of the limitation on the maximum cycle temperature and the steam turbine would likely have to deal with** the erosive effects of wet steam. Initial iterations of a product such as this might only be viable in places where there are existing high pressure steam lines where solar meets only part of the total steam requirements for the system.

Economic competitiveness

Economic competitiveness of an integrated system will depend upon lowering the XCPC costs such that the steam generated from these collectors costs less than the yearly costs of steam (\$0.015/lb⁹) incurred by a system that is installed in a location with existing high

pressure steam lines.

Market potential

The ability of the integrated system to penetrate and capture solar power generation markets will depend upon being able to beat current levelized cost of electricity from PV systems. This market as mentioned earlier is in the billions of dollars regime and to ultimately be competitive in the absence of incentives and rebates, the cost of electricity for the system would have to be less than grid electric prices.

Time to commercialization

An integrated XCPC-micro steam turbine product would probably require about five years or more (including time taken to commercialize the XCPC collectors) of development due to reasons mentioned in the feasibility assessment.

Other considerations

It is unlikely that a fully integrated system would have major legal or institutional barriers preventing adoption other than those related to leakage issues of the working fluid selected for the XCPC collector. Electrical codes and standards will apply if the system is grid connected. Steam systems in certain buildings might have significant code barriers and this is something that will need to be overcome to capture the broader market.

Stirling Cycle Based products

Technology basics

The Stirling cycle has a fixed amount of working fluid and a piston (or pistons) in a sealed space. The piston(s) are moved by heating and cooling the sealed space and this movement produces rotational, mechanical motion that can be converted to electrical energy using a generator. The choice of the working fluid is therefore one of the critical elements in the selection of an appropriate Stirling engine. It needs to be environmentally benign and work at the temperatures supplied by the XCPC collector. Dish solar collector based Stirling engines have been a topic of Department of Energy (DOE) research for several years. Some of these require working temperatures as high as 700 °C and the primary benefit of operating at higher temperatures is higher efficiency. The moderate working temperature of the XCPC compared to the higher temperatures might result in a lower efficiency operation of the Stirling engine.

Technology evaluation

Technology feasibility and viability

It is technically feasible to demonstrate a Stirling engine integrated to an XCPC array. Although the Stirling cycle has a high theoretical efficiency because it is a close approximation of the Carnot cycle, the actual efficiency is quite low because of practical limits on the effectiveness of heat exchanger devices. The efficiency and performance of such a device is unknown and it is unclear if these would perform better than the dish Stirling systems offered today.

Economic competitiveness

The system will have to be cheaper and operate at comparable efficiencies to be competitive with dish Stirling engines today. The system could compare favorably with an ORC but in this case it must meet a fairly low capital cost metric and it is unclear if some of the current Stirling systems could meet these cost metrics and stay competitive.

Market potential

The market potential in this case will also depend upon the ability of the system to offer competitive levelized cost of energy to the customer.

Time to commercialization

Stirling engine systems are commercially available from companies such as WhisperGen, Sun Power, Stirling Energy Systems etc. Time to commercialization of an integrated system will depend upon how the XCPC heat can be integrated to some of these engine systems and it is unclear at this point on how long this might take.

Other considerations

The institutional and legal barriers for an integrated system will depend upon the working fluid in the collector and the engine. Furthermore, electrical codes and standards for grid connected systems will also apply.

Heat driven water treatment technology

Water desalination and purification is important to several industrialized and developing nations. Water desalination requires removal of salt from various types of water sources including sea water, brackish water etc. with the objective of providing fresh water for every day consumer use. There are two main types of desalination technologies that are most prevalent today. The most common are various distillation processes that require high temperatures for operation. The second type is reverse osmosis which requires high pressures to drive pure water through a membrane separation process. Water purification focuses more on the removal of various particulate, organic and inorganic impurities from existing fresh water supplies or when attempting to implement water reclamation projects. Membrane technologies are popular methods for particulate removal. Other methods include adding some type of chemical such as chlorine, ozone etc., that can chemically react to remove certain organic compounds and/or biological organisms. Most of the water purification technologies do not require the high temperatures that can be generated by the XCPC for operation.

Solar desalination methodology involves using a solar still that evaporates water from sea water and collects fresh water through condensation. The process has a very slow throughput which is why even in some of the parts of the world with good solar insolation, other methods of water desalination are used. The thermally driven methods of water purification derive their thermal energy through the burning of fossil fuel (mostly natural gas). Consequently, the biggest value for XCPC generated heat might be in some of the distillation technologies as a substitute for the thermal energy generated by fuel. Two specific technologies that could fit within this realm include: a) Vacuum distillation and b) Membrane distillation.

Vacuum Distillation technology basics

Vacuum distillation works on the principle that by lowering the pressure of a salt water solution, it is possible to evaporate the water off at low temperatures (as low as 100 °F)¹⁰. The method is commonly used in large scale co-generation plants that produce electricity from natural gas and uses the waste heat from the process to distill sea water. A key tradeoff that occurs with the technology is that with lower quality waste heat, the vacuum pump may have to be designed to provide very low pressures and this may increase the electrical power consumed by the pump. Companies such as WasTech offer packaged vacuum distillation products for industrial use.

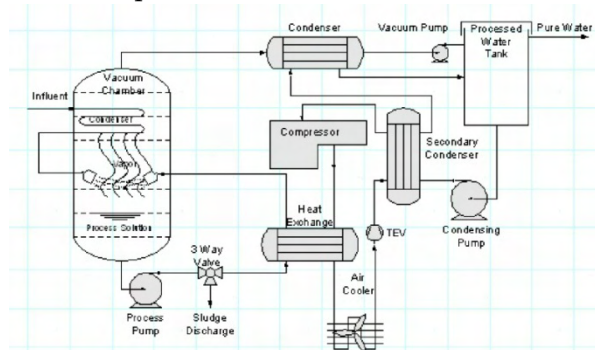


Figure 12. Vacuum distillation system¹⁰

Source: The Regents of University of California

Technology evaluation

Technical feasibility and viability

It should be technically feasible to use heat from the XCPC to drive a low temperature vacuum distillation process. The temperatures required are low enough that the process could even be driven by low temperature collectors today. It is possible that one of the reasons why a system such as this has not been implemented is due to the fact that these units operate in industrial processes where there should be other sources of low quality waste heat by negating the need for solar driven processes.

Economic competitiveness

It is unlikely that an XCPC driven vacuum distillation system would give any significant competitive advantage unless the power consumed by the vacuum pump is substantially reduced by adapting the system to operate at higher grade heat. In this case the realized cost savings due to lowered electricity consumption would have to be traded against the cost of utilizing XCPC heat.

Market potential

The integrated product if commercially and technically viable should have tremendous market potential because of growing demands for water desalination products both in California and worldwide.

Time to commercialization

The integrated product could take between 5-10 years to commercialize if an appropriate skilled vendor is identified in the field of water desalination to support the development project.

Other considerations

The legal and regulatory barriers for the integrated technology will be associated with demonstrating the quality of the water obtained from the process.

Membrane Distillation technology basics

Membrane distillation operates using a temperature differential driving force that creates vapor pressure differentials between two sides of a membrane module. One side of the membrane circulates cool, clean water with heated brine solution flowing on the opposite side. The temperature differential between the solutions results in vapor being formed from the brine solution and transported across the membrane pores where it condenses to fresh water upon contacting the cold side. This technology has been demonstrated for temperatures up to 80 °C in university studies¹¹ but there are no products available in the market place today that are based on membrane distillation.

Technology evaluation

Technical feasibility and viability

It is difficult to say if an integrated XCPC-membrane distillation system can be successfully demonstrated primarily because it may be difficult to obtain a durable membrane that operates at the higher temperatures (>150 °C) provided by the collectors.

Economic competitiveness

The current technology if successfully commercialized could compete favorably with reverse osmosis and other distillation processes. Initial costs of these units however may be high to factor in recovery of research and development expense.

Market potential

The product could compete well in the global water desalination market if the technology can be commercialized and it beats the more mature desalination product technologies in the market place today.

Time to commercialization

High temperature membranes will have to be developed so that the distillation process can operate at the thermal output provided by the XCPC. This requires technology development and it is conceivable that the system itself could take several years to develop.

Other considerations

The major institutional barrier to be considered is the fact that the integrated product would have to be qualified in terms of the quality of water provided by the systems. The barriers can be successfully overcome if appropriate testing protocols and standards are first developed for a standalone membrane distillation process.

Heat driven industrial processes

The thermal energy from the XCPC can certainly be integrated into industrial processes that require supplemental heat to drive certain processes. One such application is in industrial drying processes. The large food production and processing industry in California uses enormous amounts of heat for cooking, packaging and cleaning and this could be another potential market for the heat collected by the XCPC. The complication with implementing the XCPC in these scenarios is that industrial processes tend to be highly integrated in terms of their thermal management schemes. These processes also often require continuous 24/7 or 16/5 supply of the heat. The value for the thermal energy from an economic perspective is consequently lower in these cases compared to building integrated power generation and/or cooling and heating applications.

The generation of renewable solar fuels is an area that could offer a future application space for the XCPC. Several technology options in this area have been identified as critical areas of research by the DOE Office of Basic Energy Sciences (BES)¹². Advanced catalytic and biomimetic approaches that convert biological waste, carbon dioxide, water etc. to fuels, requiring process temperatures in the neighborhood of 250 °C could be a good fit with XCPC generated process heat. This report has avoided providing an evaluation of these options due to their low technology maturity. It is important to note however that if these breakthrough technologies are successfully commercialized, a whole new area could be opened up for applying XCPC derived solar thermal energy

Ranking Technology options

The five categories for technology evaluation were assigned the following weights based on preferred importance: a) Technology feasibility and viability (TF-0.3), b) Economic competitiveness (EC-0.2), c) Market potential (MP-0.2), d) Time to commercialization (TC-0.2) and e) Other considerations (OC-0.1). The possible scores for each category used were in the range of 1-3. The market potential in our assessment follows the order power generation > cooling/heating > water desalination. This is based on the fact that there are products for the first two applications that encompass the residential, commercial and industrial markets. Water desalination is primarily industrial and commercial with limited application in the residential space. Table 3 below presents the decision matrix used to guide high level system design efforts for Task 3 of the contract.

Table 3. Decision matrix for technology down selection

Application	Technology	TF (0.3)	EC (0.2)	MP (0.2)	TC (0.2)	OC (0.1)	Total Score
Cooling/Heating	Absorption	3	2.5	2.5	3	2.51	2.75
	Adsorption	2.5	2	2.5	2.5	3	2.45
	Desiccant	2	2	2.5	2.5	3	2.3
Power Generation	ORC	2.5	3	3	2.5	2.52	2.7
	Steam cycle	2	3	3	2.5	2.5	2.55
	Stirling Cycle	2	2	3	2.5	2.52	2.35
Water Desalination	Vacuum Distillation	2	2	2	2	2	2
	Membrane Distillation	1.5	2.5	2	1.5	2	1.85

Source: The Regents of University of California

Conclusions and recommendations

Based on the assessment in this report it is recommended that an ideal near term focus for a future project would be XCPC integration with absorption cooling and ORC electrical power generation technologies. Next generation efforts could focus on integration with distributed steam (the micro-steam turbine for example) and Stirling cycles. Finally, over the longer term, the XCPC integration with water desalination technologies is worth considering. It is also recommended that UC Merced partner with other universities and/or companies in the development of basic technology for the emerging area of solar fuels with a focus around processes that operate at < 250 °

2.2. Task 3.0

2.2.1. Technical System Architectures for Application of Solar Heat

This report summarizes conceptual system architectures for the five potential applications for process heat from the XCPC that were identified from a broad survey that was conducted earlier (Task 2 report – “Report on Application Areas of Solar Heat”).

System configurations that are discussed in this report include:

XCPC driven single effect chilling

XCPC driven double effect chilling (b1: oil or b2: steam as hot working fluid)

XCPC driven triple effect chilling

XCPC driven combined chilling and heating

XCPC ORC

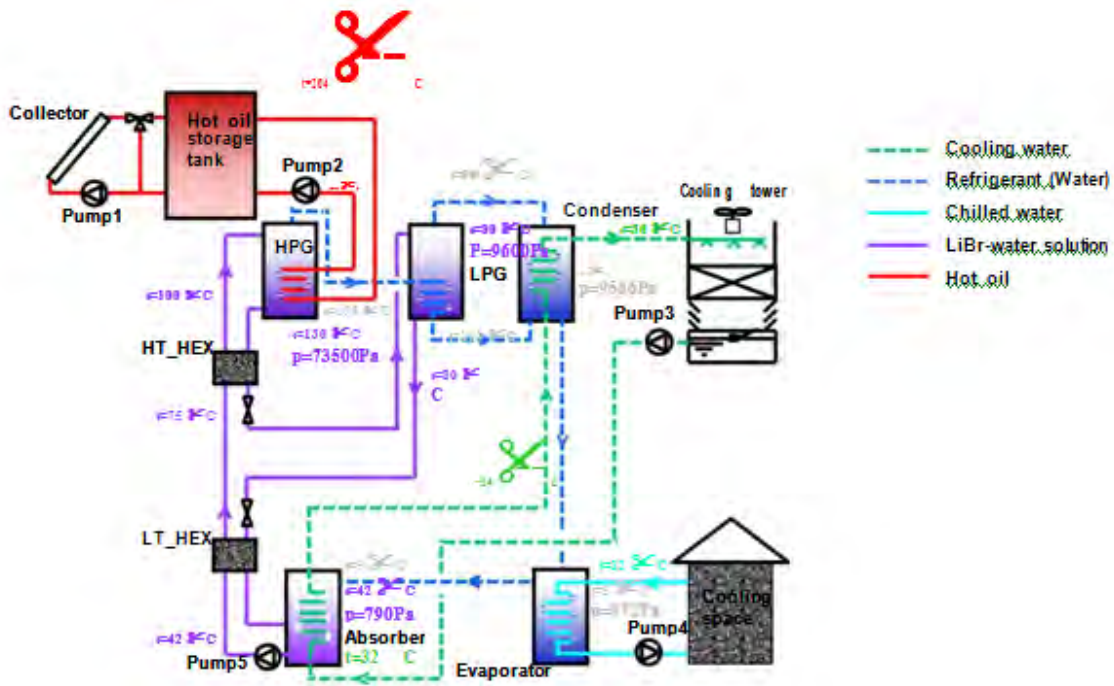
To compare different architectures, we assume the same chilling capacity of 120 refrigeration tons (RT) for all chillers, which is good for a mid-size office building in a moderate hot climate such as Washington, D.C., in summer. The solar thermal capacity needed to drive the absorption chiller will match the cooling capacity.

The technical specifications are provided are as generic as possible. Commercial data are referenced wherever appropriate to better illustrate the system working characteristics. Conceptual designs have been arrived at using simple high level engineering calculations that also provide details on the key operating parameters for the system.

XCPC driven single effect chilling

The diagram of a solar thermal driven single effect chilling system is shown in Figure 13 below.

Figure 13. Solar Thermal Driven Single Effect Chilling System



Source: The Regents of University of California

In this system, water is pumped to the solar collector and then heated to a temperature below the boiling point. The heated water is sent to a hot water storage tank. Hot water leaving the storage tank enters into the generator of a single effect Lithium bromide (LiBr) absorption chiller. The absorption chiller produces chilled water through the evaporator to cool the desired space. A cooling tower is needed to serve as the heat sink for the system.

Table 4. Major design specifications for solar thermal driven single effect absorption chillers

Design Specifications	Value (SI)	Unit (SI)	Remarks
Solar collector capacity	670	kW	
Water heating system efficiency	0.90		Assumed value
Hot water temperature produced	92	C	Assume water supply temperature + 2C
Design incoming hot water temperature	78	C	Assume return water temperature - 2C
Pump flow rate	11.4	kg/s	181 GPM
Hot water pump type	Variable speed		
Storage tank capacity	41	m ³	Assume 1 hour full load supply
Chiller type	Single effect		
Chiller capacity	120	RT	Assumed benchmark capacity
Chiller COP	0.7		A typical value

Design Specifications	Value (SI)	Unit (SI)	Remarks
Hot water inlet temperature	90	C	
Hot water leaving temperature	80	C	
Hot water flow rate	14.4	kg/s	228 GPM
Generator solution design temperature	80.0	C	
Chilled water leaving temperature	6.7	C	Typical design value
Chilled water returning temperature	12.2	C	Typical design value
Chilled water flow rate	18.1	kg/s	288 GPM
Cooling water leaving temperature	35.0	C	Typical design value
Cooling water returning design temperature	29.4	C	Typical design value
Cooling water flow rate	44.1	kg/s	698 GPM
Chiller water charge amount	152	liter	40 gallon
LiBr charge amount	417	liter	110 gallon

Source: The Regents of University of California

There is no significant performance difference between single effect chillers from different manufactures. Therefore, the above parameters are generally applicable to most single effect chillers. The Carrier 16 JB single effect absorption chiller (a hot water driven product) can be used as a prototype, Figure 2.

During normal operation, the water storage tank maintains a constant temperature profile. When there is no sufficient solar insolation, the pump supplying hot water to the solar collector should reduce the water flow rate, so that the hot water temperature can be maintained as constant as possible which implies that a variable speed pump is preferred.

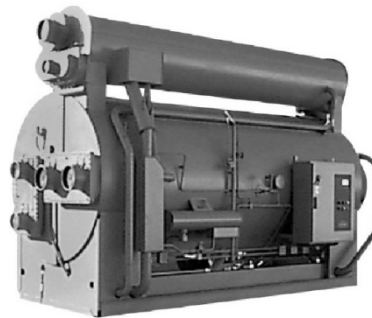


Figure 14. Carrier 16JB single effect LiBr absorption chiller

Source: The Regents of University of California

When the cooling load is low but the solar insolation is high, excess thermal energy can be stored in the storage tank. A radiator is not likely needed because the solar collector does not have to produce hot water if not needed; and the water storage tank can be oversized to absorb most of the excess solar energy. The option will need to be carefully considered during the detailed system design phase.

When there is high cooling demand but low solar energy, hot water in the storage tank is drained at a rate higher than the thermal energy produced in the collector. The average hot water temperature in the tank will decline. When the hot water temperature going to the chiller deviates within a few degrees, the absorption chiller cannot work properly and the building backup chillers, usually electrically driven vapor compression chillers, have to be used.

The advantage of single effect absorption chillers that they requires relatively low hot water temperature which means the water can be pumped at atmospheric pressure. The system is simple, commercially available, and the reliability is high. The major disadvantage is that the COP of the chiller is low and a larger solar collector is needed to provide the same amount of cooling load. Furthermore, since the quality of waste heat required for these chillers is lower than the temperature delivery capabilities projected for the XCPC, there may be a need to use the chiller as a bottoming cycle which works of the exhaust heat from a higher temperature component.

XCPC driven double effect chilling

A double effect absorption chiller can be used when the heating fluid temperature is sufficiently higher than the solution temperature in the high pressure generator (HPG) of the chiller. The solution temperature in the HPG is typically around or below 130 C. Therefore the XCPC heat source providing temperatures in the 150 C – 250 C range would work well with this system. The chiller can be driven by oil or steam, as shown below.

b1: Oil as hot working fluid

An oil driven double effect absorption chiller with solar heating is shown in Figure 16.

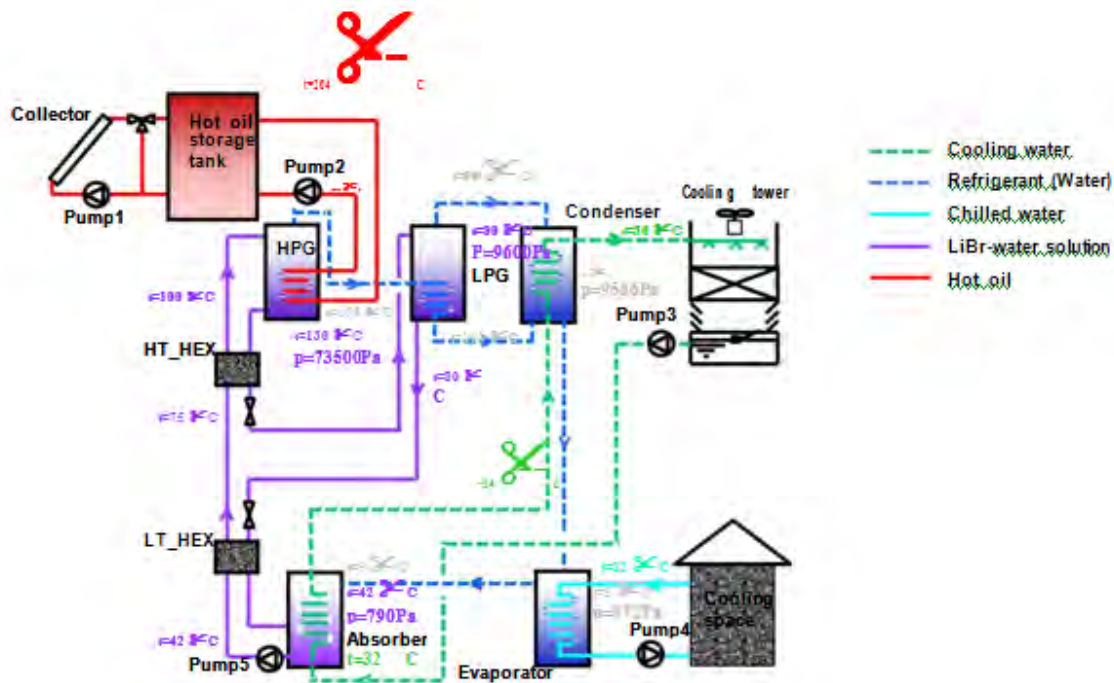


Figure 15 Diagram of a solar thermal driven double effect absorption chiller: using hot oil
Source: The Regents of University of California

When the chiller is driven by oil, the oil can reach high temperature of ~250 C while being maintained at atmospheric pressure. The working principle of an oil driven double effect absorption chiller is similar to that of a hot water driven single effect chiller. The oil is heated in the solar collector and then enters an oil storage tank. Hot oil leaving the storage tank enters the high pressure generator where the solution is heated to produce refrigerant (water) steam. The oil then returns to the hot oil tank at a lower temperature. The water steam enters the low pressure generator (LPG) where additional refrigerant is produced from the solution in the LPG.

The detailed technical specifications are shown in Table 2. The specifications are made as generic as possible, since the performance of double effect chillers made by different manufactures do not vary greatly. The 16DN direct fired double effect absorption chiller made by Carrier shown in Figure 4 is used as a commercial reference model wherever helpful. In reality, the 16DN chiller has been modified to use exhaust gas from microturbines as the heating medium¹. The 16 DE products can work with high pressure steam.

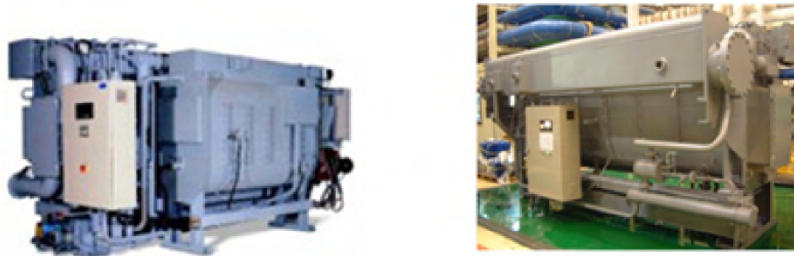


Figure 16. DN and 16 DE double effect chiller made by Carrier

Source: The Regents of University of California

With higher COP, a double effect absorption chiller requires much less heat than a single effect chiller to produce the same amount of cooling load. Even though the solar collector efficiency drops nominally from 0.90 to 0.80 and the oil has smaller specific heat than water, only a small oil flow rate is needed and the storage tank size is smaller as well. The insulation around the tank, however, should be more effective and more expensive than the low temperature tank that can be used in single effect systems.

Table 5. Major design specifications for oil driven solar thermal double effect absorption chillers

Design Specifications	Value (SI)	Unit (SI)	Remarks
Solar collector capacity	422	kW	
Oil heating system efficiency	0.80		Assumed value
Hot oil temperature produced	214	C	Assume oil supply temperature + 10C
Design hot oil temperature leaving storage	120	C	Assume return oil temperature - 10C
Pump flow rate	2.2	kg/s	36 GPM

	Value	Unit	
Hot oil pump type	Variable speed		
Storage tank capacity	8.1	m³	Assume 1 hour full load supply
Chiller type	Double effect		Oil driven
Chiller capacity	120	RT	Assumed benchmark capacity
Chiller COP	1.25		A typical value
Hot oil inlet temperature	204	C	
Hot oil leaving temperature	130	C	
Hot oil flow rate	2.3	kg/s	36 GPM
HPG solution design temperature	130	C	
LPG solution design temperature	80	C	
Chilled water leaving temperature	6.7	C	Typical design value
Chilled water returning temperature	12.2	C	Typical design value
Chilled water flow rate	18.1	kg/s	288 GPM
Cooling water leaving temperature	35.0	C	Typical design value
Cooling water returning design temperature	29.4	C	Typical design value
Cooling water flow rate	32.7	kg/s	518 GPM
Chiller water charge amount	235	liter	62 gallon
LiBr charge amount	640	liter	169 gallon

Source: The Regents of University of California

The oil tank storage and control logic are similar to that mentioned for the solar thermal driven single effect chillers. The reliability considerations are critical because of the possible leakage of oil in the solar collector. In addition, the oil pump and piping, etc., all require good sealing to prevent oil leakage. The oil based system in general however could be easier to seal than high pressure steam. Another possible issue with oil is the corrosion of the tubes that are used to

transport the oil to the chiller which means that material compatibility issues must be addressed in selection of the oil.

Due to the less common usage of oil as the heating fluid for absorption chillers, customized design is needed for the high stage generator. The development cost associated with designing this feature and the expected relatively small sales volume implies that the cost of the oil driven chiller will be somewhat higher than non-oil driven absorption chillers.

b2: Steam as hot working fluid

A steam driven double effect absorption chiller with solar heating is shown:

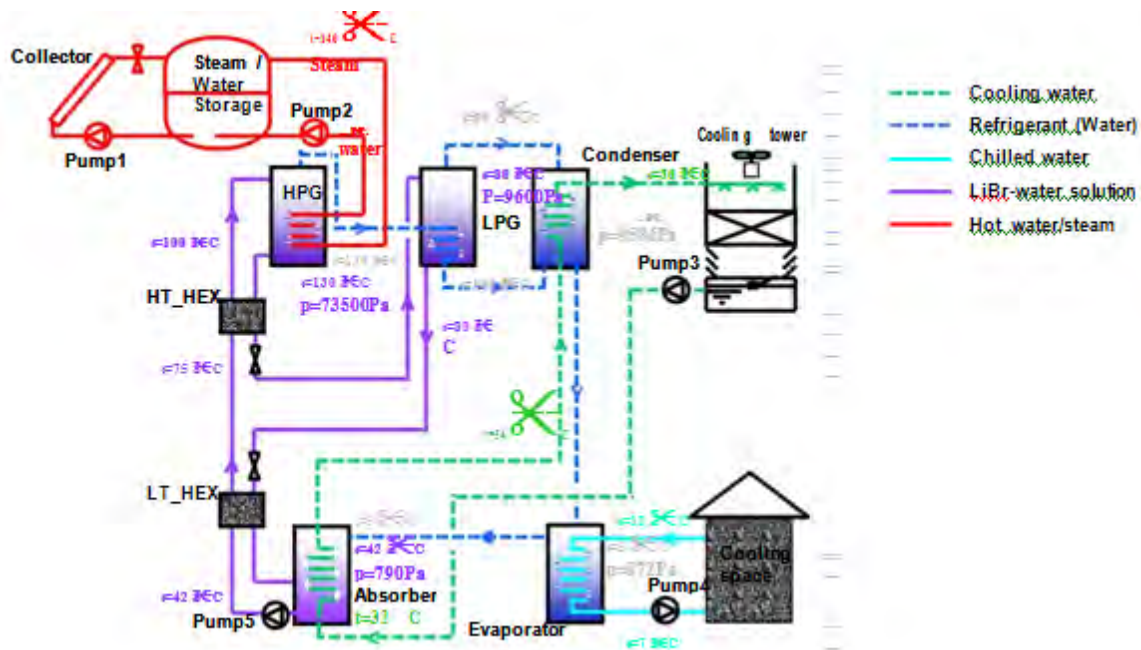


Figure 17. Diagram of a solar thermal driven double effect absorption chiller: using steam

Source: The Regents of University of California

The double effect absorption chiller driven by steam is similar to that driven by oil in the case of b1. The only differences are the high pressure generator (HPG) and heating fluid loop.

The hot solution in the HPG is heated using the steam latent heat. The steam condensing or saturation temperature therefore has to be higher than the solution temperature. Since the hot solution in the HPG of a double effect chiller needs to be around 130 C, the corresponding minimum steam saturation temperature needs to be a few degrees higher than 130 C, e.g., 140 C or above. The temperature difference of 5-10 C between the solution temperature and the steam condensing temperature would be sufficient because the phase change heat transfer coefficient of the steam side is several orders higher than that in the case of non-phase changing oil heat transfer.

A saturation temperature of 140 C or above corresponds to the steam pressure of 3.6 bar. The steam loop, including the solar collector, the storage tank and the valves, etc., needs to be pressurized. The system reliability and maintenance may be a concern. The detailed specifications are shown below in Table 6, in which the chilled water and the cooling water flow rates remain the same.

Table 6. Major design specifications for oil driven solar thermal double effect absorption chillers

Design Specifications	Value (SI)	Unit (SI)	Remarks
Solar collector capacity	422	kW	
Steam heating system efficiency	0.80		Assumed value
Steam saturation temperature	140	C	HPG solution temperature + 10 C
Steam saturation pressure	3.6	bar	From steam table
Pump flow rate	0.21	kg/s	3.4 GPM
Hot water pump type	Fixed speed		Fixed speed is sufficient
Storage tank capacity	~1	m³	Water level should be ~half @steady state
Chiller type	Double effect		Steam driven
Chiller capacity	120	RT	Assumed benchmark capacity
Chiller COP	1.25		A typical value
Heating fluid (steam) inlet quality	0.98		There is some condensation in the pipe
Heating fluid outlet temperature	135	C	Slightly above solution temperature, with some subcooling
Heating fluid flow rate	0.17	kg/s	2.7 GPM
HPG solution design temperature	130	C	
LPG solution design temperature	80	C	
Chilled water leaving temperature	6.7	C	Typical design value
Chilled water returning temperature	12.2	C	Typical design value
Chilled water flow rate	18.1	kg/s	288 GPM

	Value	Unit	
Cooling water leaving temperature	35.0	C	Typical design value
Cooling water returning design temperature	29.4	C	Typical design value
Cooling water flow rate	32.7	kg/s	518 GPM
Chiller water charge amount	235	liter	62 gallon
LiBr charge amount	640	liter	169 gallon

Source: The Regents of University of California

Before the chiller is started, the heating fluid system may be below the working pressure of 3.6 bar. It will take some time to build up the pressure and the overall system start up time may be longer than one hour. This is a major drawback and will significantly limit the use of steam driven absorption chiller.

Solar thermal driven triple effect chilling: oil driven

A triple effect absorption chiller adds another steam generator on top of the two generators in a double effect absorption chiller. The added generator produces more refrigerant steam with the same amount of heating load which translates to a higher COP.

Without detailed information on the triple effect chiller design, the following concept of solar thermal driven triple effect cooling is based on the assumption that the solution temperature in the highest stage generator is 160 C. As long as the hot heating fluid temperature is higher than this temperature, the solar collector would be able to drive the triple effect chiller. The system diagram is shown in Figure 19.

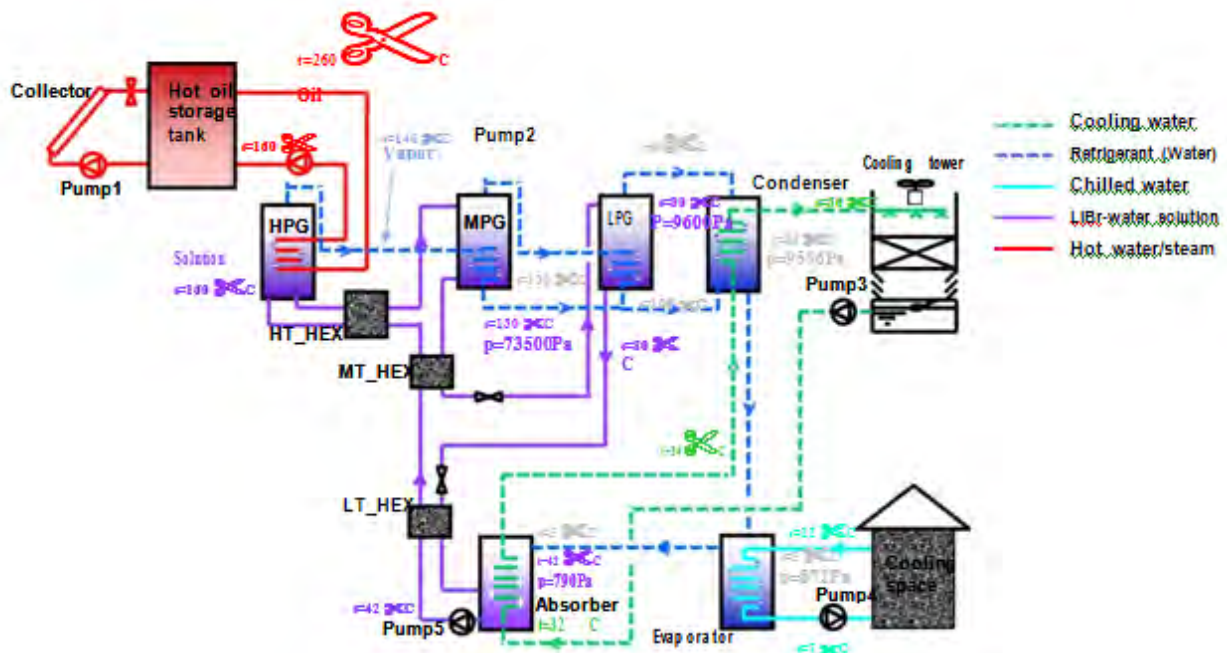


Figure 18. Diagram of a solar thermal driven triple effect absorption chiller

New Energy Development Organization (NEDO) of Japan developed triple effect absorption chillers from 2001-2004, in cooperation with Japan Gas Association and four major absorption chiller manufactures. With the help of US Department of Energy², Trane and York each had developed their own triple effect chillers based on the double effect technology (Figure 20). However, no triple effect chillers are commercially available today.



375 Ton 1.6 COP - Trane



400 Ton 1.6 COP - York

Figure 19. Trane and York triple effect chillers

Source: The Regents of University of California

Compared to an oil driven double effect chiller, the COP of the triple effect is higher. Higher heating fluid temperature means higher loss and lower solar collector efficiency. In addition, triple effect chillers are susceptible to corrosion due to very high solution temperature. The cost of triple effect chillers are also expected to be much higher with a smaller sales volume and possibly higher maintenance costs. Overall, using triple effect chillers today seems a less favorable option than using double effect chillers.

Steam may be considered as well to drive triple effect chillers. However, since the solution temperature is even higher, close or above 160 C, the heating steam should be at a pressure close to 9 bar. That makes the steam storage and sealing more difficult. The startup time will be longer than in a steam driven double effect chiller. These are likely to be the show-stopper for steam driven triple effect chillers.

Table 7. Major design specifications for oil driven solar thermal triple effect absorption chillers

Design Specifications	Value (SI)	Unit (SI)	Remarks
Solar collector capacity	406	kW	
Oil heating system efficiency	0.65		Assumed value
Hot oil outlet temperature	270	C	Assume oil supply temperature + 10C
Design hot oil temperature leaving			Assume return oil temperature -

storage	160	C	10C
Pump flow rate	1.8	kg/s	29 GPM
Hot oil pump type	Variable speed		
Storage tank capacity	6.6	m³	Assume 1 hour full load supply
Chiller type	Triple effect		Oil heating
Chiller capacity	120	RT	Assumed benchmark capacity
Chiller COP	1.6		A typical value
Hot oil inlet temperature	260	C	500 F
Hot oil leaving temperature	170	C	HPG solution temperature + 10C
Hot oil flow rate	1.5	kg/s	23 GPM
HPG solution design temperature	160	C	High pressure generator
MPG solution design temperature	130	C	Mid pressure generator
LPG solution design temperature	80	C	Low pressure generator
Chilled water leaving temperature	6.7	C	Typical design value
Chilled water returning temperature	12.2	C	Typical design value
Chilled water flow rate	18.1	kg/s	288 GPM
Cooling water leaving temperature	35.0	C	Typical design value
Cooling water returning design temperature	29.4	C	Typical design value
Cooling water flow rate	29.5	kg/s	518 GPM
Chiller water charge amount	TBD	liter	Data unavailable
LiBr charge amount	TBD	liter	Data unavailable

Source: The Regents of University of California

Hot oil temperature produced	150	C	transfer
Design hot oil temperature leaving storage	100	C	Assumed value to allow good heat transfer
Pump flow rate	5.0	kg/s	79 GPM
Hot oil pump type	Variable speed		
Storage tank capacity	17.9	m³	Assume 1 hour full load supply
(The previous chilled water loop now serves as the space heating water)			
Heating capacity	422	kW	
Heating water leaving temperature	65.0	C	Typical design value
Heating water returning temperature	55.0	C	Typical design value
Heating water flow rate	10.1	kg/s	160 GPM
(The previous cooling water loop now is disconnected)			

Source: The Regents of University of California

Compared to the cooling case, the solar collector pump flow rate is larger in the heating mode and the heating/chilled water flow rate is lower. Large pump sizes can be chosen such that the pumps satisfy both the cooling and heating needs. Certain double effect chillers are capable of delivering both chilled water and hot water on days when cooling demands are relatively low.

XCPC driven ORC

Figure 22 shows a potential conceptual architecture for an integrated XCPC/ORC system. The balance of systems components for the architecture is identical to those presented for the previous architectures. There is a possibility that other components and interfaces might emerge as requirements once a detailed design is created (part of a product development activity).

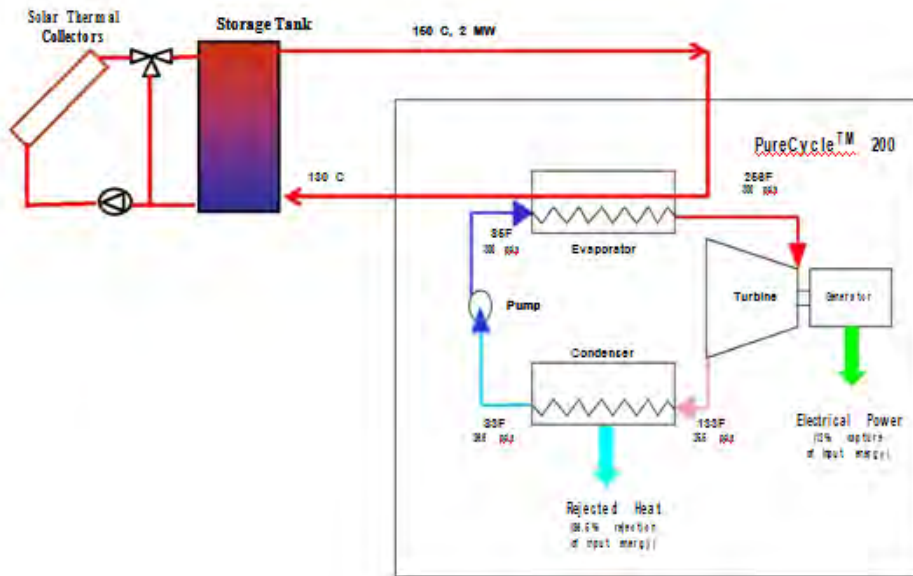


Figure 21 Solar ORC conceptual system architecture

Source: The Regents of University of California

The PureCycle™ ORC product offered by UTC Power uses waste heat for power generation and has been demonstrated for geothermal applications with a source heat temperature of < 100 C. Figure 23, shows a picture of the product which uses several components that are already available in volume production.

Figure 22. UTC Power PureCycle™ product



Source: The Regents of University of California

The product can currently produce about 220 kW of electricity at approximately ~10% efficiency (thermal to electricity) and there are designs that are currently being developed to increase the generation capacity and improve the efficiency of the system. Solar thermal Rankin cycles have been demonstrated for utility scale operations using solar trough or power tower technology. The advantage of this product is that it is a good fit for distributed power generation applications. Depending on the capabilities of the collector, the design could be further adapted in such a way that exhaust from this system feeds a single or double effect chiller thereby providing a combined cooling, heating and power (CCHP) product.

Table 9 presents design parameters for the ORC when fed with 150 C working fluid (hot water) from the XCPC. The parameters presented in the table were obtained from high level models

used by UTRC to estimate impact of source temperatures and other design parameters on ORC performance.

Table 9. Major design specifications for XCPC driven ORC cycle

Design Specifications	Value (SI)	Unit (SI)	Remarks
Solar collector capacity	2	MW	Calculated assuming 12% cycle efficiency for 220 kW
Heat source temperature (hot water)	150	C	Assumed lower bound in current design (high temperatures might require change of working fluid)
Heat source mass flow rate	38	kg/s	Steam flow rate would be ~ 1 kg/s
Heat source exit temperature	130	C	
Turbine inlet pressure	20	atm	Refrigerant loop
Turbine inlet temperature	124	C	Refrigerant loop
Condenser inlet pressure	1.7	atm	Refrigerant loop
Condenser inlet temperature	56	C	Refrigerant loop
Pump inlet pressure	1.8	atm	Refrigerant loop
Pump inlet temperature	28	C	Refrigerant loop
Evaporator inlet pressure			Refrigerant loop
Evaporator inlet temperature	29	C	Refrigerant loop
Electrical power efficiency	12	%	

Source: The Regents of University of California

The current design of the ORC uses a copper evaporator to transfer heat from hot water to the refrigerant. If the working fluid is hot oil, it could conceivably be pumped directly into the existing copper heat exchanger which serves as the evaporator. Corrosion and leakage issues could become a concern in this case. The use of high or low pressure steam also might require some re-design of this evaporator and this will work its way into the final system cost. In the case where the XCPC collector reaches its target 250 C design goal there is the possibility of creating higher efficiency ORC configurations. Improving efficiencies in this case would require major redesign of all the ORC components to deal with the new refrigerant and the overall system will need to be re-qualified.

Conclusions and Recommendations

Conceptual technical system architectures for five major applications of XCPC derived solar energy have been explored in this report and high level engineering estimates point to the fact

that designs are technically feasible. A common theme that will impact detailed design for all the architectures is the choice of the working fluid for the collector. This choice could impact heat exchanger designs across all the proposed architectures. The chiller and ORC products today operate at pre-determined design points and transient behavior of the heat source could have a negative impact on performance and reliability. The use of a thermal storage tank in all the architectures could help abate some of the concerns but it is likely that a supervisory control subsystem would need to be developed to seamlessly integrate the XCPC to the various products.

Task Component and Equipment Interfaces for System Integration and on Technical and Economic Performance Requirements for Solar Thermal Collectors

Introduction

This report is a complement to the report on preferred system architectures (“Report on Technical System Architectures for Application of Solar Heat”) that summarized some of the conceptual XCPC integrated system architectures and technical features for these architectures. The architectures considered included:

- e) XCPC driven single effect chilling
- f) XCPC driven double effect chilling
- g) XCPC driven triple effect chilling
- h) XCPC driven cooling and heating
- i) XCPC driven ORC

The previous report focused on products that could be integrated with the XCPC and presented some potential conceptual designs for the complete system. This report focuses around some of the key components and interfaces required to create the integrated system. An emphasis is placed on understanding some of the cost and reliability considerations associated with these systems. This helps guide some of the performance and cost requirements for the XCPC collectors. The cost parameters presented in this report have been estimated using some in house expertise guided cost estimation obtained from various HVAC design manuals.

Appendix A presents a summary of these cost estimates for the five configurations (less the collector and storage tank). These numbers will be further validated prior to use in the system modeling analysis task (Task 9) where 24/7 building electric, cooling and heating load data will be used to further determine the economic competitiveness of proposed options.

XCPC driven single effect chilling

Components and interfaces

The system architecture for this concept has been described in some detail in the earlier report. The balance of system components required for this design includes:

- One (or two) pumps to circulate the XCPC working fluid in between the collector and the chiller

- A thermal storage tank (hot water or oil) that serves the function of minimizing the impact of temperature transients in the XCPC working fluid by providing a steady temperature source to the moderate temperature generator of the chiller
- A three way valve that allows bypassing of the storage tank especially when the tank is full
- A cooling tower (with a fan) and an associated pump used to circulate cool water to the absorber especially in some of the warmer climates
- Supervisory controller that interfaces data collected from the XCPC with chiller modes of operation so that optimal control decisions are made from a system performance perspective
- A radiator that might also be needed to dump some of additional heat when tanks are full (also needed from a safety standpoint)

The technical requirements for these chillers indicate that the collector performance should match the heat source specifications provided in the previous report (6.700.0013-3b). Briefly, the XCPC when coupled with a single effect chiller will only need to provide ~ 92 C. Since this is close to the lower bound temperature for the XCPC, one possibility is to design the collectors at a low cost with capacity of delivering hot water at these temperatures. Alternatively, higher temperatures would mean that the chiller could be used as a bottoming cycle with an intermediate heat exchanger that can generate process fluid capable of driving a thermally activated technology (potentially an ORC) that operates at a higher temperature. This option however would mean that the collector should be capable of heating working fluid entering at 80 C to the higher target temperature (possibly as high as 250 C). This type of hybrid configuration maybe worth considering once the operational capabilities of the XCPC have been demonstrated and qualified.

System economics considerations

One of the key economic considerations when installing chillers is the impact of parasitic power on the overall value proposition of the system. Parasitic power for chiller includes electrical power needed to run the solution and refrigerant pumps, the fan used in the cooling tower and the chilled water and condenser pumps. Figure 24, shows the anticipated parasitic power required for a single effect chiller at various cooling capacities and distances between the chiller and cooling tower. The numbers are based on engineering estimates arrived at using product literature data and standard HVAC design guidelines. Specifically, Carrier air conditioning system design manual #3 of 12 which includes

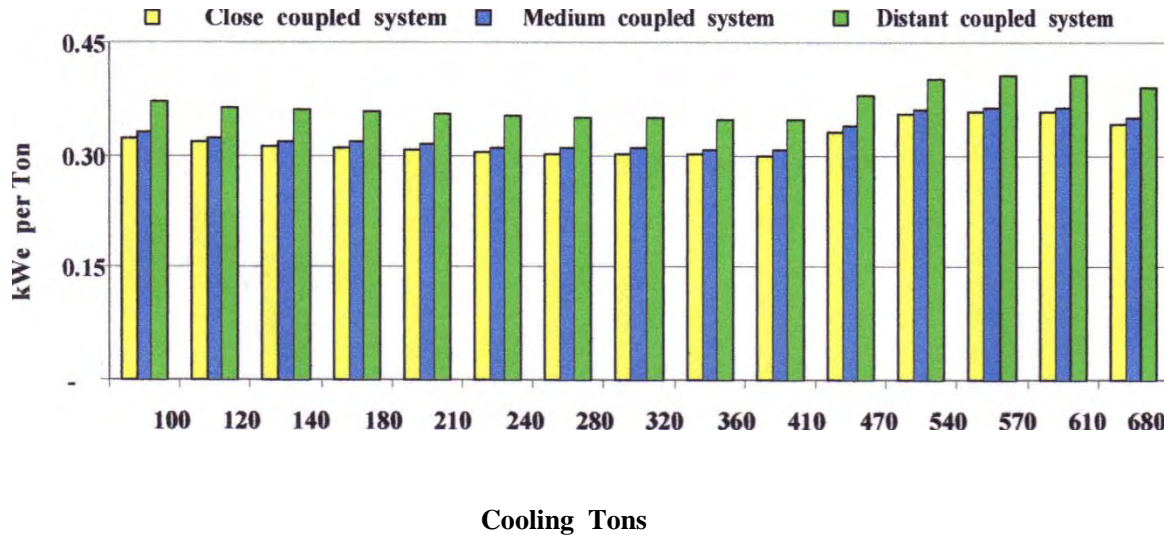
- Open and closed pipe sizing and pressure drops for pipe specification including valves, strainers and fittings.
- Hydraulic pressure drop for each of the sub components reflected in the chiller - condenser and hot water pump energy calculations.

The highest parasitic power consumption for a single effect chiller is in the distant coupled

system configuration and this value is roughly 0.35 kW per cooling ton. This implies that a 100 ton system would consume about 35 kW of electrical power and if the system is operated for approximately 2000 hours (average number of hours for a solar energy system) in the year, the total energy consumption is 70000 kWh.¹ Single effect chillers range from 100 – 680 RT.

System Parasitic Electric Consumption Sensitivity at full load

On-board solution & refrigerant pumps, tower fan, chilled & condenser pumps) Baseline - Single Effect Absorption Chillers 100 through 680 tons



Notes: Coupled distance between chiller and farthest AHU / distance between chiller and cooling tower Close = 25 ft / 60 ft, Medium = 200 ft / 100 ft, Distant = 600 ft / 800 ft
Chilled water flow 2.4 GPM/Ton, Condenser water flow 3.6 GPM/Ton, 80% Pump efficiency, 5 ft/100ft wg

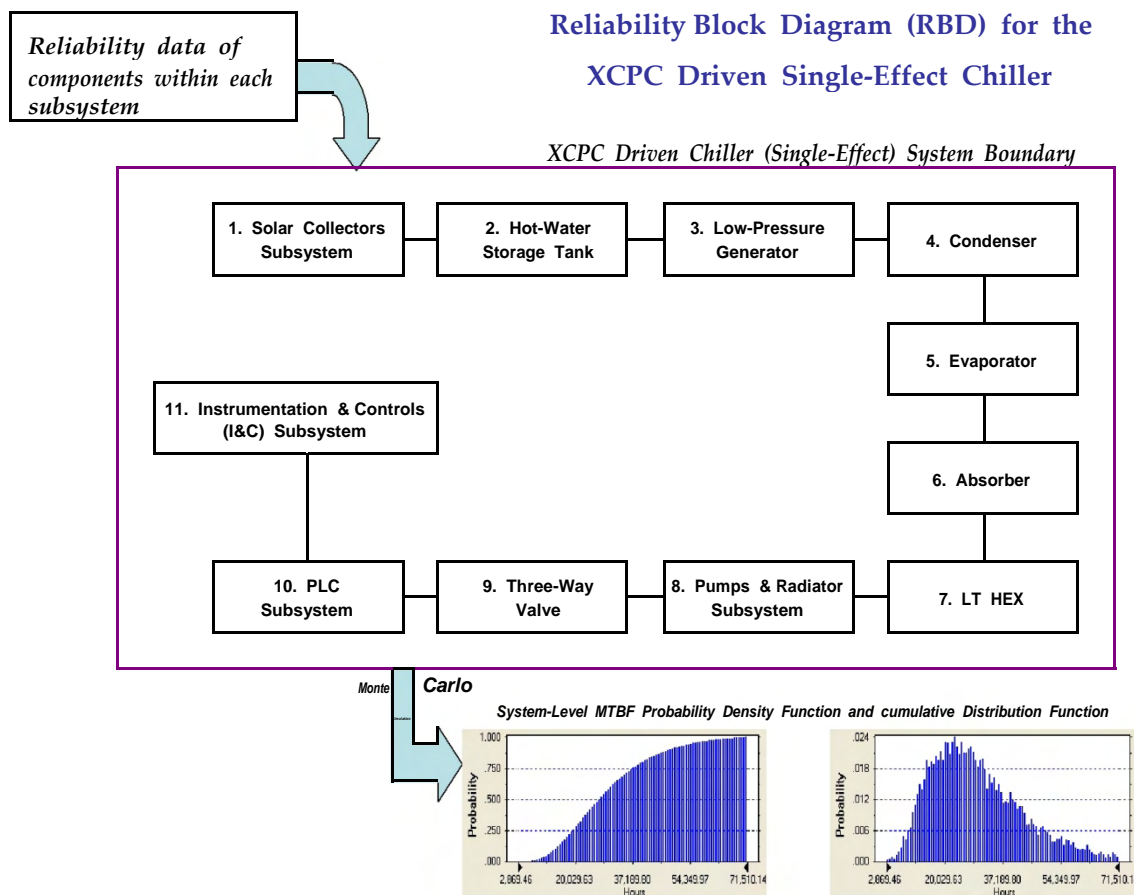
Figure 23. System parasitic power for single effect chillers

Source: The Regents of University of California

Operating costs for a hot water driven absorption cooling system will also include the costs associated with consumption of this resource in the system. The levelized cost (\$/kWh-economic requirement) of installing and operating the collector should therefore be lower than the cost associated with simply utilizing a hot water thermal source and this could be challenging.

¹Estimated by indexing actual cooling capacity to ARI published gallons per minute and pressure drop - unique to each size chiller.

System reliability considerations



As shown in Figure 25, the reliability block diagram (RBD) for the single-effect solar-driven chiller consists of 11 subsystems (modules). Each subsystem contains components and parts with their associated reliabilities expressed by probability density functions (pdf). Each subsystem contains a set of components and parts required for the subsystem to perform a specific function. The subsystem could be a single component such as the condenser, evaporator, or heat exchanger. The subsystem could also be a collection of more than one component, for example, the instrumentation & controls subsystem contains all process proportional–integral–derivative (PID) controllers, level indicators, flow indicators, pressure indicators, process alarms, etc. The reliability of each subsystem is determined by the product of

reliabilities of its constituent components and parts. The latter are typically estimated from historical failure rate data of the components and parts within the subsystem.

The reliability metrics for most of the components and subsystems associated with the chiller are well known which means the collector subsystem and hot water storage tanks are the components for which the data is currently unavailable. In order for a XCPC integrated system to work, the reliability numbers on the additional balance of system components in this configuration would have to be comparable to reliability numbers for a conventional hot water driven chiller system.

A Monte Carlo simulation technique can be used to predict the system-level reliability (R) by quantifying the reliability block diagram (RBD). The system reliability is the product of its subsystems reliabilities as described by the equation: $R = R_1.R_2.R_3.R_4.R_5.R_6.R_7.R_8.R_9.R_{10}.R_{11}$, where $R_1, R_2, R_3 \dots$ etc represents the reliability of subsystem 1, 2, 3, etc, respectively. The predicted system-level reliability is typically measured by the mean time between failures (MTBF). As the Monte Carlo simulation allows for propagation of uncertainties in the reliabilities of the various subsystems, the predicted system-level MTBF will be given in the form of a probability density function with a mean value (best estimate), standard deviation, lower bound, and upper bound values. This simulation can be performed as part of a detailed design effort once the metrics of performance and reliability have been clearly established for the XCPC collectors. These reliability results should help identify then estimate some of the maintenance costs that could be required for the system.

XCPC driven double effect chilling

Components and interfaces

The components and interfaces required to design an integrated XCPC and double effect chiller system are identical to those required for a single effect chiller with the possibility of the following additions:

- a. A compressor if high pressure steam is used as the input into the high temperature generator (preferred for 16DE design)
- b. A heat exchanger that is adequately integrated into the high temperature generator if heat transfer fluid such as hot oil becomes the working fluid of choice

The first choice is not preferred due to regulatory complexity (steam codes). Maintaining the temperature of the fluid entering the high temperature generator (at approximately 200 C) is of great importance in the second system configuration because this enables operation at the optimized design point. A system that works with a collector and hot storage tank front end may be inadequate in maintaining this temperature especially during transient operation. This suggests the possible need for a supplemental burner to provide heat to the generator in case the designed front end does not work adequately. The decision on adding this component will greatly depend upon the target capacity of the chiller and the type of building that the integrated system will service. There may be some additional complexity needed in the supervisory control to allow for functioning of the chiller using the supplemental burner.

System economics considerations

Double chillers are sized between 70 – 520 RT. System parasitics (pumps, cooling towers etc.) are a consideration for double effect chillers as well. Figure 26, summarizes these as a function of cooling capacity and distance. Energy consumption is in the range of 0.45/kW (versus 0.35/kW) for single effect systems. Known high pressure double effect chillers are more fully optimized than low pressure single effect chillers. On-board parasitic losses are actually comparable for single effect and double effect machines with the latter having the added benefit of a higher COP. External pump, tower fan and other auxiliary power consumption however are higher for the double effect chiller. This penalty could trade favorably against the improved chiller COP

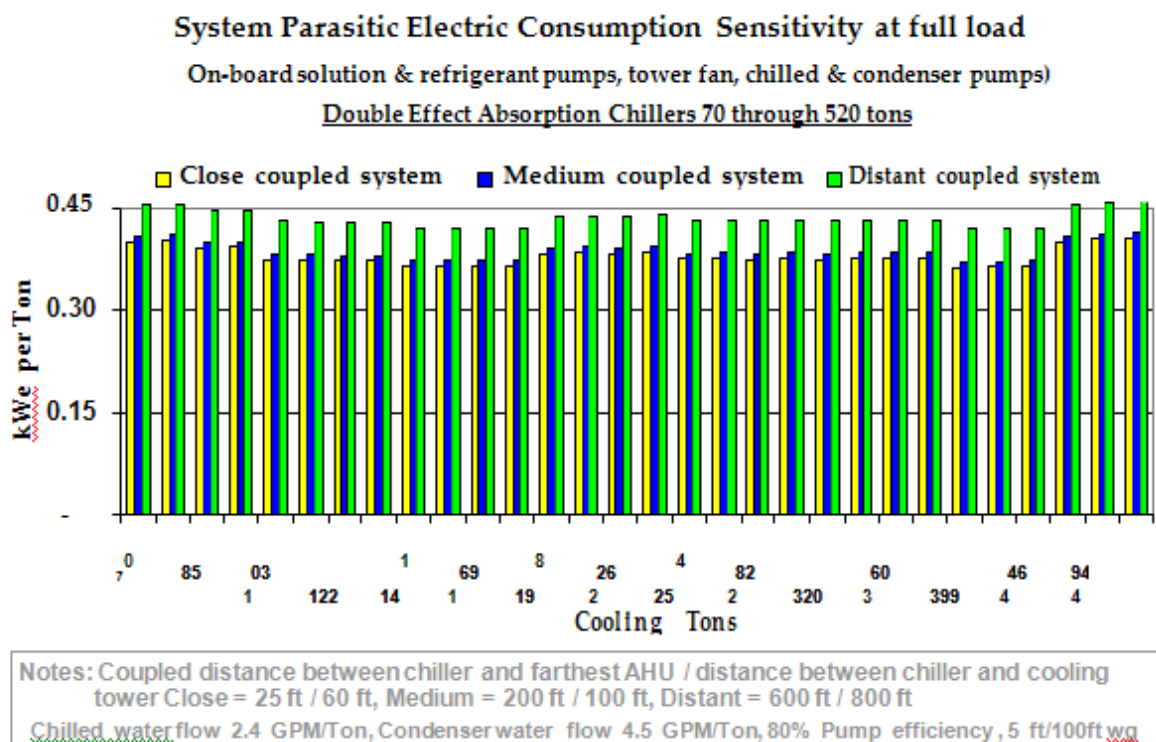


Figure 25. System parasitic power for double effect chillers

Source: The Regents of University of California

Double effect chillers can work with steam or on natural gas with the latter being more common due to avoidance of high pressure steam in several buildings. The yearly operating costs for a natural gas driven system would therefore in large part include the yearly fuel consumption (natural gas price * volume) incurred by the customer. This implies that in order for a system to be economically viable, the overall capital cost incurred by the XCPC plus balance of systems should be recovered through deferral of fuel costs. The economics of the system consequently changes substantially with increased fuel costs. Assuming a 300 kW cooling requirement, a double effect chiller operating at a COP of 1.1 would require ~273 kW of thermal energy or ~546,000 kWh (assuming 2000 hours of operation). At \$0.04/kWh (\$12/mm BTU) natural gas cost, yearly fuel savings from an XCPC system would be ~\$22,000 which means that the cost of the XCPC plus balance of systems should be no more than \$100,000 to have a simple payback of 5 years (assuming the chiller equipment already exists in the building). In order to obtain 273 kW of thermal energy, the XCPC field should be ~550 m² (assume 0.5 kW/m² collected) which

means that the \$/m² for a fully installed collector field should be well under \$200/m² to create a reasonable value proposition.

The system's competitiveness is even more challenging if the building uses electrically driven vapor compression systems that have a COP which is about three times higher than thermally driven processes. In such a scenario, a chiller that provides 300 kW of cooling requires only 100 kW (at a COP of 3) of electricity. A system that operates over a year would consume ~200,000 kWh (assuming 2000 hours of operation) that translates to yearly costs (at \$0.20/kWh) of ~\$40,000. The total system (including cost of replacement absorption chiller) should therefore cost no more than \$200,000 to have a simple payback of 5 years².

Electric chillers can be considered as having an emission footprint associated with the electricity (typically derived from coal plants) required to drive the cooling process. Double effect chillers running on natural gas could have a lower carbon foot print and the advantage is enhanced when using solar energy as the heat source. The economics for the systems would therefore be more favorable when the cost of natural gas is higher and when additional benefits are realized by applying carbon credits.

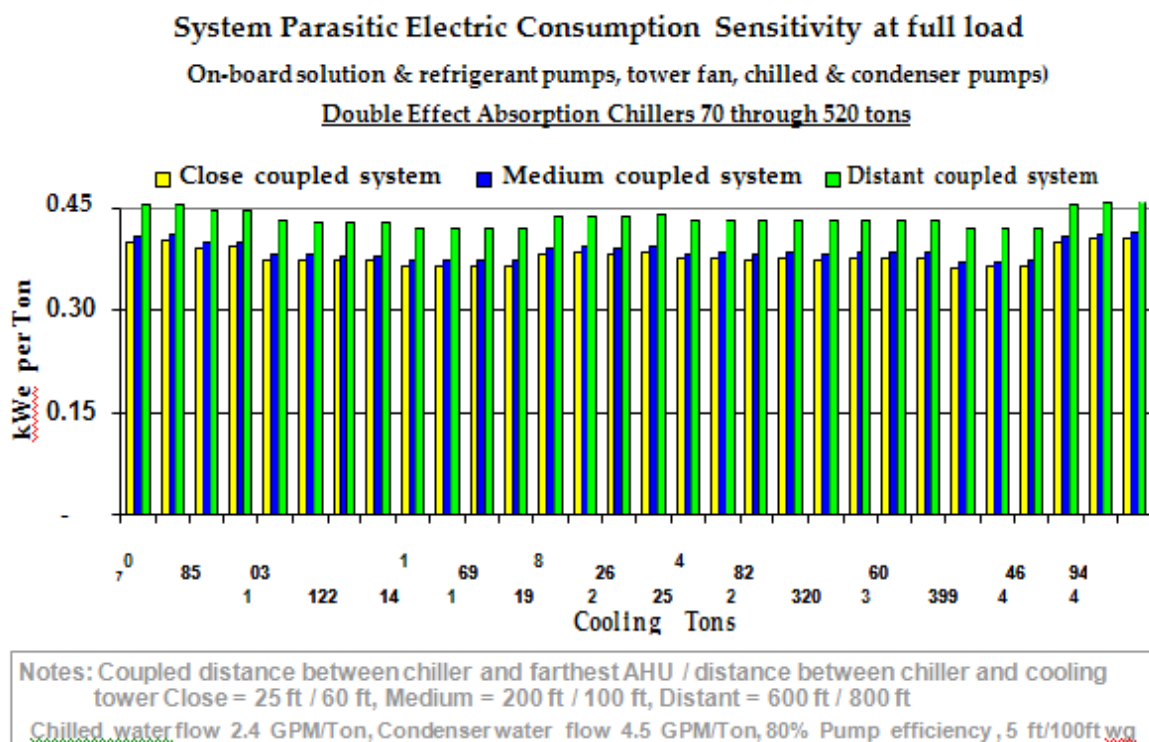


Figure 26. System Parasitic Electric Consumption Sensitivity at full load

Source: The Regents of University of California

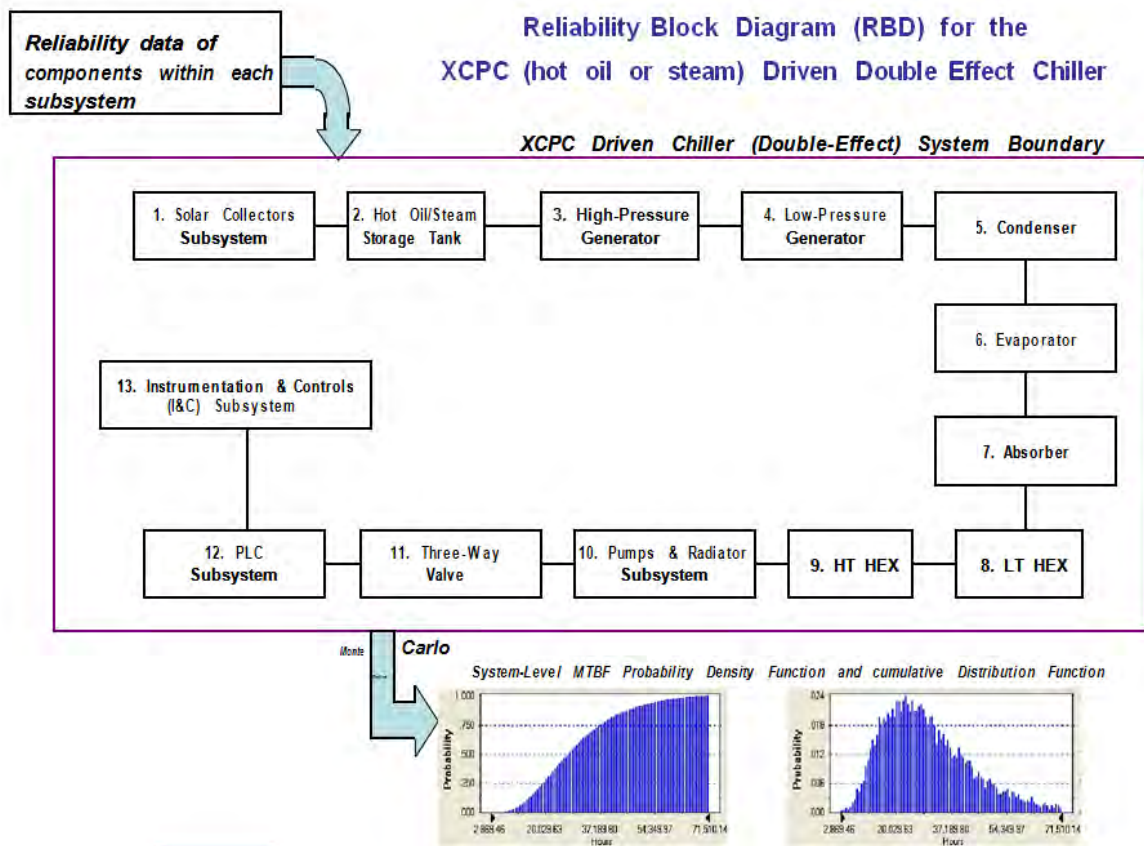


Figure 27. Reliability block diagram XCPC driven double effect chillers

Source: The Regents of University of California

² Note: These are simple high level calculations. Actual economics depends on system performance and real building loads that will be part of Task 5 assessment.

Compared to the single-effect solar-driven chiller which has 11 subsystems, the reliability block diagram (RBD) for the double-effect (hot oil) solar-driven chiller consists of 13 subsystems (modules) primarily due to the increased number of components within the chiller. The reliability expression will have two additional terms that correspond to this increased part count. Typically from a reliability perspective, increase part count results in lower reliability for the system. Besides the reliability metrics for the XCPC collector, the metrics for the hot oil / steam storage tank are also an unknown at this point. Additionally, if there is any alteration that is made to the high pressure generator (e.g. to make it compatible with hot oil), the reliability numbers for this design will need to be collected.

XCPC driven triple effect chilling

Components and interfaces

The system that uses the XCPC integrated with a triple effect chiller would be identical to the double effect chiller option in terms of the balance of system components required for integration with the XCPC. There may be significant redesign required for the high temperature generator to make it compatible with hot oil. Since triple effect chillers are not commercially available in volume, the non recurring engineering has not been sunk into a sub optimal design. The system will also require a supplemental burner and additional control logic (similar to

requirements for the double effect chiller) to facilitate seamless performance during transient operation of the solar thermal collectors.

System economics considerations

The parasitic power associated with on-board electrical consumption (not including remote pumps or a cooling tower) for the three different types of chillers have been summarized in Figure 29. Since there is limited actual data on the triple effect devices, the electrical parasitic power for this application have been projected based on high level system parameters that were gathered in the previous report (Task 3 report 6.700.0013-3a).

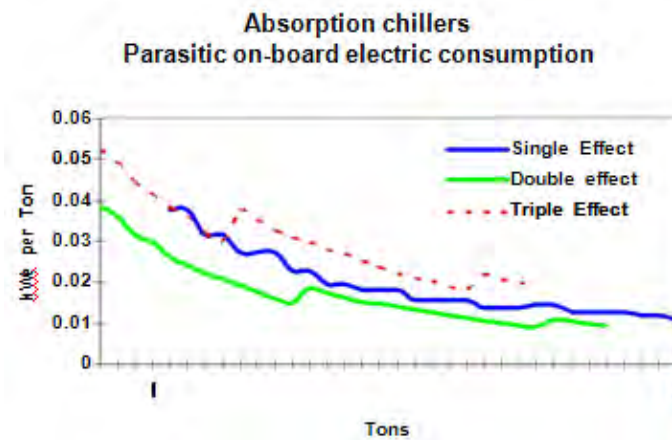


Figure 28. On board parasitics for chillers

Source: The Regents of University of California

The total parasitic power for the triple system benefits from derivation from the double effect machines but will likely consume more energy. The economic competitiveness of triple effect chillers compared to the double effect has not yet been validated. The higher COP of these systems could result in ~30% lesser consumption of fuel but the increased complexity of the system could increase maintenance costs thereby diminishing the value proposition for the small capacity chiller systems.

System reliability considerations

The reliability block diagram (Figure 30) for the XCPC driven triple effect chiller shows that the part count in this system has gone up by an additional two components. The concerns about LiBr temperature controllability and the effect of increased temperature induced corrosion problems make this system less desirable from a reliability perspective. Redesign of the HPG to be compatible with hot oil will also add uncertainty in the final reliability numbers for the system.

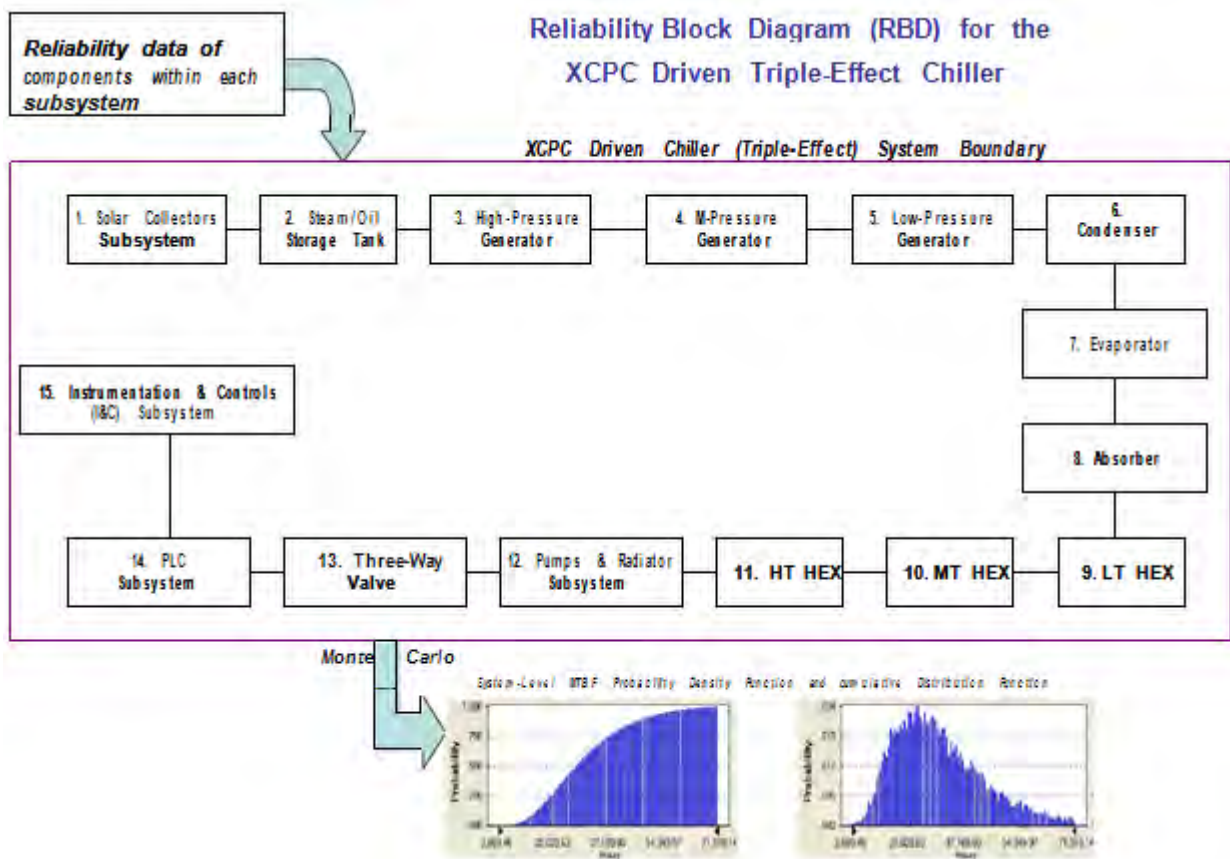


Figure 29. Reliability block diagram XCPC driven double effect chillers

Source: The Regents of University of California

XCPC driven cooling and heating

Components and interfaces

The components and interfaces required for this configuration are largely the same as the double effect configuration. There could be the need for an intermediate heat exchanger that is used to provide the hot water supply to the building. This might require some change in the control logic of the supervisory control for the system which enables managing demand side management for the cooling and heating needs of the building.

System economics consideration

The integrated system would only be marginally more expensive than the double effect configuration (see Appendix A). This would be the case if a secondary heat exchanger is used to obtain the hot water and if there is plumbing required to interface the system with existing building hot water supplies. There are chillers available that can operate in dual mode (both cooling and heating) which could be ideal for situations where the cooling load is low (mild summer days). Providing heating to the building could help defer fuel costs (natural gas) if heating is provided through traditional boilers or electricity costs if the building uses electrical heating. The latter would be more favorable from a value proposition standpoint given the higher cost of electricity (in general) compared to the cost of natural gas and the lower cost of strip electric resistance heaters to hydronic boiler assisted systems.

System reliability considerations

The addition of a heat exchanger and additional plumbing to the double effect configuration would add one more component to the reliability equation and this also introduces another point of failure for the system. The failure will likely not be catastrophic since the default of any controller would be to revert to existing back up hot water lines to meet the requirements of the building in case the heating subsystem in the configuration fails.

XCPC driven ORC

Components and interfaces

The components and interfaces required for the XCPC driven ORC configuration are identical to those considered for the double effect chiller option. The choice of thermal oil is the most attractive option from an ease of integration and implementation standpoint. The technical requirements dictate that roughly 2 MW of thermal energy at 150 C must be supplied to the ORC evaporator to obtain approximately 200 kW of electric power. The ORC supervisory controller may need to be modified to operate at part load under transient solar insolation conditions. The variable speed controller on the working fluid pump for the current ORC enables operation at part load.

System economics considerations

The economics of an XCPC driven ORC should be compared to the most common method for obtaining distributed solar electricity namely solar PV. The volume cost of an ORC unit is projected at \$2.7/W (installed). The total cost (installed) for the integrated system could therefore be in the neighborhood of \$4/W today (approximately half the cost of an installed PV system). This system assuming 50% total collection efficiency and 20% ORC efficiency would operate at a net efficiency of 10% which is comparable in efficiency to installed PV systems today implying that the overall electricity generated by the system could be equivalent to that provided by identically sized PV systems. The main deficiency in the ORC concept is that the moving parts associated with the machine and the overall system could result in higher maintenance costs compared to flat panel PV systems thereby reducing the factor of 2 advantages on levelized energy costs (realized through reduced system capital costs).

System reliability

The block diagram presented in Figure 31, is a simplified picture of the overall XCPC driven ORC concept because it uses a single subsystem to represent the ORC which is itself comprised of 5 or more components. It is represented this way because it is conceivable that no modification is required to interface the system with hot water, steam or oil (not true for chillers where some modification of generator heat exchangers may be required). In any event, the ORC reliability number would be a product of the reliability of the individual components that comprise the system and the total number of "parts" for the integrated system would be in the range of that for the double effect chiller configuration. The uncertainty in reliability metrics is again primarily associated with the solar collector subsystem and the storage tank component. There is the additional possibility that the reliability metrics for ORC components might change should the refrigerant be altered to achieve higher system efficiencies.

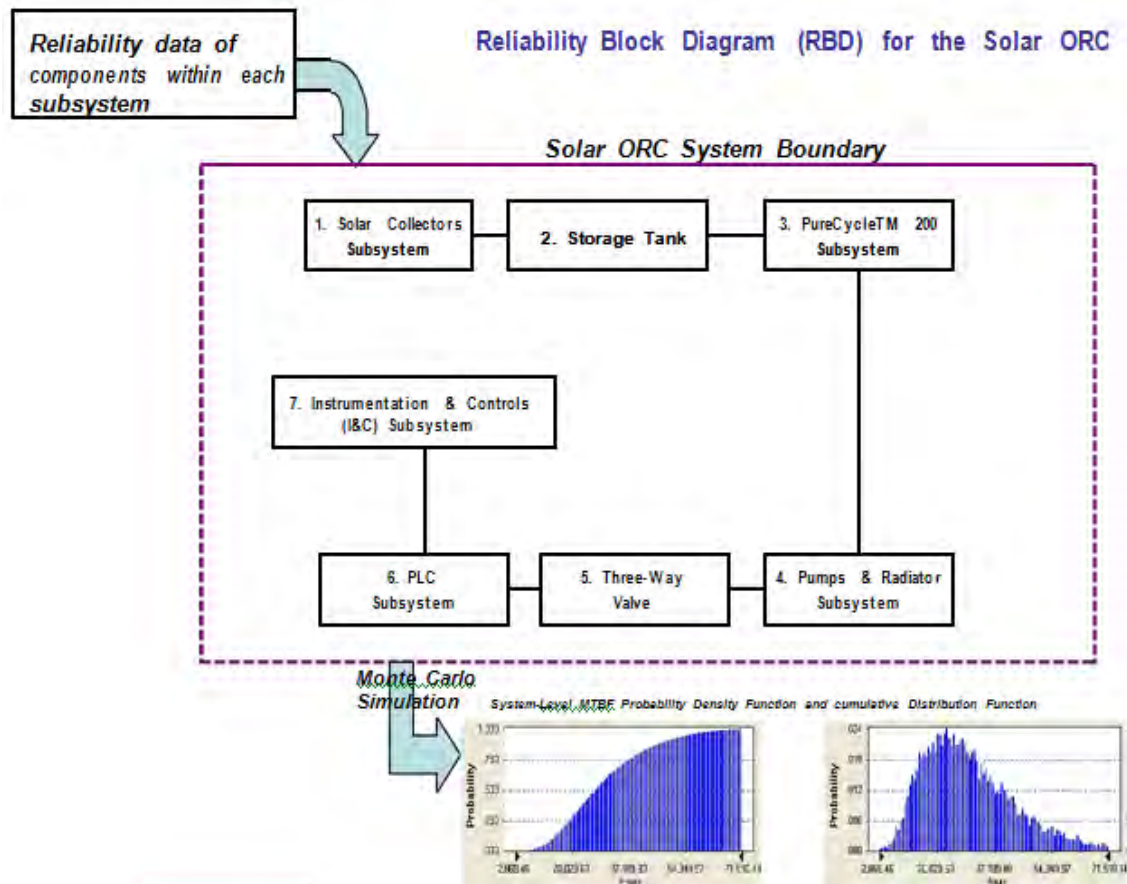


Figure 30. Reliability block diagram XCPC driven ORC

Source: The Regents of University of California

Conclusions and recommendations

Analyzing the XCPC integrated system architecture options from a components, interfaces and economics perspective shows that there could be major challenges in launching these systems. All these systems require additional off the shelf components and interfaces compared to traditional methods of implementing the product. The ability of the XCPC to achieve cost targets of less than \$100/m² with minimal maintenance costs coupled with increases in fuel and other utility costs will largely dictate the economic attractiveness of the various systems. Estimation of system maintenance costs will be contingent upon high level reliability metrics for the integrated systems.

Based on the current analysis³, it is recommended that system modeling and economic viability calculations focus on the double effect chiller and solar ORC configuration. It is also recommended that UC Merced provide UTRC with specifications of the working fluid, collector costs (and breakdown) and collector reliability so that some of these elements can be incorporated into the system and economic modeling tasks that will follow as part of Task 5.

³ Analysis conducted by synthesizing real world experience from interviews with service contractors, professionals, reviewing long term proprietary service records

Table 10. Equipment cost estimates (less collector, storage tank and front end collector to tank piping)

	1-Stage Chiller	2-Stage Chiller	3-Stage Chiller	2-Stage Chiller/Heater	ORC Generator	Electric Centrifugal Chiller
Cooling Tons	375	375	375	375		375
Power generated [kWe]					220	
Equipment:						
Pipe - Hot / Chilled / Condenser	\$ 18,755	\$ 21,725	\$ 23,705	\$ 20,790	\$ 11,055	\$ 17,600
Pipe Specialties - Valves, Strainers	\$ 21,900	\$ 28,470	\$ 35,040	\$ 24,310	\$ 11,400	\$ 17,100
Auxiliaries - Pumps, Cooling Tower Exhaust Duct & Stack	\$ 67,188	\$ 87,250	\$ 131,375	\$ 80,250	\$ 58,224	\$ 48,125
Chiller	\$ 187,500	\$ 243,750	\$ 300,000	\$ 225,000		\$ 103,125
Organic Rankine Cycle					\$ 286,000	
Water Treatment	\$ 7,500	\$ 10,000	\$ 12,500	\$ 7,500	\$ 10,000	\$ 7,500
Subtotal:	\$ 302,843	\$ 391,195	\$ 502,620	\$ 397,850	\$ 376,679	\$ 193,450
Installation:						
Labor	\$ 90,853	\$ 117,359	\$ 150,786	\$ 119,355	\$ 75,336	\$ 38,690
Materials	\$ 8,384	\$ 10,650	\$ 15,222	\$ 15,475	\$ 26,268	\$ 28,384
Overhead & Profit	\$ 84,796	\$ 109,535	\$ 140,734	\$ 111,398	\$ 105,470	\$ 54,166
Reserve	\$ 15,142	\$ 19,560	\$ 25,131	\$ 19,893	\$ 18,834	\$ 9,673
Subtotal:	\$ 199,175	\$ 257,102	\$ 331,873	\$ 266,121	\$ 225,907	\$ 130,913
Total:	\$ 502,018	\$ 648,297	\$ 834,493	\$ 663,971	\$ 602,586	\$ 324,363
\$/Ton:	1,339	1,729	2,225	1,771		865
\$/kWe:					2,739	

Source: The Regents of University of California

2.2.2. Safety Considerations for XCPC Applications

This report summarizes some of the main safety considerations for system architectures that have been discussed extensively in the two previous reports of Task 3 (“Report on Technical System Architectures for Application of Solar Heat” and “Report on Component and Equipment Interfaces for System Integration and on Technical and Economic Performance Requirements for Solar Thermal Collectors”).

This report summarizes the safety considerations in terms of two broader categories: a) XCPC driven absorption cooling, b) XCPC driven ORC.

XCPC driven absorption cooling

Safety considerations for XCPC driven absorption cooling/heating technologies are mainly associated with three sources: 1) heating fluid with high temperature and/or high pressure; 2) corrosive LiBr solution in absorption chillers; and 3) general equipment malfunctioning such as motor winding high temperature and leakage of hermetic pumps. The degree of safety concerns varies with the system configuration. Here we will focus on configuration specific safety issues, i.e., 1) & 2) only.

Solar thermal driven single effect chilling

In this system, the hot water is below 100 C and at atmospheric pressure. The solution temperature in the single effect chiller is low. Both the chiller and the solar collector are mature technologies, thus this configuration has the least safety concern.

Solar thermal driven double effect chilling (b1: oil or b2: steam as hot working fluid)

Direct fired or steam driven double effect chillers are also mature technologies and are not of great safety concerns. Major concern comes from the fact that hot oil needed to drive the double effect chiller may leak into the solar collector or the LiBr solution in the HPG. For steam driven system, the safety issue arises when the heating fluid loop, including the solar collector, the water storage tank and the pump, all need to be pressurized to approximately 3.6 bar. The pressurization cycle will have a daily cycle, a severe condition for a pressurized system. This may drive system configuration to a hot oil temperature.

Solar thermal driven triple effect chilling

For triple effect chillers, assuming hot oil is used, the oil temperature needs to be even higher. Possible leakage or contact with the oil becomes more dangerous and poses an increased safety concern than the double effect chillers. In addition, the solution in triple effect chillers, with much higher temperature, becomes very corrosive. The piping, valve, pump and heat exchanger life are likely to be affected. Possible spill of the solution can be a great safety hazard.

Solar thermal driven combined chilling and heating

Heating option in the solar driven chillers does not add any significant safety concerns because the modification to the system is minimal, consisting of a plate heat exchanger and valves. These technologies are simple and mature.

XCPC driven ORC

The choice of the XCPC working fluid will also impact some of the safety considerations in the integrated ORC system design. The use of hot oil will require appropriate design of lines and storage devices so that leaks are minimized (particularly important for roof top applications where there may be no access to drains). The use of high pressure steam as the working fluid may be less problematic from a safety aspect since there are several existing examples of high pressure steam being pumped in and out of buildings for heating purposes.

The refrigerant used in the ORC could become a source of future safety/environmental considerations. Phase out of chloro-fluoro carbon based refrigerants might occur and this coupled with the need to adapt the design to higher efficiencies could mean the use of newer refrigerants that will need to be qualified for safety.

Conclusions and recommendations

Current assessment of the XCPC integrated systems indicates that the choice of the working

fluid through the collector will be the most important safety consideration in system design. Storage and buffering conveniences associated with the ability to thermal cycle and the stringent requirements on steam code might drive towards the design choice of hot oil. It is recommended that the hot oils be selected only after it is completely clear that there are no existing or emerging regulatory bans that are imminent on these substances. This may require doing some assessment work with the California Environmental Protection Agency (EPA) prior to down selecting the preferred working fluid.

2.3. Task 4.0

The design team (SolFocus and UC-Merced) formulated three competing conceptual level designs for the External Compound Parabolic Concentrator (XCPC) that is to be developed during the course of this project. All three designs are believed to have the potential to reach the performance and cost goals defined in the agreement, which are to develop a manufacturable stationary solar thermal collector system with a system efficiency of at least 50 percent at a temperature of 400°F, and also have a production cost of less than \$10 per square foot. Each of the formulated designs consists of an assembly of stationary evacuated tube absorbers with external non-imaging reflectors.

The three competing design concepts that have been formulated are:

1. All glass dewar: Direct Flow
2. All glass dewar filled with thermal fluid: Indirect Flow
 - (a) with metal tube
 - (b) with heat pipe
3. Metal absorber with glass-to-metal seal
 - (a) with metal tube
 - (b) with heat pipe

Concept 1 - All glass dewar: Direct Flow

The design concept is depicted in Figure 32. The heat transport fluid flows directly inside the all-glass dewars – hence we use the term “direct flow”. The design concept uses very inexpensive all glass Dewar solar thermal absorbers that are mass produced in China. The dewars are cylindrical borosilicate glass bottles with an evacuated annulus between the two glass walls. The vacuum surface of the inner wall is coated with a selective surface (usually aluminum nitride cermet) with a high solar absorptance and low thermal emittance. Popular dimensions of off-the-shelf Chinese Dewars are 44mm (inside diameter), 58mm (outside diameter) and 1800mm length. Other Dewar dimensions are also available. The glass dewars are to be attached to a plumbing manifold using O-ring compression seals. The manifold will incorporate a unique design feature – the inlet tube (item 8 in Figure 32) will be integral to the manifold itself. This eliminates the need for a separate part (the inlet tube), which speeds field

installation and also eliminates a potential leak path (at the connection of the inlet tube to the manifold). Each dewar is placed so that an external reflector concentrates the solar irradiance onto the inner dewar wall of with the selective coating. The shape of the reflector is designed so that all sunlight incident on the aperture plane of the collector within a defined angular acceptance angle is redirected onto the absorber. The acceptance angle can be designed according to the desired concentration factor, the concentrated flux profile and the orientation of the absorber tubes (East-West or North-South/tilted). Orienting the absorber tubes North-South requires larger acceptance angles to ensure sufficient illumination throughout the day, which reduces the concentration factor. Therefore, an East-West orientation is generally advantageous. However, a North-South oriented reflector (with the larger acceptance angle) does accept more diffuse solar irradiation and so too has some positive performance attributes. Additionally, reflectors with larger acceptance angles will generally require less reflector area, which provides an economic advantage. Designs for both East-West and North-South orientations will be designed and evaluated as part of this project. To achieve our collector cost goals, the reflector must also be low in cost and be easily shaped into the desired CPC profile. And to produce the desired optical performance, the reflectance of the reflective surface must be high (preferably in the '90's). Various reflector materials will be examined and evaluated as part of this project. Also an optional glass or plastic glazing will be considered to cover the reflector and absorbers. The heat transfer fluid (e.g. mineral oil) will be circulated through the absorber tubes. The flow pattern may be in series, in parallel, or a combination of both. The fluid will enter the glass dewar from the manifold, through the inlet tube into the lower part of the absorber tube and will then flow back to the upper end of the dewar in a counter flow direction where it will reenter the manifold. The flow pattern may be such that either the cold or the hot fluid enters through the center inlet tube. Also, the direction of the outlet flow (#3 in Figure 1) may also be configured in the opposite direction. This may offer thermal advantages as well as provide more convenient plumbing connections since the outlet of one collector would then feed into the inlet of an adjacent collector. The manifold may be as depicted in Figure 1 (a tube in a tube) or, as two separated tubes (one supply and the other the return). Analysis of all these options will help us assess the preferred configuration.

Features

Heat Transfer: This design is expected to have excellent heat transfer from the black selective surface to the working fluid because the heat collected on the coated wall of the inner dewar has only to conduct through the inner dewar wall (typically 2mm thick) to reach the circulating working fluid that flows in the dewar.

Cost: This design is very likely to be the lowest cost option of the three competing designs in terms of material cost. However, the operating cost (pumping) may suffer slightly due to the counter flow path and the larger pressure drop where the flow reverses in direction. If that becomes an issue, the design can be modified to reduce pressure drop.

Manufacturability: This design is amenable to low cost manufacturing.

Installation: This design is very easily installed as the dewars can be attached to the manifold on site. Broken dewars can be easily replaced.

Orientation: This design allows all possible tube orientations (East-West, North-South).

Robustness: The fluid is circulated in double-walled glass dewars so leakage will occur if both dewar walls break. The risk can be reduced by adding safety valves and/or covering the tubes in a box/framework. The concept of solar collectors using all-glass evacuated tubes is not

entirely new. Schott Inc. manufactures and sells all-glass ICPC collectors and the collectors passed the required performance and safety tests. However, the Schott collectors do not utilize external reflectors, not do they have a tube inlet (part #8) that is integral with the manifold.

Durability: Potential durability issues may be glass breakage due to thermal shock and/or temporary pressure surges within the circulating flow stream. In the event of collector stagnation, the dewar surfaces coated with the selective coatings can achieve temperatures in excess of 500°F. Should cold working fluid be suddenly introduced into very hot dewars, it is possible that thermal shock could result in dewar breakage. Another durability concern with this design is the pressure limitation (about 90 psi) imposed by the use of glass as a containment vessel for the circulating working fluid. The durability and/or integrity of the O-ring compression seals, which are exposed to high and fluctuating temperature, are a concern. All of these various durability issues will be addressed during the performance of this project.

Technical Risk: We consider the technical risk of this concept to be reasonably low since heat transfer from the absorber coating to the circulating working fluid is expected to be excellent (i.e. very little thermal resistance along this thermal path) and also because the manifold design is relatively straightforward (although there are a variety of possible design permutations that must be assessed). But, the durability issues identified above are of real and practical concern, so some technical risk is present

Concept 2 - All glass dewar filled with thermal fluid: Indirect Flow

This design concept allows for two versions: (a) with a metallic tube insert (see Figure 2a); and (b) with a heat pipe insert (see Figure 2b). Both versions of this concept use the same inexpensive all glass Dewar solar thermal absorber tubes as our concept 1. However, in this concept the circulating fluid does not directly contact the glass dewars. The circulating fluid is confined to the manifold and the metallic tubes reaching into the glass dewars (as in version a), or confined to just the manifold itself (as in version b). In both cases the metallic inserts are immersed within a thermal fluid (e.g. a mineral oil) in order to enhance thermal transport from the blackened/coated inner dewar to the metallic insert. Prior research has shown that thermal transport from the dewar to these kinds of thermal inserts is poor because of the poor thermal contact between the inserts and the glass dewars. The addition of the thermal fluid is aimed at greatly enhancing the heat transfer because the thermal fluid will have much better thermal conductivity than does the thin air gaps that are present when the inserts are simply placed inside dry dewars. Another simple variation of this design concept is to use highly-viscous thermal grease rather than a thermal fluid.

Version (a) uses metal tubes to direct the circulating fluid into the dewars to remove the thermal energy. The metal tubes are immersed into a heat transfer fluid to enable and enhance heat transfer from the coated dewar wall to the metallic tube. The tubes may be configured as a “double-D” (as depicted in Figure 2a) or as a simple bent u-tube (not shown). The size and shape of these metallic tubes (part #8 in Figure 2a) will be evaluated from the perspective of heat transport, pressure drop and cost before a selection is finalized. These immersed tubes may also have fins attached to enhance thermal performance, and we will also consider minimization of the needed thermal fluid

Version (b) uses heat pipes to transfer the heat from the coated dewar to the manifold. Similar to version (a), the heat pipes are immersed in a heat transfer fluid to enable and enhance heat transfer from the coated dewar wall to the heat pipe. Heat pipes of this basic design are

currently mass produced in China, but to our knowledge no one has successfully enhanced the thermal transport with the addition of thermal fluid or thermal grease.

The absorber tubes are placed so that external reflectors concentrate sunlight onto the evacuated dewars, just as in concept 1.

Features

Heat Transfer: The heat transfer in this design will not be as good as in our concept 1. The heat has to pass from the coated Dewar wall through three barriers to reach the circulating fluid: The inner glass Dewar wall, the thermal fluid, and the wall of the metal tube/heat pipe. The limiting factor will be the conduction/natural convection through the non-circulating thermal fluid.

Also, with design 2b (the heat pipe design) the operation and performance of the heat pipe is unknown at this point. The heat pipes that are produced in volume in China are used at much lower temperatures than we need, and performance/operation data at the higher operating temperatures is unavailable. Concerns are the “dry out” temperature of these standard heat pipes as well as whether their performance deteriorates significantly as operating temperatures increase.

Cost: This design is likely to have low production cost, albeit not as low as our concept 1. However, pumping cost should be lower, especially for design 2b since the use of the heat pipe eliminates all the pressure drop aside from that of the manifold.

Manufacturability: This design is amenable to low cost manufacturing.

Installation: This design is not as easy to install as concept 1 as the dewars have probably to be filled on site with the thermal fluid.

Orientation: This design restricts the possible tube orientation to North-South as the tubes have to be tilted to keep the thermal fluid from spilling. The North-South orientation requires a higher optical acceptance angle which reduces the concentration.

Robustness: The heat transfer fluid contained in the Dewars is in contact with air. It will be important to select a heat transfer fluid with a flash point above the stagnation temperature of the collector. Some form of container will be needed to prevent spilling of the heat transfer fluid. Oil expansion issues have to be considered. Alternatively, a thermal grease (if found to work sufficiently well) will

Durability: Version (a) of this concept is expected to be very durable. The same applies to version (b) assuming satisfactory heat pipe longevity. Since the glass dewars are not used to contain the circulating fluid, there is no risk of dewar breakage in the event of pressure surges within the circulating fluid loop. Similarly, thermal shock is greatly minimized (probably eliminated) because the thermal fluid within the dewars will act to dampen thermal transport.

Technical Risk: The technical risk of this concept is higher than concept 1. Potential technical barriers are the heat transfer and the performance and longevity of heat pipes operated at high temperatures.

Concept 3 - Metal absorber with glass-to-metal seal

This concept allows for two versions: (a) with metal tube (see Figure 3a); and (b) with heat pipe (see Figure 3b). In both versions an evacuated glass tube with an innovative glass-to-metal seal is used to insulate the metal absorber. The metal absorber is a thin cylindrical copper fin with a selective coating that enables high solar absorptance and reduces radiative heat loss. The fin is welded to a metal counter flow tube (version a) or a heat pipe (version b). In version (a) the heat

absorbed by the fin is transferred to the manifold by the circulating fluid in the metal tube. In version (b) the heat is transferred from the fin to the manifold by a heat pipe. The absorber tubes are placed so that external reflectors concentrate sunlight onto the evacuated dewars, just as in concepts 1 and 2.

Features

Heat Transfer: This design has good heat transfer, but not as good as concept 1 because the absorbed thermal energy must be conducted around a metallic fin before it passes into the working fluid.

Cost: This design is likely to have higher production costs than concepts 1 and 2. This is due to the high metal content and especially the glass-to-metal seals. Pumping cost might be an issue with the counter flow metal tube of version (a). In this case, a metal U-tube could be used instead.

Manufacturability: The manufacturing is more complex than in concepts 1 and 2.

Installation: Version (b) is very easy to install as the heat pipes can be plugged onto the manifold on site. Version (a) requires plumbing.

Orientation: Version (a) can be oriented East-West or North-South. Version (b) needs some tilt because of the heat pipes.

Robustness: The concept is very robust. The fluid is contained in metal pipes.

Durability: Thermal stress issues and the longevity of the glass-to-metal seals have to be analyzed.

Technical Risk: Version (a) has very little technical risk. Version (b) has higher technical risk due to the unknown performance and longevity of heat pipes operated at high temperatures.

The design team (SolFocus and UC-Merced) formulated three competing conceptual level designs for the External Compound Parabolic Concentrator (XCPC) that is to be developed during the course of this project. All three designs are believed to have the potential to reach the performance and cost goals defined in the agreement, which are to develop a manufacturable stationary solar thermal collector system with a system efficiency of at least 50 percent at a temperature of 400°F, and also have a production cost of less than \$10 per square foot. Each of the formulated designs consists of an assembly of stationary evacuated tube absorbers with external non-imaging reflectors.

The three competing design concepts that have been formulated are:

4. All glass dewar: Direct Flow
5. All glass dewar filled with thermal fluid: Indirect Flow
 - (a) with metal tube
 - (b) with heat pipe
6. Metal absorber with glass-to-metal seal
 - (a) with metal tube
 - (b) with heat pipe

Concept 1 - All glass dewar: Direct Flow

The design concept is depicted in Figure 1. The heat transport fluid flows directly inside the all-glass dewars – hence we use the term “direct flow”. The design concept uses very inexpensive all glass Dewar solar thermal absorbers that are mass produced in China. The dewars are

cylindrical borosilicate glass bottles with an evacuated annulus between the two glass walls. The vacuum surface of the inner wall is coated with a selective surface (usually aluminum nitride cermet) with a high solar absorptance and low thermal emittance. Popular dimensions of off-the-shelf Chinese Dewars are 44mm (inside diameter), 58mm (outside diameter) and 1800mm length. Other Dewar dimensions are also available.

The glass dewars are to be attached to a plumbing manifold using O-ring compression seals. The manifold will incorporate a unique design feature – the inlet tube (item 8 in Figure 1) will be integral to the manifold itself. This eliminates the need for a separate part (the inlet tube), which speeds field installation and also eliminates a potential leak path (at the connection of the inlet tube to the manifold). Each dewar is placed so that an external reflector concentrates the solar irradiance onto the inner dewar wall of with the selective coating. The shape of the reflector is designed so that all sunlight incident on the aperture plane of the collector within a defined angular acceptance angle is redirected onto the absorber. The acceptance angle can be designed according to the desired concentration factor, the concentrated flux profile and the orientation of the absorber tubes (East-West or North-South/tilted). Orienting the absorber tubes North-South requires larger acceptance angles to ensure sufficient illumination throughout the day, which reduces the concentration factor. Therefore, an East-West orientation is generally advantageous. However, a North-South oriented reflector (with the larger acceptance angle) does accept more diffuse solar irradiation and so too has some positive performance attributes. Additionally, reflectors with larger acceptance angles will generally require less reflector area, which provides an economic advantage. Designs for both East-West and North-South orientations will be designed and evaluated as part of this project.

To achieve our collector cost goals, the reflector must also be low in cost and be easily shaped into the desired CPC profile. And to produce the desired optical performance, the reflectance of the reflective surface must be high (preferably in the '90's). Various reflector materials will be examined and evaluated as part of this project. Also an optional glass or plastic glazing will be considered to cover the reflector and absorbers.

The heat transfer fluid (e.g. mineral oil) will be circulated through the absorber tubes. The flow pattern may be in series, in parallel, or a combination of both. The fluid will enter the glass dewar from the manifold, through the inlet tube into the lower part of the absorber tube and will then flow back to the upper end of the dewar in a counter flow direction where it will reenter the manifold. The flow pattern may be such that either the cold or the hot fluid enters through the center inlet tube. Also, the direction of the outlet flow (#3 in Figure 1) may also be configured in the opposite direction. This may offer thermal advantages as well as provide more convenient plumbing connections since the outlet of one collector would then feed into the inlet of an adjacent collector. The manifold may be as depicted in Figure 1 (a tube in a tube) or, as two separated tubes (one supply and the other the return). Analysis of all these options will help us assess the preferred configuration.

Features

Heat Transfer: This design is expected to have excellent heat transfer from the black selective surface to the working fluid because the heat collected on the coated wall of the inner dewar has only to conduct through the inner dewar wall (typically 2mm thick) to reach the circulating working fluid that flows in the dewar.

Cost: This design is very likely to be the lowest cost option of the three competing designs in terms of material cost. However, the operating cost (pumping) may suffer slightly due to the counter flow path and the larger pressure drop where the flow reverses in direction. If that becomes an issue, the design can be modified to reduce pressure drop.

Manufacturability: This design is amenable to low cost manufacturing.

Installation: This design is very easily installed as the dewars can be attached to the manifold on site. Broken dewars can be easily replaced.

Orientation: This design allows all possible tube orientations (East-West, North-South).

Robustness: The fluid is circulated in double-walled glass dewars so leakage will occur if both dewar walls break. The risk can be reduced by adding safety valves and/or covering the tubes in a box/framework. The concept of solar collectors using all-glass evacuated tubes is not entirely new. Schott Inc. manufactures and sells all-glass integrated compound parabolic collector (ICPC) collectors and the collectors passed the required performance and safety tests. However, the Schott collectors do not utilize external reflectors, not do they have a tube inlet (part #8) that is integral with the manifold.

Durability: Potential durability issues may be glass breakage due to thermal shock and/or temporary pressure surges within the circulating flow stream. In the event of collector stagnation, the dewar surfaces coated with the selective coatings can achieve temperatures in excess of 500°F. Should cold working fluid be suddenly introduced into very hot dewars, it is possible that thermal shock could result in dewar breakage. Another durability concern with this design is the pressure limitation (about 90 psi) imposed by the use of glass as a containment vessel for the circulating working fluid. The durability and/or integrity of the O-ring compression seals, which are exposed to high and fluctuating temperature, are a concern. All of these various durability issues will be addressed during the performance of this project.

Technical Risk: We consider the technical risk of this concept to be reasonably low since heat transfer from the absorber coating to the circulating working fluid is expected to be excellent (i.e. very little thermal resistance along this thermal path) and also because the manifold design is relatively straightforward (although there are a variety of possible design permutations that must be assessed). But, the durability issues identified above are of real and practical concern, so some technical risk is present

Concept 2 - All glass dewar filled with thermal fluid: Indirect Flow

This design concept allows for two versions: (a) with a metallic tube insert (see Figure 2a); and (b) with a heat pipe insert (see Figure 2b). Both versions of this concept use the same inexpensive all glass Dewar solar thermal absorber tubes as our concept 1. However, in this concept the circulating fluid does not directly contact the glass dewars. The circulating fluid is confined to the manifold and the metallic tubes reaching into the glass dewars (as in version a), or confined to just the manifold itself (as in version b). In both cases the metallic inserts are immersed within a thermal fluid (e.g. a mineral oil) in order to enhance thermal transport from the blackened/coated inner dewar to the metallic insert. Prior research has shown that thermal transport from the dewar to these kinds of thermal inserts is poor because of the poor thermal contact between the inserts and the glass dewars. The addition of the thermal fluid is aimed at greatly enhancing the heat transfer because the thermal fluid will have much better thermal conductivity than does the thin air gaps that are present when the inserts are simply placed inside dry dewars. Another simple variation of this design concept is to use highly-viscous thermal grease rather than a thermal fluid.

Version (a) uses metal tubes to direct the circulating fluid into the dewars to remove the thermal energy. The metal tubes are immersed into a heat transfer fluid to enable and enhance heat transfer from the coated dewar wall to the metallic tube. The tubes may be configured as a “double-D” (as depicted in Figure 33) or as a simple bent u-tube (not shown). The size and shape of these metallic tubes (part #8 in Figure 33) will be evaluated from the perspective of heat transport, pressure drop and cost before a selection is finalized. These immersed tubes may also have fins attached to enhance thermal performance, and we will also consider minimization of the needed thermal fluid

Version (b) uses heat pipes to transfer the heat from the coated dewar to the manifold. Similar to version (a), the heat pipes are immersed in a heat transfer fluid to enable and enhance heat transfer from the coated dewar wall to the heat pipe. Heat pipes of this basic design are currently mass produced in China, but to our knowledge no one has successfully enhanced the thermal transport with the addition of thermal fluid or thermal grease.

The absorber tubes are placed so that external reflectors concentrate sunlight onto the evacuated dewars, just as in concept 1.

Features

Heat Transfer: The heat transfer in this design will not be as good as in our concept 1. The heat has to pass from the coated Dewar wall through three barriers to reach the circulating fluid: The inner glass Dewar wall, the thermal fluid, and the wall of the metal tube/heat pipe. The limiting factor will be the conduction/natural convection through the non-circulating thermal fluid.

Also, with design 2b (the heat pipe design) the operation and performance of the heat pipe is unknown at this point. The heat pipes that are produced in volume in China are used at much lower temperatures than we need, and performance/operation data at the higher operating temperatures is unavailable. Concerns are the “dry out” temperature of these standard heat pipes as well as whether their performance deteriorates significantly as operating temperatures increase.

Cost: This design is likely to have low production cost, albeit not as low as our concept 1. However, pumping cost should be lower, especially for design 2b since the use of the heat pipe eliminates all the pressure drop aside from that of the manifold.

Manufacturability: This design is amenable to low cost manufacturing.

Installation: This design is not as easy to install as concept 1 as the dewars have probably to be filled on site with the thermal fluid.

Orientation: This design restricts the possible tube orientation to North-South as the tubes have to be tilted to keep the thermal fluid from spilling. The North-South orientation requires a higher optical acceptance angle which reduces the concentration.

Robustness: The heat transfer fluid contained in the Dewars is in contact with air. It will be important to select a heat transfer fluid with a flash point above the stagnation temperature of the collector. Some form of container will be needed to prevent spilling of the heat transfer fluid. Oil expansion issues have to be considered. Alternatively, a thermal grease (if found to work sufficiently well) will

Durability: Version (a) of this concept is expected to be very durable. The same applies to version (b) assuming satisfactory heat pipe longevity. Since the glass dewars are not used to contain the circulating fluid, there is no risk of dewar breakage in the event of pressure surges

within the circulating fluid loop. Similarly, thermal shock is greatly minimized (probably eliminated) because the thermal fluid within the dewars will act to dampen thermal transport. **Technical Risk:** The technical risk of this concept is higher than concept 1. Potential technical barriers are the heat transfer and the performance and longevity of heat pipes operated at high temperatures.

Concept 3 - Metal absorber with glass-to-metal seal

This concept allows for two versions: (a) with metal tube (see Figure 35 a); and (b) with heat pipe (see Figure 35 b). In both versions an evacuated glass tube with an innovative glass-to-metal seal is used to insulate the metal absorber. The metal absorber is a thin cylindrical copper fin with a selective coating that enables high solar absorptance and reduces radiative heat loss. The fin is welded to a metal counter flow tube (version a) or a heat pipe (version b). In version (a) the heat absorbed by the fin is transferred to the manifold by the circulating fluid in the metal tube. In version (b) the heat is transferred from the fin to the manifold by a heat pipe. The absorber tubes are placed so that external reflectors concentrate sunlight onto the evacuated dewars, just as in concepts 1 and 2.

Features

Heat Transfer: This design has good heat transfer, but not as good as concept 1 because the absorbed thermal energy must be conducted around a metallic fin before it passes into the working fluid.

Cost: This design is likely to have higher production costs than concepts 1 and 2. This is due to the high metal content and especially the glass-to-metal seals. Pumping cost might be an issue with the counter flow metal tube of version (a). In this case, a metal U-tube could be used instead.

Manufacturability: The manufacturing is more complex than in concepts 1 and 2.

Installation: Version (b) is very easy to install as the heat pipes can be plugged onto the manifold on site. Version (a) requires plumbing.

Orientation: Version (a) can be oriented East-West or North-South. Version (b) needs some tilt because of the heat pipes.

Robustness: The concept is very robust. The fluid is contained in metal pipes.

Durability: Thermal stress issues and the longevity of the glass-to-metal seals have to be analyzed.

Technical Risk: Version (a) has very little technical risk. Version (b) has higher technical risk due to the unknown performance and longevity of heat pipes operated at high temperatures.

Table 1. Comparison of Features

1 ... 4 (poor ... best)	All glass Dewar counter flow	All glass Dewar filled with heat transfer fluid		Metal absorber with glass-to- metal seal	
		with metal tube	with heat pipe	with metal tube	with heat pipe
Heat transfer / efficiency	4	2-3	2-3	3	3
Cost	4	3	3	2	2
O&M (pumping)	3	3	4	2	4
Manufacturability	4	4	4	2-3	2-3
Installation	4	3	4	3	4
Orientation	4	3	3-4	4	3-4
Robustness	2	2-3	2-3	4	3-4
Durability/Lifetime	3	4	4	2-3	2-3
Technical Risk	3	2-3	2-3	4	2-3

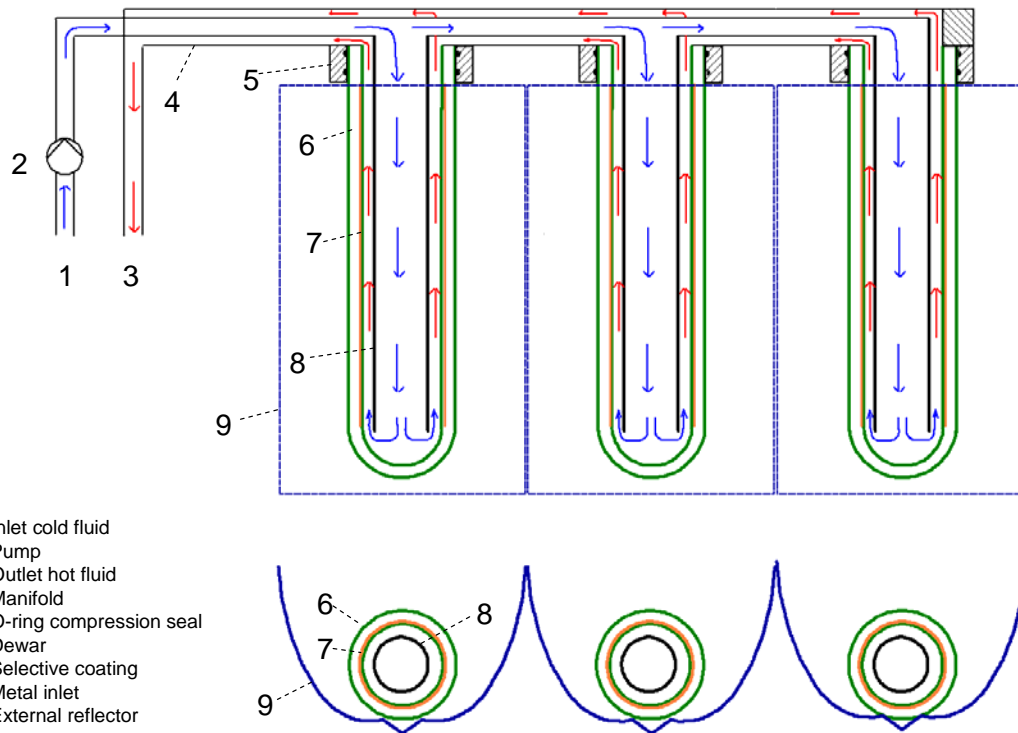


Figure 32: Top view and cross section view of XCPC concept #1 (drawing is not to scale)

Source: The Regents of University of California

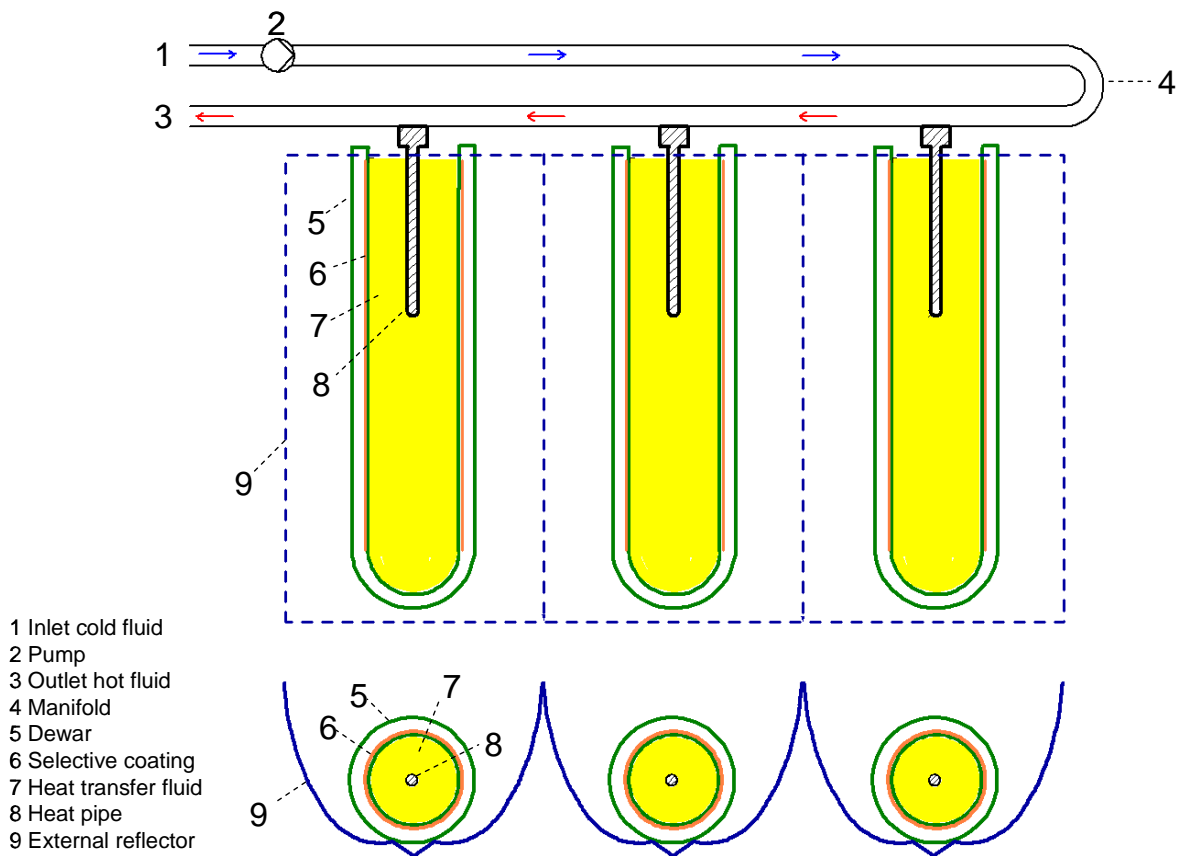


Figure 33. Top view and cross section view of XPCP concept #33 (drawing not to scale)
 Source: The Regents of University of California

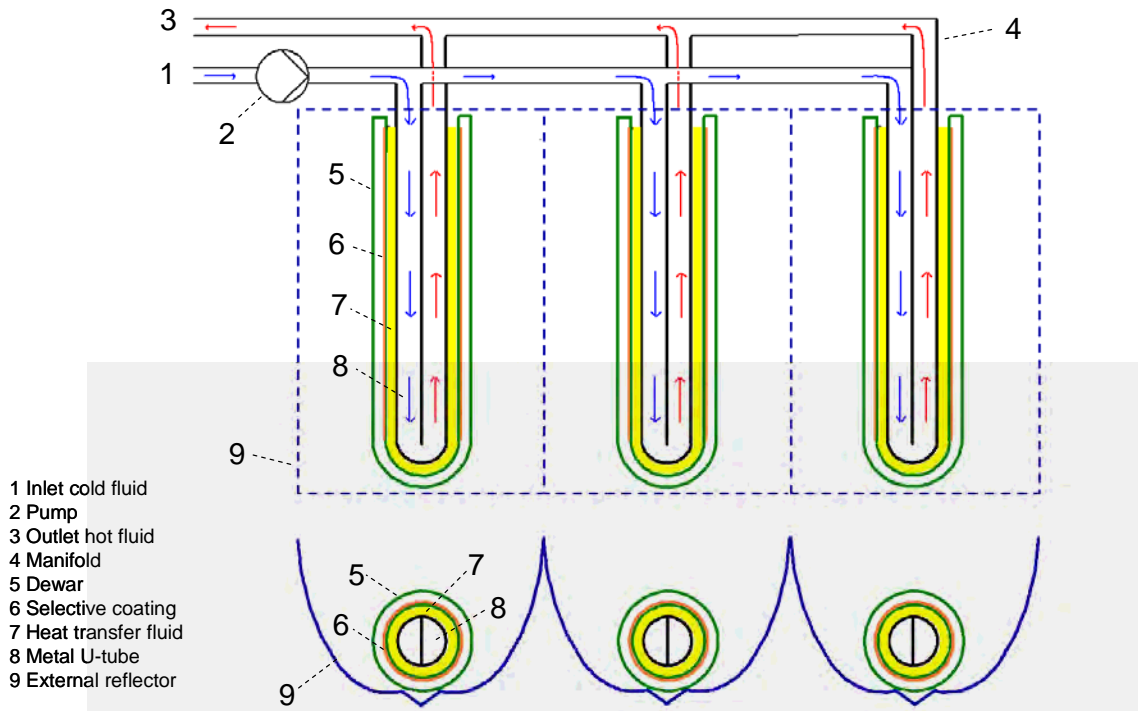


Figure 34. Top View and cross section view of XPCP concept #34 (drawing not to scale)
 Source: The Regents of University of California

Figure 35 a. Top view and cross section view of XCPC concept #3a (drawing not to scale)
 Source: The Regents of University of California

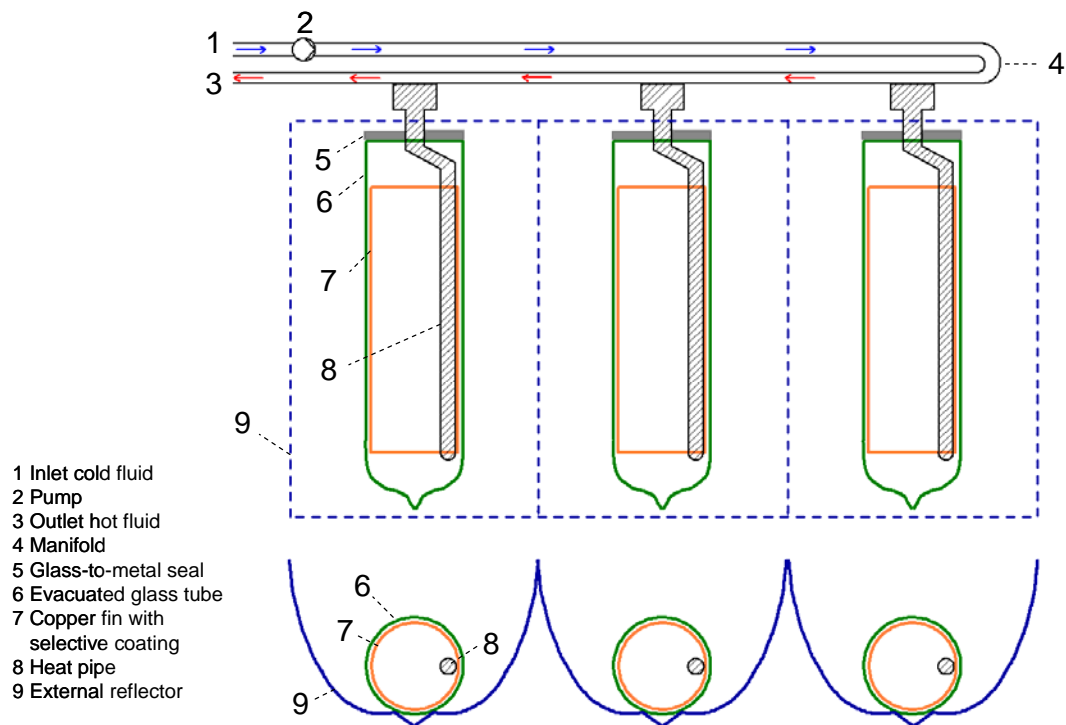
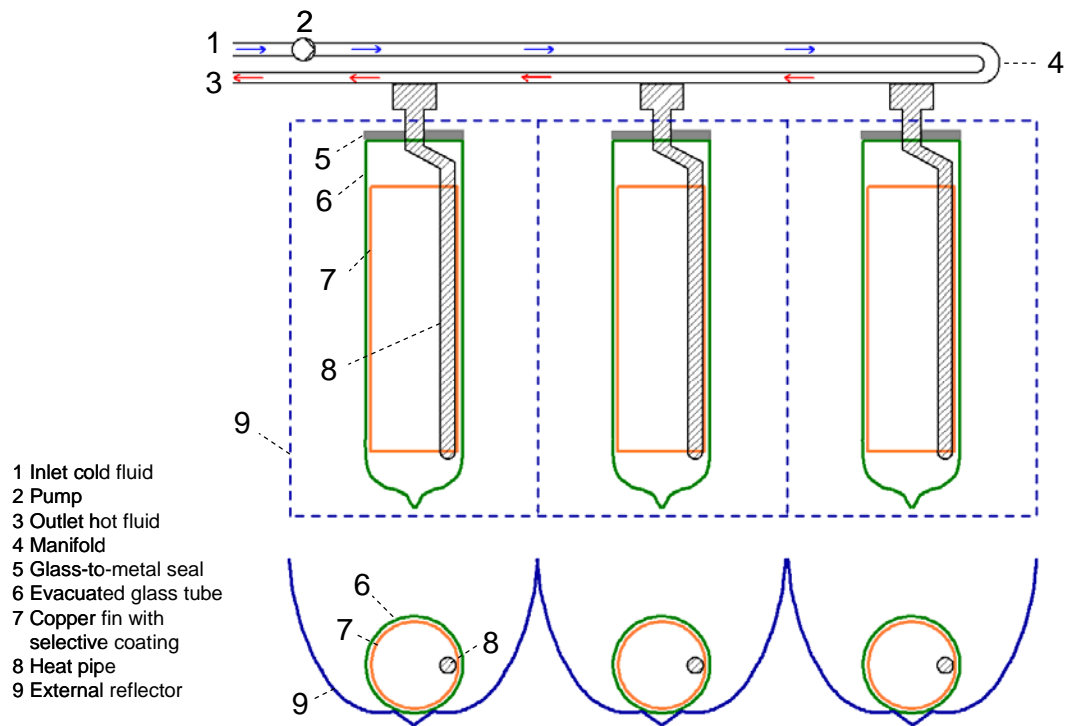


Figure 35 b. Top view and cross section view of XCPC concept #3b (drawing not to scale)
 Source: The Regents of University of California

2.4. Task 5

In Task 5, the Contractor created computer modeling tools that allow performance characterization of the conceptual XCPC designs developed in Task 4. (These conceptual designs have been described in the "XCPC Conceptual Design Report.") We developed an

optical model to analyze optical performance, thermal models to analyze thermal performance, and a system performance model to calculate the annual performance of the XCPC designs.

The evacuated receivers are the principal thermal component of our XCPC designs, and there are two basic evacuated receiver designs: a) the all-glass evacuated dewar that is already mass-produced in China very inexpensively, and b) a sealed glass evacuated tube that uses a single layer of glass and although more costly, offers higher pressure operation and reduced risk in the event of glass breakage. Thermal models for these two basic evacuated receiver approaches have been completed, as was an optical model that was used to define the CPC reflector design for the various design cases of interest. The figure below summarizes our preliminary results in the form of XCPC collector efficiency vs. temperature curve, for both the all-glass dewar (with direct flow) and the sealed glass approach.

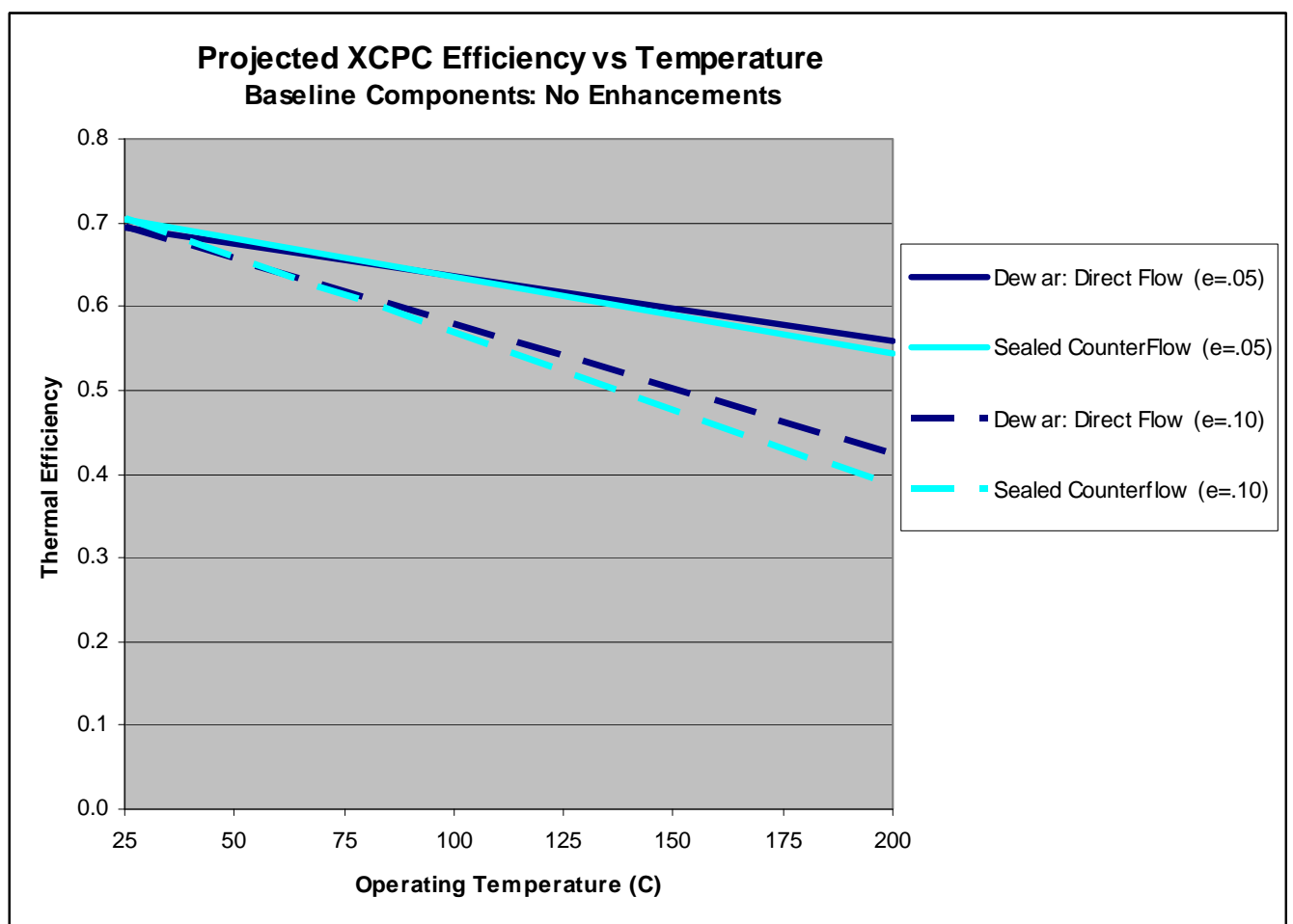


Figure 36. Projected XCPC Efficiency v Temperature

Source: The Regents of University of California

Note that two efficiency lines are given for each, one for an assumed absorber emittance of 0.05 and the other for an emittance of 0.10. This range covers the likely range in emittance for the commercially-available absorber materials of interest, which are presently not precisely known at the higher operating temperatures that are of interest. Accurate determination of the

emittance of absorber selective surfaces awaits laboratory testing, and is part of Task 6 “Detailed Component Characterization”.

Note that, depending on the emittance of the selective coatings that are found, we are expecting to be very near our design point goal of 50% efficiency at 200°C. If the emittance values are as low as 0.05, we expect to be able to achieve thermal efficiencies that are slightly above our 50% goal. If the emittance values are 0.10, we expect to be closer to 40% in thermal efficiency at 200°C. Recall also that these designs are based on using standard off-the-shelf components, and do include the potential performance enhancements that will be evaluated in Task 10. The use of improved reflective materials, anti-reflective coatings, and improved absorber coatings, for example, will boost operating these efficiencies.

Optical Analysis

For all three conceptual designs, the shape of the non-imaging external reflectors was designed so that all sunlight impinging on the aperture plane of the collector within a 34° angular acceptance angle is redirected onto the absorber. The concentration factor, the optical efficiency and the incidence angle modifiers were calculated using raytracing analysis. Optical modeling software “TracePro” was used.



Figure 37. All-glass dewars – direct flow and all-glass dewar filled with thermal fluid - indirect flow
Source: The Regents of University of California

The refractive index of the glass dewar was assumed to be 1.47 with a transmittance of 0.90. Each air/glass interface results in about a 4% reflection loss, and since there are two such interfaces the reflectance loss totals about 8%. The other 2% is due to absorption loss within the borosilicate glass.

The all glass dewar was assumed to have the following dimensions, consistent with the size of the most popular dewar that is mass-produced in China.

Diameter of outer dewar wall: 58mm

Diameter of inner dewar wall: 47mm

The vacuum surface of the inner dewar wall was assumed to be coated with a selective coating with a 92% absorptance of the solar spectrum at normal incidence. The absorptance of selective coatings is known to depend upon incidence angle, and we accounted for this variation using Figure 38.



Figure 38. Variation of selective coating absorptance with incidence angle

Source: The Regents of University of California

The external reflector was assumed to be of silver with a reflectivity of 90%, consistent with the use of Alanod's best commercially available enhanced aluminum reflective material. The dimensions and the shape of the reflector are depicted in Fig. 39.

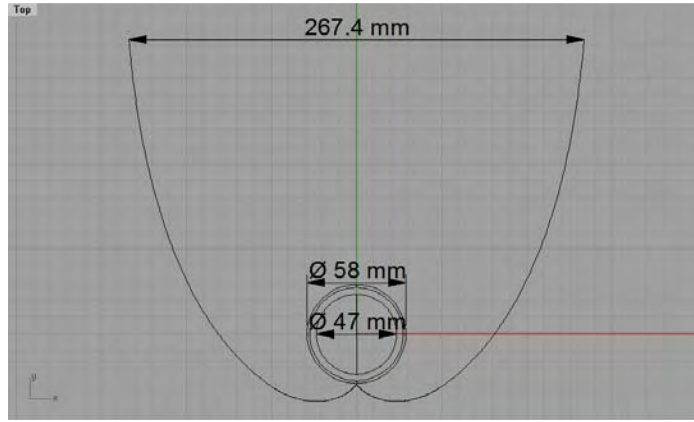


Figure 39. Shape of XPC reflector for all-glass dewars

Source: The Regents of University of California

The raytracing analysis yielded an average optical efficiency of 66.5% (averaged over all incidence angles smaller than the acceptance angle, i.e. between 0 and 34 degrees). The dependence of the optical efficiency on the incidence angle, the so-called incidence angle modifier (IAM), is depicted in Fig. 40.

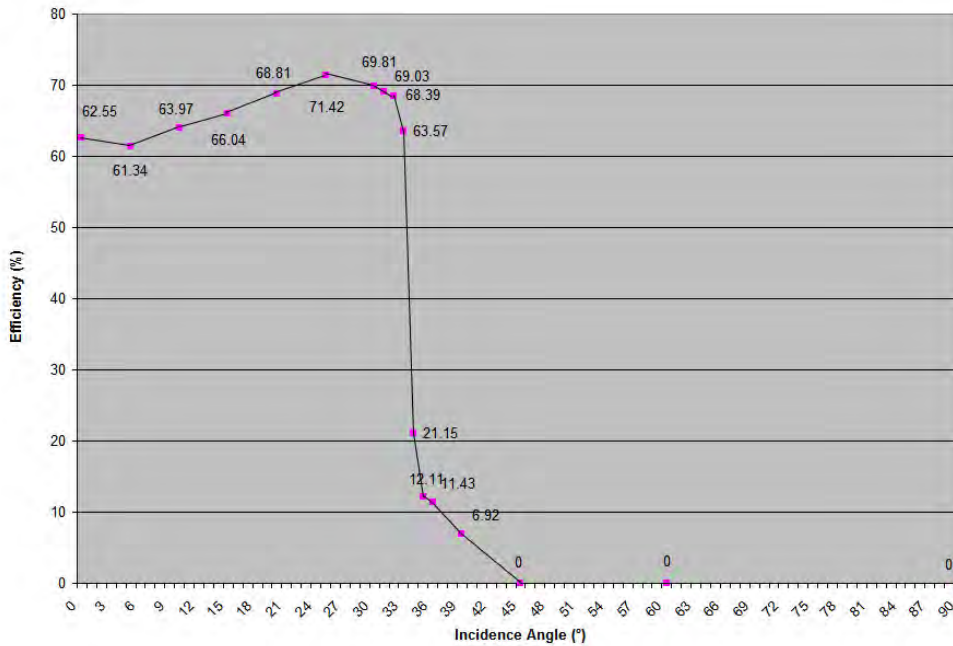


Figure 40. Incidence Angle Modifier (IAM) for 58mm OD dewars

Source: The Regents of University of California

Metal absorber with glass-to-metal seal:

The refractive index of the evacuated glass tube was assumed to be 1.47, again consistent with the normal 90% transmittance of borosilicate glass tubing. The evacuated glass tube is assumed to have the following dimensions, based on information provided by Beijing Eurocon Solar.

Diameter of outer tube wall: 65 mm

Diameter of inner tube wall: 61.8 mm

The metal absorber was assumed to be a thin cylindrical copper fin of 56 mm in diameter with a selective coating of 92%, and the variation with incidence angle depicted in Figure 38.

The external reflector was assumed to be of silver with a reflectivity of 90%, as with the previous design, based on the use of Alanod. The dimensions of the reflector are depicted in Figure 41.

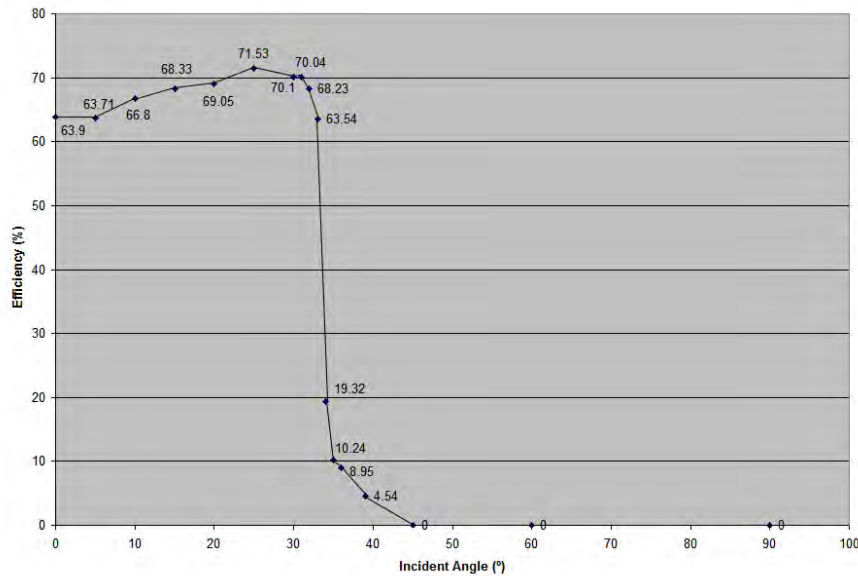


Figure 41. Incidence Angle Modifier (IAM) for design using absorber with glass-to-metal seal
Source: The Regents of University of California

The raytracing analysis yielded an average optical efficiency of 67.5% (averaged over all incidence angles smaller than the acceptance angle, i.e. between 0 and 34 degrees). The dependence of the optical efficiency on the incidence angle, the so-called incidence angle modifier (IAM), is depicted in Figure 41

Thermal Analysis

We developed thermal models (one for each of the basic conceptual designs) that describe the transfer of the heat flux from the concentrating optical system to the working fluid in the absorber tube of the XCPC. When the concentrated sunlight reaches the absorber tube, convective, conductive and radiant heat transfer mechanisms occur in the different interfaces that comprise the absorber tube. The developed model evaluates the direction and magnitude of heat transfer mechanisms associated with the evacuated tubes, and solves for the net flow of heat to/from the various materials and surfaces.

The thermal models are based on the application of Energy Conservation Laws for all the surfaces and materials that dictate the thermal performance if the collector (selective surface absorptance, selective surface emittance, material thermal conductivity, glass absorptance, and

various convective heat transfer coefficients). We applied the energy and mass conservation laws to all identified control volumes and obtained a set of equations describing the thermal performance of the system. More details are included in the appendix to this report. The equations are solved using the EES Program (Engineering Equation Solver Program), which uses an iterative mathematical technique to derive the solution.

The most important result of the model is the net heat loss from the evacuated tube for various operating temperatures and irradiance levels.

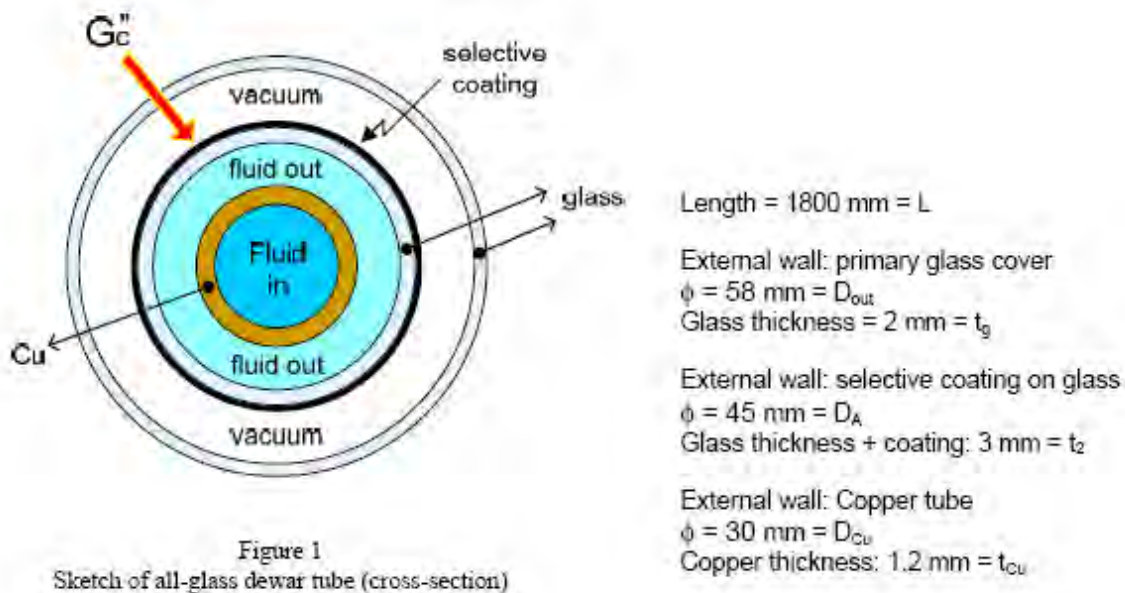


Figure 42. Sketch of all-glass dewar tube (cross-section)

Source: The Regents of University of California

Thermal analysis of this design is based on consideration of the energy transfers noted below.

1. The external glass volume that is exposed to the ambient and to a uniform solar radiation flux from the outer side. This glass volume encloses the absorber layer on the inner side.
2. The internal glass volume that is exposed on the outer surface to a uniform solar radiation flux and to the external glass cover. This glass volume encloses the working fluid on the inner side.
3. The circulating working fluid enclosed by the internal glass, including the counter-flowing fluid inside/outside the copper tube.

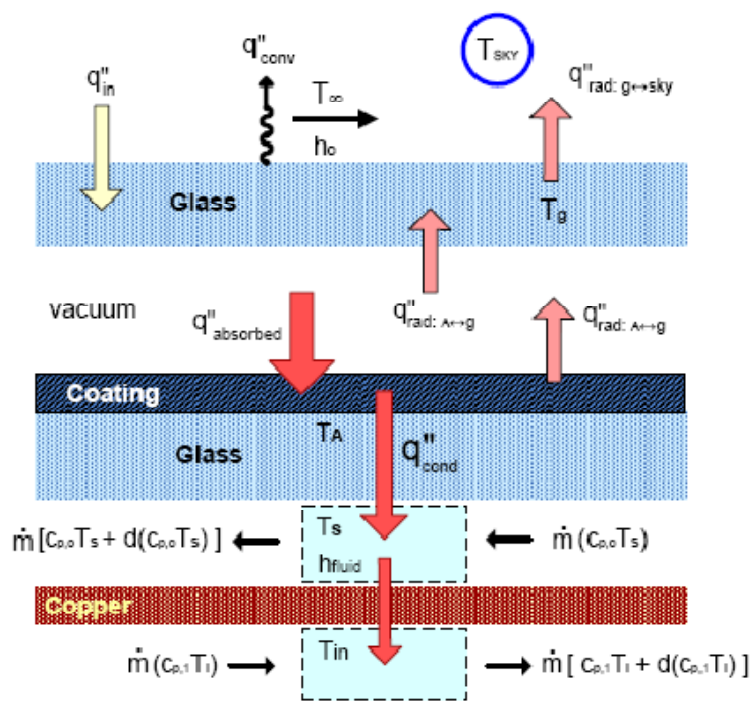


Figure 43. Sketch of all-glass dewar tube (side cross-section)

Source: The Regents of University of California

The heat loss coefficient was determined to be $0.776 \text{ W/m}^2\text{-C}$ for an assumed absorber emittance of 0.05, using the value listed by the manufacturer at a temperature of 100 C. At higher temperatures the emittance will increase, but the exact amount is unknown at present. We estimate that it will increase to no more than 0.10. At this higher emittance, the heat loss coefficient was determined to be $1.36 \text{ W/m}^2\text{-C}$. Both of these heat loss coefficients assume a concentration ratio (CR) of 1.8, the ratio between the aperture area of the CPC reflector divided by the circumference of the absorber

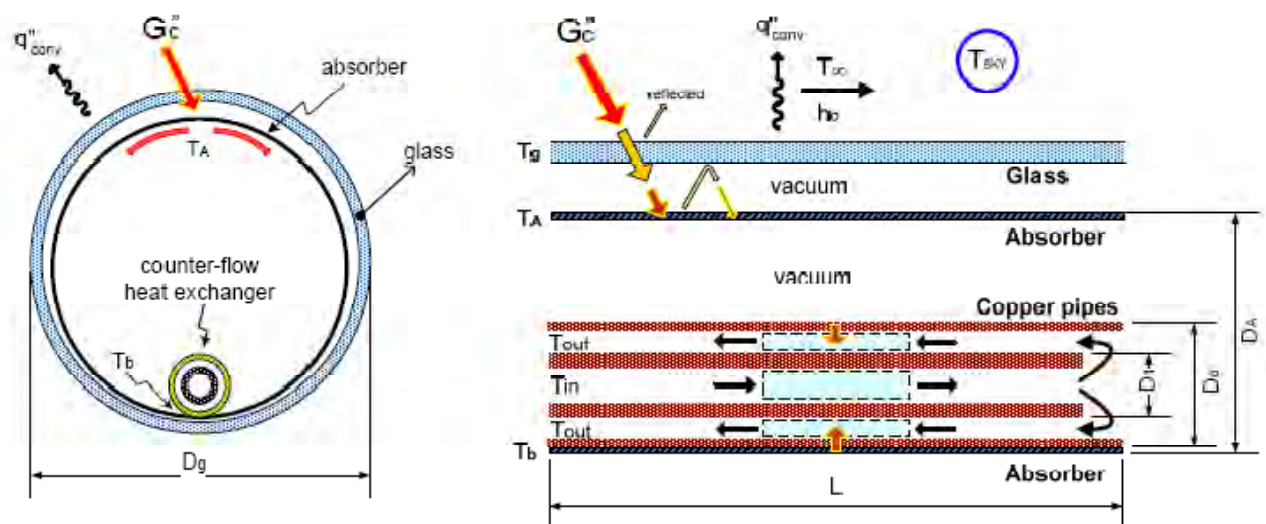


Figure 44. Metal absorber with glass-to-metal seal

Source: The Regents of University of California

The team identified three relevant control volumes:

1. The external glass volume that is exposed to the ambient and to a uniform solar radiation flux from the outer side. This glass volume encloses the metallic absorber fin on the inner side.
2. The cylindrical copper fin absorber with the selective coating. The fin is welded to a metal counter flow tube.
3. The circulating working fluid enclosed by the metal counter flow tube.

The heat loss coefficient was determined to be $0.919 \text{ W/m}^2\text{-C}$ for an assumed absorber emittance of 0.05, using the value listed by the manufacturer at a temperature of 100 C. At higher temperatures the emittance will increase, but the exact amount is unknown at present. We estimate that it will increase to no more than 0.10. At this higher emittance, the heat loss coefficient was determined to be $1.83 \text{ W/m}^2\text{-C}$. Both of these heat loss coefficients assume a concentration ratio (CR) of 1.8, the ratio between the aperture area of the CPC reflector divided by the circumference of the absorber.

Annual System Performance Analysis

The annual performance tool f-Chart has been determined to include all the necessary characteristics to provide an accurate means of determining the annual performance of the various XCPC designs. F-Chart www.fchart.com allows for user input of optical efficiencies (at normal incidence), incidence angle modifiers (as determined by our optical raytrace model), and heat loss coefficients (as determined by the thermal models). Importantly for our purposes, f-chart includes algorithms for performance analysis of CPC collectors, along with traditional flat plate collectors and evacuated tube collectors. Hence, rather than developing an entirely new annual performance model, f-chart has been purchased.

Weather data for hundreds of North American locations, the 16 California climate zones and numerous other locations are included with the program to estimate the long-term average performance of:

- Domestic Water Heating Systems
- Water Storage Space and Domestic Water Heating Systems
- Active Collection with Building Storage Space Heating Systems
- General Solar Heating Systems (e.g., process heating systems)

An example of the inputs (and descriptions of each) for the CPC collector are shown as follows:

SI units can also be used.

Compound Parabolic Concen...		
Number of collector panels	26	
Collector panel area	20.80	ft ²
FR*UL (Test slope)	0.170	Btu/hr-ft ² -F
FR*TAU*ALPHA (Test intercept)	0.600	
Concentration ratio	1.5	
Acceptance half-angle	35	degrees
Collector slope	45	degrees
Collector azimuth (South=0)	0	degrees
Receiver orientation		
Incidence angle modifier (Perpend	Ang Dep	
Incidence angle modifier (Parallel)	Ang Dep	
Collector flowrate/area	11.000	lb/hr-ft ²
Collector fluid specific heat	0.80	Btu/lb-F
Modify test values	No	
Test collector flowrate/area	11.000	lb/hr-ft ²
Test fluid specific heat	1.00	Btu/lb-F

Number of collector panels is multiplied by the area of a single collector panel to determine the total array area.

Collector panel area is either the gross or net aperture area of each collector panel. The same (gross or net) aperture area that was used to determine FR*TAU*ALPHA and FR*UL must

be used for this parameter. The ASHRAE Standard 93-77 [1977] collector test recommends the use of gross area.

FR*UL (Test Slope) is the product of the collector heat removal factor, FR, and the collector overall heat loss factor, UL. FR*UL is the negative of the slope of the straight-line efficiency plot obtained from the ASHRAE Standard 93-77 [1977] collector test.

FR*TAU*ALPHA (Test Intercept) is the product of the collector heat removal factor, FR, and the transmittance-absorptance product, TAU*ALPHA, at normal incidence. This parameter, also known as the optical efficiency, is the Y-intercept of the straight-line efficiency plot obtained from the ASHRAE Standard 93-77 [1977] collector test.

Concentration ratio is the ratio of the collector aperture area to the receiver area.

Acceptance half-angle is the maximum angle measured from the axis of the CPC for which incident beam solar radiation will strike the absorber.

Collector slope is the angle between the plane of the collector aperture and the horizontal. This parameter may have monthly values. The angle is measured in a vertical plane that is perpendicular to the line formed by the intersection of the plane of the collector aperture and the horizontal plane.

Collector azimuth (South=0) is the angle between the projection into the horizontal plane of the normal to the collector aperture and the local meridian with the zero point directly facing the equator, west positive, and east negative. The azimuth of a horizontal collector can have any value. The azimuth of a collector facing the sun at noon in the southern hemisphere (i.e. north facing) is 180°. This parameter may have monthly values.

Receiver orientation (EW, NS) toggles to indicate the axis orientation of the evacuated tubes. Specify NS if the collectors are mounted vertically with the tube pointing up and down.

parallel to the tube axis (i.e., the longitudinal plane). The incidence angle modifier is the ratio of the transmittance-absorptance product at an off-normal incidence angle in the longitudinal plane to the normal incidence transmittance-absorptance product. This parameter may have either one or ten values. A single value indicates that the incidence angle modifier is independent of solar incidence angle. The ten values, as shown above for the default parameter set, correspond to the incidence angle modifier values between 0 and 90 degrees in 10 degree increments.

Collector flow rate/area is the total mass flow rate of collector fluid through the collector array divided by the total collector array area. This flow rate may be different from the flow rate at which the collector was tested. Typical values of this flow rate are 11 lb/hr-ft² or 0.015 kg/s-m² for liquids and 9 lb/hr-ft² or 0.012 kg/s-m² for air.

Collector fluid specific heat is the specific heat of the fluid flowing through the collectors. Properties can be found in the ASHRAE handbook of Fundamentals [1985] or in any heat transfer textbook. For water, use 1.0 Btu/lb-F or 4.19 kJ/kg-K. For air use 1.0 kJ/kg-K or 0.24 Btu/lb-F.

Modify Test Values (Yes/No) toggles to indicate if the next two parameters should be used to account for differences in the collector parameters due to differences in the actual and test fluid flow rates and series-parallel fluid flow circuit arrangements. If this parameter is set to No, the following three parameters are ignored.

Test collector flow rate/area is the ratio of the collector fluid flow rate used in the collector test to the array area of the collector tested. Usually, a single collector panel is tested. In this case, this parameter is the ratio of the test collector fluid flow rate to the collector panel area. This parameter is used only if Yes has been selected for 'modify test values'.

Test fluid specific heat is the specific heat of the fluid used in the collector test. Properties of common materials can be found in the ASHRAE Handbook of Fundamentals [1985] or in any heat transfer textbook. This parameter is used only if Yes is selected for 'modify test values'.

Figure 45. Example of inputs for CPC collector
Source: The Regents of University of California

Appendix – Thermal Models for Task 5

Sealed Tube: Cylindrical Absorber, Counterflow

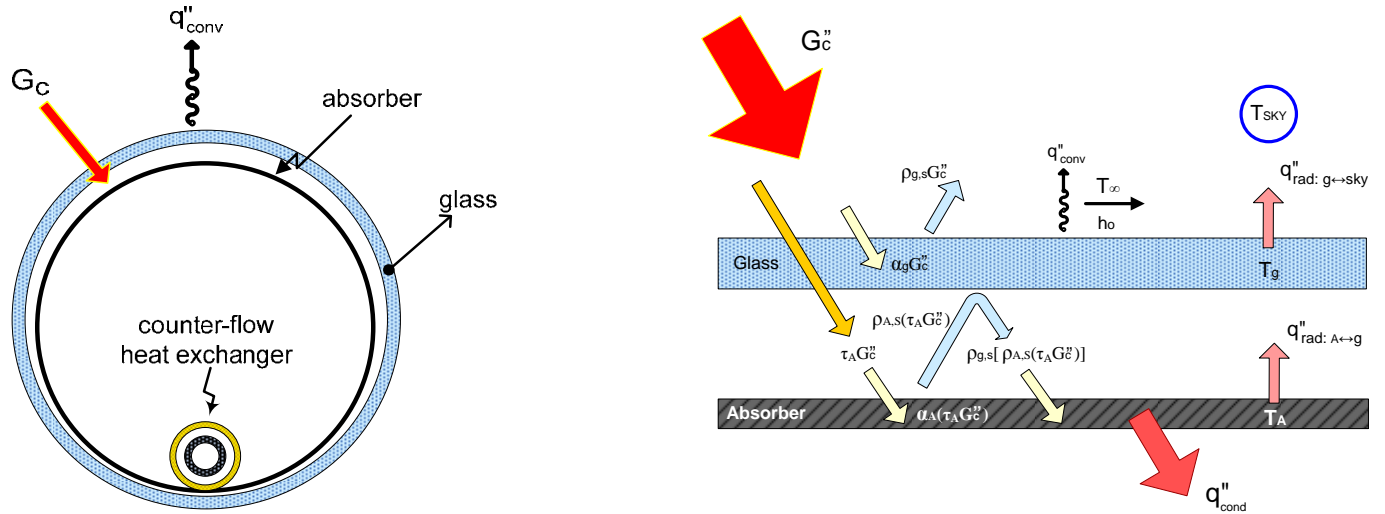


Figure 46 & 47. Transversal section and schematic of heat fluxes

Source: The Regents of University of California

G_c	Incident solar radiation	W/m^2
q''_{conv}	Heat loss by air convection on glass external surface	W/m^2
$q''_{rad: g \leftrightarrow sky}$	Net heat transfer to/from the glass from/to the atmosphere (sky) due to glass emission/absorption of heat by radiation. Gray surfaces assumed.	W/m^2
$q''_{rad: A \leftrightarrow g}$	Net heat transfer to/from the glass from/to the absorber due to emission/absorption of heat (in the infrared according to their low blackbody temperature) by radiation to/from the absorber. Gray surfaces assumed	W/m^2
q''_{cond}	Heat transferred by conduction to working fluid	W/m^2
T_g	Temperature of glass cover	K
T_A	Temperature of absorber	K
T_∞	Temperature of fluid	K
T_{sky}	Temperature of atmosphere	K
h_o	Convection coefficient	W/m^2K

Glass Properties

Solar radiation (300 – 2,700 nm)	Infrared (>2,700 nm)
$\alpha_g = \text{absorptivity} \approx \mathbf{0.02}$	$\epsilon_g = \text{emissivity} \approx \mathbf{0.92}$
$\tau_g = \text{transmissivity} \approx \mathbf{0.90}$	$\alpha_{g,IR} = \text{absorptivity as a gray surface} = \epsilon_g \approx \mathbf{0.92}$
$\rho_{g,s} = \text{reflectivity} \approx \mathbf{0.08}$ ($\alpha_c + \rho_c + \tau_c = 1$)	$\tau_g = \text{transmissivity} \approx \mathbf{0}$
	$\rho_g = \text{reflectivity} \approx (1 - \alpha_{g,IR}) = (1 - \epsilon_g) = \mathbf{0.08}$

Pyrex 7740 type: Pyrex 7740 is a low expansion borosilicate glass. Pyrex glass is good for normal use temperature of 446 degrees F and maximum use temperature 914 degrees F. Pyrex can also be tempered to increase its mechanical strength, and is also heat shock resistant. Pyrex is resistant to acid and has high optical transmission over a wide wavelength range. The low alkali content of Pyrex makes this glass ideal for high-purity laboratory applications.

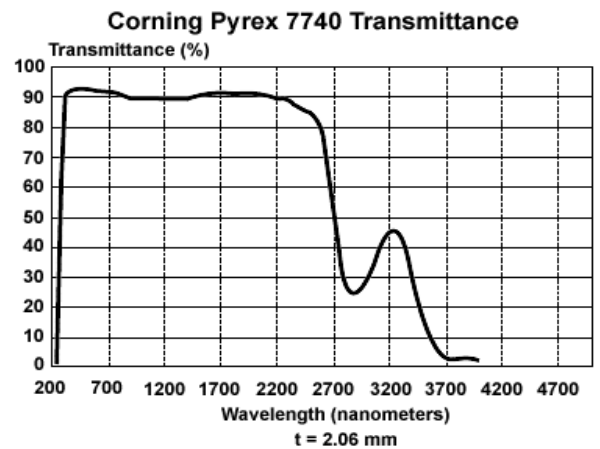


Figure 48. Corning Pyrex 7740 Transmittance curve
Source: The Regents of University of California

Absorber Properties (sputtered Al-AlN coating)

Solar radiation (300 – 2,700 nm)	Infrared (>2,700 nm)
$\alpha_A = \text{absorptivity} \approx \mathbf{0.95}$ $\epsilon_A = \text{emmissivity} \approx \mathbf{0.05}$ $\tau_A = \text{transmissivity} = \mathbf{0}$ $\rho_{A,S} = (1 - \alpha_A) = \mathbf{0.05}$	$\epsilon_A = \text{emmissivity} \approx \mathbf{0.05}$ $\rho_A = (1 - \alpha_A) \approx (1 - \epsilon_A) = \mathbf{0.95}$

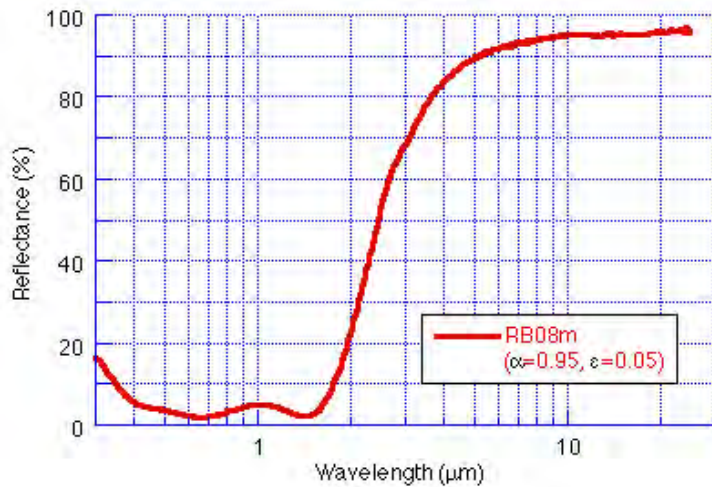


Figure 49.

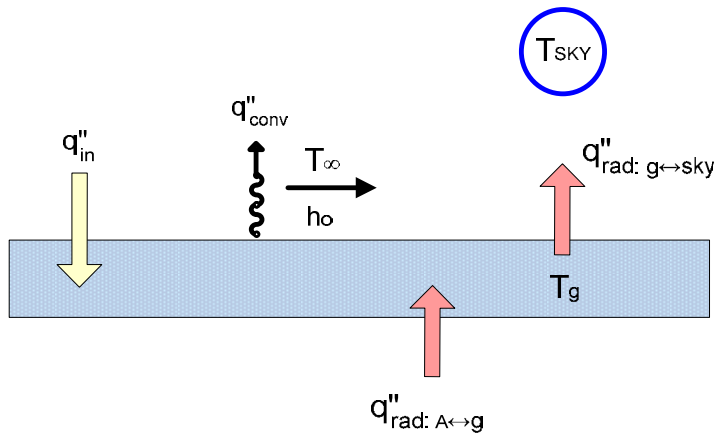
Reflectance spectrum of a SS-AlN cermet solar selective coating deposited using a commercial-scale dc sputter coater. The corresponding film has a solar absorptance of 0.95 and emissivity of 0.05 at 100°C. The coating has the double cermet film structure AlN/SS-AlN(LMVF)/SS-AlN(HMVF)/Al.

Department of Physics, University of Sidney

Source: The Regents of University of California

Applying an energy balance to the glass interface:

q_{in}''	Heat absorption by the glass in the solar spectrum.
q_{conv}''	Heat loss by air convection on glass external surface
$q_{rad: g \leftrightarrow sky}''$	Net heat loss of the glass due to glass emission of heat by radiation to the



	atmosphere (sky)
$q''_{\text{rad: A} \leftrightarrow \text{g}}$	Net heat absorption by the glass due to glass absorption of heat (in the infrared according to its low blackbody temperature) by radiation from the absorber.

Figure 50. Heat fluxes at glass interface

Source: The Regents of University of California

$$q''_{\text{in}} + q''_{\text{rad: A} \leftrightarrow \text{g}} - [q''_{\text{conv}} + q''_{\text{rad: g} \leftrightarrow \text{sky}}] = 0 \quad (1)$$

$$\alpha_g G_c'' + h_{\text{rad: A} \leftrightarrow \text{g}} \sigma (T_A^4 - T_g^4) - h_0 (T_g - T_\infty) - h_{\text{rad: g} \leftrightarrow \text{sky}} \sigma (T_g^4 - T_{\text{sky}}^4) = 0 \quad (2)$$

Where:

$$h_{\text{rad: A} \leftrightarrow \text{g}} = \frac{1}{\frac{1}{\epsilon_A} + \frac{1 - \epsilon_g}{\epsilon_g} \left(\frac{r_g}{r_A} \right)}$$

$h_0 = 2.8 + 3v$ (according to the empirical equation proposed by Watmuff for a flat plate collector)

$v = \text{wind speed (ms}^{-1}\text{)}$

$h_{\text{rad: g} \leftrightarrow \text{sky}} = \epsilon_g$ (Since the view factor between the tube and the sky is 1)

Equation (2) is more useful if expressed as a heat rate [W] :

$$A_g (\alpha_g G_c'') + A_A [h_{\text{rad: A} \leftrightarrow \text{g}} \sigma (T_A^4 - T_g^4)] - A_g [h_0 (T_g - T_\infty)] - A_g [\epsilon_g \sigma (T_g^4 - T_{\text{sky}}^4)] = 0 \quad (3)$$

Where:

$A_g = \text{Area of glass tube} = (\pi D_g)L$

$A_A = \text{Area of absorber} = (\pi D_A)L$

Applying an energy balance to the absorber:

q''_{absorbed}	Net heat absorption by the selective coating of the transmitted solar radiation plus the multiple absorber-glass reflections of transmitted solar radiation.
-------------------------	--

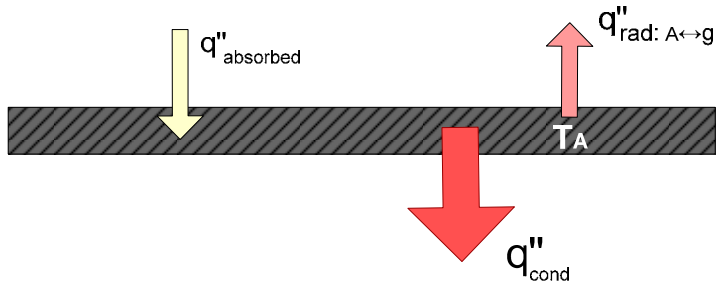


Figure 51. Heat fluxes at absorber interface

Source: The Regents of University of California

$q''_{\text{rad: A} \leftrightarrow \text{g}}$	Net heat loss of the selective coating due to selective coating emission/absorption of heat (in the infrared according to its low blackbody temperature) by radiation to/from the glass.
q''_{cond}	Heat conducted per unit area to working fluid.

$$q''_{\text{absorbed}} - q''_{\text{rad: A} \leftrightarrow \text{g}} - q''_{\text{cond}} = 0 \quad (4)$$

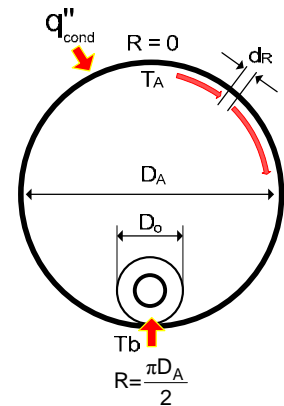
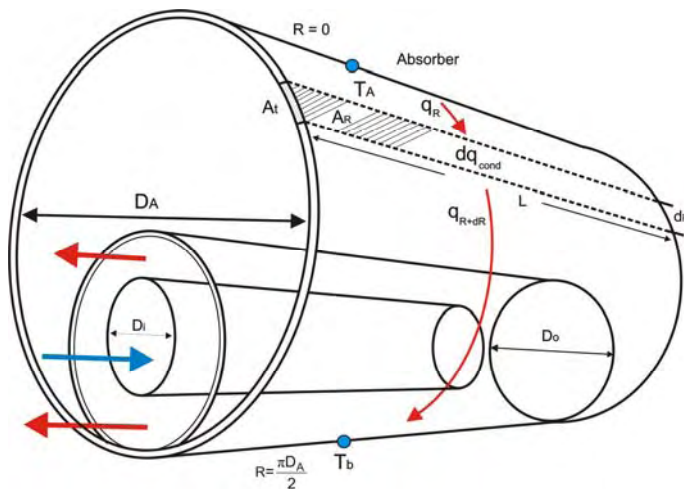
$$\frac{\alpha_A \tau_g}{1 - (1 - \alpha_A) \rho_{g,s}} G_c'' - h_{\text{rad: A} \leftrightarrow \text{g}} (T_A - T_g) - q''_{\text{cond}} = 0 \quad (5)$$

Equation (4) is more useful if expressed as a heat rate [W] :

$$A_A \left(\frac{\alpha_A \tau_g}{1 - (1 - \alpha_A) \rho_{g,s}} G_c'' \right) - A_A [h_{\text{rad: A} \leftrightarrow \text{g}} (T_A - T_g)] - A_A q''_{\text{cond}} = 0 \quad (6)$$

Where:

$$AA = \text{Area of absorber} = (\pi DA)L$$



$D_A = 56 \text{ mm}$
 $D_o = 10 \text{ mm}$
 $t_o = 1 \text{ mm}$
 $t_A = 0.3 \text{ mm}$

Figure 52. Heat fluxes at absorber / heat exchanger

Source: The Regents of University of California

From a differential conduction analysis applied to the geometry sketched in Figure 52

$$q_R + dq_{\text{cond}} = q_{R+dR} \quad (7)$$

$$A_t = (\text{thickness of absorber})(\text{Length}) = t_A L$$

$$dA_R = LdR$$

$$dq_{\text{cond}} = q''_{\text{cond}} dA_R = q''_{\text{cond}} \cdot LdR$$

$$q_R = -k_{\text{Cu}} A_t \frac{dT}{dR}$$

$$q_{R+dR} = q_R + \frac{dq_R}{dR} dR = -k_{\text{Cu}} A_t \frac{dT}{dR} - k_{\text{Cu}} \frac{dT}{dR} \left(A_t \frac{dT}{dR} \right) dR$$

Substituting in (7):

$$\frac{d^2 T}{dR^2} + \frac{L}{k_{\text{Cu}} A_t} q''_{\text{cond}} = 0 \quad (8)$$

The general solution to (8) is:
$$T(R) = -L \frac{q''_{\text{cond}}}{2k_{\text{Cu}} A_t} R^2 + BR + F \quad (9)$$

With the boundary conditions: $\frac{dT(R)}{dR} \Big|_{R=0} = 0$ and $T(R = \frac{\pi D_A}{2}) = T_b$

Thus: $B = 0$
$$F = T_b + L \frac{q''_{\text{cond}}}{2k_{\text{Cu}} A_t} \left(\frac{\pi D_A}{2} \right)^2$$

$$T(R) = T_b + L \frac{q''_{\text{cond}}}{2k_{\text{Cu}} A_t} \left[\left(\frac{\pi D_A}{2} \right)^2 - R^2 \right] \quad (10)$$

Evaluating (10) at $R=0$

$$T(R=0) = T_A = T_b + L \frac{q''_{\text{cond}}}{2k_{\text{Cu}} A_t} \left(\frac{\pi D_A}{2} \right)^2 \quad (11)$$

$$T(R=0) = T_A \quad \text{as in (2) and (5)}$$

Thus:
$$T_b = T_A - L \frac{q''_{\text{cond}}}{2k_{\text{Cu}} A_t} \left(\frac{\pi D_A}{2} \right)^2 \quad (12)$$

From the thermal circuit illustrated in Figure 53:

$$q_{\text{cond}} = \frac{T_b - T_{\text{out}}}{\frac{1}{\pi D_0 L h_{\text{in}}} + \frac{\ln[(D_o + 2t_o)/D_0]}{\pi L k_{\text{Cu}}}} \quad (13)$$

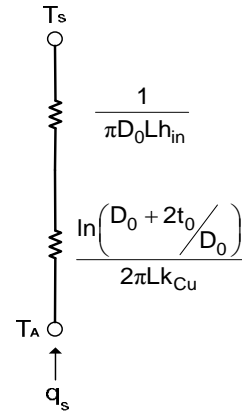


Figure 53. Thermal Circuit
Source: The Regents of University of California

From the solution of the heat exchanger:

$$\Delta T = \frac{q_{\text{cond}}}{\dot{m}_o c_{p,o}} \quad (13)$$

Where

$$\Delta T = T_{\text{out}} - T_{\text{in}} \quad (14)$$

SUMMARY:

Equations derived for the Absorber – Heat exchanger system under the following assumptions:

- Steady state
- Heat exchange by radiation between the absorber, glass and ambient is treated as a gray surface phenomena in the IR region.
- The flux in the absorber is considered to have a uniform distribution in the whole surface.
- Heat exchange by radiation between the internal wall of the absorber and the external wall of the heat exchanger is neglected.
- No temperature drop across the glass.

$$A_g (\alpha_g G_c'' + A_A [h_{\text{rad}: A \leftrightarrow g} \sigma (T_A^4 - T_g^4)] - A_g [h_0 (T_g - T_\infty)] - A_g [\epsilon_g \sigma (T_g^4 - T_{\text{sky}}^4)]) = 0 \quad (A)$$

$$A_A \left(\frac{\alpha_A \tau_g}{1 - (1 - \alpha_A) \rho_{g,s}} G_c'' \right) - A_A [h_{\text{rad}: A \leftrightarrow g} (T_A - T_g)] - A_A q_{\text{cond}}'' = 0 \quad (B)$$

$$q_{\text{cond}} = \frac{T_b - T_{\text{out}}}{\frac{1}{\pi D_0 L h_{\text{in}}} + \frac{\ln[(D_o + 2t_o)/D_0]}{\pi L k_{\text{Cu}}}} \quad (\text{C})$$

$$T_b = T_A - L \frac{q_{\text{cond}}''}{2k_{\text{Cu}} A_t} \left(\frac{\pi D_A}{2} \right)^2 \quad (\text{D})$$

$$\Delta T = \frac{q_{\text{cond}}}{\dot{m} c_{\text{po}}} \quad (\text{E})$$

$$T_{\text{out}} = \Delta T + T_{\text{in}} \quad (\text{F})$$

RESULTS

The solutions to equations A to F were obtained with the use of the EES software for a constant flow rate of 1.5 liter/min and two different conditions:

A: Constant irradiation, $G_c'' = 1000 \text{ W/m}^2$ (which translates in a heat rate of $A_g G_c'' = 326.7 \text{ W}$)

Different input temperatures of fluid, T_{in}

Table 1

Figure 52

B: Constant input temperatures of fluid, T_{in}

Different irradiation rates, G_c

Table 13

Table 14

Table 15

Figure 10

Figure 11

Figure 12

Table 12. Variation of output temperature of fluid when irradiation is kept constant at $G_c = 326.7 \text{ W}$

1	2	3	4	5	6	7	8	9	10
T_{in} [K]	T_{out} [K]	δT [K]	T_A [K]	δ Absorber [K]	T_g [K]	δ Glass [K]	q_{cond} [W]	TOTAL T [W]	Eff $_{total}$
350	355.2	5.158	429	79	301.3	-48.71	221.3	326.7	0.6772
360	365.1	5.104	438.2	78.17	302	-58	219	326.7	0.6701
370	375	5.047	447.3	77.3	302.7	-67.26	216.5	326.7	0.6626
380	385	4.986	456.4	76.37	303.5	-76.47	213.9	326.7	0.6547
390	394.9	4.922	465.4	75.39	304.4	-85.65	211.2	326.7	0.6463
400	404.9	4.855	474.4	74.36	305.2	-94.78	208.3	326.7	0.6375
410	414.8	4.785	483.3	73.28	306.1	-103.9	205.3	326.7	0.6282
420	424.7	4.71	492.1	72.15	307.1	-112.9	202.1	326.7	0.6185
430	434.6	4.633	501	70.95	308.1	-121.9	198.7	326.7	0.6083
440	444.6	4.551	509.7	69.71	309.1	-130.9	195.2	326.7	0.5976
450	454.5	4.466	518.4	68.4	310.1	-139.9	191.6	326.7	0.5864
460	464.4	4.377	527	67.04	311.2	-148.8	187.8	326.7	0.5747
470	474.3	4.284	535.6	65.62	312.4	-157.6	183.8	326.7	0.5625
480	484.2	4.187	544.1	64.14	313.6	-166.4	179.6	326.7	0.5498
490	494.1	4.087	552.6	62.6	314.8	-175.2	175.3	326.7	0.5366
500	504	3.982	561	61	316.1	-183.9	170.8	326.7	0.5229
510	513.9	3.874	569.3	59.33	317.4	-192.6	166.2	326.7	0.5087
520	523.8	3.761	577.6	57.61	318.7	-201.3	161.4	326.7	0.4939
530	533.6	3.645	585.8	55.83	320.1	-209.9	156.4	326.7	0.4786
540	543.5	3.524	594	53.98	321.5	-218.5	151.2	326.7	0.4627
550	553.4	3.4	602.1	52.07	323	-227	145.8	326.7	0.4464

Source: The Regents of University of California

Where the total efficiency is defined as:

$$Eff_{total} = \frac{q_{cond}}{A_g G_c}$$

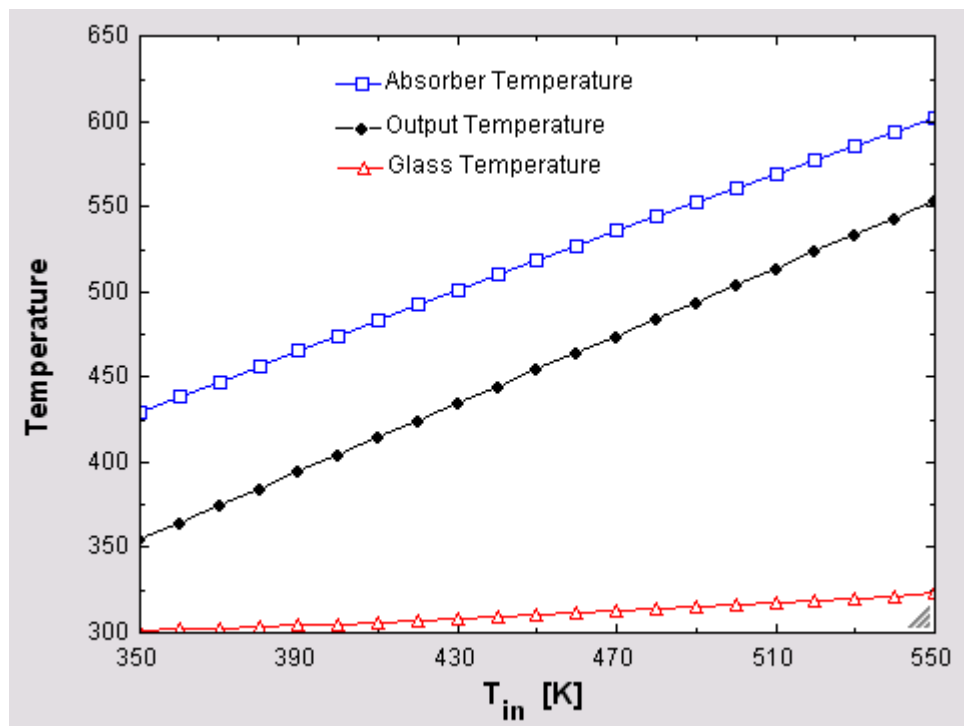


Figure 53. Output temperature of fluid when irradiation is kept constant and while fluid input temperature varies according to table 1

Source: The Regents of University of California

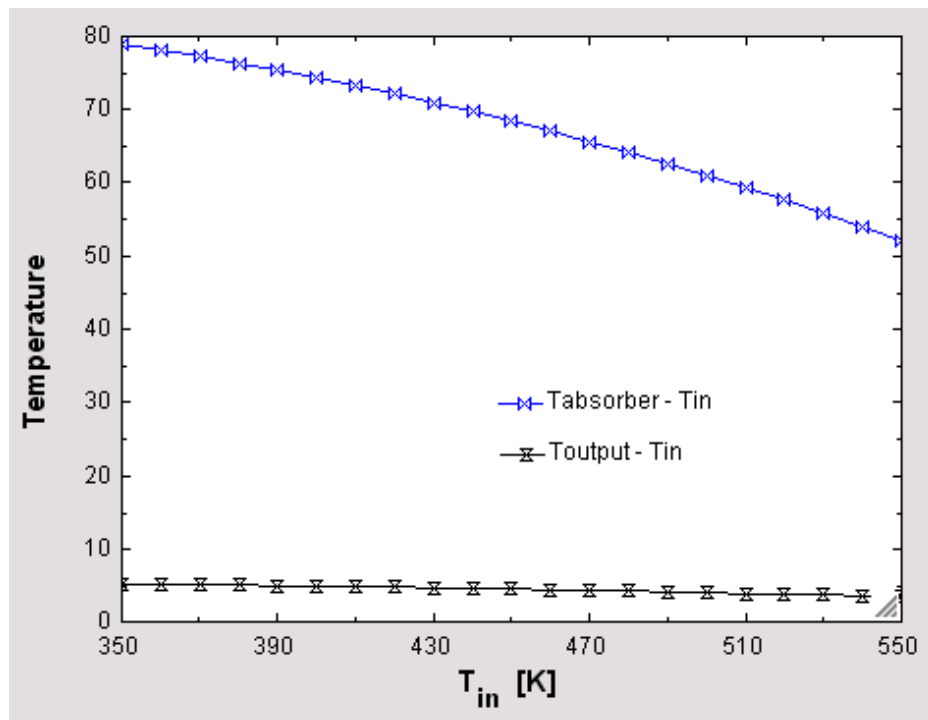


Figure 54. Differences in Temperature: Absorber – Input and Output - Input
 Source: The Regents of University of California

CONDITION B: Constant input temperatures of fluid, T_{in}

Table 13. Variation of output temperature of fluid when the input temperature is kept constant at $T_{in}=400$ K

Source: The Regents of University of California

G_s [W/m ²]	T_{out} [K]	δT [K]	T_A [K]	$\delta_{Absorber}$ [K]	T_g [K]	δ_{Glass} [K]	q_{cond} [W]	Eff_{total}
1000	404.9	4.855	474.4	74.36	305.2	-94.78	208.3	0.6375
1100	405.4	5.358	482.1	82.07	306.2	-93.81	229.9	0.6396
1200	405.9	5.858	489.7	89.73	307.2	-92.82	251.3	0.641
1300	406.4	6.356	497.3	97.35	308.2	-91.8	272.7	0.642
1400	406.9	6.851	504.9	104.9	309.3	-90.74	293.9	0.6425
1500	407.3	7.343	512.5	112.5	310.3	-89.66	315	0.6428
1600	407.8	7.832	520	120	311.4	-88.56	336	0.6427
1700	408.3	8.319	527.4	127.4	312.6	-87.42	356.9	0.6425
1800	408.8	8.802	534.8	134.8	313.7	-86.26	377.6	0.6421
1900	409.3	9.283	542.2	142.2	314.9	-85.07	398.2	0.6415
2000	409.8	9.761	549.5	149.5	316.1	-83.85	418.7	0.6408

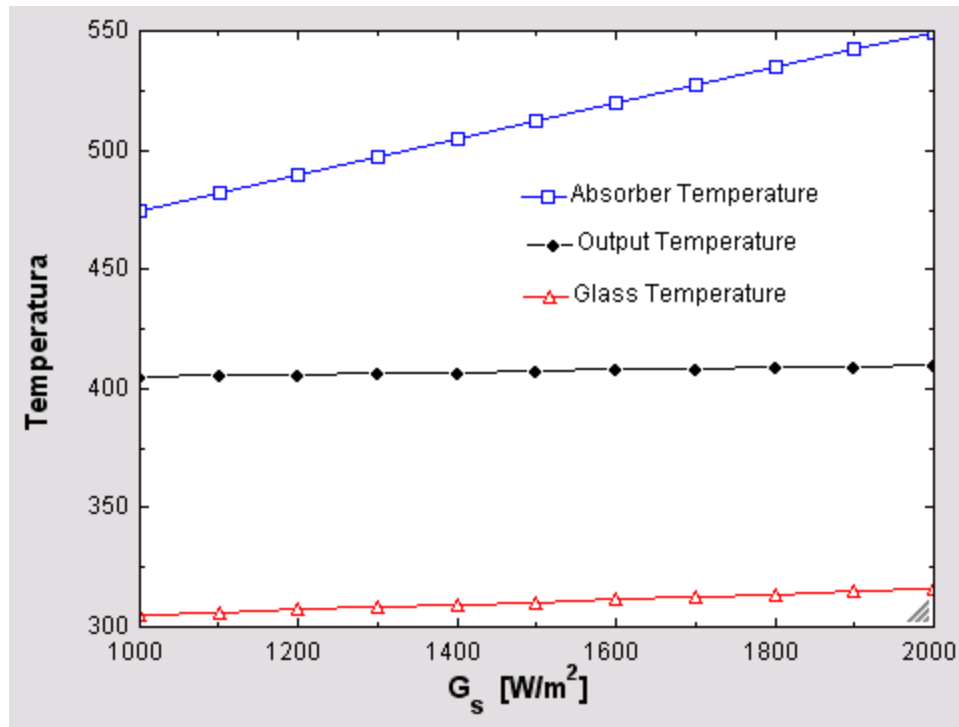


Figure 55. Output temperature of fluid when input temperature is kept constant at $T_{in}=400$ K
 Source: The Regents of University of California

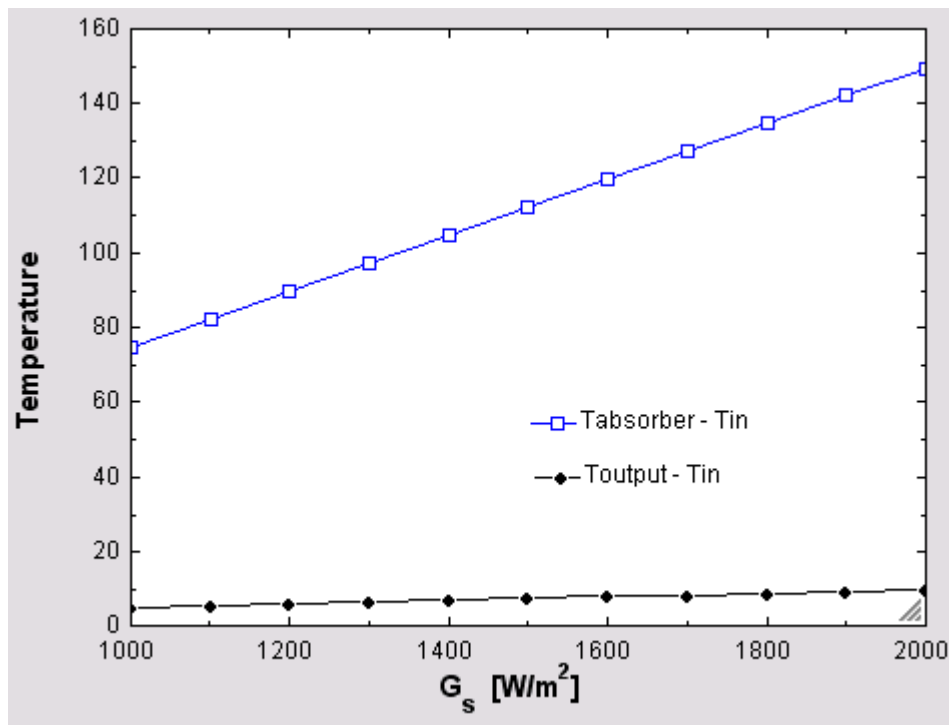


Figure 56. Differences in Temperature: Absorber – Input and Output - Input
 Source: The Regents of University of California

Table 14. Variation of output temperature of fluid when the input temperature is kept constant at $T_{in}=473$ K

Source: The Regents of University of California

G_s [W/m ²]	T_{out} [K]	δT [K]	T_A [K]	$\delta Absorber$ [K]	T_g [K]	$\delta Glass$ [K]	q_{cond} [W]	Eff_{total}
1000	477.3	4.256	538.2	65.18	312.7	-160.3	182.6	0.5588
1100	477.7	4.735	545.5	72.52	314	-159	203.1	0.5652
1200	478.2	5.212	552.8	79.82	315.2	-157.8	223.6	0.5702
1300	478.7	5.685	560.1	87.08	316.5	-156.5	243.9	0.5742
1400	479.2	6.156	567.3	94.28	317.8	-155.2	264.1	0.5773
1500	479.6	6.623	574.4	101.4	319.1	-153.9	284.1	0.5798
1600	480.1	7.088	581.6	108.6	320.4	-152.6	304.1	0.5817
1700	480.5	7.55	588.6	115.6	321.8	-151.2	323.9	0.5831
1800	481	8.008	595.7	122.7	323.2	-149.8	343.6	0.5842
1900	481.5	8.464	602.6	129.6	324.6	-148.4	363.1	0.5849
2000	481.9	8.916	609.6	136.6	326	-147	382.5	0.5854

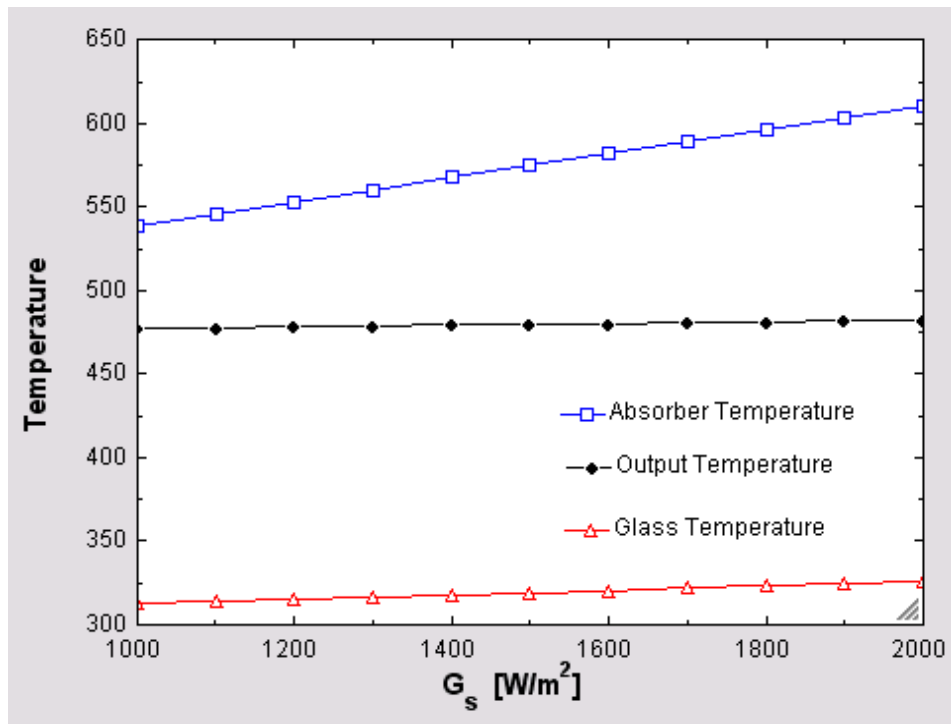


Figure 57. Output temperature of fluid when input temperature is kept constant at $T_{in}=473$ K

Source: The Regents of University of California

Considering thermal resistance of absorber

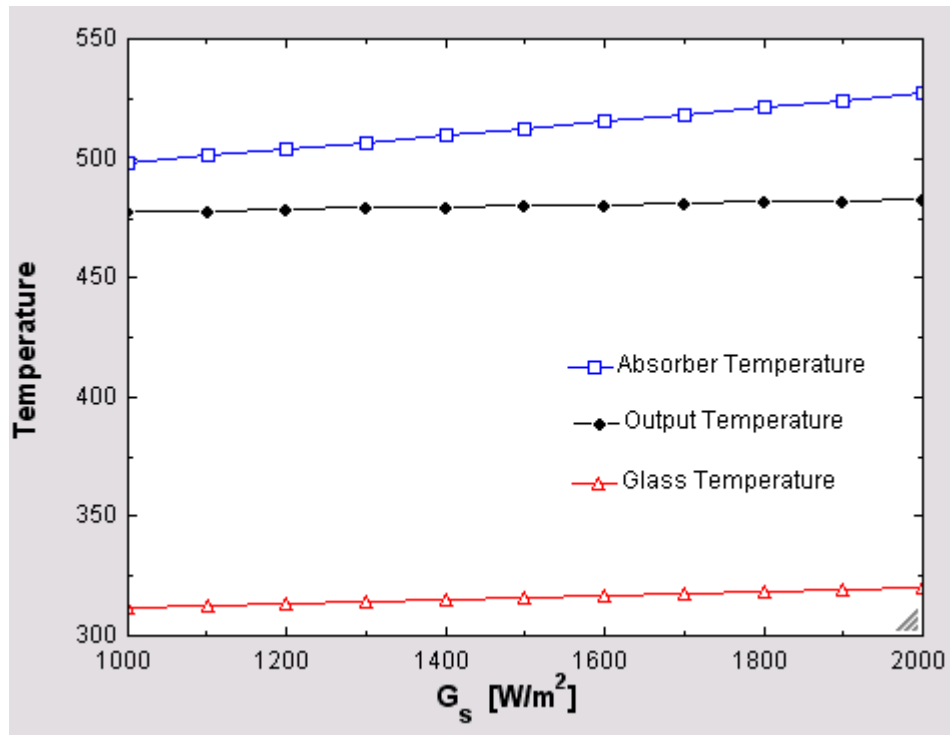


Figure 58. Output temperature of fluid when input temperature is kept constant at $T_{in}=473$ K
Source: The Regents of University of California

Neglecting thermal resistance of absorber

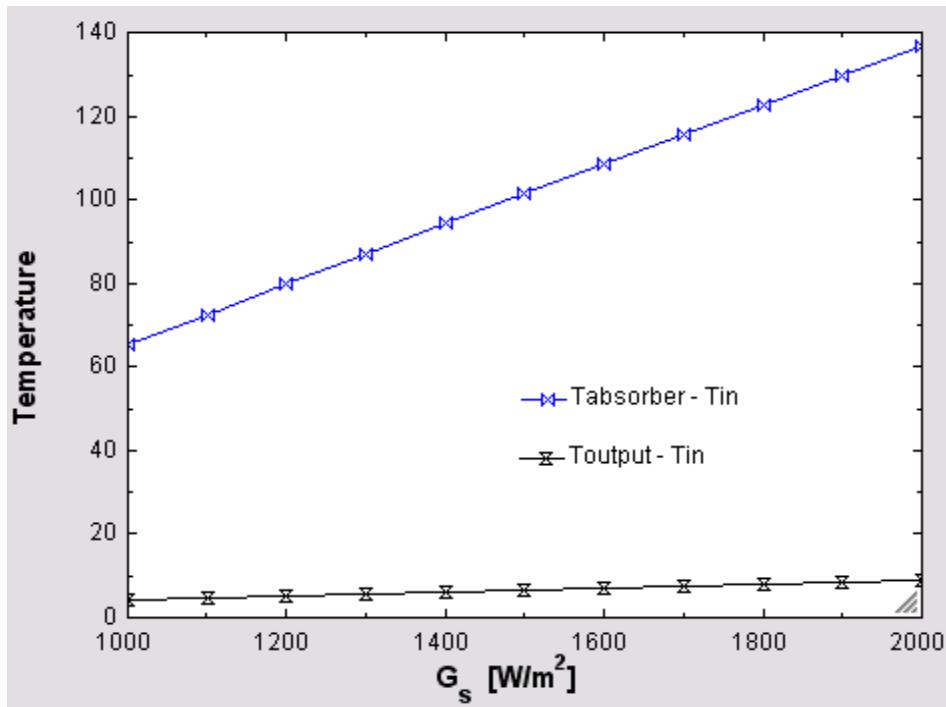


Figure 59. Differences in Temperature: Absorber – Input and Output – Input
Source: The Regents of University of California

Concept 1 - All glass dewar: Direct Flow Preliminary Results

I: Physical Dimensions:

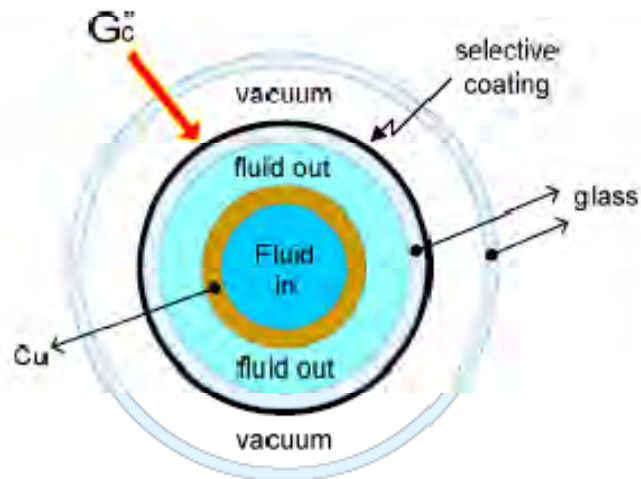


Figure 1
Sketch of all-glass dewar tube

Length = 1800 mm = L

External wall: primary glass cover

$\phi = 58 \text{ mm} = D_{out}$

Glass thickness = 2 mm = t_g

External wall: selective coating on glass

$\phi = 45 \text{ mm} = D_A$

Glass thickness + coating: 3 mm = t_2

External wall: Copper tube

$\phi = 30 \text{ mm} = D_{Cu}$

Copper thickness: 1.2 mm = t_{Cu}

II: Heat Transfer Analysis

Assumptions:

- Uniform heat flux on absorber
- Incompressible fluid.
- Constant properties of fluid.
- Constant heat transfer coefficient.
- Negligible fouling factor.
- Negligible potential and kinetic energy changes.
- Fully developed conditions throughout.

A: Glass cover to Absorber interface

Figure 2

Energy balance

B: Absorber to fluid interface

Figure 3

RESULTS

The solutions to equations A to E were obtained with the use of the EES software for two different conditions:

A: Constant irradiation, $G_c = 1000 \text{ W/m}^2$

Different input temperatures of fluid, T_{in}

Table 1

Figure 3

B: Constant input temperatures of fluid, T_{in}

Different irradiation fluxes, G_c

Table 2

Table 3

Table 4

Figure 4

Figure 5

Figure 6

Table 1: Variation of output temperature of fluid when irradiation is kept constant at $G_c = 1000 \text{ W/m}^2$

T_{in} [K]	T_o [K]	δT [K]	T_{sA} [K]	T_g [K]	q_{cond} [K]
300	304.4	4.382	453.8	315.1	188
310	314.3	4.332	462.1	316.1	185.8
320	324.3	4.279	470.2	317.2	183.6
330	334.2	4.224	478.3	318.4	181.2
340	344.2	4.166	486.3	319.5	178.7
350	354.1	4.107	494.2	320.8	176.2
360	364	4.045	502	322	173.5
370	374	3.98	509.7	323.3	170.8
380	383.9	3.914	517.4	324.6	167.9
390	393.8	3.845	525	326	165
400	403.8	3.774	532.5	327.4	161.9
410	413.7	3.701	539.9	328.8	158.8
420	423.6	3.626	547.3	330.3	155.5
430	433.5	3.548	554.6	331.8	152.2
440	443.5	3.468	561.7	333.4	148.8
450	453.4	3.385	568.9	334.9	145.3
460	463.3	3.302	575.9	336.5	141.6
470	473.2	3.215	582.9	338.2	137.9
480	483.1	3.126	589.8	339.8	134.1
490	493	3.036	596.6	341.5	130.2
500	502.9	2.943	603.3	343.2	126.3

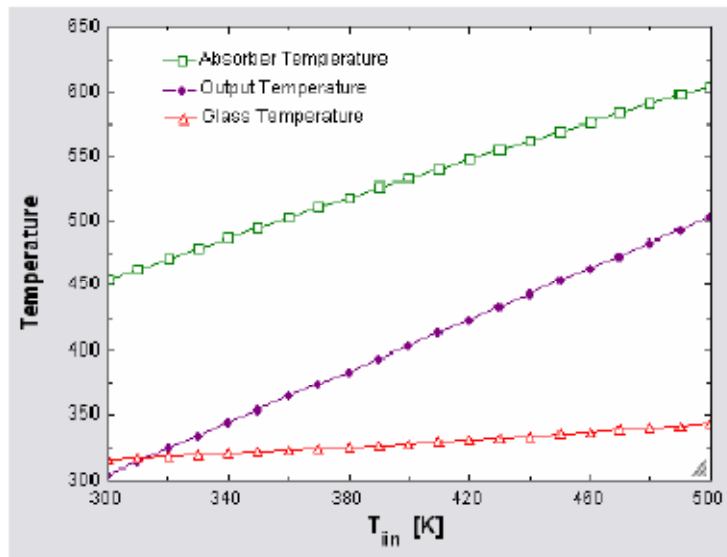


Figure 3

Output temperature of fluid when irradiation is kept constant and while fluid input temperature varies according to table 1

CONDITION B: Constant input temperatures of fluid, T_{in}

Table 2: Variation of output temperature of fluid when the input temperature is kept constant at $T_{in}=350$ K

G_s [W/m ²]	T_s [K]	T_A [K]	T_g [K]	q_{const} [K]
1000	354.1	494.2	320.8	176.2
1100	354.5	507.7	323.7	192.7
1200	354.9	521	326.7	209
1300	355.2	534	329.8	224.9
1400	355.6	546.9	333.1	240.6
1500	356	559.5	336.4	256.9
1600	356.3	571.8	339.7	271
1700	356.7	583.9	343.2	285.9
1800	357	595.8	346.7	300.4
1900	357.3	607.5	350.3	314.7
2000	357.7	619	353.9	328.7

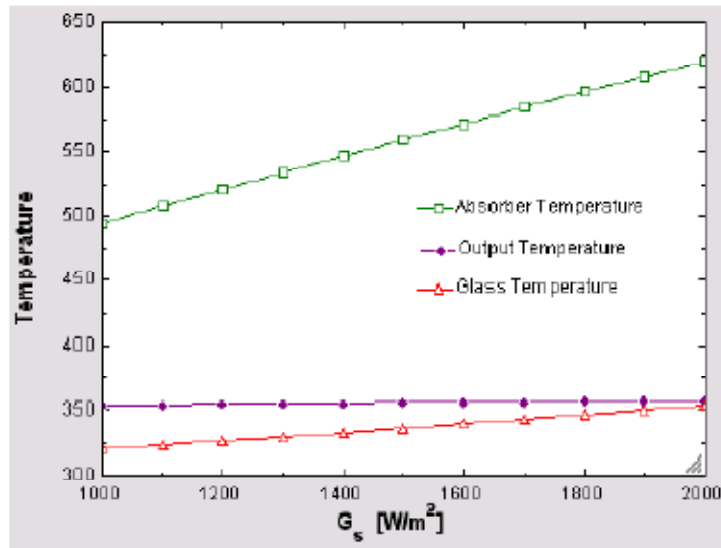


Figure 4
 Output temperature of fluid when input temperature is kept constant at $T_{in}=350$ K

Table 3: Variation of output temperature of fluid when the input temperature is kept constant at $T_{in}=400$ K

G_s [W/m^2]	T_s [K]	δT [K]	T_A [K]	T_g [K]	q_{cond} [K]
1000	403.8	3.774	532.5	327.4	161.9
1100	404.1	4.14	545.3	330.6	177.6
1200	404.5	4.499	558	333.9	193
1300	404.9	4.852	570.3	337.3	208.1
1400	405.2	5.198	582.5	340.8	223
1500	405.5	5.538	594.4	344.3	237.6
1600	405.9	5.871	606.1	347.9	251.9
1700	406.2	6.198	617.6	351.6	265.9
1800	406.5	6.519	628.9	355.3	279.7
1900	406.8	6.834	639.9	359	293.2
2000	407.1	7.144	650.8	362.8	306.5

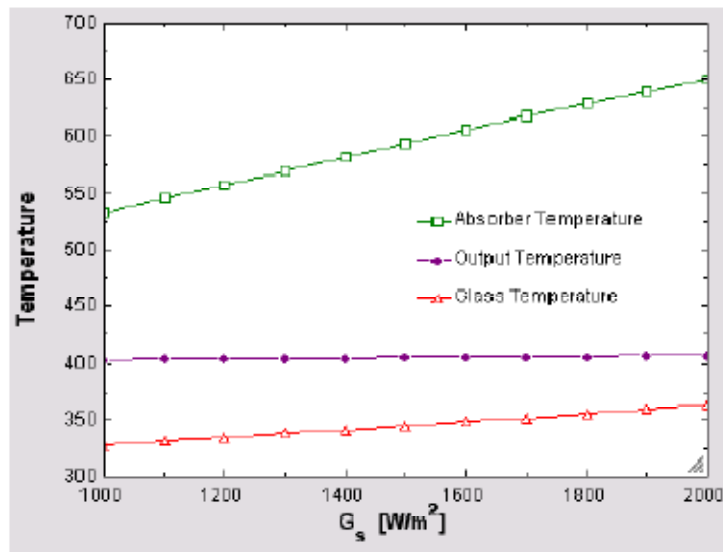


Figure 5
 Output temperature of fluid when input temperature is kept constant at $T_{in}=400$ K

Table 4: Variation of output temperature of fluid when the input temperature is kept constant at $T_{in}=473$ K

G_s [W/m^2]	T_s [K]	δT [K]	T_A [K]	T_g [K]	q_{cond} [K]
1000	476.2	3.189	584.9	336.7	136.8
1100	476.5	3.527	596.8	342.3	151.3
1200	476.9	3.859	608.5	345.9	165.5
1300	477.2	4.185	619.9	349.6	179.5
1400	477.5	4.505	631.1	353.4	193.2
1500	477.8	4.818	642.2	357.2	206.7
1600	478.1	5.126	653	361	219.9
1700	478.4	5.429	663.6	364.9	232.9
1800	478.7	5.726	674	368.8	245.6
1900	479	6.017	684.2	372.7	258.1
2000	479.3	6.304	694.3	376.6	270.4

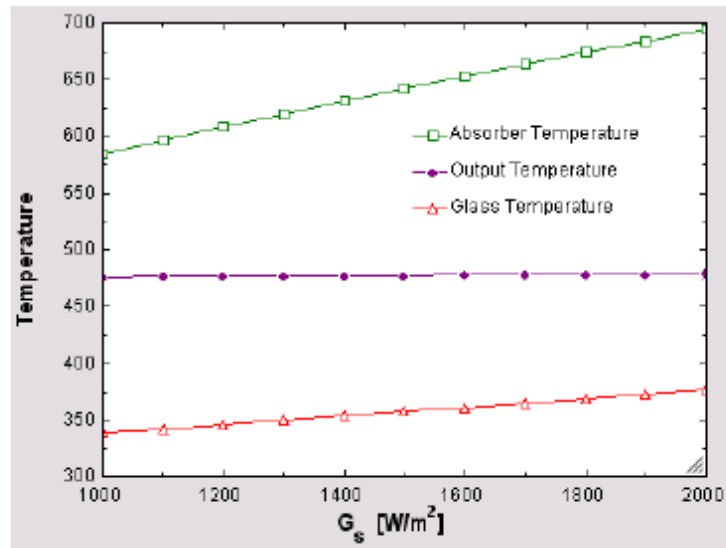


Figure 12
 Output temperature of fluid when input temperature is kept constant at $T_{in}=473$ K

2.5. Task 6

In Task 6, the Contractor has determined the important properties of the existing off-the-shelf components that are being considered for the XCPC. This report is a summary of these component properties. The analyzed components are:

- Reflector
- Glass tube
- Selective coating of absorber
- Heat pipe

Reflector Properties

The three primary types of reflectors suitable for solar concentrators are: silvered glass, polymeric films, and polished/enhanced aluminum sheet. Unfortunately, solar reflector materials have long been a “weak spot” of solar technology, and there are very few commercially-available reflector materials for use in solar concentrators. Long-term outdoor use requires good outdoor weather ability, ultra-violet stability, and good mechanical stability and durability under the extremes of the outdoor environment.

Silvered-glass reflectors offer high reflectance and good outdoor weather ability, but they are quite heavy and fragile. Also, to create the CPC-shaped reflectors that we need for the XCPC will necessitate a significant R&D effort, akin to the major effort that SolFocus is engaged in for their concentrating photovoltaic system that is under development. Since the Task 6 effort is aimed toward existing off-the shelf components, we have not considered the silvered glass approach here.

Metalized polymer films are another type of reflector, and the 3M Company offered several types of metalized films for solar use for many years. 3M manufactured an aluminized film, but it had a reflectance in the mid-80's, which was deemed to be too low and so this film was discontinued. A silvered acrylic film, called ECP-305+, was also made by 3M. But it suffered from "tunneling" problems (essentially, delaminating the acrylic from the silver layer) which ultimately results in 3M's discontinuation of this film too. A relatively recent silvered film has been developed by NREL and ReflecTech, and we consider this alternative in our Task 10 work, which includes consideration of some advanced components and possibilities for performance enhancement with further component development.

Polished aluminum reflectors are generally judged to be the most commercially-available for outdoor solar use. And while polished aluminum is known to lose significant specular reflectance after just 2 to 3 years of outdoor use, Alanod¹ (a German-based company) has made a great deal of technical progress in advancing and improving this approach. Alanod has developed specialized coating techniques that increase the reflectance of their aluminum-based reflective materials, as well as increase outdoor weatherability. Alanod has two commercially-ready reflective materials for outdoor solar energy utilization: Alanod MiroSun and Alanod 4270 KKSP. Both are aluminum based reflectors, and samples of these materials were supplied to NREL for optical measurements. The measured hemispherical reflectance vs. wavelength values is shown below.

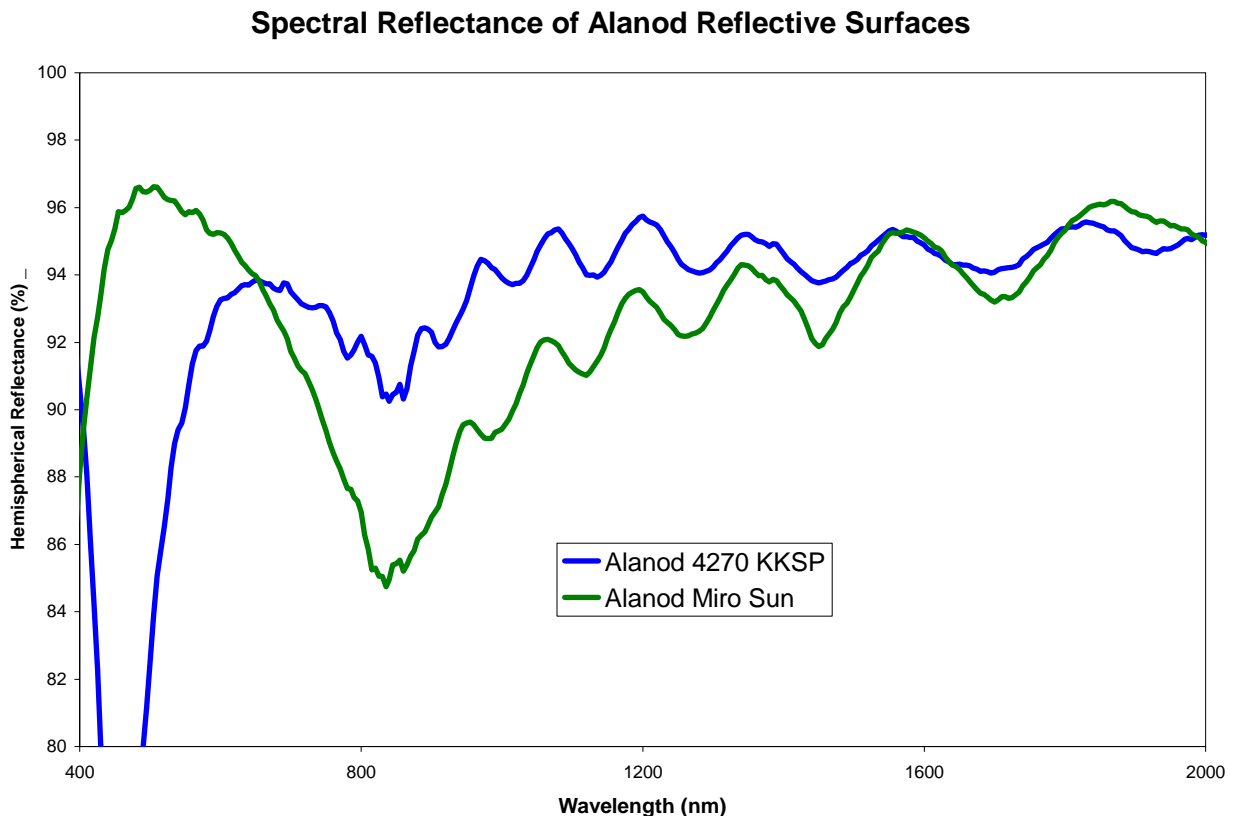


Figure 60. Spectral reflectance of Alanod Reflective Surfaces
 Source: The Regents of University of California

¹ <http://www.alanod.com/opencms/sites/alanod.de/en/miro/MIRO-SOLAR/mirosun.html>

Weighting the reflectance values by an airmass-1.5 solar spectrum allows determination of the overall hemispherical reflectance for solar thermal applications, since the entire solar spectrum provides useful energy for thermal conversion. The solar-weighted hemispherical reflectance of Alanod Miro Sun is 91.9%. The solar-weighted hemispherical reflectance of Alanod 4270 KKSP is 91.5%. Hemispherical reflectance includes all reflected light from the sample, regardless of its reflected direction.

Another common way to characterize reflective surfaces is to measure specular reflectance, which excludes reflected light that is scattered, that is, reflected outside a specified acceptance cone angle. The Devices and Services portable specular reflectometer Model 15R provides this measurement, but for a specific wavelength of 660 nm. This instrument was used to measure specular reflectance of both Alanod reflector materials, with the largest acceptance angle (46 milliradians) available on the Model 15R. Alanod MiroSun measured 86%, and the 4270 KKSP measured 90.0%. There is a significant difference between the specular reflectance values at 660 nm and the hemispherical reflectance (also taken at 660 nm), indicating that there is a significant amount of scattering. Given the high acceptance angles of the CPCs, we expect that performance will be more closely governed by hemispherical reflectance than specular reflectance, but will be somewhere in between. To be conservative, in our modeling efforts to date we have assumed a reflectance value of 90%.

The specularly of reflective materials is known to sometimes be affected by material forming operations (such as bending, roll-forming, etc.) since these operations can sometimes alter the front portions of the reflective material. To determine whether this might be the case with Alanod, for the radii needed for our CPC, a virgin piece of flat Alanod 4270 KKSP was measured with the Devices and Services portable specular reflectometer, then formed/rolled to a radius of 1.12 inches (28 mm) as shown in the left-most photo below.

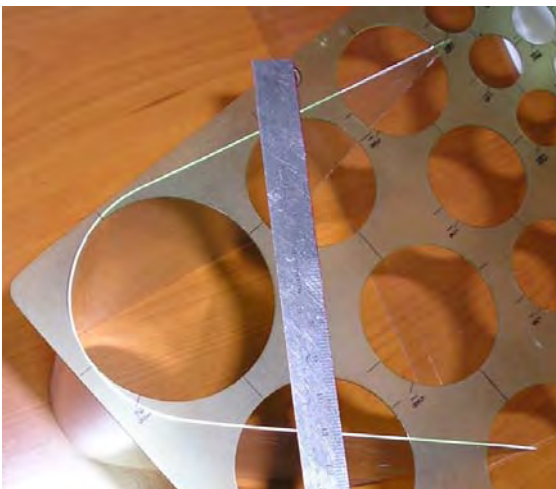


Figure 61: Measuring radius
Source: The Regents of University of California

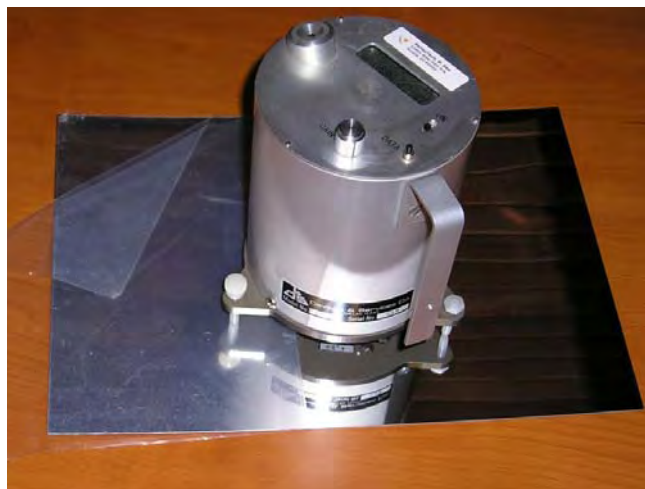


Figure 62: Reflectivity measurements of Alanod
Source: The Regents of University of California

The formed sheet was then flattened, and measurements were obtained again with the D&S specular reflectometer², as shown in the right-most photo above. These measurements were within 0.1% of the original values, indicating that specular loss is not anticipated to be an issue for the amount of roll-forming required to form the CPC profiles.

Glass Transmittance

The commercially available evacuated tubes that are mass-produced in China use borosilicate glass. Borosilicate glass is a high quality glass with low thermal expansion and excellent solar transmittance. Solar energy absorption within the glass is very small; the optical loss of borosilicate glass is dominated by reflection losses (Fresnel losses) due to the higher index of refraction of glass compared to air. As light passes through a glass cylinder (e.g. a glass dewar) to the absorber surface within it, the light encounters two interfaces: one at the outer surface of the glass and one at the inner surface of the glass. Each interface yields a loss of about 4%, so the total reflectance loss is about 8%.

The transmittance of a typical borosilicate glass (Corning 7740) sample is shown below, and yields a solar-y

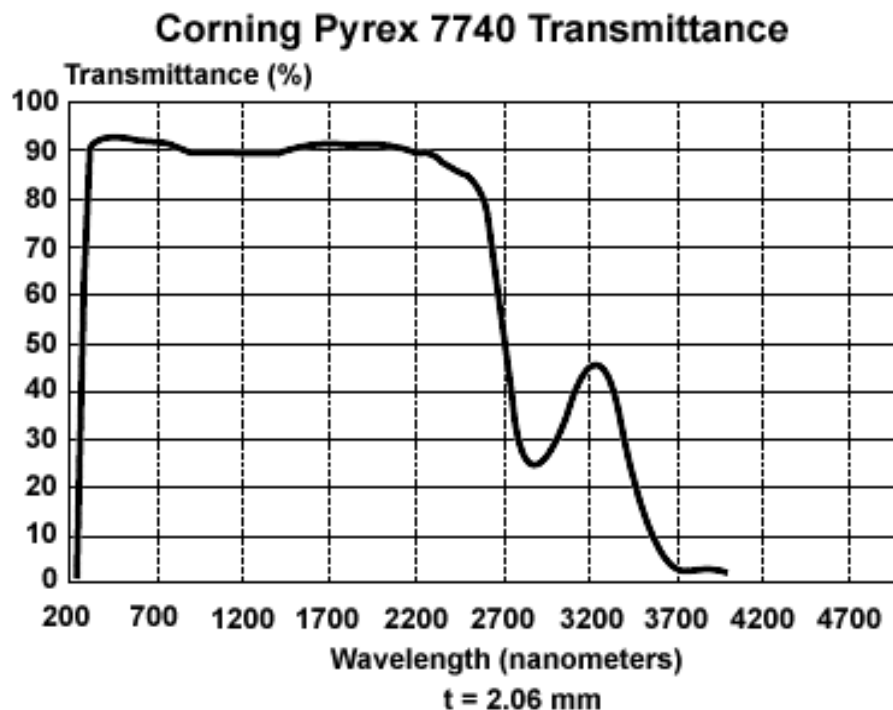


Figure 63. Corning Pyrez 7740 Transmittance

Source: The Regents of University of California

To verify that the glass used in the Chinese-manufactured evacuated tubes is of the same high quality as noted above, samples were taken from a Chinese-manufactured evacuated tube (i.e. the standard dewars we contemplate using in certain of our XCPC designs) and tested at NREL

² <http://www.devicesandservices.com/>

by Cheryl Kennedy for transmittance with their Perkin-Elmer spectrophotometer. The instrument is pictured below to the left, and a close up of the glass sample, mounted in the instrument, as shown on the next page:



Figure 64. Perkin-Elmer spectrophotometer
Source: The Regents of University of California



Figure 65. Perkin-Elmer spectrophotometer
Source: The Regents of University of California

The measured transmittance vs. wavelength is shown below.

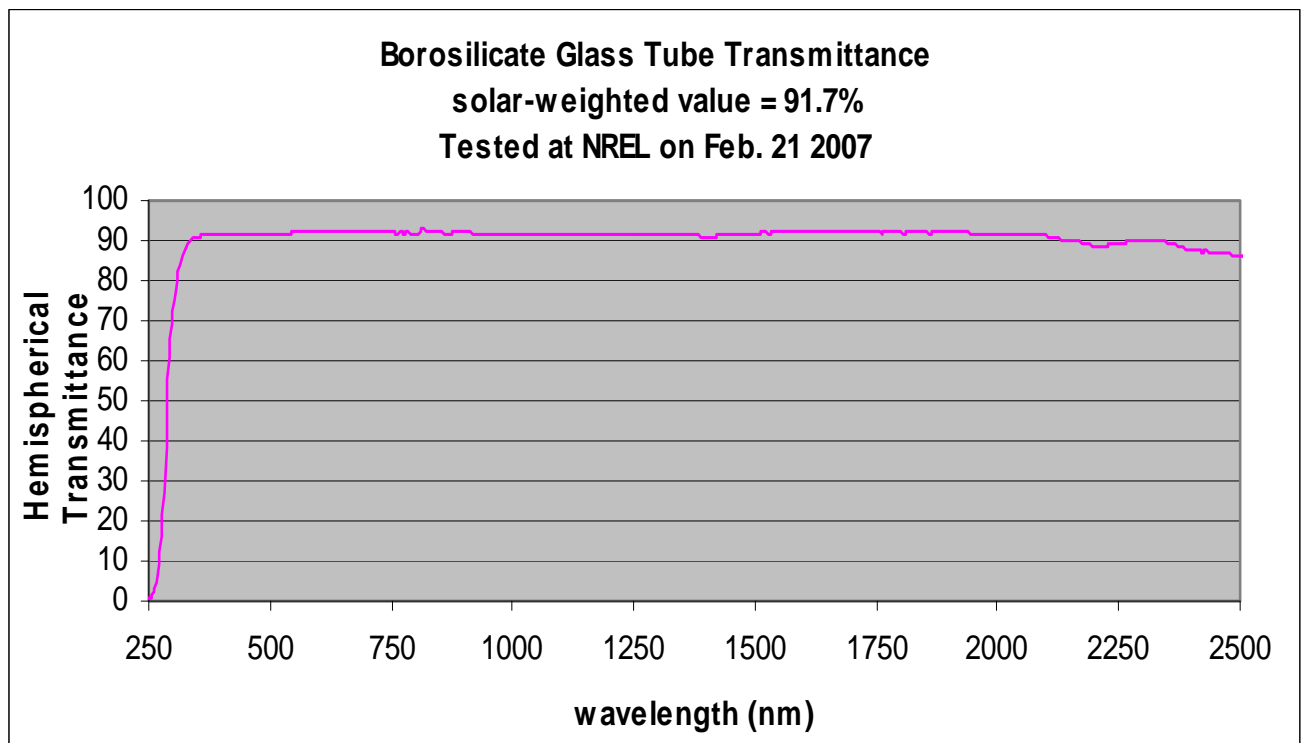


Figure 66. Borosilicate Glass Tube Transmittance
Source: The Regents of University of California

The solar-weighted transmittance was found to be 91.7%, a bit higher than anticipated and a good indication that the glass is indeed of high quality.

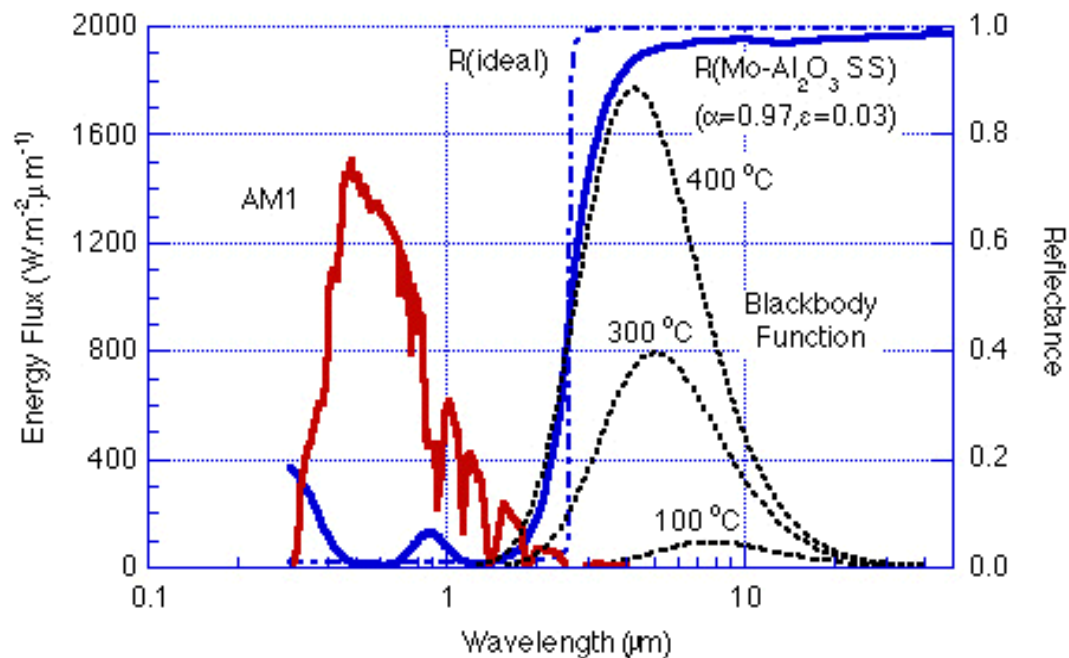


Figure 67. Selective coating properties

Source: The Regents of University of California

Selective Coatings

The two performance-related properties of the selective coatings are absorptance and emittance. Although there are some limited absorptance and emittance values available from product suppliers, we have taken steps to determine these two properties through independent testing.

Most of the commercially available evacuated tubes that are mass-produced in China use an aluminum nitride vacuum sputtered coating that provides for selective properties. With the term “selective” we mean spectrally selective, an absorber that has different spectral reflectance at different wavelengths. We desire that the reflectance of the coating over the solar spectrum is very low, while the reflectance of the coating over most of the infra-red spectrum is very high. An example of a very high quality highly-selective Mo-Al₂O₃-on-stainless coating is illustrated in the figure below as the heavier solid blue line. Note that the reflectance increases sharply just above the wavelengths of the solar spectrum (the solid red line). Note also that the blackbody spectrum for temperatures of 100°C, 300°C and 400°C are also indicated on the figure. Since the blackbody spectrum increasingly extends into the lower wavelength regions as the temperature increases, it is clear that selective surfaces can be expected to have increased emittance as temperatures increase.

There is another factor at work here also, which can further increase the emittance of the selective coating as temperature increases. The reflectance vs. wavelength relationship of surfaces (and selective coatings) can change, depending on temperature. The heavy blue solid line reflectance values are typically obtained using a spectrophotometer, with the sample at

room temperature. But at higher temperatures, the reflectance values can be different. To account for this change, and be sure that the proper emittance is known (especially if thermal models are being used for performance prediction) it is best to measure the selective coating reflectance values at the higher temperatures of interest. Since the selective coating emittance is a key determinant of the performance of our XCPC collectors, samples have been measured at room temperature and 200°C, as part of this Task 6 work effort. Few laboratories have the capability to measure emittance at 200°C. NREL presently does not, for example, but they referred us to Surface Optics Corporation (SOC) in San Diego.

SOC measured the optical properties of selective coating samples that we provided to them from:

- a) three commercially available Chinese dewars manufacturers (Paradigma, Tsinghua, and SunRain),
- b) a commercially-available selective foil (TiNOX) that can be used within our sealed-glass design, and
- c) a custom-produced vacuum-deposited selective foil manufactured in China by Eurocon, the vendor that has manufactured our sealed-glass prototype tubes.

The emittance results obtained by SOC for these various selective coatings are provided below in Table 1, along with the solar-weighted absorptance of the coatings, another key optical characteristic that is of primary importance. A coatings solar-weighted absorptance is the fraction of the solar spectrum that will be absorbed by the coating.

	Solar-Wt	Emittance	Emittance	Coating
Chinese all-glass dewars	Absorptance	@ 27C	@ 200C	Substrate
Paradigma	0.883	0.1	0.15	glass
Tsinghua	0.923	0.05	0.074	glass
SunRain	0.913	0.047	0.088	glass
Metal Foils for Sealed Glass Tubes				
TiNOX	0.958	0.035	0.158	copper
Eurocon	0.902	0.05	0.064	aluminum

Also, to gain a full understanding of absorptance, we need to determine the variation of absorptance with incidence angle. This can have a significant impact on performance. A typical illustration of this affect is shown below. (We have used this figure for our performance estimates.)

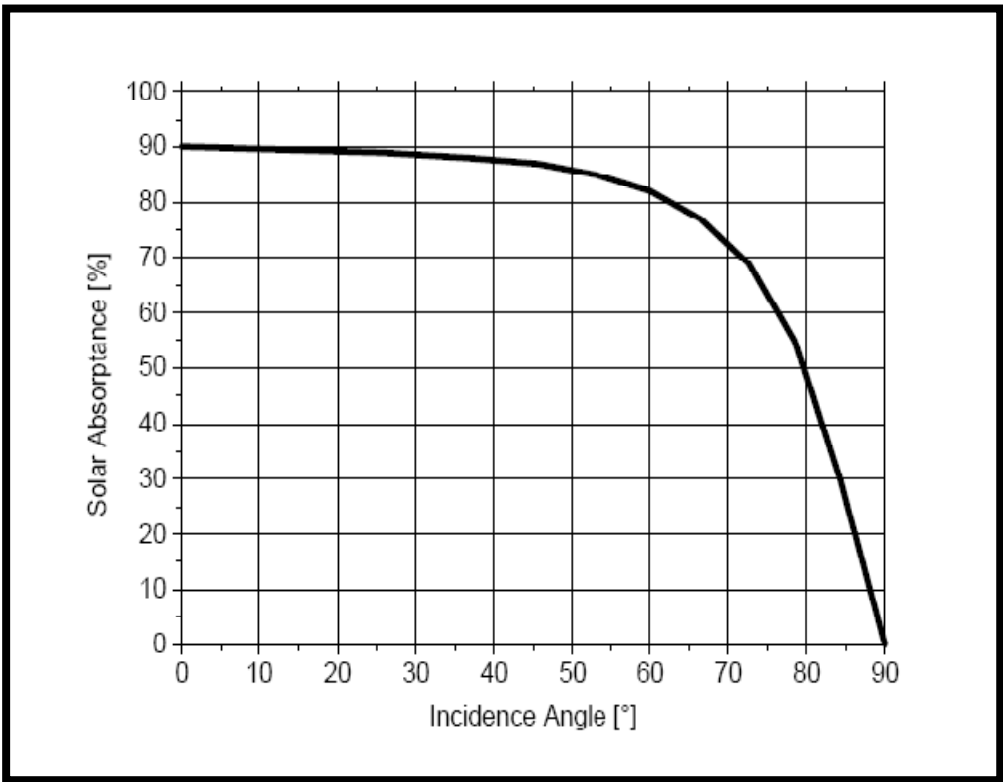


Figure 68. Expected absorbance of selective coating as a function of incidence angle
 Source: The Regents of University of California

To check whether the commercially-available selective coatings that we are evaluating do indeed have an absorbance drop-off with incidence angle of approximately this amount, we have tested two of the materials at incidence angles of 60 and 75 degrees (the range of greatest absorbance

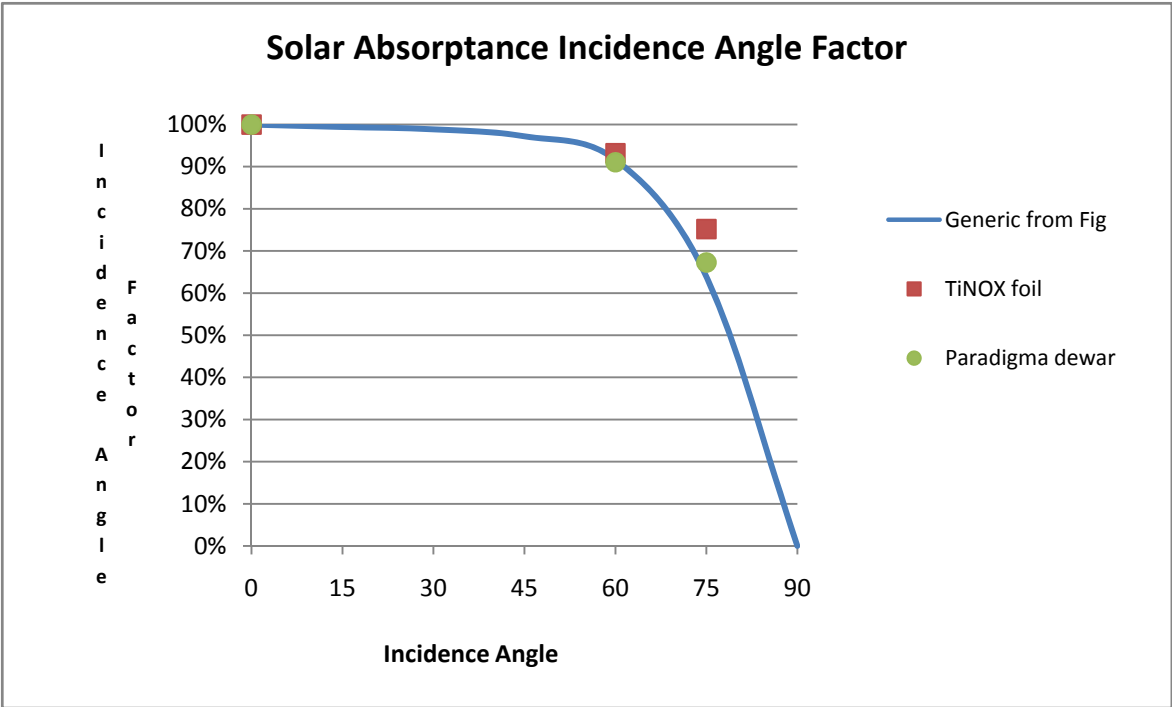


Figure 69: Measured absorbance of selective coating as a function of incidence angle
 Source: The Regents of University of California

decrease) and compared these values with their normal-incidence absorptance values. The data points obtained (for the TiNOX foil and the Paradigma dewar) are plotted onto the generic figure shown earlier. Note that the values are in quite good agreement with what had been expected.

Heat Pipes

The approximate capacity of the Chinese heat pipes that we consider using for the XCPC has been estimated by United Technologies Research Center using simple modeling techniques from first principles. It is to be noted that the analysis was done based on the external geometrical dimensions and the data provided by the manufacturer about internal construction and contents of the tube.

Background

Thermosyphons and heat pipes are devices that transport heat from one location to another (or one fluid stream to another) by using a cyclic process of vaporization and condensation of a charge (working fluid) inside a sealed tube. Heat is supplied to the evaporator (or hot end) of the tube which conducts across the tube wall and heats the working fluid inside which upon reaching its vaporizing temperature evaporates to the center of the tube and travels towards the cold end (condenser) of the tube. Typically the cold end is cooled by external means, whereby the vapor inside the tube reaching the cold end condenses, giving up the latent heat of vaporization. The condensed fluid inside the tube then must return back to the evaporator end of heat pipe, so that the cycle can continue. In heat pipes this return of the condensed fluid back to the evaporator end is achieved by intricate wick structures through which the liquid can travel using surface tension. In thermosyphons there are no wicks and hence return of fluid to evaporator is solely aided by gravity. As such in thermosyphons the devices must be so installed that the condenser is at an elevated level with respect to the evaporator. In this report, however, the terms “heat pipes” and “thermosyphons” will be used interchangeably unless a distinction needs to be made.

In both devices, however, since the heat transfer occurs by means of evaporation/ condensation of a fluid at or near its saturated state, there is very little temperature gradient between the hot and cold ends (in other words there is very little difference in “quality” of the heat as it travels from hot to cold end, unlike solid metal conductors). Also, since latent heats of vaporization of the commonly used fluids are large, a relatively high rate of heat transfer is possible, depending on the mass flow rate of the fluid inside. Furthermore, the operating temperature of a heat pipe is fairly constant at its design temperature, since the saturation temperature of any fluid is constant at a given pressure and once manufactured there is no way to change the pressure inside sealed heat pipes.

Heat Transfer Limitations of a Heat Pipe

The amount of thermal energy that a heat pipe can transport from its hot end to its cold end can be limited by three major ways:

1. Maximum heat that can be radially transferred from the hot external source to the working fluid inside – Evaporator Limit – which is a function of the tube wall properties and geometry, surface area of heat pipe at the evaporator section, and temperature difference between source and the operating temperature of the heat pipe.
2. Axial heat transport limit of the heat pipe – Axial Heat Flux Limit – which can be due to Capillary Limit, Boiling Limit, Entrainment Limit, Sonic Limit and some other limiting criteria, some of which will be discussed in detail below.
3. Maximum heat that can be radially transferred from the working fluid inside at the cold end to the external sink – Condenser Limit - which is a function of the tube wall properties and geometry, surface area of heat pipe at the condenser section, and temperature difference between sink and the operating temperature of the heat pipe.

In this analysis, the Evaporator Limit of the heat pipe is not evaluated. The work here focuses on estimating the Axial Heat Flux Limit and the Condenser Limit.

Assumptions

The purchased Chinese off-the-shelf devices (from Beijing Eurocon Solar Energy Tech. Co. Ltd.) are clearly thermosyphons, since they do not have any internal wick structure. The charge inside is a proprietary mixture which is 80% by volume water and water is the only fluid that participates in heat transfer. It is assumed that while the pipe is designed for 80 – 100 C operation, it can be operated safely at a much elevated temperature of 200 C. The intent of this analysis is to estimate the performance of the device as it operates at 200 C. Fig.1 shows the heat pipes and the known key physical attributes.

Calculation of Axial Heat Flux

Axial transport of heat in a thermosyphon can be limited by a number of physical phenomena like attainment of sonic velocity in the heat pipe vapor, entrainment of the heat pipe liquid by its vapor or the onset of boiling in the heat pipe liquid. There are some other means of limiting the heat flux and Table 1 (Ref. 1) provides a list and a brief explanation. Based on our understanding of the operating procedures of these heat pipes, it is thought that only limits due to entrainment or vapor reaching sonic velocity are of relevance.

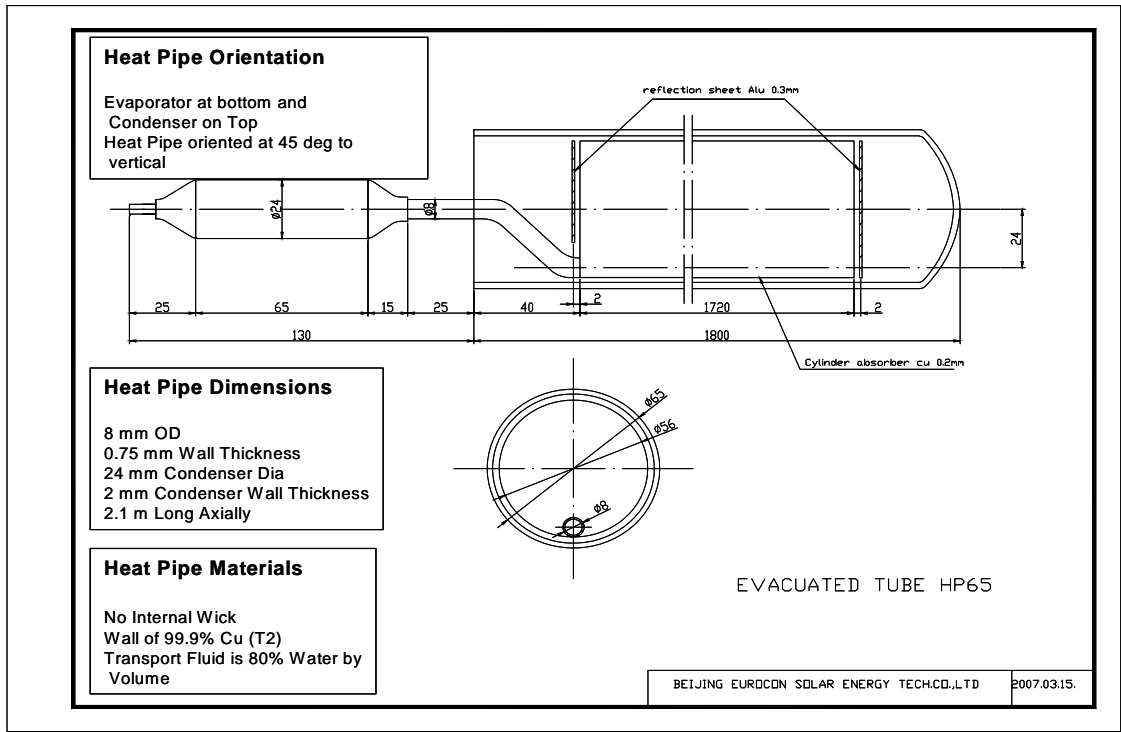


Figure 70. Beijing Eurocon Heat Pipe Geometry and Characteristics

Source: The Regents of University of California

Sonic Limit

Sonic Velocity Limit is calculated based on the maximum allowable velocity of the vapor in the evaporating section of the heat pipe which cannot exceed the sonic velocity of vapor at the operating temperature of the heat pipe. Based on this limiting velocity, density of vapor and latent heat of vaporization, the maximum axial heat flux limit Q_s (Eqn. 1) is calculated. The Sonic Limit is simply this axial heat flux multiplied by the available cross-section for vapor flow.

$$Q_s = \frac{\rho V L}{1 + (1 + FM) * \Gamma} \sqrt{\frac{1 + \Gamma}{2}} \dots\dots\dots \text{Eqn. 1}$$

where ρ = Density of vapor,

V = Sonic velocity in evaporator

L = Latent heat of vaporization

Γ = Gas Constant for steam

& FM = Momentum Correction Factor

Calculation of Sonic Limit was performed at 100 C, 150 C, 200 C and 250 C and the results are shown in Table 15.

Heat Transport Limit	Description	Cause	Potential Solution
Viscous	Viscous forces prevent vapor flow in the heat pipe	Heat pipe operating below recommended operating temperature	Increase heat pipe operating temperature or find alternative working fluid
Sonic	Vapor flow reaches sonic velocity when exiting heat pipe evaporator resulting in a constant heat pipe power transport and large temperature gradients	Power/temperature combination, too much power at low operating temperature	This is typically only a problem at start-up. The heat pipe will carry a set power and the large ΔT will self correct as the heat pipe warms up
Entrainment –Flooding	High velocity vapor flow prevents condensate from returning to evaporator	Heat pipe operating above designed power input or at too low of an operating temperature	Increase vapor space diameter or operating temperature
Capillary	Sum of gravitational, liquid and vapor flow pressure drops exceed the capillary pumping pressure of the heat pipe wick structure	Heat pipe input power exceeds the design heat transport capacity of the heat pipe	Modify heat pipe wick structure design or reduce power input
Boiling	Film boiling in heat pipe evaporator typically initiates at about 5-10 W/cm ² for screen wicks and 25-35 W/cm ² for powder metal wicks	High radial heat flux causes film boiling resulting in heat pipe dryout and large thermal resistances	Use a wick with a higher heat flux capacity or spread out the heat load

Table 15. Heat Pipe Heat Transport Limitations

Source: The Regents of University of California

Entrainment Limit

Entrainment Limit is essentially due to the fact that water returning from the condenser is entrained in the vapor flowing towards the condenser and this water is lost from the evaporation process, thereby limiting the heat transfer rate. In a thermosyphon, this can happen due to two separate processes which can be interrelated. However, since an analysis that accounts for these two effects together can be very complicated, in this first order analysis the two phenomena are considered independently.

The first of these effects is due to the vapor inertia force acting over the vapor space cross-section, which can result in liquid drops being stripped by vapor and being carried back to condenser without getting a chance to evaporate. In this study, this entrainment limit is denoted as $Q_{E,vap}$. This vapor inertia force is countered by the stabilizing force of surface tension of the liquid, acting over the circumference of the vapor space, which prevents droplet formation. Typically, this competing nature of two forces is quantified in the Weber Number ($We = \rho V^2 D / 4\sigma$), where V is the velocity of the vapor, D is the vapor space diameter and ρ and σ are explained below. For Weber Number more than 1, it is assumed that entrainment takes

place. After solving for the vapor velocity by setting Weber No to 1, the vapor-based entrainment limit flux $Q_{E,vap}$ is calculated according to Eqn. 2. In typical heat pipes with wicks, this is the only limit that is relevant.

$$Q_{E,vap} = L^* \sqrt{\frac{2\Pi \sigma \rho}{\Omega D}} \dots\dots\dots \text{Eqn. 2}$$

where Ω = Momentum Factor = 2.2 for turbulent flow,

ρ = Density of vapor

σ = Surface tension of liquid water

An additional mechanism for entrainment should be investigated in the thermosyphons under consideration, since they are wickless and the liquid return is solely under the influence of gravity. In such a situation, the liquid “trickles” down the walls of the pipe from the condenser and the film thickness and velocity of flow are determined by well defined correlations that depend on the viscosity and the surface tension of the liquid. For films thicker than this limiting thickness, the water film will develop instabilities on the surface and break down into drops which can be entrained in the vapor flowing out of the evaporator. This entrainment limit, denoted by $Q_{E,liq}$, is also based on Weber Number being equal to or more than 1. However, the Weber No is defined as $We = \rho_l V^2 \delta / 2\mu$, where ρ_l and V refer to liquid density and film velocity respectively and δ is the thickness of the liquid film. The velocity of a liquid film falling under gravity is given by the well-known Eqn. 3. Combining with the definition of Weber No and setting We to 1, one can derive Eqn. 4 to calculate the liquid film thickness. This will lead to the calculation of liquid film velocity and hence the limiting rate of liquid return. The $Q_{E,liq}$ can be calculated as the product of this liquid flow rate and the latent heat of vaporization of water as in Eqn.5.

$$V_l = \frac{\rho_l g \cos \theta}{3\mu} \delta^2 \dots\dots\dots \text{Eqn. 3}$$

and

$$\delta = \sqrt[5]{\frac{18\mu^2 \sigma}{\rho_l^2 (g \cos \theta)^2}} \dots\dots\dots \text{Eqn. 4}$$

where μ = Viscosity of water,

g = Acceleration due to gravity

& θ = the angle with the vertical

$$Q_{E,liq} = A^* L^* \rho_l V_l \dots\dots\dots \text{Eqn. 5}$$

Table 16 shows the calculated values of $Q_{E,vap}$ and $Q_{E,liq}$ for operating temperatures of 100 C, 150 C, 200 C and 250 C. For 200C, this limiting flux is 1.25 kW. Since the needed heat transport

capacity of these devices - based on solar irradiation - is no more than 300 W, the pipes are adequate to perform this task.

Table 16. Estimated Heat Transport Limits

Temperature (C)	Sonic Limit (W)	Entrainment Limit(vapor) (W)	Entrainment Limit (liq) (W)	Overall Heat Transport Limit (W)
100	8000	414	2200	414
150	31700	1180	1700	1180
200	96000	5310	1250	1250
250	232751	16400	850	850

Source: The Regents of University of California

Condenser Limit

The maximum heat transfer limit at the condenser is a function of not only the heat pipe condenser design but also the design of the manifold through which the external cooling liquid flows. Fig.2 shows a detailed picture of this manifold at a typical condenser location. The Cu walled thermosyphon condenser is snugly fit into a Cu sleeve that is inserted perpendicular to the flow of the external cooling fluid in the manifold.

The calculation assumes that the cooling fluid (Duratherm) flows over the cylindrical condenser and based on the effective area at the junction, flow velocity is calculated. The Reynolds No based on the velocity and the outside diameter of the sleeve is in the turbulent range. Nusselt number is calculated based on this Reynolds No and Prandtl No for Duratherm according to the following equation (Eqn.6):

$$Nu = C \cdot Re^m \cdot Pr^n \dots\dots\dots Eqn.6$$

where C = 0.26, m = 0.6, n = 0.36

Once the external heat transfer coefficient, h, is calculated from the Nusselt number based on the sleeve OD, equation for conjugate heat transfer through tube wall cooled on one side is used to calculate the net heat transferred in the condenser. Since the process inside the condenser is a phase change process, it is assumed that the resistance to heat transfer inside the condenser is negligible and the inside wall of the copper tube is at the condensing temperature. Table 3 lists key results of the calculations. It is shown that the current condenser design can transmit only 80 W of heat under the specified assumptions.

Discussion

The above analysis clearly establishes the overall limits of the Beijing Eurocon thermosyphons at different operating conditions. Particularly at 200 C – the operating temperature of interest, the device transfers 80 W of heat, limited by the condenser performance. It is imperative that the condenser (and/or manifold) design be improved to be able to use them in solar applications, where the demand is to transfer 300 W per pipe. However, a few other issues are of concern too.

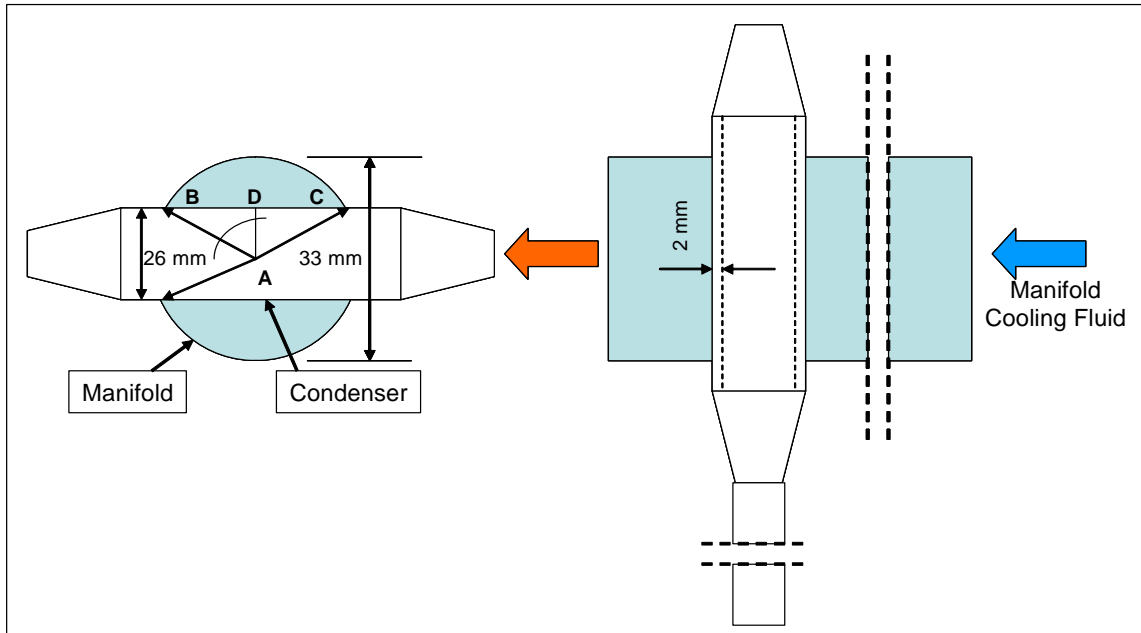


Figure 71. Manifold and Heat Pipe Arrangement

Source: The Regents of University of California

Table 17: Condenser Side Heat Transfer Estimates

Source: The Regents of University of California

Flow Rate of Duratherm	gpm	1
Prandtl No.		25.7
Effective Flow Area in Manifold	cm ²	9.67
Reynolds No		8700
Nusselt No		194
Heat Transfer Coefficient, h	W/m ² /K	1010
Temperature Difference Across Condenser	C	30
Heat Transfer from Condenser	W	81

Firstly, it has been suggested that these pipes are originally designed to operate between 80 and 100 C and to transfer about 100 W (consistent with condenser design and Table 16 data). If they are operated at 200 C, then the vapor inside is operating at a superheated state. The pressure of superheated steam at 200 C is about 1.5 MPa. So one hopes that the tubes are strong enough to withstand this pressure for which they were not built.

Secondly, the only way it will operate at 200 C is if the minimum temperature of the manifold fluid is 200 C. In the manifold, the thermosyphons are arranged in series and the first one in the series will encounter fluid returning from CHP heat exchanger at approximately 130° C (according to current design). It is United Technologies' belief that the heat pipe will operate around this temperature rather than 200 C. The subsequent pipes in the same manifold will each operate at progressively higher temperature. But given the expected temperature rise of 30° C across the entire manifold, it is expected no heat pipe will operate above 160° C.

2.6. Task 7

As described in the XCPC Conceptual Design Report (Task 4), we formulated three competing conceptual level designs for the External Compound Parabolic Concentrator (XCPC) that were developed during the course of this project. The performance goal was a collector efficiency of at least 50 percent at a temperature of 400°F, and a cost goal (uninstalled) of \$10 per square foot,

or lower. Each of the formulated designs consists of an assembly of stationary evacuated tube absorbers with external non-imaging reflectors.

The three competing design concepts that were formulated are:

1. All glass dewar: Direct Flow
2. All glass dewar filled with thermal fluid: Indirect Flow
1. Metal absorber with glass-to-metal seal

Each of these designs was considered, one by one, and is presented with the expected performance for.

Design #1 - All glass dewar: Direct Flow

The heat transport fluid flows directly inside the all-glass dewar – hence we use the term “direct flow”. The design uses very inexpensive all-glass dewar solar thermal absorbers that are mass produced in China. The dewars are cylindrical borosilicate glass bottles with an evacuated annulus between the two glass walls. A cross-sectional diagram of the dewar is shown in Figure 72. The vacuum surface of the inner wall is coated with a selective surface (usually aluminum nitride cermet) with a high solar absorptance and low thermal emittance. A popular size of off-the-shelf Chinese dewars are 44mm (inside diameter), 58mm (outside diameter) and 1.8-m in length. Our preliminary design was based on the use of dewars that are this size.

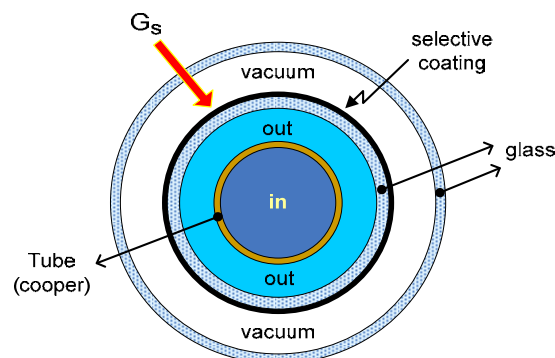


Figure 72. Direct Flow All Glass Dewar

Source: The Regents of University of California

Fluid is fed into each dewar through a central feed-tube, made of copper, to the end of the glass dewar where the flow reverses and then passes back in the annulus between the copper feed-tube and the ID of the inner glass cylinder.

The glass dewars are attached to a plumbing manifold using a compression seal system. The inlet tube is integral to the manifold itself, which speeds field installation and also eliminates a potential leak path (at the connection of the inlet tube to the manifold). For the analysis the manifold is configured so that the outlet of one collector can feed into the inlet of an adjacent collector.

Each dewar is placed so that an external reflector concentrates the solar irradiance onto the inner dewar wall where the selective surface is coated. The shape of the reflector has been designed so that all sunlight incident on the aperture plane of the collector (within a defined angular acceptance angle) is redirected onto the 47-mm OD absorber. Figure 73 shows ray traces over the design acceptance angle range of +34 degrees to -34 degrees.

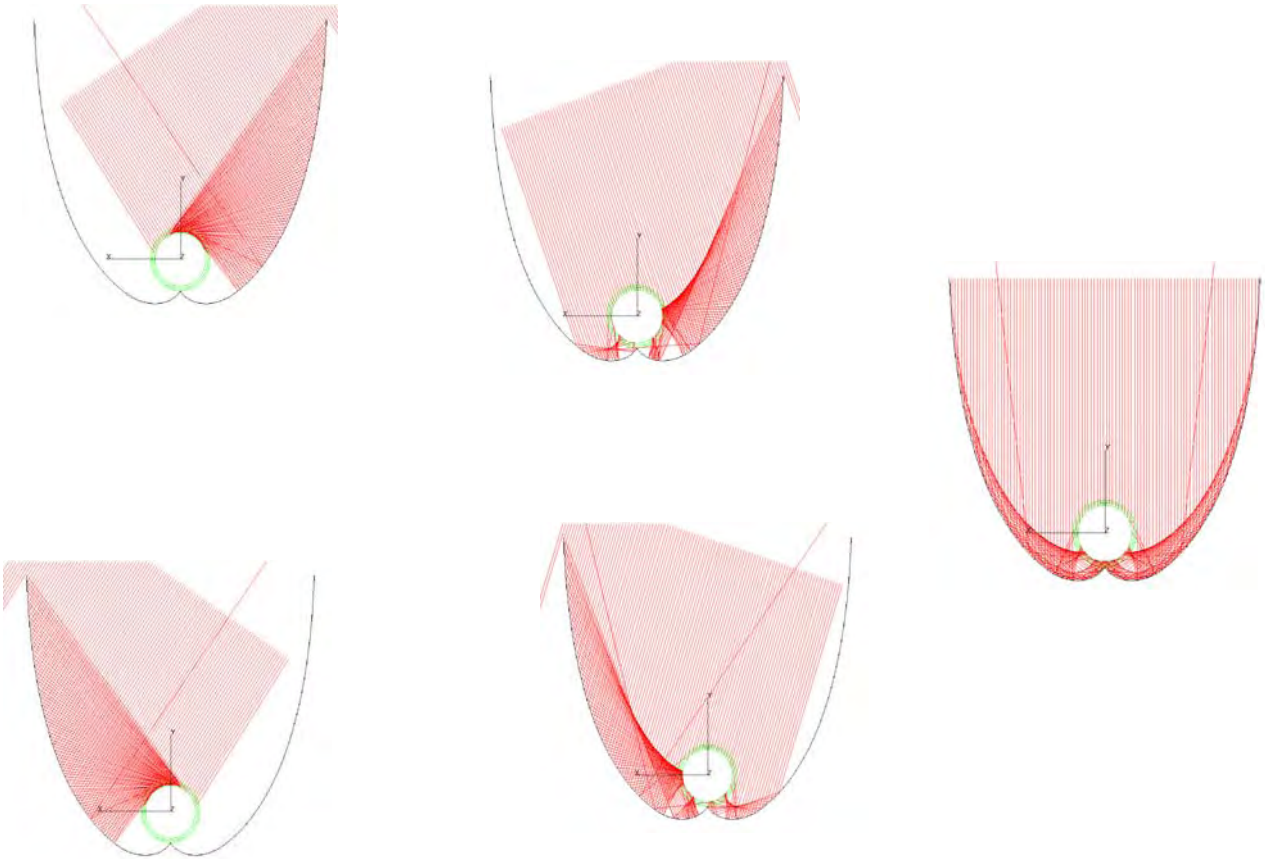


Figure 73. Ray Traces over the Design Acceptance Angle

Source: The Regents of University of California

This reflector design (dimensioned below in Fig- 7-3) is based on dewars that are oriented horizontally as part of an XCPC collector. This configuration yields the highest concentration ratio that is possible for a fixed collector, and reduces the number of evacuated tubes to a minimum (on a per unit area basis), which leads to the least amount of heat loss.

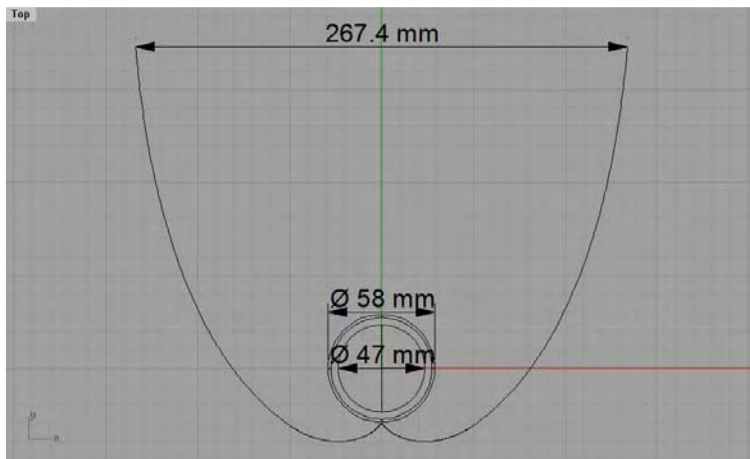


Figure 74. Horizontal Dewar Reflector Dimensions

Source: The Regents of University of California

The design shown above in Figure 74 is a CPC that has been truncated by 20%. This means that the arc length of the reflector has been reduced by 20% compared to the full CPC (untruncated) in order to reduce the required amount of reflector. With 20% truncation, the ratio of the aperture area to absorber area is 1.81 ($267.4 \text{ mm} / (47 \text{ mm} \times \pi) = 1.81$). This geometric concentration ratio (CR) is high for a fixed non-tracking solar collector and was a key attribute of the proposed design. This means that evacuated tubes can be spaced 58-mm OD apart by 267 mm and still capture essentially all the energy that is available. Using an XCPC collector with just six evacuated tubes spaced apart by about 10.5 inches (a center-to-center spacing of 267 mm) will yield a collector area of about 3.1 ft², about the same size as a traditional 4 x 8 ft flat plate collector.

Detailed optical and thermal modeling determined the expected performance of this horizontal XCPC design, using off-the-shelf components. Expected collector thermal efficiency³ is shown in Fig. 75 for temperatures from 25°C up to 200°C. The collector efficiency curve⁴ is in its simplest single-order form. It assumed the use of a high-quality selective coating within the dewars, like those produced by Tsinghua Solar, which was measured to have an absorptance of 0.923, an emittance of 0.050 at room temperature, and an emittance of 0.074 at 200°C. The SunRain tubes had optical properties nearly this good, while the Paradigma tubes were significantly poorer (see Task 6 Report for details).

³ A total irradiance in the aperture plane of the collector is assumed to be 1000 W/m², and an ambient temperature of 25°C is assumed.

⁴ The collector efficiency curve has two numerical constants. The first term is the optical efficiency and the second term is the heat loss coefficient. DT means delta-T (the temperature difference between the collector fluid temperature and the ambient temperature) in degrees C, and I is the total irradiance in the aperture of the collector in W/m².

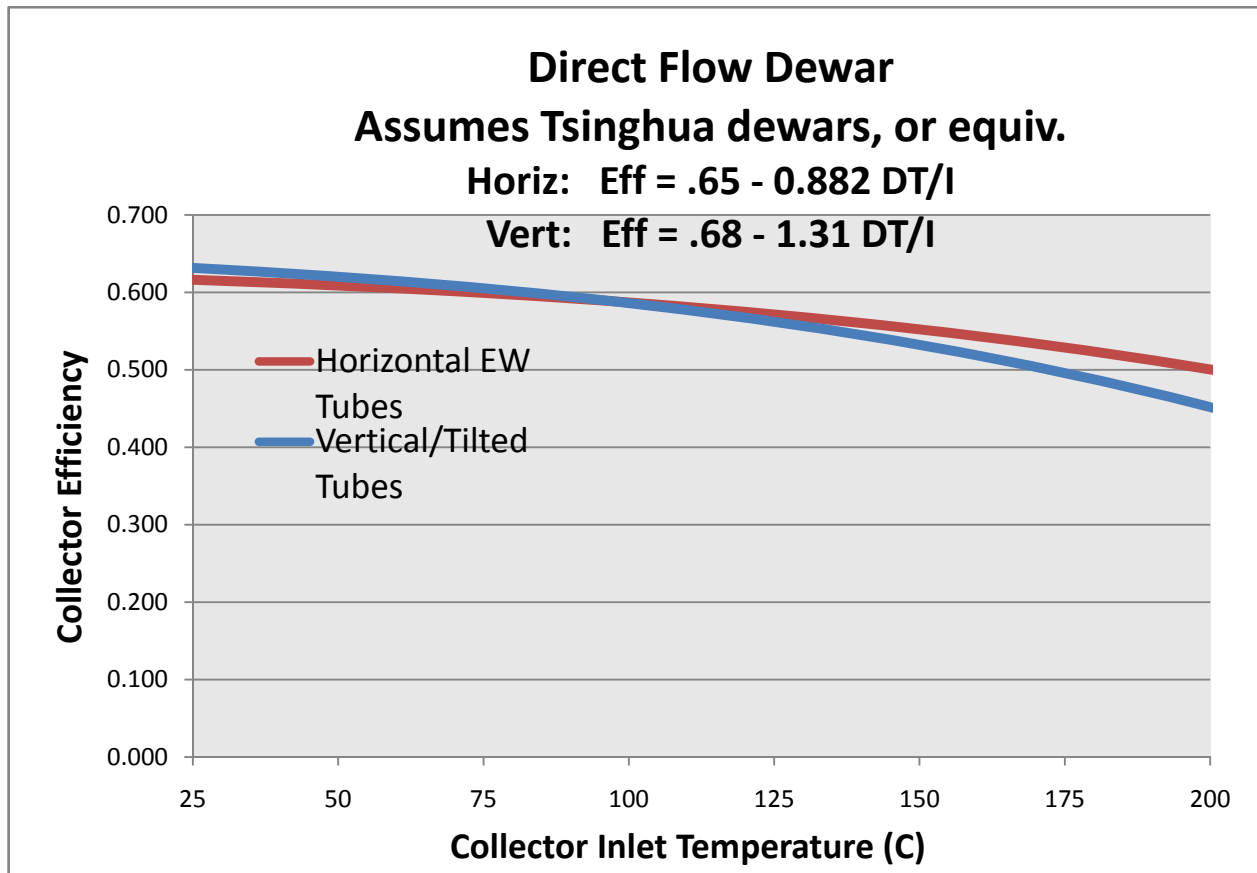


Figure 75. Direct Flow Dewar Efficiency

Source: The Regents of University of California

If we orient the tubes vertically (tilted), a somewhat different design results. A south-facing vertical/tilted orientation means that the CPC must be designed to a larger acceptance angle (e.g. 60 degrees) because the sun traverses a wider range, as seen from the tilted collector. The reflector shape and size is different for this design compared to that of Design #1 (see Figure 76 below). It has been designed to yield the highest concentration ratio that is possible for a non-tracking collector with a 60 degree acceptance angle, but allowing for 20% truncation in order to reduce the amount of reflector material that is required. The concentration ratio for this design is 1.16. The concentration ratio is lower than the horizontal orientation because of the need for a higher acceptance angle for vertically-oriented evacuated tubes.

A positive characteristic of this vertical/tilted design is that the required reflector area per unit of aperture area is considerably lower than the horizontal orientation. This means a lower cost per unit of aperture area can be achieved, making it easier to achieve our cost goals. But a negative characteristic is that the concentration ratio is considerably lower. This means higher heat loss, making it harder to achieve our performance goals. Figure 75 clearly quantifies this performance difference.

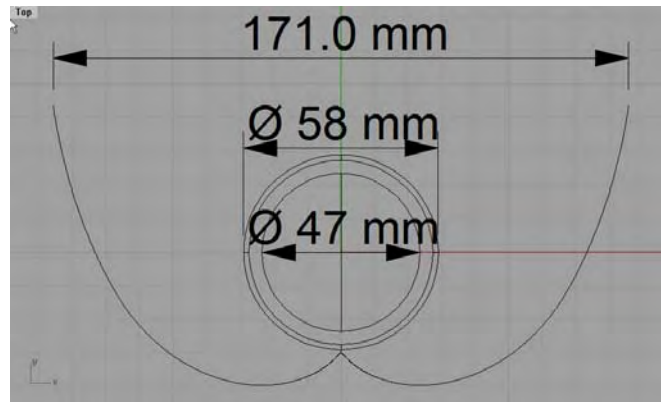


Figure 76. Vertical Dewar Reflector Dimensions

Source: The Regents of University of California

Referring again to the Collector Efficiency in Figure 75, note that the optical efficiency of the collector using vertical/tilted tubes is higher than the collector with the horizontal east-west tubes. This is so because the vertical orientation design has a lower concentration ratio, allowing more of the diffuse irradiation to be collected⁵. The collector with the horizontally-oriented tubes does have a “flatter” efficiency curve, owing to the reduced heat loss that results from the higher concentration ratio.

Finally, note that these performance estimates indicate that the XCPC design with the horizontal orientation can nearly achieve our performance goal of 50% thermal efficiency at 400°F (approx. 200°C), and this is with the use of commercial off-the-shelf components. The vertical/tilted XCPC design falls about 5% short at 200°C.

Design #2 - All glass dewar: Indirect Flow -- Dewars filled with thermal fluid

This design uses the same inexpensive all-glass dewars as our design #1. However, in this concept the circulating fluid does not directly contact the glass dewars. The circulating fluid is confined to the metallic inserts reaching into the glass dewars. The metallic inserts are immersed within a thermal transport fluid (e.g. a mineral oil or a highly-viscous thermal grease) in order to provide for thermal energy transport from the blackened/coated inner dewar to the metallic insert.

The basic idea of this design is to contain the fluid within the metallic insert, allowing for high pressures within the circulated fluid as compared to the Direct Flow designs (i.e. Design #1) where peak operating pressures are limited by the burst pressure of the glass dewars (90 psig). The other advantage of this design is that there is much reduced leak potential from the circulated fluid, since the circulated fluid does not contact the glass dewars. This “indirect” heat transport requires heat exchange from the heated glass dewar surface to the metallic insert,

⁵ To calculate the portion of the diffuse irradiance that is collected, we use the traditional assumption that the fraction of the diffuse insolation captured is equal to $1/C$ (where C = geometric concentration ratio). Also, for our efficiency calculations we assume that 85% of the insolation is direct irradiance, and the other 15% is diffuse irradiance.

which introduces a thermal heat transfer penalty, owing to the thermal resistance between the metallic insert and the heated dewar surface. If this space between the metallic insert and the ID of the glass dewar was filled with just air, which has poor heat transfer characteristics, the heat transfer penalty would be very large. So instead, we fill the gap with heat transfer oil (like Duratherm 600) in order to reduce this heat transfer resistance. Design #2 is shown in Figure 77.

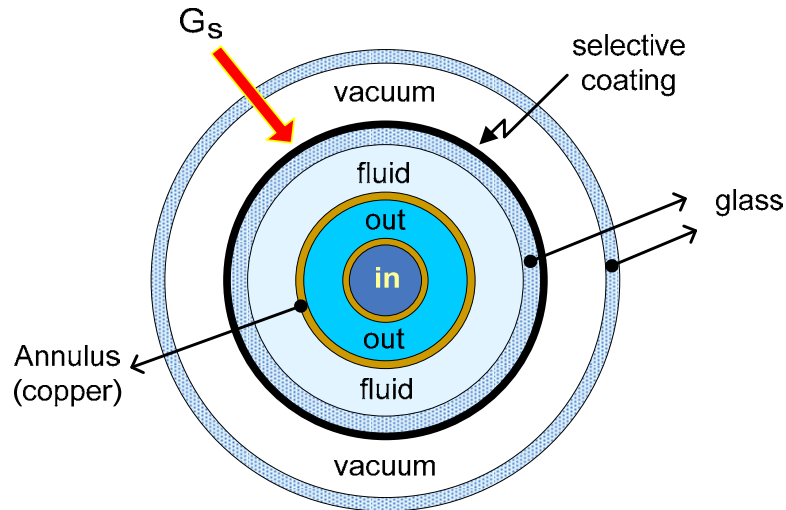


Figure 77. Indirect Flow Dewar

Source: The Regents of University of California

The other major difference between Design #1 and Design #2 is that the evacuated tubes must be oriented vertically (at a tilt) in order to contain the thermal fluid within the dewars. This means we cannot use the higher-concentration horizontal/EW design, and so we have evaluated just the vertical tilted/EW design with a 1.16 concentration ratio.

The expected performance of this XCPC design is shown in the Figure 78, based on the optical and thermal models. Again, we have assumed the use of a high-quality selective coating within the dewars, like those produced by Tsinghua Solar, which was measured to have an absorptance of 0.923, an emittance of 0.050 at room temperature, and an emittance of 0.074 at 200°C. The SunRain tubes had optical properties nearly this good, while the Paradigma tubes were significantly poorer (see Task 6 Report for details).

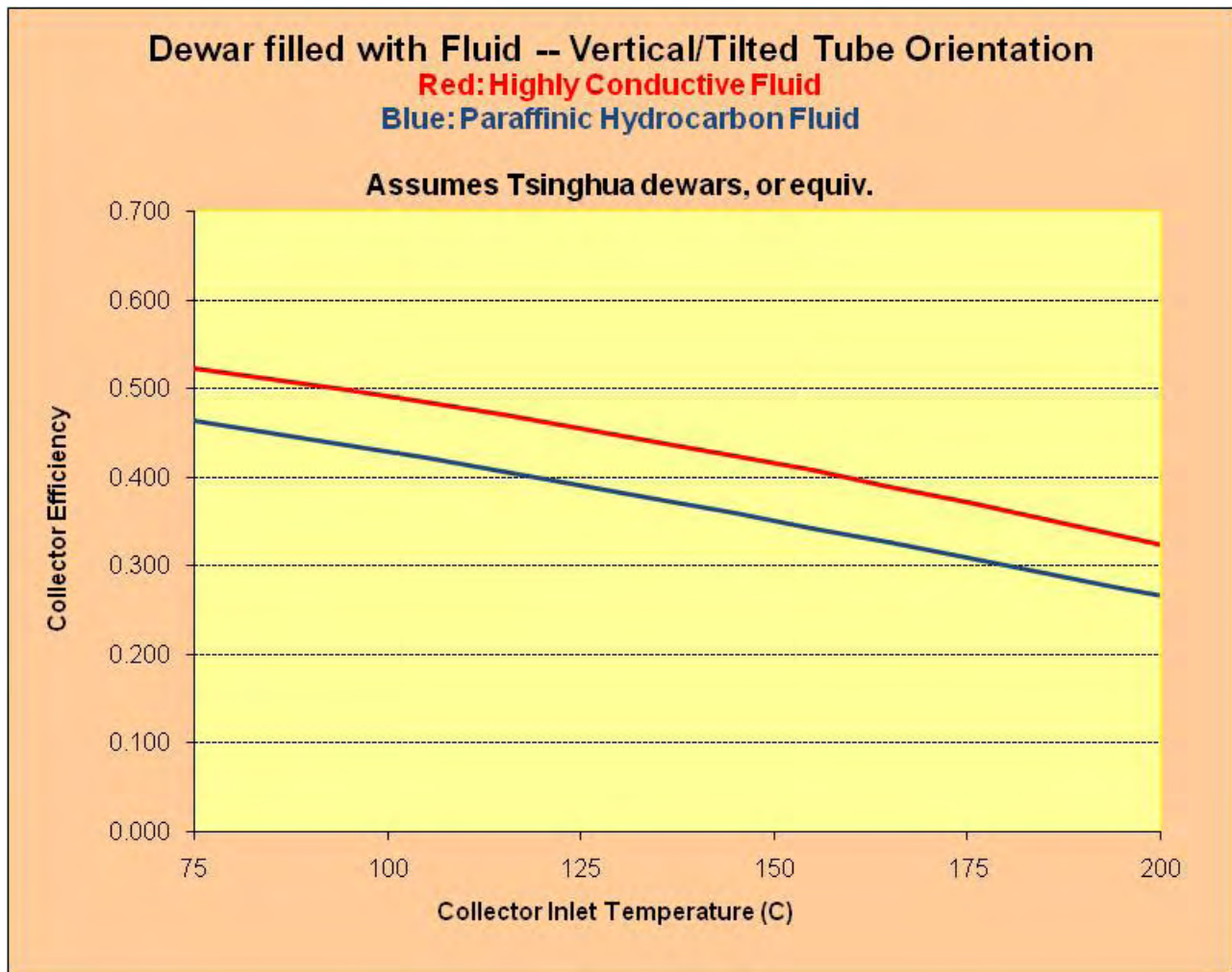


Figure 78. Expected Performance for Indirect Flow Dewar

Source: The Regents of University of California

Based on these results, this design will not achieve our thermal performance goal of 50% at 400°F (approx. 200°C). There are two primary reasons for this shortfall, based on our modeling. First, as noted above, the concentration ratio for this vertically-oriented design is lower, resulting in additional heat loss since the amount of heat loss is directly related to the concentration ratio of the collector. Second, our thermal model indicates that the heat transfer capability of the thermal fluid within the dewar is relatively poor. Analysis indicates that relatively low Grashof numbers (i.e. poor natural convection) will occur under our operating conditions. Combined with a relatively low thermal conductivity for the typical fluids that might be used inside the dewars, we end up with relatively poor heat transfer. To explore the sensitivity of this result to the predicted heat transfer coefficients of this heat transfer fluid, we have shown two sets of results. The blue line is based on the properties of a typical paraffinic hydrocarbon fluid (e.g. Duratherm 600), while the red-colored line assumes the Nusselt numbers have been doubled, that is the calculated heat transfer coefficients have been doubled. In neither case do we achieve our performance goals. However, we should note that the prediction of these convective heat transfer coefficients is subject to some uncertainty. It would be desirable to verify the predicted performance with actual testing. Also, it is worth further

exploration of various heat transfer fluids to see if significantly better fluids might be found that would allow much improved results.

Design #3 - Metal absorber with glass-to-metal seal

This design, shown in Figure 79 uses an evacuated glass tube with a glass-to-metal seal at one end that maintains the vacuum to insulate the metal absorber. The metal absorber is a thin cylindrical metallic fin with a selective coating that enables high solar absorptance and reduces radiative heat loss. The fin is welded to a metal counter flow tube. The heat absorbed by the fin is transferred to the manifold by the circulating fluid within the metal tube.

The evacuated glass tube has the following dimensions.

- Diameter of outer tube wall: 65 mm
- Diameter of inner tube wall: 61.8 mm
- Diameter of absorber: 56 mm

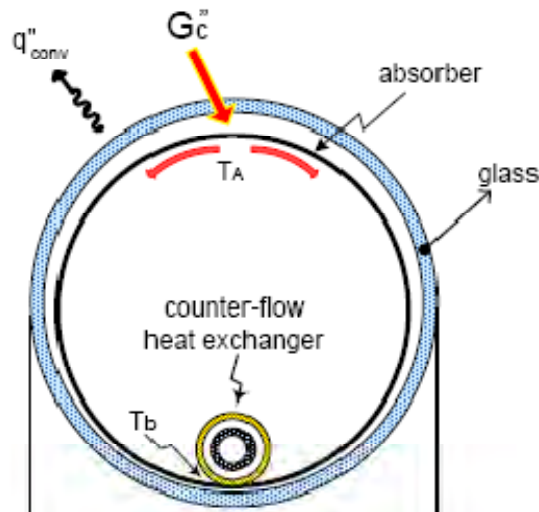


Figure 79. Metal Absorber Tube (Counter Flow)

Source: The Regents of University of California

The absorber tubes are placed so that external reflectors concentrate sunlight onto the evacuated glass tubes, just as in designs #1 and #2. But the diameter of the cylindrical absorber in this design is larger (56 mm) than that of the all-glass dewars (47 mm) used in the other designs. This results in a proportionally larger CPC reflector, as shown in Figure 80. The concentration ratio is 1.80, consistent with the 34 degree acceptance angle of horizontally oriented tubes. The center-to-center spacing of each tube is 316 mm (12.5 inches).

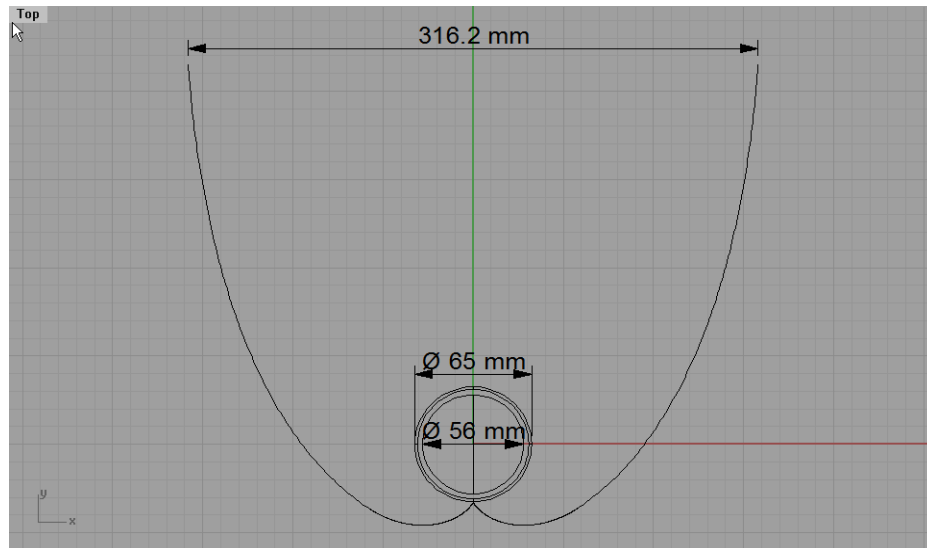


Figure 80. Horizontal Metal Absorber Tube Reflector Dimensions

Source: The Regents of University of California

Detailed optical and thermal modeling has determined the expected performance of this XCPC design, and the expected performance is shown in the next figure for temperatures from 75°C to 200°C (167°F to 392°F).

Our analysis of this design has shown that the thermal performance is significantly affected by:

- the solar-weighted absorptance of the selective coating on the metallic absorber, and
- the thermal emittance of the selective coating on the metallic absorber, and
- the thickness of the cylindrically-shaped metallic absorber.

Figure 80 shows performance predictions for three types of selective absorbers:

- a) TiNOX
- b) a custom vacuum-deposited absorber labeled as Eurocon because this is the Chinese company that produced the coating
- c) Alanod Mirotherm

TiNOX is thin copper foil that has been vacuum-coated with titanium and quartz. It is available in only one thicknesses, 0.2 mm. The absorptance of TiNOX was measured to be 0.958, a very good absorptance. And while the thermal emittance was measured to be 0.035 at room temperature, it dramatically increased to 0.158 at 200°C. This large increase in emittance at elevated temperatures results in a severe performance drop at our 200°C design point. In addition, the availability of TiNOX in just the 0.2 mm thickness is a significant performance constraint. Our analysis of this design has shown that the thermal performance is significantly affected by the thickness of the cylindrically-shaped metallic absorber, because the cylindrical absorber acts as a fin since it must conduct heat around its entire surface to the point of contact with the copper tube where all the heat is extracted. Analysis indicates that a copper thickness of at least 0.6 mm is needed to achieve good results with a copper absorber. However, as noted above, the high emittance of TiNOX at 200°C is another severe performance limitation.

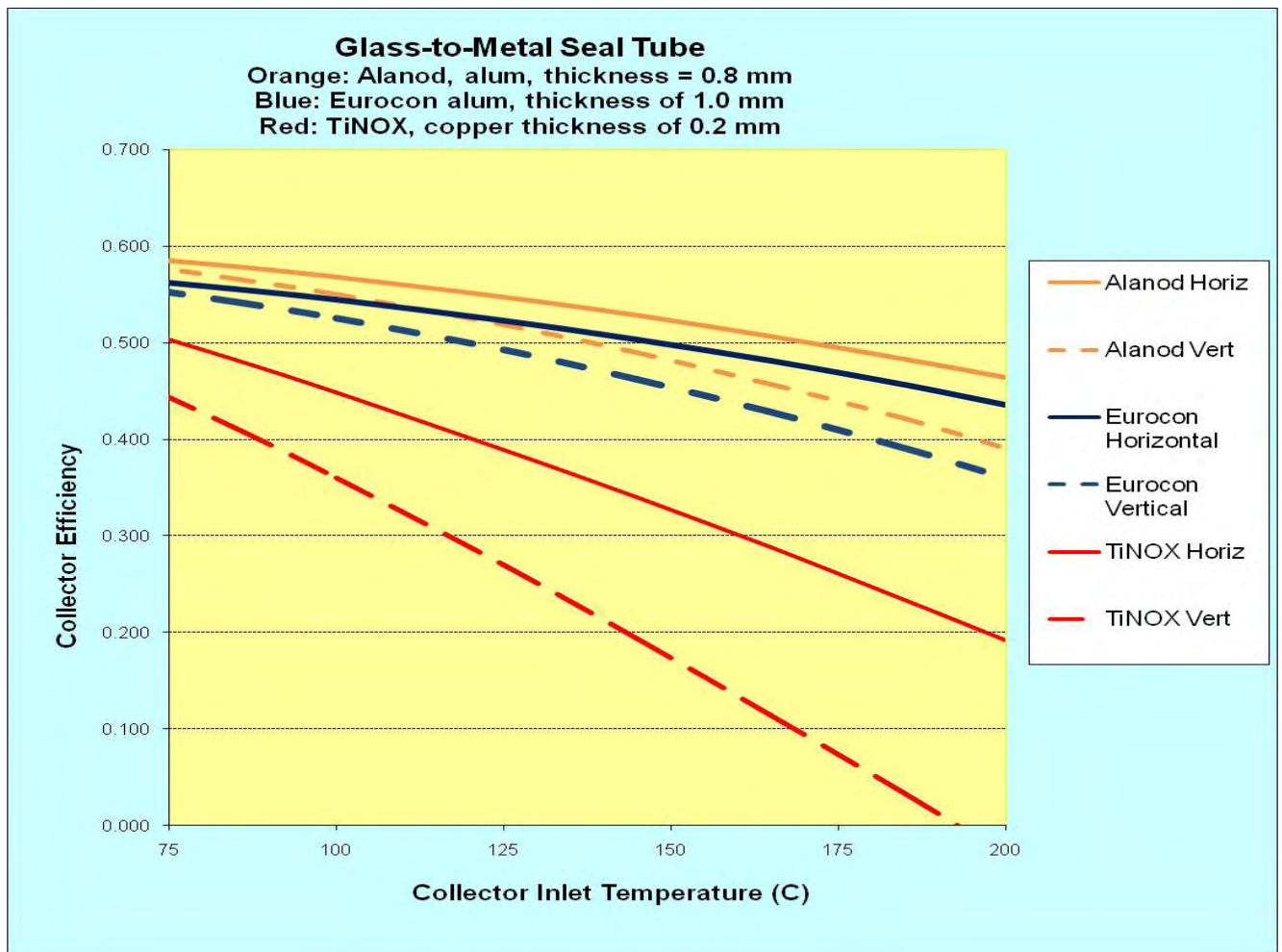


Figure 81 Performance predictions for three types of selective absorbers

In order to stay on schedule with this XCPC development project, the XCPC Design Team had to order prototypes of this sealed-end tube design during February. Our vendor, Eurocon, was prepared to use TiNOX, as this is a high quality and widely used selective absorber. Fortunately, our early analysis of this design revealed that the 0.2 mm TiNOX thickness would result in a significant performance limitation. So instead, Eurocon was authorized to use an alternative selective coating that the company had been developing. This alternative absorber uses aluminum and has a much greater thickness (1 mm), to its great advantage. When the optical properties of this custom coating were measured the absorptance was found to be 0.904, with an emittance of 0.050 at room temperature, and an emittance of 0.064 at 200°C. Although the absorptance is a bit low, the emittance values are very good, and the 1 mm thickness is a big advantage.

As our investigation into other selective coating alternatives continued we became aware of an Alanod product called Mirotherm. Mirotherm is an aluminum based selective absorber that uses physical vapor deposition to apply several layers to anodized aluminum. The material is available in several thicknesses, up to 0.8 mm. As reported in Task 6 Report, optical property measurements at Surface Optics showed that Mirotherm has a solar-weighted absorptance of 0.934, an emittance of 0.043 at room temperature, and an emittance of 0.057 at 200°C. As can be seen above in the Glass-To-Metal Seal Tube collector efficiency figure, Alanod’s Mirotherm

offers a preferred metallic coated absorber. Had we become aware of this material earlier in our development program, we would have recommended its use in the prototypes that have now been manufactured by Eurocon.

Finally, the various collector efficiency equation coefficients have been tabulated in Figure 82 for the two Direct Flow and the Sealed End designs. These coefficients will be useful in annual performance calculations (e.g. f-Chart).

Design	Optical Efficiency	Heat Loss Coefficient
Direct Flow- Tsinghua (or equiv) all-glass dewers		
Horizontal/East-West	0.646	0.882
Vertical/Tilted (facing South)	0.678	1.309
Glass-to-Metal Sealed End Tubes		
Microtherm absorber		
Horizontal/East-West	0.664	1.145
Vertical/Tilted (facing South)	0.697	1.746
Eurocon absorber		
Horizontal/East-West	0.641	1.172
Vertical/Tilted (facing South)	0.673	1.787
TiNOX Absorber		
Horizontal/East-West	0.681	2.792
Vertical/Tilted (facing South)	0.715	4.26

Figure 82. Various collector efficiency equation coefficients

Source: The Regents of University of California

2.7. Task 8

This report compares the cost of possible designs for the External Compound Parabolic Concentrator (XCPC) that is to be developed during the course of this project. The cost goal of this project is to design a XCPC collector that costs less than \$10 per square foot to manufacture.

As described in the XCPC Conceptual Design Report (Task 4), we have formulated three competing conceptual level designs for the XCPC. The three competing design concepts that have been formulated are:

- j) All glass dewar: Direct Flow
- k) All glass dewar filled with thermal fluid: Indirect Flow
- l) Metal absorber with glass-to-metal seal

The Draft XCPC Preliminary Design Report (Task 7) analyzed the expected performance of the three design concepts. The study found that design concept #2 will probably not achieve our performance goal of 50% system efficiency at 400°F. Therefore, we made the cost estimate only

for design concepts #1 and #3.

There are several variations possible within each design concept, mainly whether the orientation of the tubes is West-East or North-South and, for design concept #3, if the metal absorber tube operates in flow-through configuration or with a heat pipe.

The analyzed concepts are:

- 6) All glass dewar: Direct Flow – East-West orientation
- 7) All glass dewar: Direct Flow – North-South orientation
- 8) Metal absorber flow-through – East-West orientation
- 9) Metal absorber flow-through – North-South orientation
- 10) Metal absorber heat pipe (only North-South orientation possible)

The cost comparison is shown in Table 18.

Table 18 shows that the all-glass dewar designs have BOM cost of around \$10 per square foot. The XCPCs using metal absorber tubes show slightly higher BOM cost, around \$12 per square foot.

It is noted that this cost estimate reflects the baseline design, to be developed during Phase I of the project. We expect that the BOM cost of the final improved XCPC design, to be developed in Phase II of the project, will be lower.

XPCP concept	All-glass dewar: Direct Flow	All-glass dewar: Direct Flow	Metal absorber flow-through	Metal absorber flow-through	Metal absorber heat pipe
Orientation	East-West	North-South	East-West	North-South	North-South

Bill of Materials

Source of estimate:

Absorber tube					
Tube type	Sunrain All-glass dewar with improved selective coating (TTY-MC)	Sunrain All-glass dewar with improved selective coating (TTY-MC)	Beijing Eurocon metal absorber tube with counterflow insert	Beijing Eurocon metal absorber tube with counterflow insert	Beijing Eurocon metal absorber tube with heat pipe
Length of tube	1800 mm	1800 mm	1800 mm	1800 mm	1800 mm
OD of tube	58 mm	58 mm	65 mm	65 mm	65 mm
Diameter of absorber	47 mm	47 mm	56 mm	56 mm	56 mm
Price of one tube	\$3.20	\$3.20	\$22.00	\$22.00	\$21.00
Price of tubes [per aperture of reflector (m2)]	\$6.40	\$9.94	\$37.19	\$58.27	\$55.62

Vendor quotes

Reflector					
Material	Alanod	Alanod	Alanod	Alanod	Alanod
Reflectivity	90%	90%	90%	90%	90%
Acceptance angle	± 34°	± 60°	± 34°	± 60°	± 60°
Function	20%	20%	20%	20%	20%
Length of reflector (mm)	1860	1860	1860	1860	1860
Width (mm) of reflector opening (incl. 1mm spacing)	269	173	318	203	203
Depth (mm) of reflector	212	83	261	97	97
Arc length of reflector (mm)	562.6	278.8	685.6	327.8	327.8
Aperture of one reflector (m2)	0.50034	0.32178	0.59148	0.37758	0.37758
Reflector material needed per tube (m2)	1.046436	0.518568	1.275216	0.609708	0.609708
Price of reflector material per m2	\$20.00	\$20.00	\$20.00	\$20.00	\$20.00
Cost of reflector bending (per m2)	\$0.22	\$0.22	\$0.22	\$0.22	\$0.22
Price of bent reflector per tube	\$21.16	\$10.49	\$25.78	\$12.33	\$12.33
Price of reflector [per aperture of reflector (m2)]	\$42.29	\$32.59	\$43.59	\$32.65	\$32.65

Vendor quote Estimate from Madifac Solar

Manifold					
Length of manifold	~2.2m	~1.1m	2.6m	1.265m	1.265m
Tubes per manifold	8	6	8	6	6
Price of manifold	\$176.74	\$93.02	\$128.37	\$63.26	\$50.23
Price of manifold per tube	\$22.09	\$15.50	\$16.05	\$10.54	\$8.37
Price of manifold [per aperture of reflector (m2)]	\$44.16	\$48.18	\$27.13	\$27.92	\$22.17

Vendor quote

Collector frame and rack					
Dimensions of one collector	~2.2m x 2m	~1.1m x 2m	2.6m x 2m	1.3m x 2m	1.3m x 2m
Price of one frame including rack	\$88.00	\$44.00	\$104.00	\$51.00	\$51.00
Price of one frame including rack per tube	\$11.00	\$7.33	\$13.00	\$8.50	\$8.50
Price of frame and rack [per aperture of reflector (m2)]	\$21.99	\$22.79	\$21.98	\$22.51	\$22.51

Estimate from UC Merced

Total BOM [per aperture of reflector (m2)]	\$114.83	\$113.50	\$129.90	\$141.35	\$132.95
Total BOM [per aperture of reflector (sf)]	\$10.67	\$10.54	\$12.07	\$13.13	\$12.35

Table 18. Cost comparison of XPCP design concepts in high volume production (10,000 tubes)

Source: The Regents of University of California

2.8. Task 9

This analysis has been performed by United Technologies Research Center (UTRC). It summarizes the results from the system performance evaluation studies conducted by UTRC to better understand the techno-economic viability of system architectures for XPCP driven cooling and ORC (identified as promising application areas for the XPCP in Task 2 report of this project).

The general approach, for both cooling and power generation, includes two steps: design and off-design or performance analysis. In the design point, the system specifications are determined, including the chiller or ORC capacity, solar collector size, inlet and outlet fluid temperatures. In the off-design, the cooling or power generated by the system at each of the 8760 hours throughout the year is calculated with the hourly weather data.

The analysis focused on evaluating system viability for four different areas in California (Los Angeles, Sacramento, San Diego and San Francisco) and four different building types (retail

store, supermarket, hotel and hospital). The rest of this report includes a summary of the modeling approach used to evaluate the system architectures, the results of the modeling approach, the limitations of the current study and recommendations for future work that can be used to further enhance the fidelity of the modeling calculations.

Solar Insolation and Building Data

Solar insolation and weather data (used to get the dry bulb and wet bulb temperatures) were obtained using EnergyPlus⁶ software. Building load simulation results were obtained using DOE-2 software⁷. The appendices contain typical representative excel file outputs that were used in all of the analysis that follows. Figure 1 below presents how the solar insolation data can be used to estimate thermal energy output for the entire year (8760 period).

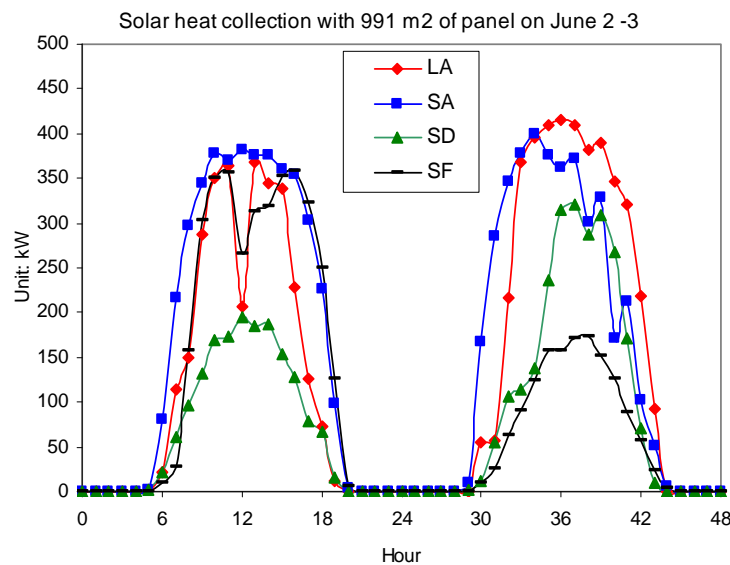


Figure 83 Solar thermal energy output (assuming 50% efficiency) for a 991 m² collector for a two day period June 2-3

Source: The Regents of University of California

Four cities were studied including Los Angeles, Sacramento, San Diego and San Francisco. For each city, four types of buildings were analyzed: 80k ft² supermarket, 120k ft² retail store, 270k ft² hospital and 270 ft² hotel. Figure 84 presents typical building load information that is provided by the DOE-2 simulation program for the four different building types. The numbers next to the building type indicates footprint (120 K -> 120,000 ft²).

⁶ http://www.eere.energy.gov/buildings/energyplus/cfm/weatherdata/weather_request.cfm

⁷ <http://www.doe2.com/>

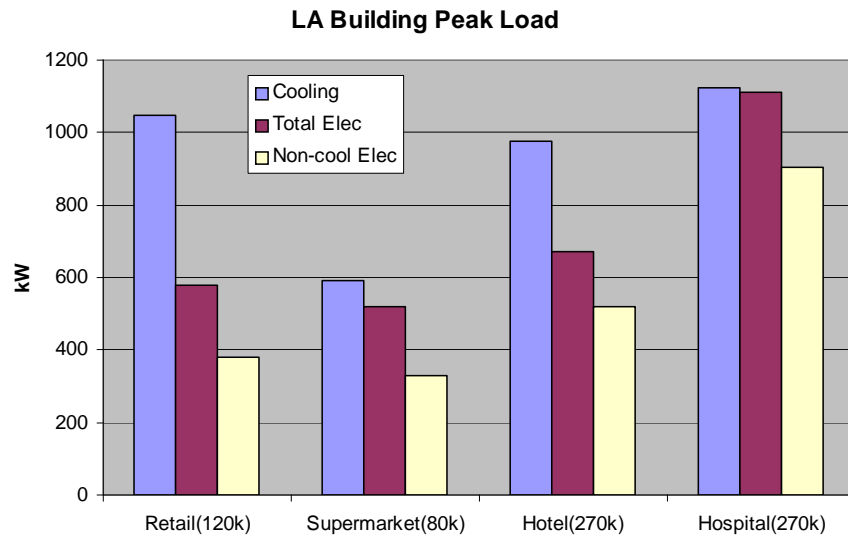


Figure 84. DOE-2 output for four building types in Los Angeles

Source: The Regents of University of California

Estimating both these data sets is important in determining if the cooling and electrical power generation solutions are appropriately sized for the associated regions and building types. It was determined from these preliminary calculations that the 120 RT chiller and the 220 kW ORC could be driven with thermal energy derived from solar (through the XCPC) and that the cooling and electrical power loads provided by the systems were appropriately sized given the building types.

XCPC driven double effect absorption chiller analysis

Factors affecting the absorption chiller performance mainly include solar heat available, building cooling load needed, equipment size, the minimum part load ratio below which the equipment cannot work, and the wet bulb temperature.

The chiller performance is assumed to be mainly affected by the cooling water temperature, which is a function of the wet bulb temperature. The chiller performance map or the COP as a function of the cooling water temperature is shown in Figure 85.

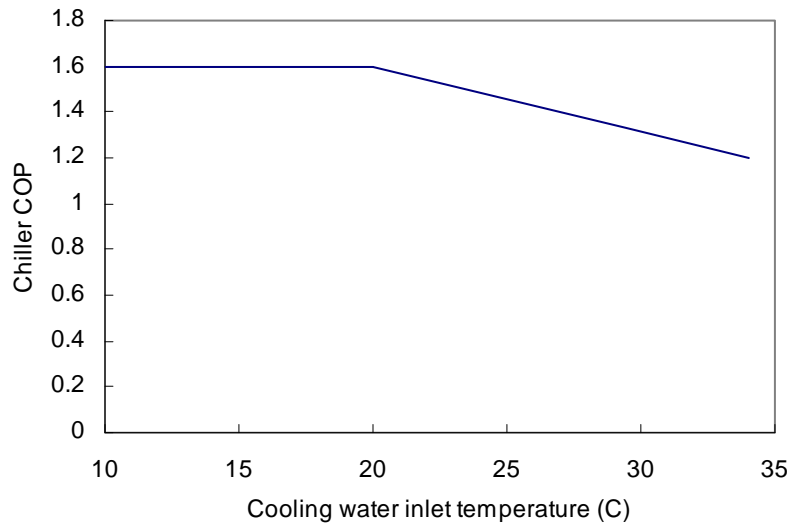


Figure 85. Absorption chiller COP as a function of the cooling water inlet temperature

Source: The Regents of University of California

The chiller has a nominal COP at the design inlet temperature of 29.4 C (85F). When the cooling water temperature decreases, the chiller COP increases. But if the cooling water temperature is too low, it will cause crystallization so a limit of 20 C is set for the minimum cooling water temperature, corresponding to COP of 1.6.

For cooling, the off-design procedure used to analyze the data was as follows:

- Choose a city and get the 8760 solar data for the city
- Calculate the wet bulb temperature based on EnergyPlus file
- Get the chiller COP based on wet bulb temperature
- Calculate the maximum cooling available with the given solar heat
- Chiller stops running when the cooling load < 25% of nominal capacity
- Run DOE2 to get the building cooling load needed
- Calculate the actual cooling that the chiller will provide
- Economic analysis

In economic analysis, the cost of electricity is calculated that is needed to generate the same amount of cooling as solar cooling with a vapor compression chiller (VCC). The cost of natural gas needed in an otherwise direct fired absorption chiller is also calculated. The assumed VCC COP is 5. The grid electricity and utility gas price are assumed \$0.20/kWh and \$0.05/kWh (\$1.465/therm), respectively.

XCPC driven cooling - Results

Based on the design point analysis, the system specifications are summarized in Table 19.

Table 19. System specifications for solar cooling system

Source: The Regents of University of California

Specifications	Value	Unit
Chiller COP	1.33	
Chiller capacity	120	RT
Chiller hot oil inlet temperature	150	C
Chiller hot oil outlet temperature	120	C
Chiller hot oil flow rate	4.23	kg/s
Oil design specific heat	2.5	kJ/kgC
Chiller design cooling water inlet	29.3	C
Solar collector design insolation	800	W/m ²
Solar collector design efficiency	50%	
Solar collector area	991	m ²
Chiller minimum part load ratio	25%	

In the performance analysis, the 8760 cooling load for a 120k ft² retail store in Los Angeles and the solar heat available are shown in Figure 86(a) and 86(b), respectively. The cooling load shows higher cooling load in summer and lower in winter. On the other hand, the solar heat *peak value* is relatively uniform.

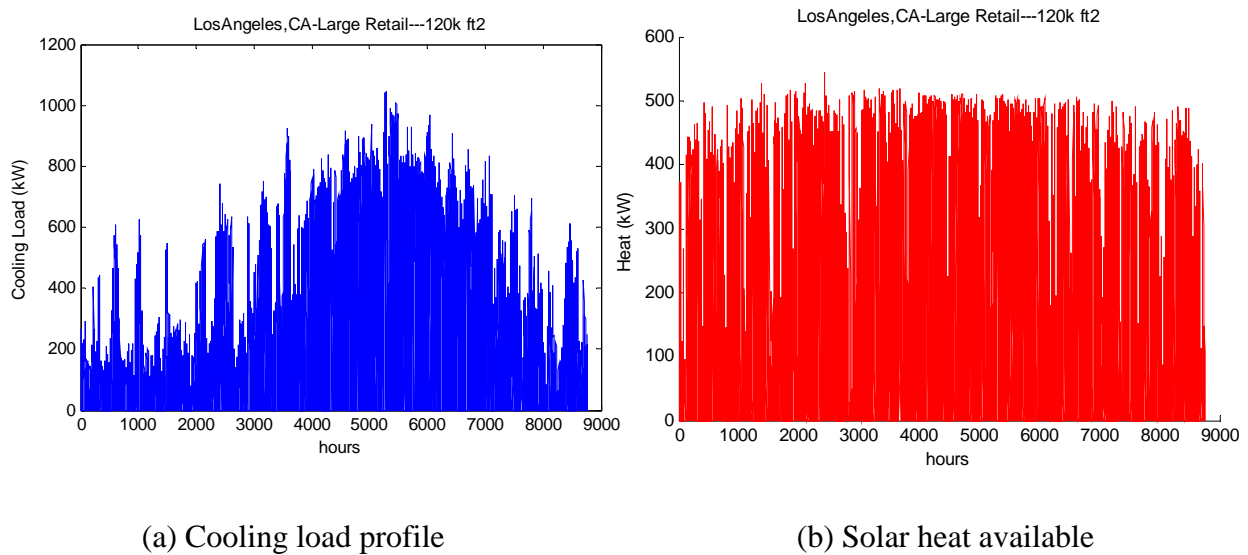
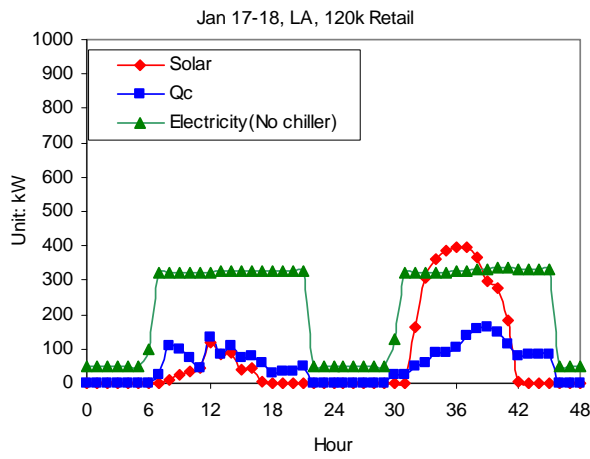


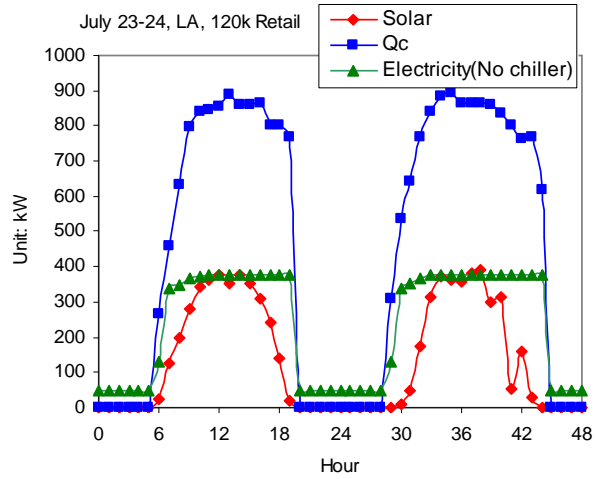
Figure 86. Los Angeles retail store cooling load and solar heat profiles

Source: The Regents of University of California

To display the profiles more clearly, Figure 87(a) and 87(b) show the building electricity demand, cooling demand Q_c and the solar heat in a 48-hour period in winter and in summer, respectively. Summer cooling load is much higher than the winter cooling load. Although the peak solar heat in winter is similar to that in summer, the solar insolation has a different profile between summer and winter. The total amount of heat received by the solar collector is higher in summer.



(a) Winter profile



(b) Summer

Figure 87. Typical 48-hour solar, cooling and electricity profiles of Los Angeles 120 ft² retail

Source: The Regents of University of California

The solar driven chiller provides the cooling as shown in Figure 88, with a zoomed version of a mid-year 3-day profile shown in Figure 89. The chiller produces a maximum of 422 kW, the rated capacity. The unmet cooling demand needs to be provided by a backup vapor compression (VC) chiller. At certain times, e.g., in the early morning, even if the cooling demand is less than the rated chiller capacity, the absorption chiller still cannot meet the cooling demand because of insufficient solar heat, as shown in Figure 89

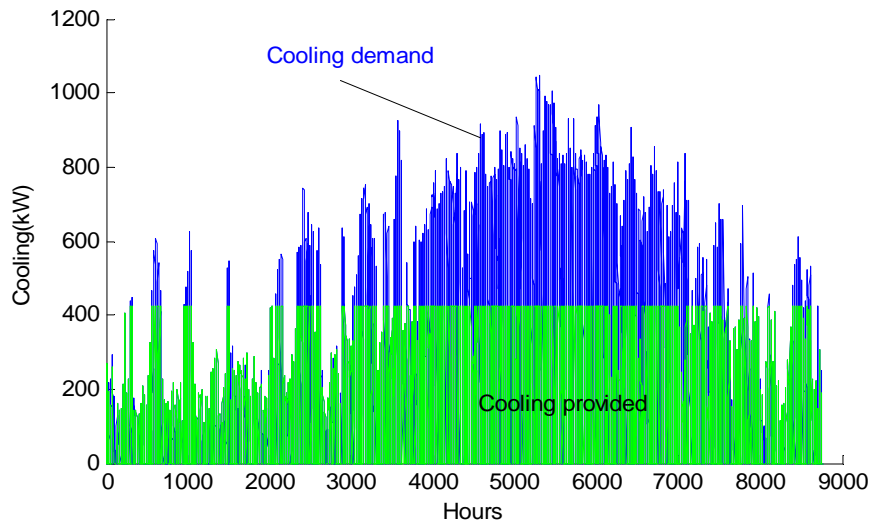


Figure 88. Annual profile of cooling generation compared with the cooling demand

Source: The Regents of University of California

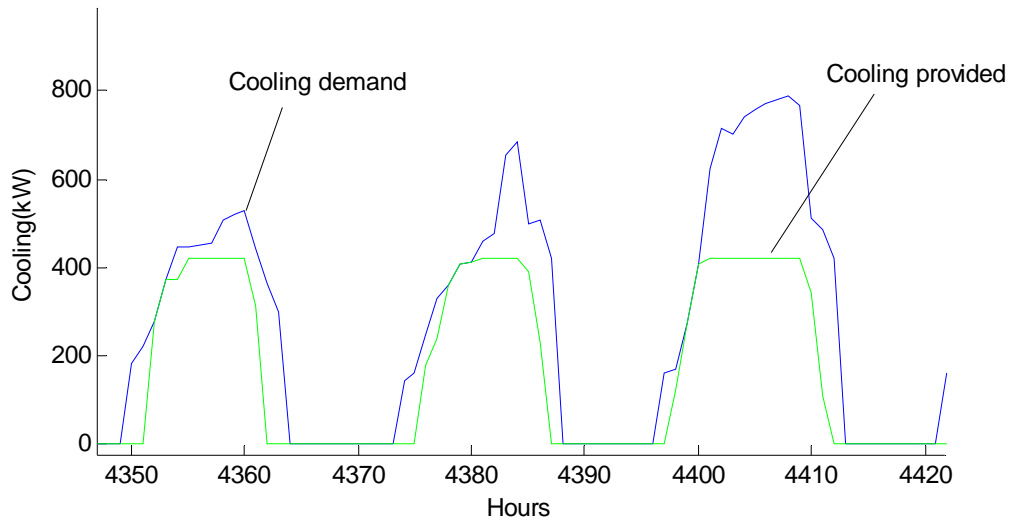


Figure 89. A 3-day profile of cooling generation compared with the cooling demand
 Source: The Regents of University of California

With the annual solar cooling profile, the solar cooling ratio is calculated as shown in Figure 90. The solar cooling ratio is defined as the total solar cooling kWh, the area under the green curve in Figure 89, divided by the total cooling demand kWh, the area under the blue curve in Figure 89. When the load of the building is higher, e.g., the hospital, solar cooling portion is smaller and the backup chiller has to supply the unsatisfied load. In San Francisco, the building cooling is generally lower than that in other cities and solar cooling ratio becomes relatively larger.

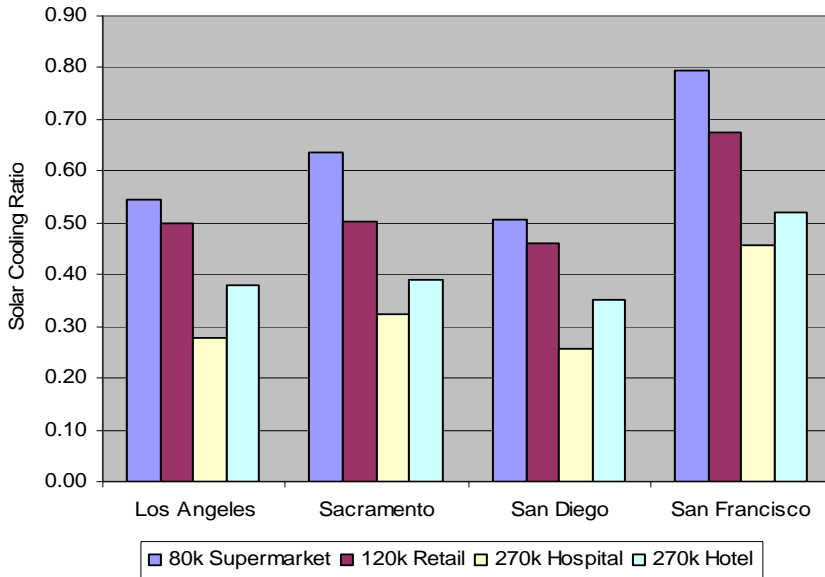


Figure 90. Solar cooling ratio for the four buildings in the four cities.

$$\text{(Solar cooling ratio = Total cooling kWh from solar / Total cooling demand kWh)}$$

Even though the solar cooling does not meet the full demand of the building, some solar heat is left unused. This happens in three cases: 1) The solar heat is more than the chiller can consume, even if the chiller is running at full capacity; 2) In some days, there is solar heat but the cooling demand is small; and 3) The solar heat, even though available, is not enough to drive the chiller

above its minimum part load ratio of 25%. Figure 91 shows that the solar utilization ratio, defined as the solar heat used by the chiller vs. the total solar heat available from the collector, is around 0.7. A potential application for the rest of the solar heat can be domestic hot water. In buildings such as hotels or hospitals, this could create additional value.

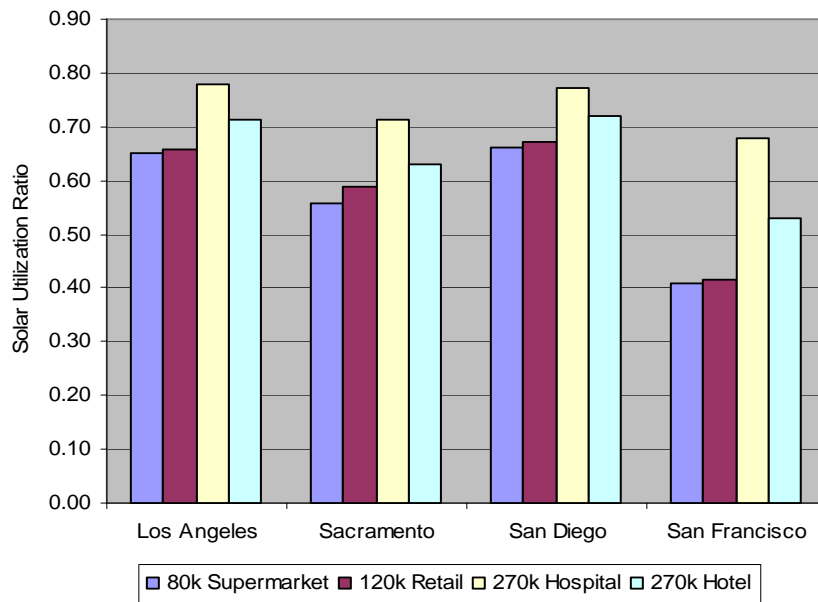


Figure 91. Solar utilization ratio for the four buildings in the four cities.

Source: The Regents of University of California

Figure 92 shows the solar cooling capacity statistics. The chiller runs for about 3400 hours per year, which is equal to the 8760 hours minus the ~5400 hours of idle time, as indicated by the bar on the left.

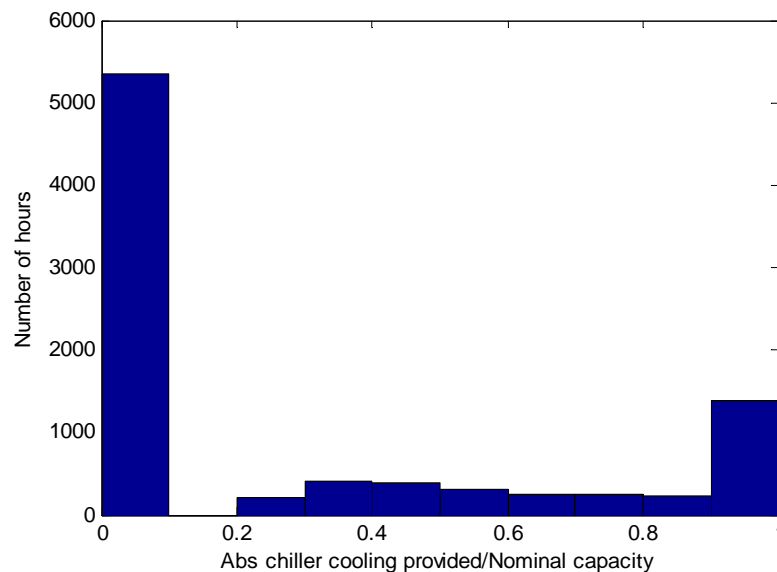


Figure 92. Solar cooling capacity statistics

Source: The Regents of University of California

XCPC driven cooling – Economics

The total solar cooling generation can be converted to the electricity savings based on assumed typical VCC COP and electricity unit price. Figure 93 shows that the 120 RT solar driven chillers here can save in the neighborhood of \$40,000.

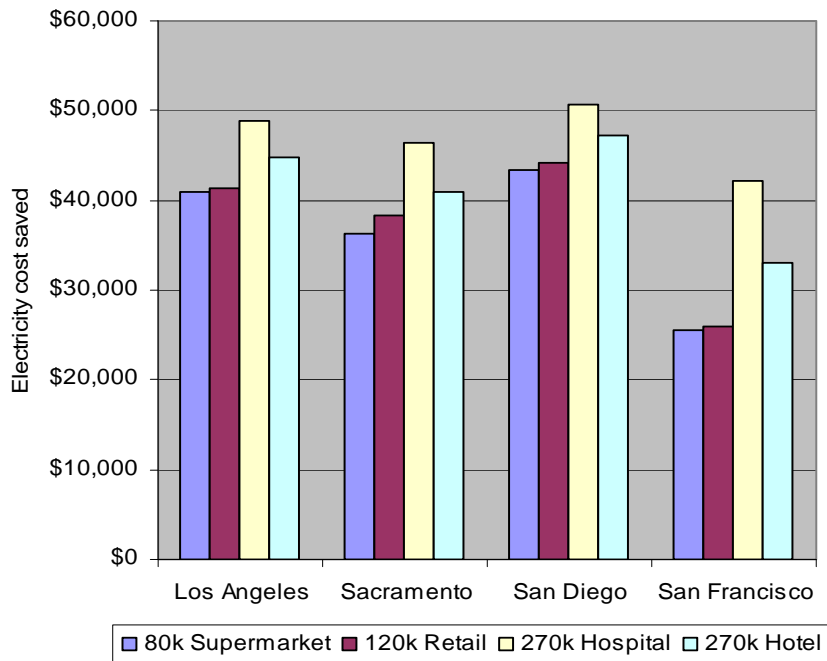


Figure 93. Solar cooling capacity statistics

Source: The Regents of University of California

Instead of comparing with VC chiller, the cost savings can also be compared with the gas cost in direct fired absorption chillers. The detailed analysis results in Table 20 show that the gas savings is approximately the same as the electricity savings.

Table 20. Detailed analysis results for 120k ft² retail store with solar cooling

	120k sq ft Retail Store			
	Los Angeles	Sacramento	San Diego	San Francisco
Total Cool Need (MWh)	2073	1910	2396	960
Chiller Q Provided (MWh)	1032	959	1104	647
Total Solar Hours Available	3452	3527	3545	3422
Total Cooling Hours Provided	3401	2976	3582	2544
Electricity cost saved	\$40,919	\$36,199	\$43,405	\$25,576
Natural gas cost saved	\$38,458	\$34,022	\$40,794	\$24,038
Solar Utilization Ratio	0.66	0.59	0.67	0.41

Source: The Regents of University of California

*: Solar hours available are defined as the hours with solar insolation larger than 100 W/m². Costs assumed 0.20 cents/kWh electric and \$1.465/therm natural gas.

The system payback can be calculated as the solar panel and the chiller installed cost divided by the electricity cost savings. Assume the chiller cost is \$500/RT and the solar panel cost of \$150/m², the payback is around 4 years for 120 retail stores in Los Angeles. Different stores with other assumed equipment price are shown in Figure 94.

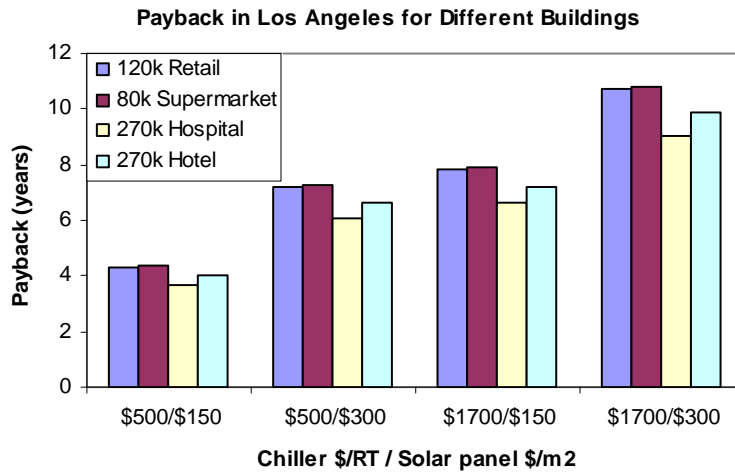


Figure 94. Payback of the solar cooling system in Los Angeles

Source: The Regents of University of California

The payback periods may be severely impacted when including the parasitic electrical power that the systems can consume. The value can be as high as 0.4 kWe/RT; depending on the distance between chiller and the solar thermal equipment, electrical consumption of the fan in the cooling tower etc. This would thereby result in an additional 48 kWe consumed that over a 3400 hour period would result in an additional operating cost of \$33000 thereby seemingly negating payback periods and savings for most markets. It must however be noted that almost 90% of these costs are also incurred by conventional water cooled, electrically driven chillers so a more accurate number to use for parasitics is the incremental amount used by the lithium bromide solution pumps. These values are in the neighborhood of 0.04 kW/RT (or 4.8 kW for a 120 RT chiller). Detailed results from the modeling has been reported in Appendix 2.

XCPC driven cooling – Modeling limitations and future work

The model can be improved to consider the following factors: 1) Part load effect on the chiller performance. Keeping other conditions the same, at part load, the chiller COP will be higher; 2) Detailed utility price structures, e.g., to include the demand charge and the utility rate at the solar cooling hours; 3) Maintenance cost in the solar cooling system to get the payback with higher fidelity; 4) Parasitic power for the pump used to feed the hot oil to the chillers needs to be included in the overall system model as this may substantially impact value proposition (due to consumption of additional electricity).

XCPC driven organic Rankine cycle (ORC)

The XCPC driven ORC system here is physics based modeling at the component level. The system diagram is shown in Figure 13. Factors affecting the ORC power generation mainly include solar heat available, equipment size, the minimum part load ratio and the ambient temperature (dry bulb if air cooled and wet bulb if water cooled).

In the design mode, the ORC inlet and outlet temperatures of the heating and cooling fluids are chosen. Based on the heat source temperature, the working fluid of the ORC and the approach to Carnot efficiency are selected based on experience. Then the solar panel area is calculated.

In the off-design mode, the modeling procedure is:

- Get the solar and weather data
- With the given outlet and inlet hot fluid temperature, calculate the hot fluid flow rate
- With the available solar heat, using a loop gradually increase the heat transfer rate in the evaporator, and then calculate the evaporating and condensing temperature. The turbine power can be calculated then. The heat transfer and the power generation are not balanced until increasing the evaporator heat transfer rate to a certain point.
- Move onto next hour
- Integrate the solar power throughout the year
- Economic analysis

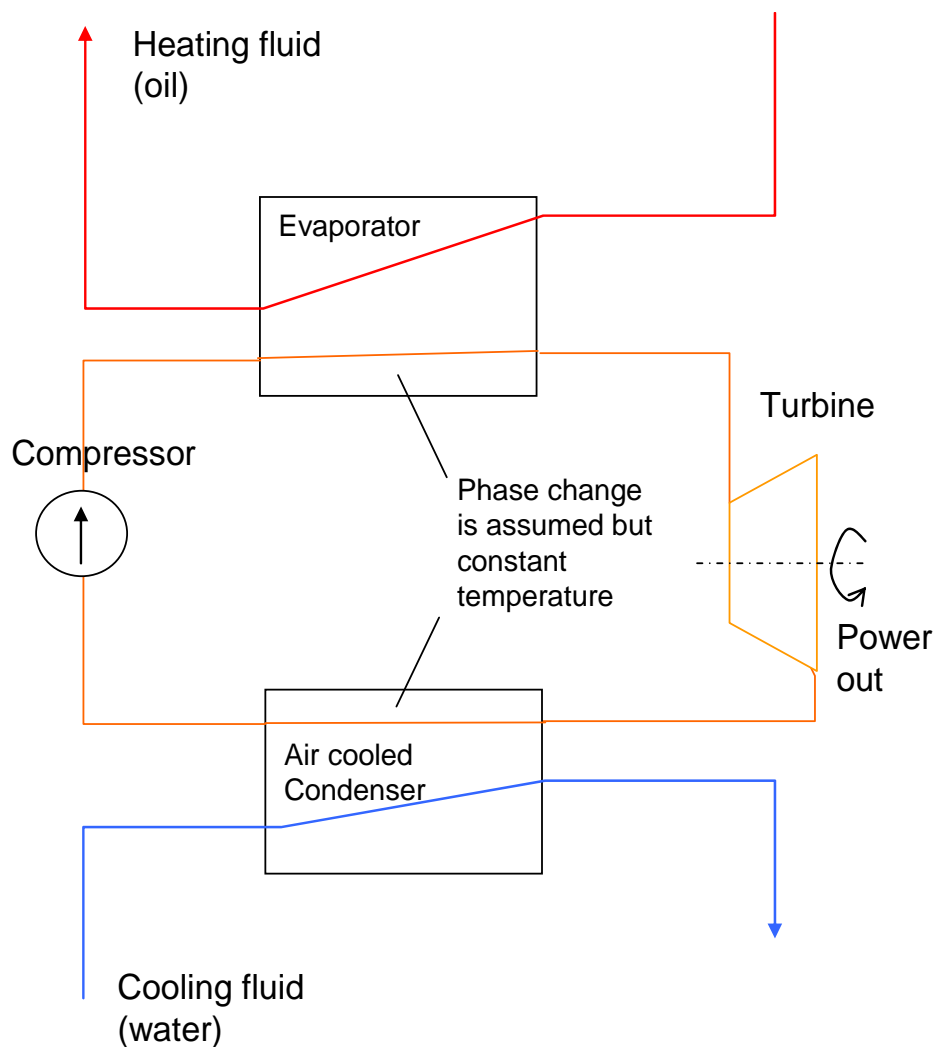


Figure 95. Diagram of solar driven ORC

Source: The Regents of University of California

XCPC driven ORC - Results

The design specifications of a 220kW solar driven ORC is shown in Table 21.

Table 21. System specifications for solar power generation system with ORC

Specifications	Value	Unit
ORC Design Efficiency	0.12	
Approach to Carnot efficiency	0.7	
ORC electric capacity	220	kW
ORC hot oil inlet temperature	150	C
ORC hot oil outlet temperature	120	C
ORC hot oil flow rate	24.1	kg/s
Oil design specific heat	2.5	kJ/kgC
ORC working fluid	R245fa	
Turbine pressure ratio	5.9	
Cooling fluid	Water	
Cooling fluid flow rate	38	kg/s
Cooling fluid inlet temperature	15	C
Cooling fluid outlet temperature	25	C
Cooling tower pinch temperature	10	C
Solar collector area	4761	m ²
ORC minimum part load ratio	35%	

Source: The Regents of University of California

Here water cooled ORC with a cooling tower is assumed, which tends to have higher efficiency than an air cooled ORC.

The power generation and the solar heat available throughout the year are shown in Figure 96(a) and (b). More detailed profiles for a 48-hour period are shown in Figure 97. The peak solar heat power is likely to be higher in summer than in winter, but in general rather uniform throughout the year. The longer solar hours in summer tends to generate more power than in winter.

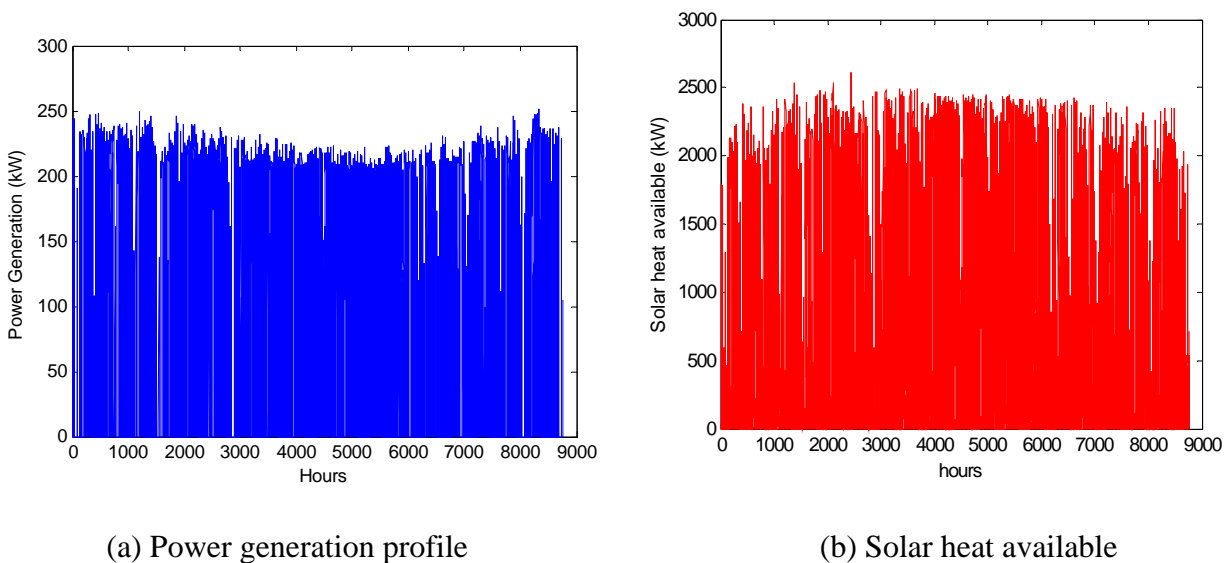
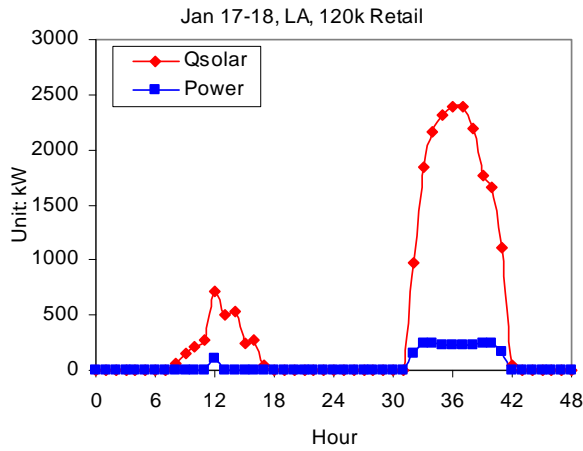
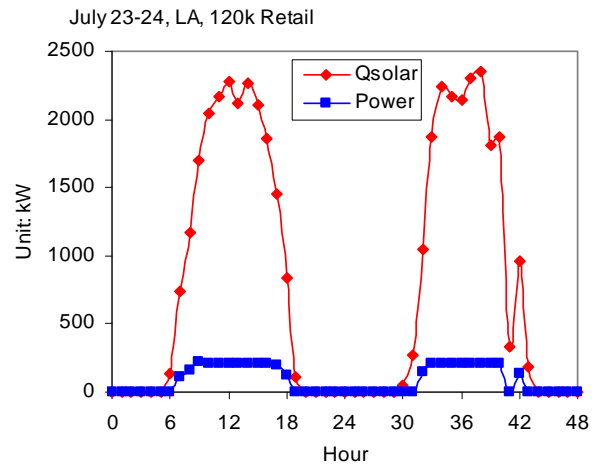


Figure 96. Los Angeles ORC power generation and solar heat profiles

Source: The Regents of University of California



(a) Winter profile

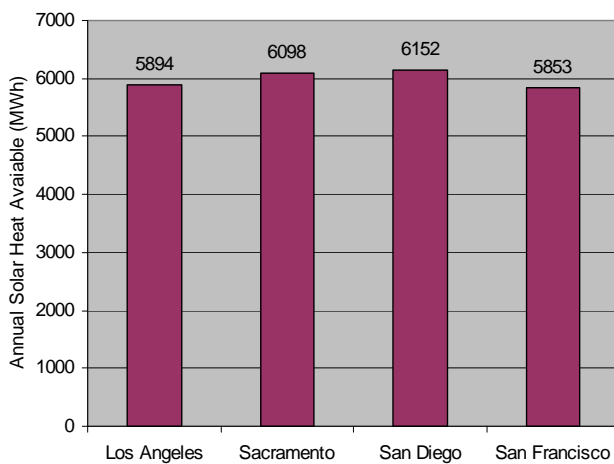


(b) Summer

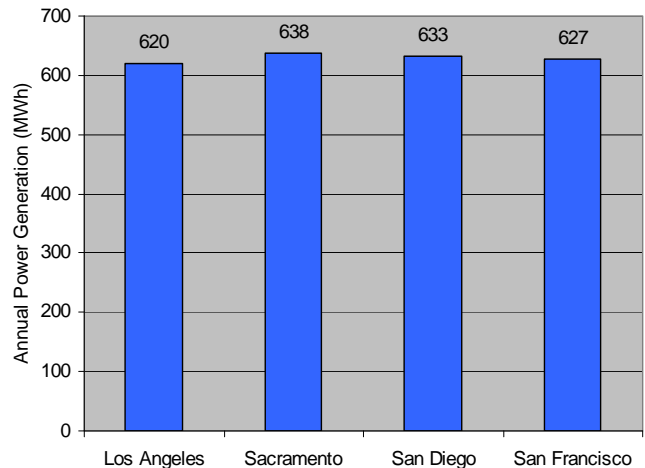
Figure 97. Typical 48-hour solar heat and electricity generation profiles in Los Angeles

Source: The Regents of University of California

The annual total solar heat available and the total power generation are shown in Figure 98. The 220kW ORC delivers approximately 630 MWh of electricity per year with about 6000 MWh of solar heat. The total power generation does not vary greatly with the city. This is because it is assumed that the power generated by the ORC can always be sent to the grid, so that the power generation is only limited by the solar heat available, which does not vary with the cities in this study.



(a) Annual total solar heat available



(b) Annual total power generation

Figure 98. Total solar heat and power generation in four cities

Source: The Regents of University of California

The ORC operation statistics are shown in Figure 99. The ORC runs at nominal capacity for about 3200 hours per year, among which about 1000 are at full capacity or above. For ORC, when the ambient condition is favorable, e.g., very low ambient temperature, the ORC can produce slightly beyond its nominal capacity.

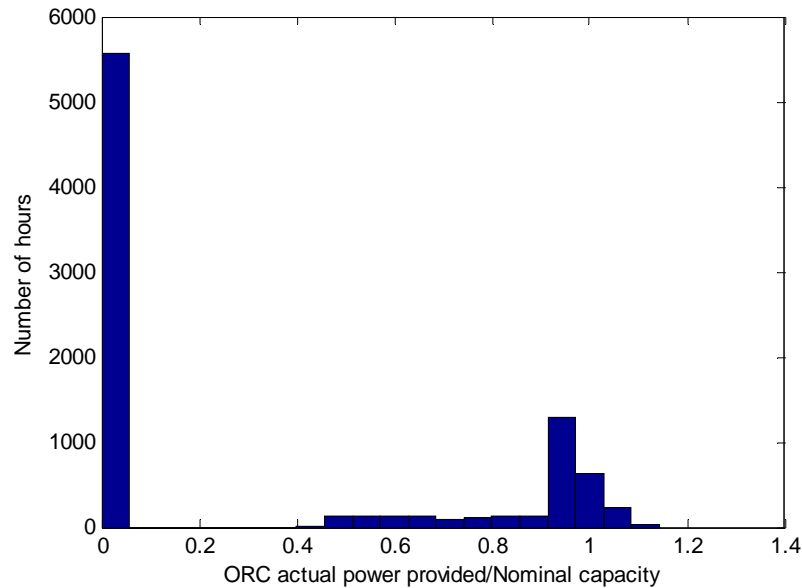


Figure 99. ORC operation statistics
 Source: The Regents of University of California

The overall solar heat utilization for ORC is around 0.85, higher than the typical cooling solar heat utilization ratio mentioned before, as shown in Table 22.

Table 22. Detailed analysis results with solar ORC

	Los Angeles	Sacramento	San Diego	San Francisco
Total Electricity Generated (MWh)	620	638	633	627
Total Solar Hours Available	3452	3527	3545	3422
Total Orc Operation Hours Provided	3186	3240	3253	3144
Solar Utilization	0.85	0.85	0.84	0.85

Source: The Regents of University of California

XCPC driven ORC – Economics

Similar power generation total amount directly translates to similar electricity savings, assuming the electricity cost is \$0.20/kWh for all the cities. Similarly, there is no much variation with cities. The efficiency number for an XCPC driven ORC could be further lowered when factoring in pump power requirements to move the hot oil from the collectors to the ORC evaporator. This value is currently and unknown and incorporating these additional electrical demands to the system would reduce the cost savings further.

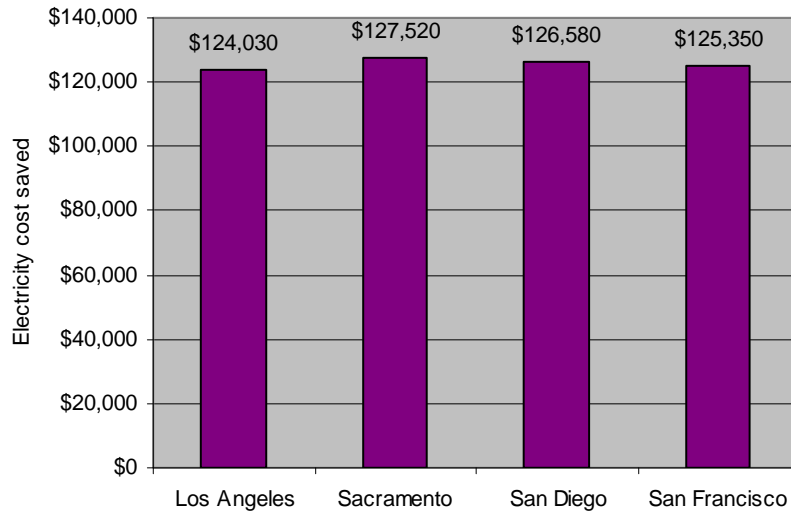


Figure 100. Solar driven ORC electricity savings

Figure 101, presents how payback periods could vary as a function of ORC cost/collector costs based on current estimates of electricity costs saved.

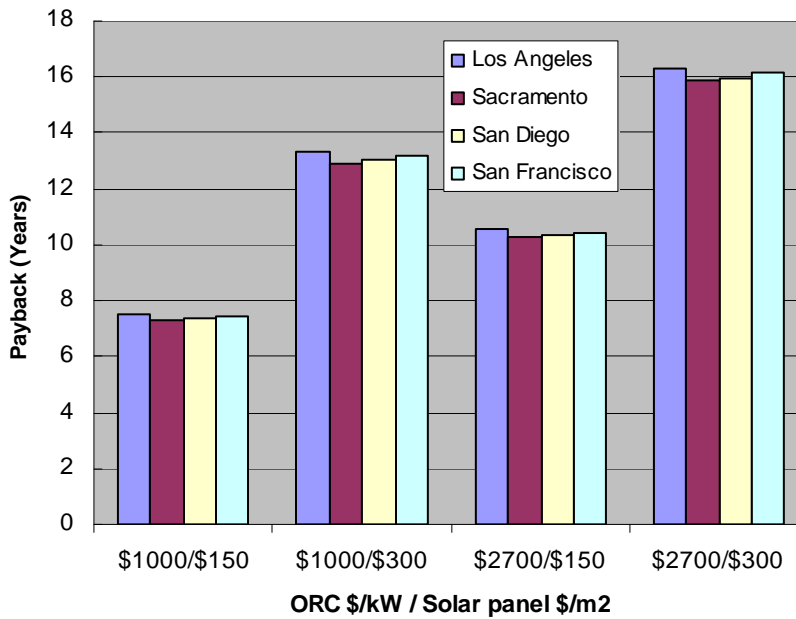


Figure 101. XCPC driven ORC payback as a function of ORC and solar collector costs

Source: The Regents of University of California

The conclusion drawn from these observations is that the XCPC driven ORC is an application that requires further consideration for building applications especially in the face of rising costs of electricity.

XCPC driven ORC – Modeling limitations and future work

Currently, several major assumptions are taken in the model such as the constant temperature of the refrigerant in the evaporator and condenser. Future work to improve the model can focus on: 1) Using more detailed heat transfer models for the evaporator and the condenser; 2) Improving the turbine model to go beyond a constant efficiency assumption; 3) Using variable electricity costs to reflect the demand charges, the city-specific rates and the time of power generation; 4) Creation of comprehensive detailed models for the collector and balance of systems which will help further refine the efficiency and cost benefits of the XCPC driven ORC systems.

Other considerations - Sensitivity Analysis

Sensitivity analysis has been conducted to understand the system performance characteristics. In the first study, we look at the solar cooling system payback at different cities, as shown in Figure 102. The payback in San Francisco is slightly higher, because of lower cooling load generated. With optimistic cost estimate of \$500/RT for the chiller and \$150/m² for the solar panel, this creates about 7 years of payback in San Francisco and about 4 years in the other 3 cities (not factoring in parasitics).

In a second study, a 50 RT chiller is used. Because a smaller system can be used more often than a larger chiller in supplying the building cooling demand, the smaller system has better payback, as shown in Figure 103. However, it should be pointed out that the chiller unit cost in \$/RT tends to go higher with a smaller chiller. Therefore the benefit of using smaller chiller should be discounted.

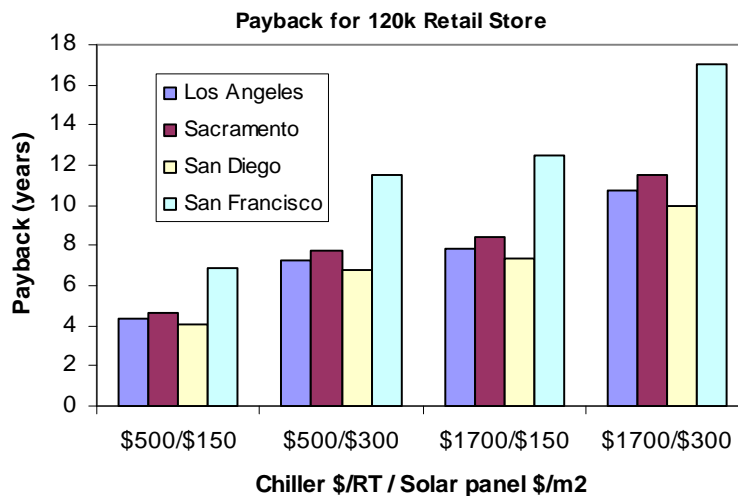


Figure 102. Payback of solar driven cooling system at different cities

Source: The Regents of University of California

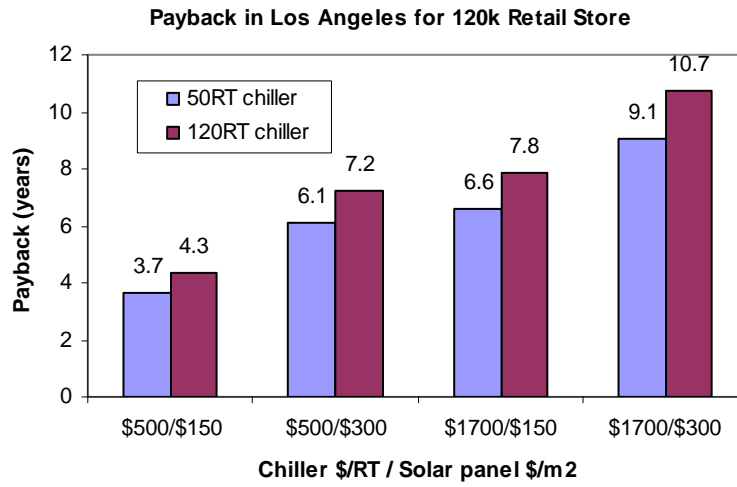


Figure 103. Payback of solar driven cooling system with different chiller capacity

Appendix 1: Solar, weather and building raw data used in the analysis - Sample

Hour	EnergyPlus						DOE2 (LA, 120k s.f. Retail)		
	Tdb K	Twb K	ITotal W/m2	RH	IDirect W/m2	IDiffuse W/m2	Cooling kW	Total Elec kW	Chiller Elec kW
1	282.55	276.905	0	0.36	0	0	0	5.03E+01	0
2	280.95	276.368	0	0.44	0	0	0	5.03E+01	0
3	280.95	275.723	0	0.36	0	0	0	5.03E+01	0
4	279.25	274.971	0	0.43	0	0	0	5.03E+01	0
5	279.85	275.186	0	0.4	0	0	0	5.03E+01	0
6	279.25	274.864	0	0.42	0	0	0	5.03E+01	0
7	280.95	275.401	0	0.33	0	0	0	1.00E+02	0
8	282.55	276.046	37	0.27	8	29	0	2.93E+02	0
9	283.15	277.335	315	0.35	217	98	2.20E+01	3.31E+02	1.07E+01
10	285.35	277.872	393	0.25	193	200	7.52E+01	3.57E+02	3.68E+01
11	288.15	279.161	574	0.19	340	234	1.41E+02	3.75E+02	5.40E+01
12	290.35	280.342	649	0.17	372	277	1.97E+02	3.82E+02	5.88E+01
13	290.35	279.913	754	0.14	553	201	1.97E+02	3.83E+02	5.89E+01
14	291.45	280.557	693	0.14	522	171	2.42E+02	3.91E+02	6.31E+01
15	292.05	281.094	550	0.15	400	150	2.68E+02	3.96E+02	6.57E+01
16	291.45	280.557	291	0.14	193	98	2.56E+02	3.97E+02	6.45E+01
17	288.75	279.698	46	0.2	17	29	1.69E+02	3.89E+02	5.64E+01
18	287.05	278.624	0	0.21	0	0	1.23E+02	3.83E+02	5.26E+01
19	286.45	278.194	0	0.21	0	0	1.10E+02	3.82E+02	5.16E+01
20	285.95	277.872	0	0.21	0	0	9.44E+01	3.76E+02	4.62E+01
21	285.35	277.442	0	0.21	0	0	0	5.03E+01	0
22	284.85	277.442	0	0.24	0	0	0	5.03E+01	0
23	283.75	277.012	0	0.27	0	0	0	5.03E+01	0
24	284.25	277.12	0	0.25	0	0	0	5.03E+01	0
25	283.75	277.012	0	0.27	0	0	0	5.03E+01	0
26	282.55	276.26	0	0.29	0	0	0	5.03E+01	0
27	283.15	276.583	0	0.27	0	0	0	5.03E+01	0
28	282.55	276.153	0	0.28	0	0	0	5.03E+01	0
29	282.55	276.153	0	0.28	0	0	0	5.03E+01	0
30	283.15	276.475	0	0.26	0	0	0	5.03E+01	0
31	280.95	275.723	0	0.36	0	0	0	1.00E+02	0
32	283.75	277.012	107	0.27	66	41	3.55E+01	3.37E+02	1.74E+01
33	284.25	277.657	479	0.3	391	88	4.74E+01	3.43E+02	2.33E+01
34	287.55	278.838	495	0.2	354	141	1.25E+02	3.73E+02	5.27E+01
35	289.85	280.02	751	0.17	620	131	1.82E+02	3.80E+02	5.75E+01
36	290.35	280.342	520	0.17	358	162	1.96E+02	3.82E+02	5.88E+01
37	290.95	280.235	207	0.14	10	197	2.18E+02	3.86E+02	6.08E+01
38	289.25	281.417	204	0.31	1	203	1.75E+02	3.84E+02	5.70E+01
39	288.15	280.879	283	0.33	93	190	1.50E+02	3.83E+02	5.48E+01
40	287.55	280.45	129	0.33	6	123	1.38E+02	3.82E+02	5.38E+01
41	287.55	280.235	24	0.31	5	19	1.40E+02	3.83E+02	5.40E+01
42	286.45	279.698	0	0.34	0	0	1.07E+02	3.81E+02	5.13E+01
43	285.35	279.805	0	0.42	0	0	7.61E+01	3.66E+02	3.73E+01
44	284.85	279.483	0	0.43	0	0	6.25E+01	3.59E+02	3.07E+01
45	285.95	282.383	0	0.62	0	0	0	5.03E+01	0
46	285.95	281.631	0	0.55	0	0	0	5.03E+01	0
47	286.45	279.483	0	0.32	0	0	0	5.03E+01	0
48	286.45	279.913	0	0.36	0	0	0	5.03E+01	0
49	283.75	279.268	0	0.5	0	0	0	5.03E+01	0
50	283.75	278.624	0	0.43	0	0	0	5.03E+01	0

Appendix 2: Detailed modeling results for XCPC cooling using a 120 RT absorption chiller
Additional information provided here includes:

- Total cooling hours needed: the hours with cooling load great than zero
- Total solar heat available in MWh: total solar heat accumulation in a year with the given solar area
- Total solar heat used in MWh: total solar heat used by the chiller
- Total solar heat remaining in MWh: the solar heat not used by the chiller
- Electricity saved in MWh, the amount of electricity that would be used with a vapor compression chiller with COP of 5 to replace the solar cooling
- Natural gas saved in MWh, the amount of natural gas that would be used otherwise with an absorption chiller with COP 1.3
- Solar cooling ratio, the solar cooling provided divided by the total cooling demand

Table 23 Modeling of solar driven cooling for a 80k sq ft supermarket

	80k sq ft Supermarket			
	Los Angeles	Sacramento	San Diego	San Francisco
Total Cool Need (MWh)	1873	1421	2142	805
Chiller Cooling Provided (MWh)	1023	905	1085	639
Total Cooling Hours Needed	6171	4126	6705	3234
Total Solar Hours Available	4132	4209	4208	4142
Total Cooling Hours Provided	3016	2498	3210	1856
Total Solar Heat Available (MWh)	982	1016	1025	975
Total Solar Heat Used (MWh)	639	566	678	400
Total Solar Heat Remaining (MWh)	343	451	347	576
Electricity saved (MWh)	205	181	217	128
Electricity cost saved	\$40,919	\$36,199	\$43,405	\$25,576
Natural gas saved (MWh)	769	680	816	481
Natural gas cost saved	\$38,458	\$34,022	\$40,794	\$24,038
Collector Area (m2)	793	793	793	793
Solar Cooling Ratio	0.55	0.64	0.51	0.79
Solar Utilization Ratio	0.65	0.56	0.66	0.41

Note: Parasitic estimation can be done as follows LA = 3016 hours of operation with 4.8 kW for pumps (120 RT chiller estimate) implying operational costs of 14477 kWh*0.2 cents/kWh = ~\$2895 per yr which is < 10% of net savings from the system. Similar estimates for other cities/building types can be done.

Table 24: Modeling of solar driven cooling for a 120k sq ft retail store

	120k sq ft Retail Store			
	Los Angeles	Sacramento	San Diego	San Francisco
Total Cool Need (MWh)	2073	1910	2396	960
Chiller Q Provided (MWh)	1032	959	1104	647
Total Cooling Hours Need	5504	4462	5517	4827
Total Solar Hours Available	3452	3527	3545	3422
Total Cooling Hours Provided	3401	2976	3582	2544
Total Solar Heating Available (MWh)	982	1016	1025	975
Total Solar Heating Used (MWh)	645	599	690	404
Total Solar Heat Remaining (MWh)	337	417	335	571
Electricity saved (MWh)	206	192	221	129
Electricity cost saved	\$41,279	\$38,351	\$44,153	\$25,883
Natural gas saved (MWh)	776	721	830	487
Natural gas cost saved	\$38,796	\$36,045	\$41,497	\$24,326
Collector Area (m2)	793	793	793	793
Solar Cooling Ratio	0.50	0.50	0.46	0.67
Solar Utilization Ratio	0.66	0.59	0.67	0.41

Table 25: Modeling of solar driven cooling for a 270k sq ft hospital

	270k sq ft Hospital			
	Los Angeles	Sacramento	San Diego	San Francisco
Total Cool Need (MWh)	4405	3586	4967	2308
Chiller Q Provided (MWh)	1223	1158	1269	1056
Total Cooling Hours Need	8695	7858	8726	8188
Total Solar Hours Available	3452	3527	3545	3422
Total Cooling Hours Provided	3571	3366	3659	3341
Total Solar Heating Available (MWh)	982	1016	1025	975
Total Solar Heating Used (MWh)	765	724	793	660
Total Solar Heat Remaining (MWh)	218	292	232	315
Electricity saved (MWh)	245	232	254	211
Electricity cost saved	\$48,930	\$46,322	\$50,752	\$42,251
Natural gas saved (MWh)	920	871	954	794
Natural gas cost saved	\$45,986	\$43,536	\$47,700	\$39,709
Collector Area (m2)	793	793	793	793
Solar Cooling Ratio	0.28	0.32	0.26	0.46
Solar Utilization Ratio	0.78	0.71	0.77	0.68

Table 26: Modeling of solar driven cooling for a 270k sq ft hotel

	270k sq ft Hotel			
	Los Angeles	Sacramento	San Diego	San Francisco
Total Cool Need (MWh)	2945	2618	3355	1583
Chiller Q Provided (MWh)	1118	1023	1178	826
Total Cooling Hours Need	8682	7368	8729	8139
Total Solar Hours Available	3452	3527	3545	3422
Total Cooling Hours Provided	3427	3063	3577	2868
Total Solar Heating Available (MWh)	982	1016	1025	975
Total Solar Heating Used (MWh)	699	640	736	516
Total Solar Heat Remaining (MWh)	283	377	289	459
Electricity saved (MWh)	224	205	236	165
Electricity cost saved	\$44,737	\$40,937	\$47,134	\$33,047
Natural gas saved (MWh)	841	770	886	621
Natural gas cost saved	\$42,046	\$38,475	\$44,299	\$31,059
Collector Area (m2)	793	793	793	793
Solar Cooling Ratio	0.38	0.39	0.35	0.52
Solar Utilization Ratio	0.71	0.63	0.72	0.53

2.9. Task 10

Three competing XCPC design concepts were formulated in Task 4.

1. All glass dewar: Direct Flow
2. All glass dewar filled with thermal fluid: Indirect Flow
3. Metal absorber with glass-to-metal seal

In Task 7, relying on only off-the-shelf components, the thermal efficiency of each design was estimated as a function of operating temperature. It was found that the “Direct Flow” design and the “Metal Absorber with Glass-to-Metal Seal” design could nearly achieve the performance goal of 50% thermal efficiency at 400°F. This was a very positive result. But before selecting a “Preferred XCPC Design” (Task 11 of this project), the extent that future component could improve the performance of the top two XCPC design alternatives development (Phase 2 activities during the second year of this project) was quantified. The “Fluid-filled dewar” design was not considered since Task 7 showed that the concept offers little potential to achieve the performance goal.

Component Improvements

There are a number of ways to increase the performance of the XCPC through the development of improved components that can then be incorporated into the design of an advanced XCPC. Some of these component improvements require a significant R&D effort, while others do not and can be implemented quite quickly into an improved XCPC design.

Four primary component improvements were identified. The difficulty of successfully implementing various component improvements was examined, and their performance impacts were quantified.

- A. Improved Selective Coating
- B. Anti-Reflective Coating on Glass
- C. Higher Reflectance CPC
- D. Thicker Absorber (applies only to Metal absorber with glass-to-metal seal)

A) Improved Selective Coating

First, the “Metal absorber with glass-to-metal seal” design, which uses a thin metallic foil that has a black selective coating, was considered.

Alanod's Mirotherm selective foil possesses very good optical properties⁸, as noted in table 27 below. Only the TiNOX has a higher absorptance, but TiNOX has an unacceptably high emittance (e = .158) at 200°C.

	Solar-Wt Absorptance	Emittance @ 27C	Emittance @ 200C	Coating Substrate
Metal Foils for Sealed Glass Tubes				
TiNOX	0.958	0.035	0.158	copper
Eurocon	0.902	0.05	0.064	aluminum
Alanod Mirotherm	0.934	0.043	0.057	aluminum

Table 27. Selective Foil Properties
Source: The Regents of University of California

To put the optical properties of Alanod's Mirotherm into perspective, it was compared against the highly advanced cermet coatings that have been developed for use in higher-temperature evacuated receivers used for parabolic troughs. Table 28 shown below was taken from NREL research⁹ and shows that the properties of Mirotherm at 200°C compare favorably with these highly-advanced cermet coatings. The absorptance of the "Improved Cermet" is 2% points higher than Mirotherm, but the emittance is also higher (.085 vs .057 for the Mirotherm) – not a preferred tradeoff for the XCPC. The more advanced coating labeled "NREL 6A" does indicate some potential for modest improvement, but these "NREL 6A" values were laboratory-based and the final product turned out not to be for exterior commercial production environments.

	Original Mo- Al ₂ O ₃ Cermet	Improved Al ₂ O ₃ - based Cermet	NREL 6A
Solar α	0.938	0.954	0.959
Thermal ε (α)			
25°C	0.061	0.052	0.027
100°C	0.077	0.067	0.033
200°C	0.095	0.085	0.040
300°C	0.118	0.107	0.048
400°C	0.146	0.134	0.061
450°C	0.162	0.149	0.070
500°C	0.179	0.165	0.082

Table 28. Cermet Properties
Source: The Regents of University of California

Overall, given this background information, it is reasonable to consider that with extensive R&D, we might be able to increase the absorptance to 0.954, while

⁸ The solar-weighted absorptance and the emittance data was measured by Surface Optics Corporation, and documented in the Task 6 Final Report.

⁹ Source: *Progress toward Developing a Durable High-temperature Solar Selective Coating*, Cheryl Kennedy and Hank Price, NREL, Trough Workshop, March 2007.

maintaining the 200°C emittance at 0.05. Figure 104 below is a comparison of the impact this improved selective coating should have on the XCPC's thermal efficiency. Note that at our 200°C design point, it was calculated that the thermal efficiency would increase from 46.4% to 50.5%.

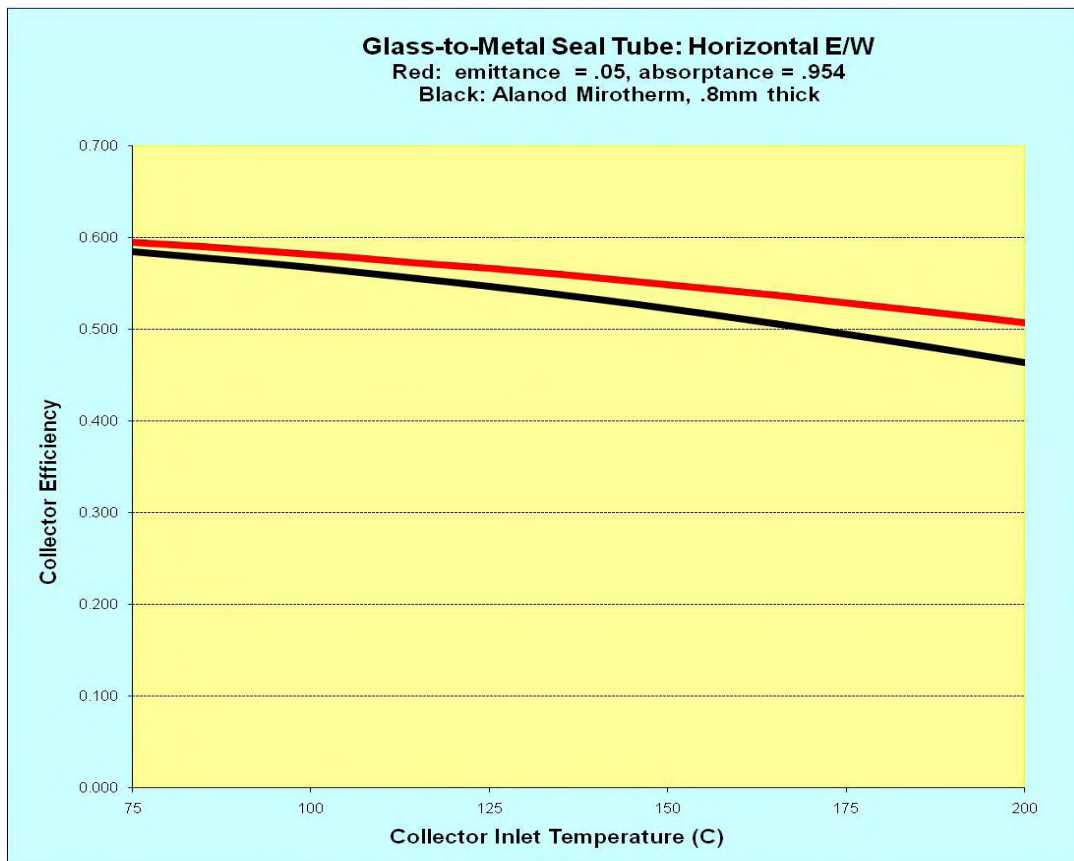


Figure 104. Horizontal Glass to Metal Tube Efficiency

Source: The Regents of University of California

It was also useful to compare this advanced cermet coatings with the coatings used within the all-glass dewars, which are tabulated in Table 29 below.

Chinese all-glass dewars	Solar-Wt	Emittance	Emittance	Coating Substrate
	Absorptance	@ 27C	@ 200C	
Paradigma	0.883	0.1	0.15	glass
Tsinghua	0.923	0.05	0.074	glass
SunRain	0.913	0.047	0.088	glass

Table 29: All Glass Dewar Advanced Cermet Coatings

The Tsinghua dewar has the best optical properties of the dewar coatings. The absorptance of the Tsinghua coating is about 1% point lower than for Mirotherm, and the emittance at 200°C is slightly higher (0.074 vs. 0.064 for the Mirotherm). Achieving the improved selective coating properties we noted above (absorptance = .954 and emittance = .05 at 200°C), was expected to be more difficult for the all-glass dewars. This is because the emittance of glass is high, while the emittance of aluminum (or copper and most other metals) is relatively low. To achieve low

emittance on glass requires that a highly reflective layer be deposited onto the glass, an extra requirement compared to metal-based selective foils. In any case, for the sake of continuity and ease of comparison, we have made these same assumptions for the improved coating (i.e. an absorptance of 0.954 and an emittance of 0.05).

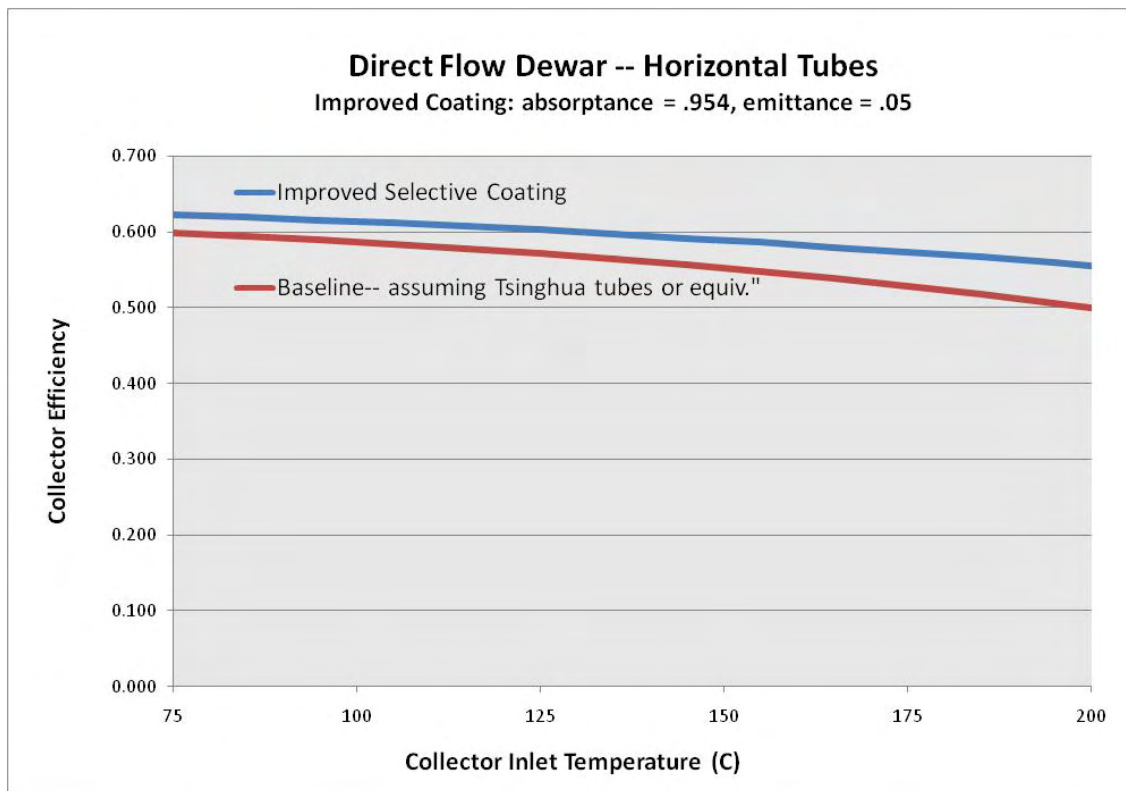


Figure 105. Horizontal Dewar Efficiency

Source: The Regents of University of California

As shown in Figure 105 above for these assumptions (absorptance = .954 and emittance = .05 at 200°C), the “Direct Flow” collector efficiency increases to 55% with the improved selective coating, compared to a baseline collector efficiency at 200°C of 50%,

B) Anti-Reflective Coating on Glass

The solar-weighted transmittance of the borosilicate glass used in the dewars was found to be 91.7%, as reported in the Task 6 Final Report. With the addition of an anti-reflective layer to both surfaces of the glass cylinder (just the 57 mm OD glass cylinder, in the case of the all-glass dewars), the solar-weighted transmittance can be increased to 96%, see Figure 106. The most cost-effective method to add the anti-reflective coating is with the application of a sol-gel coating – typically implemented as a dip process, followed by a bakeout process. Several solar companies have successfully developed this process for parabolic trough evacuated receivers in the last ten years, including Abengoa/Solucar and Schott Solar (for their highly advanced evacuated receivers). But none of the millions of the evacuated tubes that are manufactured in China employed this AR-coating technology.

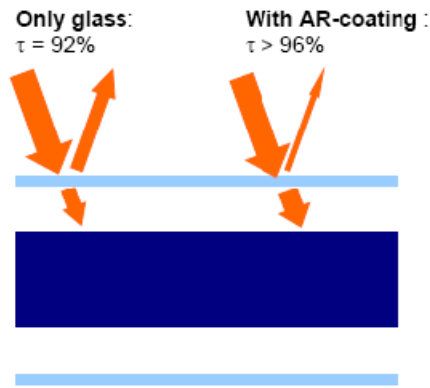


Figure 106. Transmittance with Anti Reflective Coating

Source: The Regents of University of California

The transmittance of borosilicate glass vs wavelength is shown in the figure 107 below, both with the addition of a sol-gel anti-reflective coating and without.

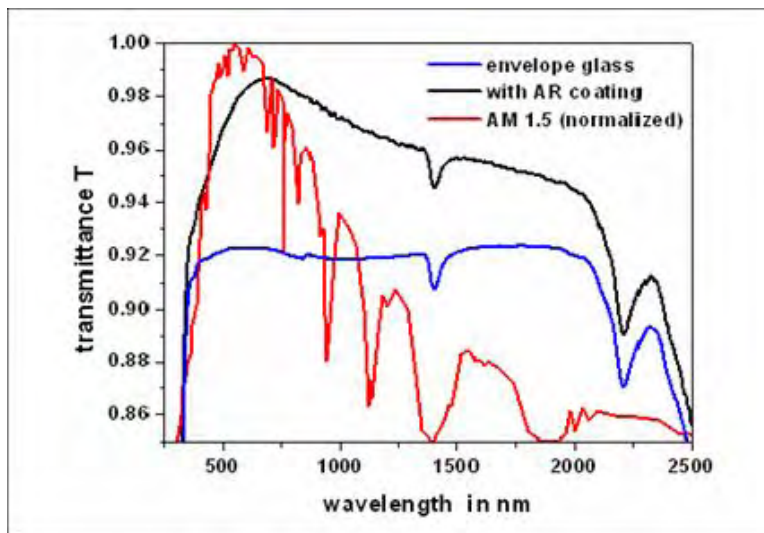


Figure107. Transmittance by Wavelength

Source: The Regents of University of California

With the addition of the anti-reflective coatings to the glass, the collector efficiency at 200°C of the baseline “Metal absorber with glass-to-metal seal” collector increases from 46.4% to 49.5%. Figure 108.

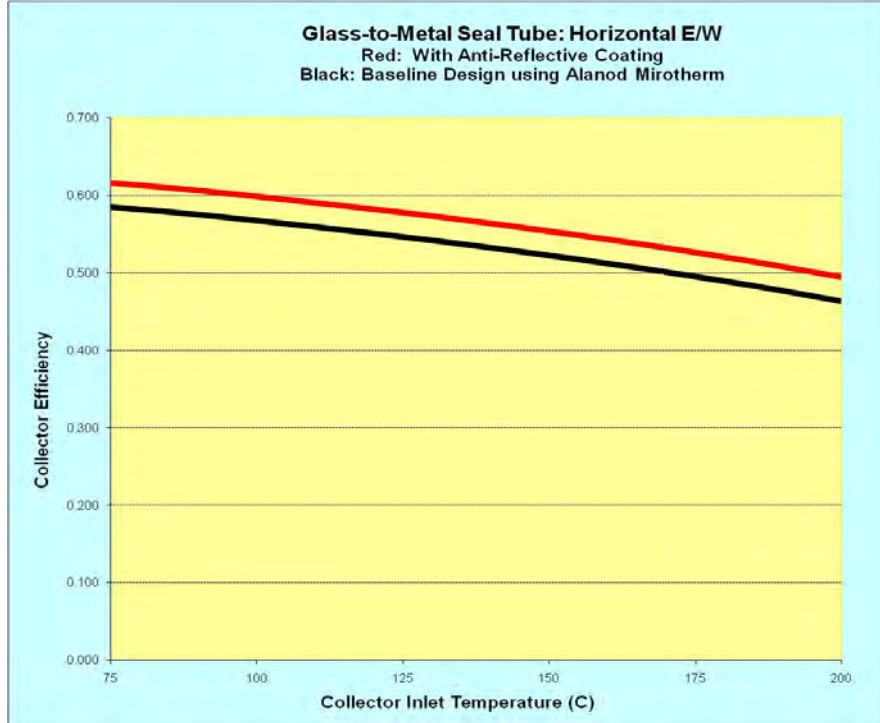


Figure 108. Metal Absorber Collector with AR
 Source: The Regents of University of California

Similarly, with the addition of anti-reflective coatings to the glass dewars for the “Direct Flow” design, the collector efficiency increases from 50% at 200°C to 53%. Figure 109.

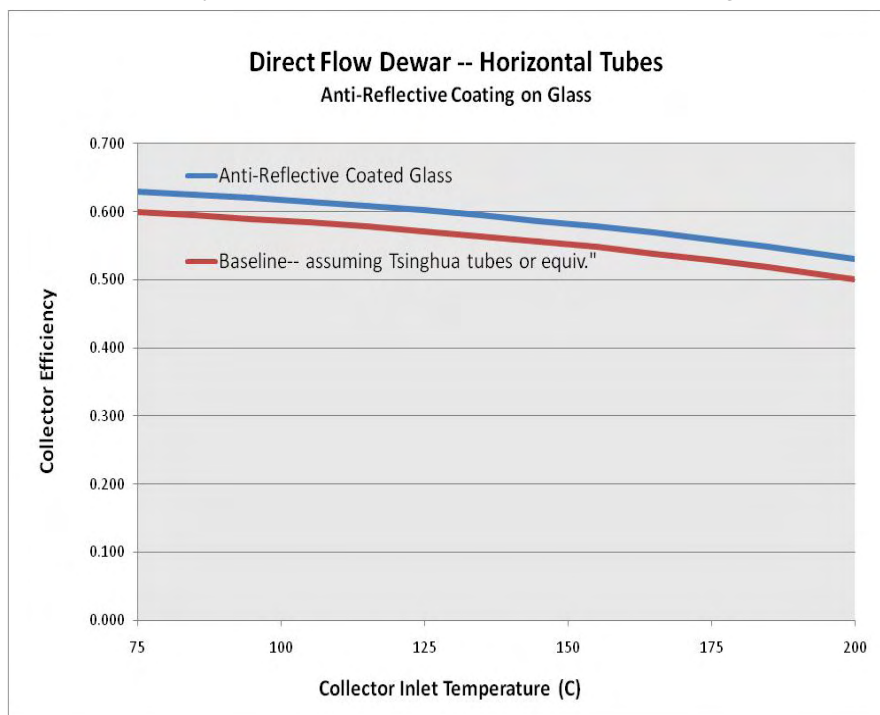


Figure 109. Direct Flow Dewar with AR
 Source: The Regents of University of California

C Higher Reflectance CPC

For our baseline XCPC designs, we assumed the use of Alanod Miro Sun, an advanced aluminum reflector with a specialized coating that increases the reflectance as well as increasing outdoor weatherability. The solar-weighted hemispherical reflectance of Alanod Miro Sun is

91.9%, but it measures 86% with the Devices and Services portable specular reflectometer Model 15R (D&S), which measures at 660 nm, a wavelength that happens to be a bit low with Miro Sun and thereby would be expected to provide a reading on the low side. The D&S also excludes light that is scattered, since it is intended to just measure specularly-reflected light. Given the high acceptance angles of the CPCs, we expected that performance would be more closely governed by hemispherical reflectance than specular reflectance, but would be somewhere in between. To be conservative, in our modeling efforts we assumed a reflectance value of 90%.

Metallized polymer films are another class of reflective surfaces. A relatively recent silvered film has been developed by NREL and ReflecTech (www.reflectechsolar.com) that has recently reached commercial status after years of R&D. The hemispherical reflectance and the specular reflectance (using the D&S) of ReflecTech film both exceed 94%. The measured hemispherical reflectance vs. wavelength values are shown in Figure 110 for Alanod’s Miro Sun and the ReflecTech film. These measurements were obtained at NREL.

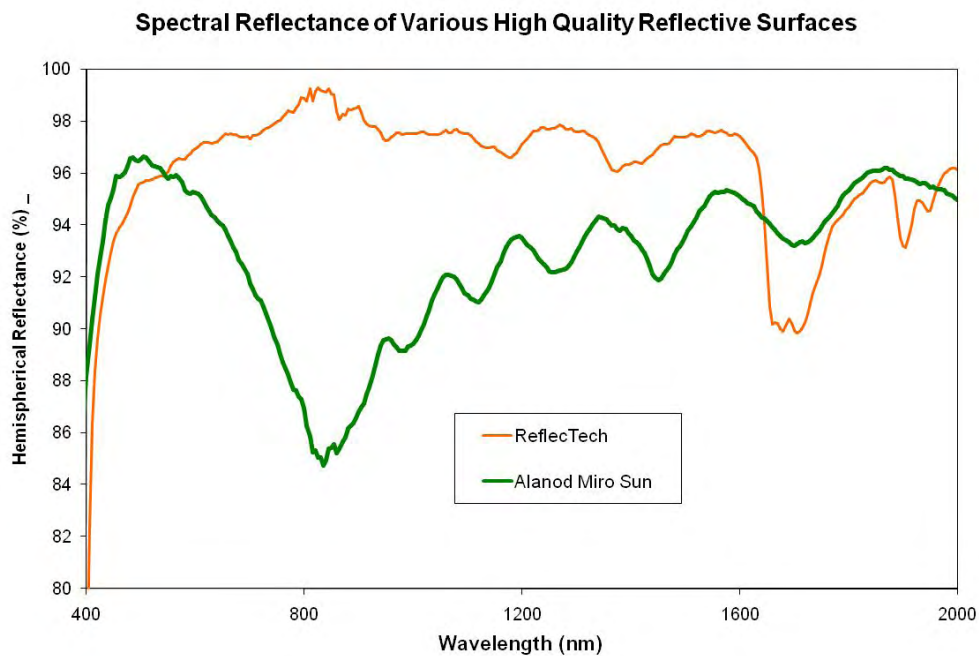


Figure 110. Spectral Reflectance
 Source: The Regents of University of California

Alanod (www.alanod.de) was also expected to offer a higher-reflectance alternate to their Miro Sun. This new reflector utilizes silver in order to achieve a higher reflectance than the aluminum based Miro Sun. Alanod introduced this new material for commercial use in 2008. The materials turned out to be only for protected (lighting and TV displays) environments.

With the use of ReflecTech film, the collector efficiency at 200°C of the baseline “Metal absorber with glass-to-metal seal” collector increases from 46.4% to 48.3%.

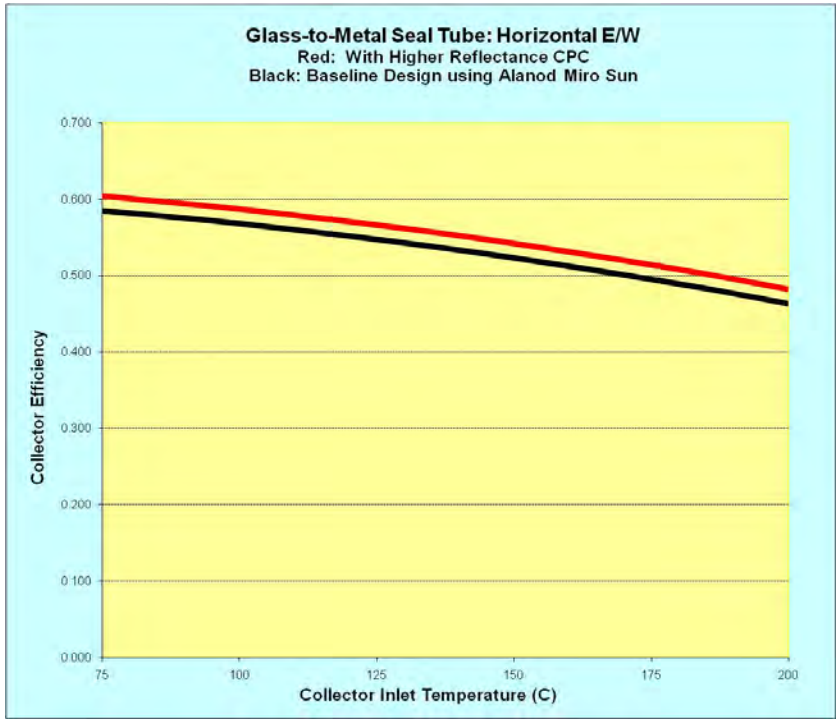


Figure 111. Metal Absorber with Reflectec
 Source: The Regents of University of California

Similarly, with the use of ReflecTech film for the “Direct Flow” design, the 200°C collector efficiency increases from 50% to 52 %.

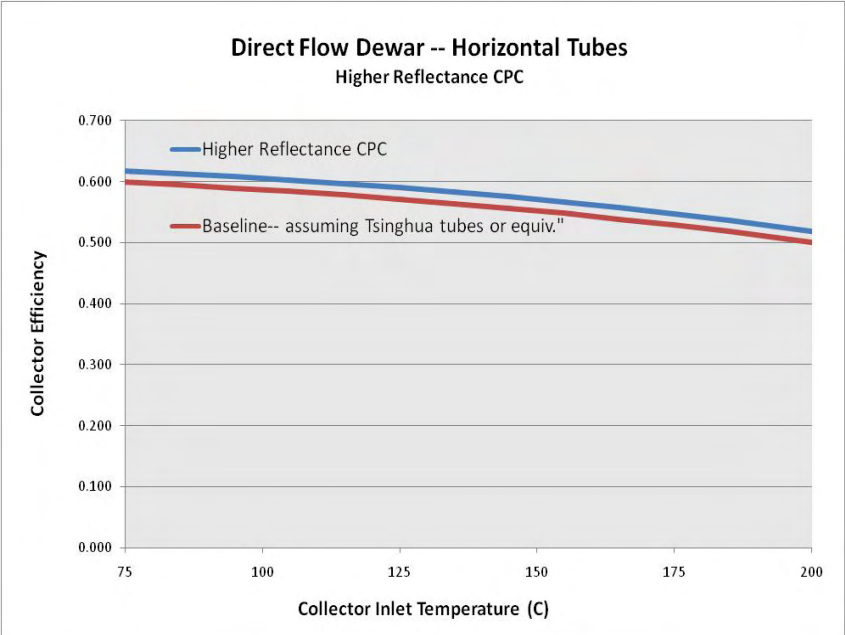


Figure 112. Direct Flow with Reflectec
 Source: The Regents of University of California

Thicker Absorber (applies only to “Metal absorber with glass-to-metal seal” design)

The design pictured in Figure 113 to the right uses an evacuated glass tube with a glass-to-metal seal at one end that maintains the vacuum to insulate the metal absorber. The metal absorber is a thin cylindrical metallic fin with a selective coating that enables high solar absorptance and reduces radiative heat loss. The fin is welded to a metal counter flow tube. The heat absorbed by the fin is transferred to the manifold by the circulating fluid within the metal tube.

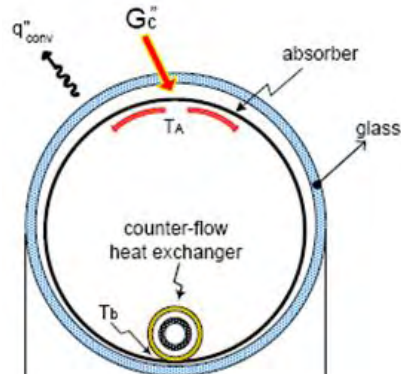


Figure 113. Metal Absorber Design

Source: The Regents of University of California

Our analysis of this design has shown that the thermal performance is significantly affected by the thickness of the cylindrically-shaped metallic absorber, because the cylindrical absorber acts as a fin since it must conduct heat around its entire surface to the point of contact with the copper tube where all the heat is extracted.

Figure 114 shows how the XCPC collector efficiency is affected by the thickness of the absorber. It indicates that an absorber thickness of at least 0.6 mm is needed to achieve good results with an aluminum absorber. Our baseline design (using Alanod’s Miro Sun absorber) uses an aluminum absorber of 0.8 mm. It is clear from the figure that there is virtually no performance incentive to increase the absorber thickness above this baseline 0.8 mm thickness.

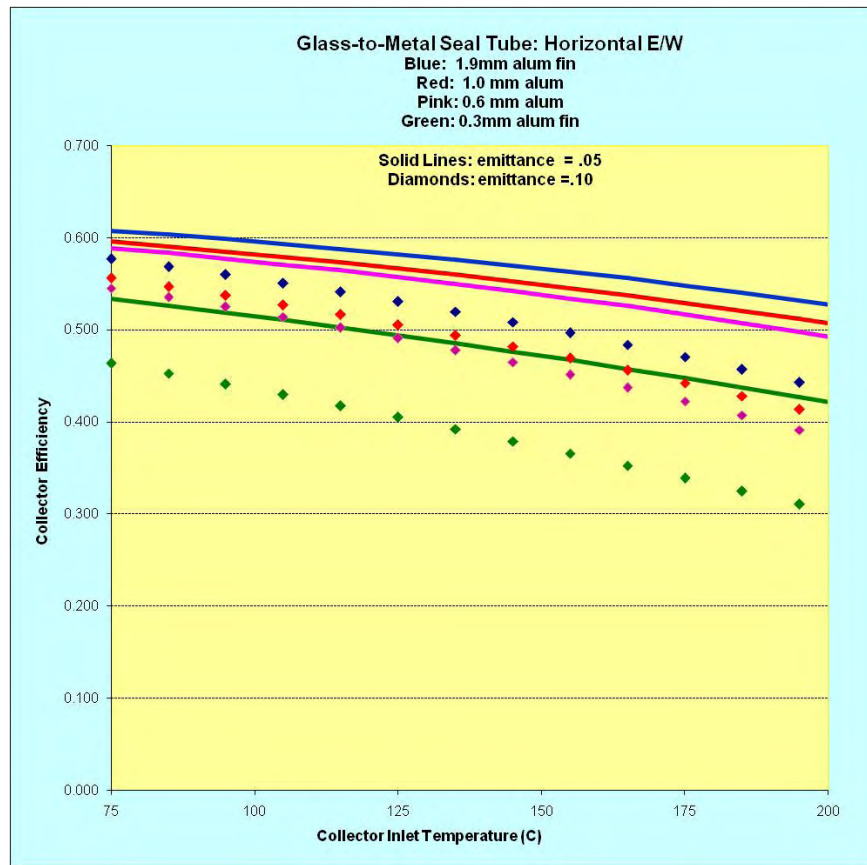


Figure 114. Metal Absorber Thickness

C) AR Coating Combined with Higher Reflectance CPC

In this section, we evaluate the addition of two simultaneous improvements – the two improvements that can be most assuredly incorporated with the little technical risk and at little or no cost (past any R&D and testing activities). The two improvements that are most readily incorporated into an advanced XCPC are the AR-coating and the higher reflectance CPC. The higher reflectance CPC can be most easily accomplished with the use of ReflecTech silvered film. And as noted previously, Alanod is working on a higher reflectance material. The AR-coating will require a significant R&D effort, but not one that has any risk of failure because the addition of sol-gel coatings on borosilicate glass is well understood.

Figure 115 below shows that the collector efficiency of the “Metal absorber with glass-to-metal seal” design at 200°C is estimated to increase from the baseline of 46.4% up to 52.6% with the addition of both the AR-coating and the higher reflectance CPC.

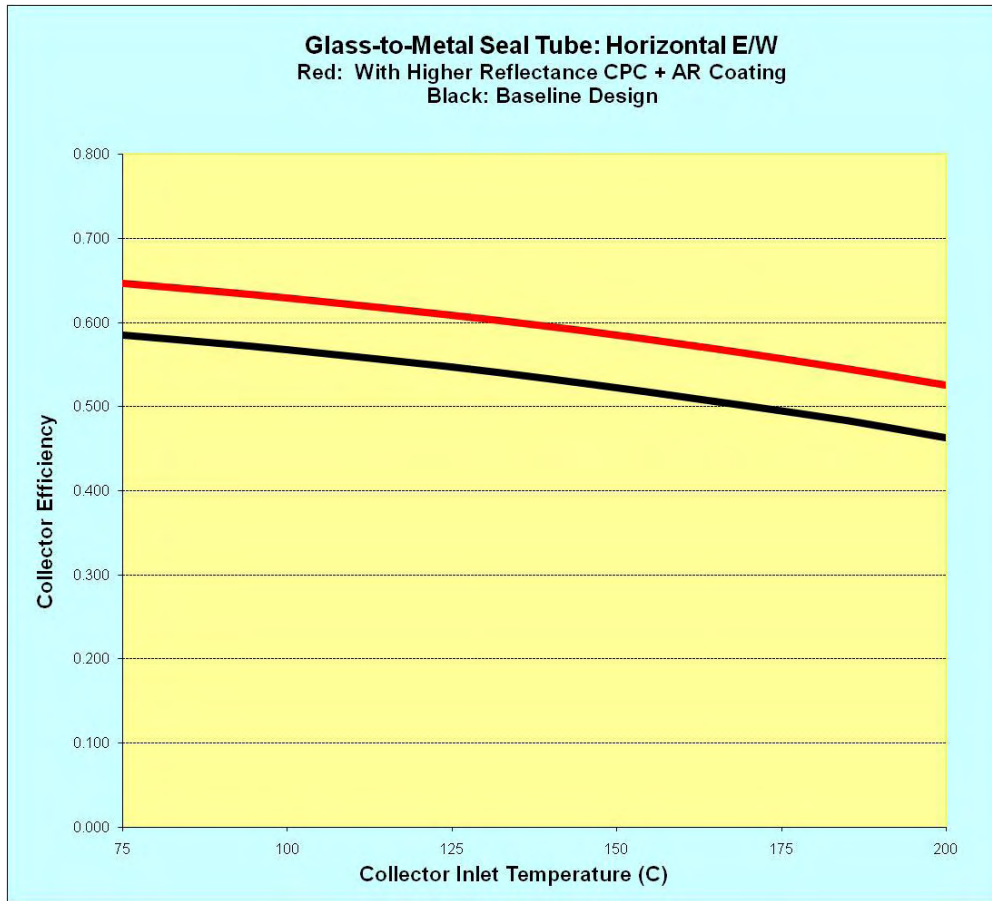


Figure 115 Metal Absorber with AR and Reflectec

Source: The Regents of University of California

Figure 116 shows that the 200°C collector efficiency of the “Direct Flow Dewar” design is estimated to increase from the baseline of 50% up to 56% with the addition of both the AR-coating and the higher reflectance CPC.

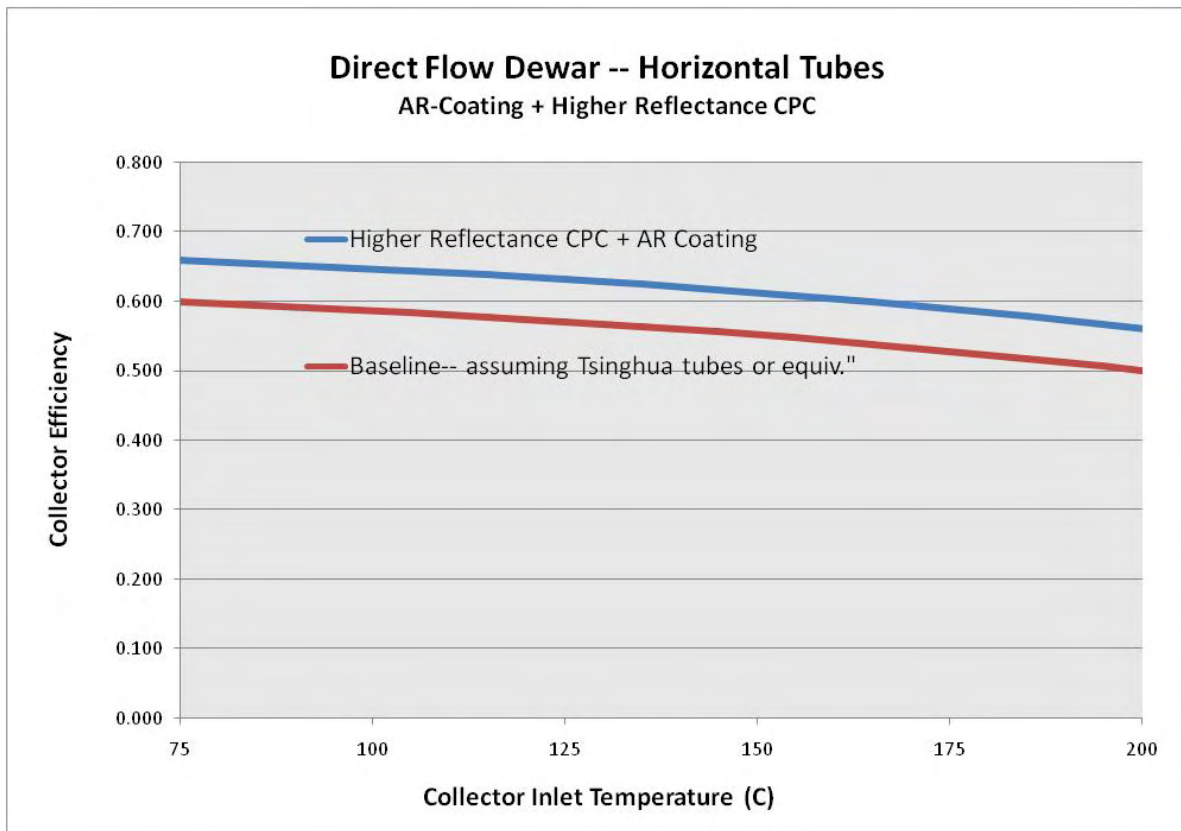


Figure 116. Direct Flow Tube with AR and Reflectec

Source: The Regents of University of California

Summary Table

Table 30 summarizes the findings of this Task 10 analysis.

Component Improvement	Difficulty (1=easy , 5=difficult)		Thermal Efficiency at 200 deg C	
	Direct Flow	Glass-to-Metal Seal	Direct Flow	Glass-to-Metal Seal
Improved Selective Coating	4	5	55%	50.5%
A-R Coated Glass	2	2	53%	48.3%
Higher Reflectance CPC	1	1	52%	48.3%
Thicker Absorber (1 mm)	N/A	2	N/A	47.0%
Higher Reflectance + A-R Coated Glass	N/A	2	56%	52.6%

Baseline = 50% Baseline = 46.4%

Table 30. Component Improvement Summary

Source: The Regents of University of California

2.10. Task 11

Summary

This Task identified a single preferred external compound parabolic concentrator (XCPC) design based on:

- ✓ performance estimates of Task 7,
- ✓ cost estimates of Task 8, and
- ✓ Task 10 analysis of the potential for improvements to each major XCPC design option.

The task provides the XCPC design down-select methodology and all significant data behind the methodology. The methodology is based on a matrix-based evaluation of solar collector system and component characteristics (e.g. cost and efficiency) that are important in determining the technology's overall desirability for likely application(s). The characteristics used for collector selection are:

- Performance
 - Efficiency
 - Actual annual energy production
- Risk
 - Technical
 - Marketing – reputation/potential for leakage
- Cost
- O&M – cost and convenience
- Manufacturability
- Installation
- Robustness, durability/lifetime

The purpose of this down-select process is to determine the single preferred XCPC design that is to be the focus of further work under this project effort. It should be noted that much of the technical data, as well as some of the more qualitative information used in this down-select process, is based on theoretical information and models that have not yet been validated with field testing. Therefore, although this report recommends a preferred XCPC design for further consideration, this recommendation will be confirmed upon field testing the recommended design – for general operability and performance model validation – as part of Task 15 and Task 16.

Collector Design Concepts

The XCPC collector cost and performance goals set forth in this agreement were as follow:

- 50% collector efficiency at 204°C (400 °F)
- Production cost (high volume) less than \$108/m² (\$10/ft²).

Originally (Task 4), the Contract design team (SolFocus and UC Merced) formulated three competing, conceptual-level designs for the XCPC collector. All three designs were believed to have the potential to reach the Contract performance and cost goals. The three original design concepts were as follow:

1. All glass dewar: direct flow Figure 117
2. All glass dewar filled with heat transfer fluid: indirect flow
 - with metal pipe
 - with heat pipe
3. Metal absorber with glass-to-metal seal Figure 118
 - with metal tube
 - with heat pipe

All features of the above design concepts are described in detail in the Contract Task 4 report.

Results from performance analysis documented in the Draft Preliminary Design Report under Task 7 clearly illustrated that the indirect flow collector concept (design concept #2, above) likely did not have the potential to meet our performance goals of 50% efficiency at 200°C. Therefore, this design concept was removed from consideration in our down-select process. Further preliminary analysis showed that for the two remaining design concepts, collector orientation was potentially an influential factor. Therefore, the following design concepts and variations were considered for the final Task 7 performance analysis and Task 8 cost analysis:

1. All glass dewar: direct flow
 - a. east-west orientation
 - b. north-south orientation
2. Metal absorber flow-through
 - a. east-west orientation
 - b. north-south orientation
3. Metal absorber heat pipe (only north-south orientation possible)

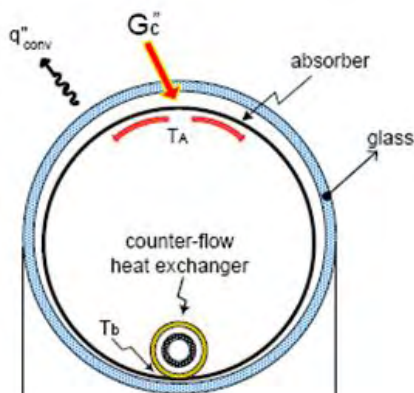


Figure 117. All glass dewar: direct flow
Source: The Regents of University of California

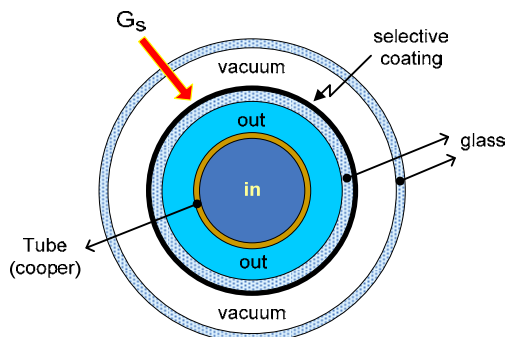


Figure 118. Metal absorber with glass-to-metal seal
Source: The Regents of University of California

Collector Performance Analysis

The project team has looked to the collectors' projected performance as a significant determinant in the down-select process. A precursory performance analysis of the five original design concepts was first performed as part of Task 4. The Task 6 Component Characterization Report provided the performance-critical, material properties of the off-the-shelf components that are being considered for the XCPC. The projected collector efficiency as a function of heat-transfer-fluid temperature was calculated as part of Task 7. And the Task 10 Report assessed ways in which the collector efficiencies might be improved through R&D, and quantified the impact this improvements would make on the XCPC collector designs.

The heat pipe design was eliminated from the performance analysis of the down-select process because the heat pipe analysis performed by United Technologies Research Center, which is included in Task 6, determined that it did not have temperature capability above 160°C.

The “baseline” collector efficiencies for the two primary XCPC designs are shown in figure 119 and Figure 120 below, along with the higher collector efficiencies that can be achieved using relatively straight forward component improvements.

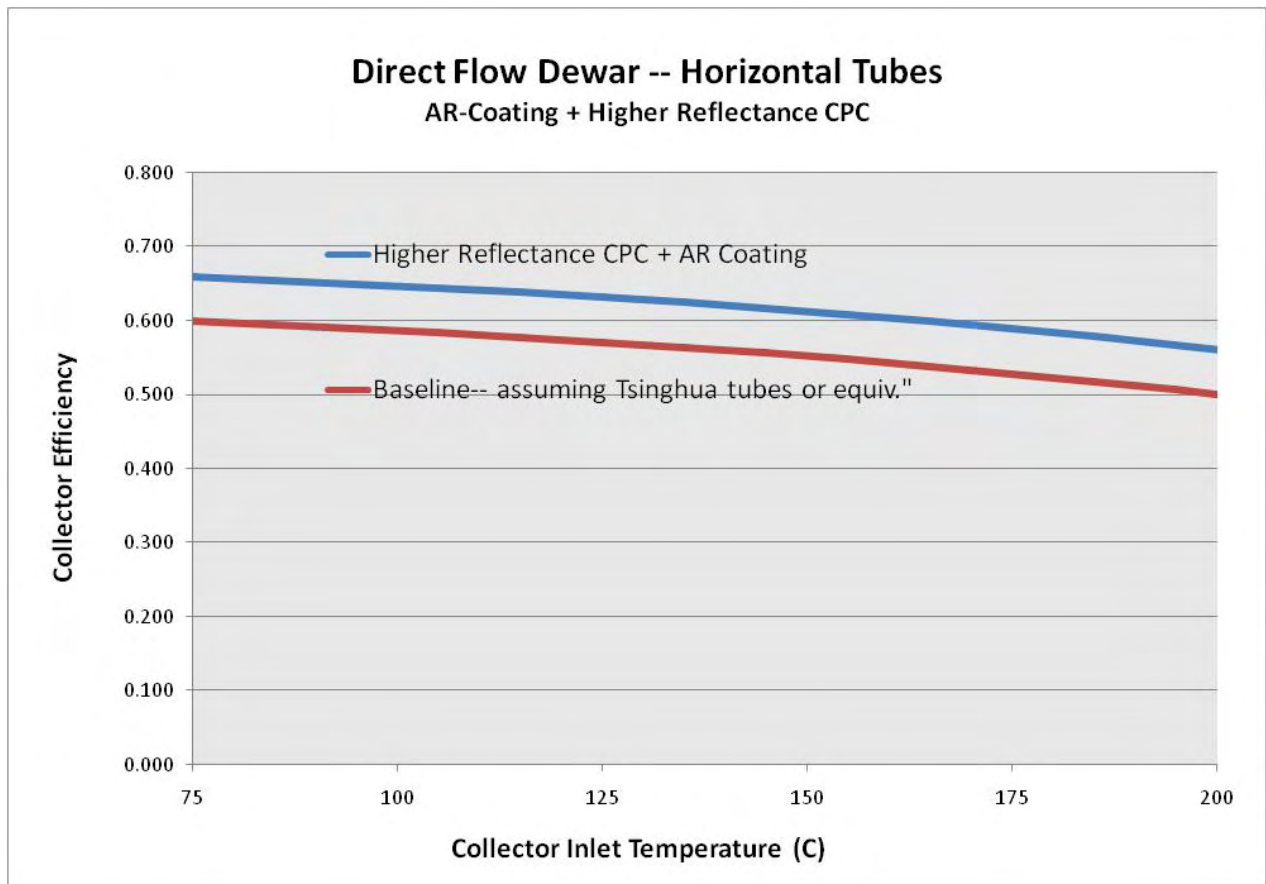


Figure 119. Direct Flow Dewar

Source: The Regents of University of California

Note that the direct-flow dewar design is expected to achieve the 50% collector efficiency goal at 200°C using off-the-shelf components, and has the potential to surpass this performance goal with the development of improved components.

The metal absorber with glass-to-metal seal design, as shown in Figure 120 below, falls just short of the 50% performance goal (at 200° C), but can surpass this goal with the development of improved components. Although the baseline collector efficiency for this design falls slightly below the 50% efficiency goal, the efficiency curve still shows exceptional performance.

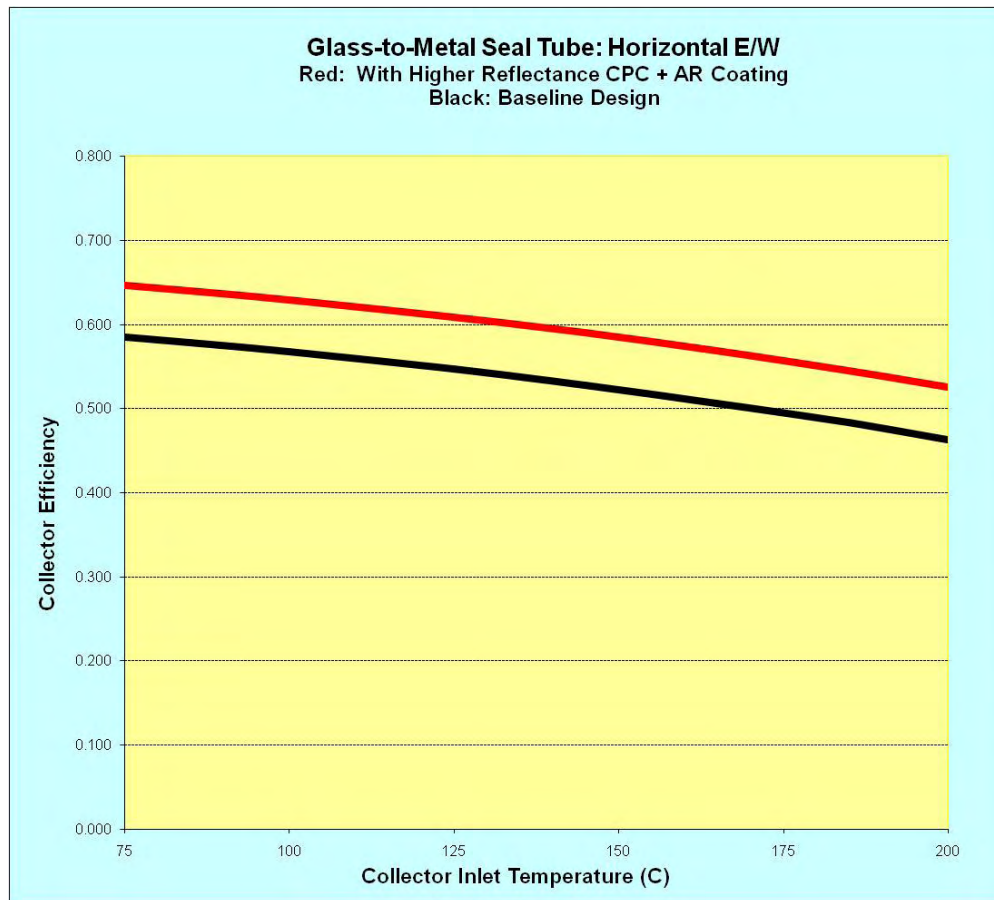


Figure 120. Metal Absorber

Source: The Regents of University of California

In Task 5, the annual performance modeling tool f-Chart was determined to be an appropriate analysis tool for this stage of the XCPC collector development. F-chart (see www.fchart.com) uses the following as input parameters: optical efficiencies, acceptance half angle, incident angle modifiers (as determined by the project's raytrace model) and heat-loss coefficients (as determined by the project team's heat transfer analysis). F-Chart was used for the analysis presented in this report to examine and compare the area-normalized, annual performance of the two design concepts and orientations. The results of this analysis for two California climates – San Francisco (diffuse solar resource) and Daggett (strong direct-normal solar resource) – are shown in Figure 121 and Figure 122 respectively.

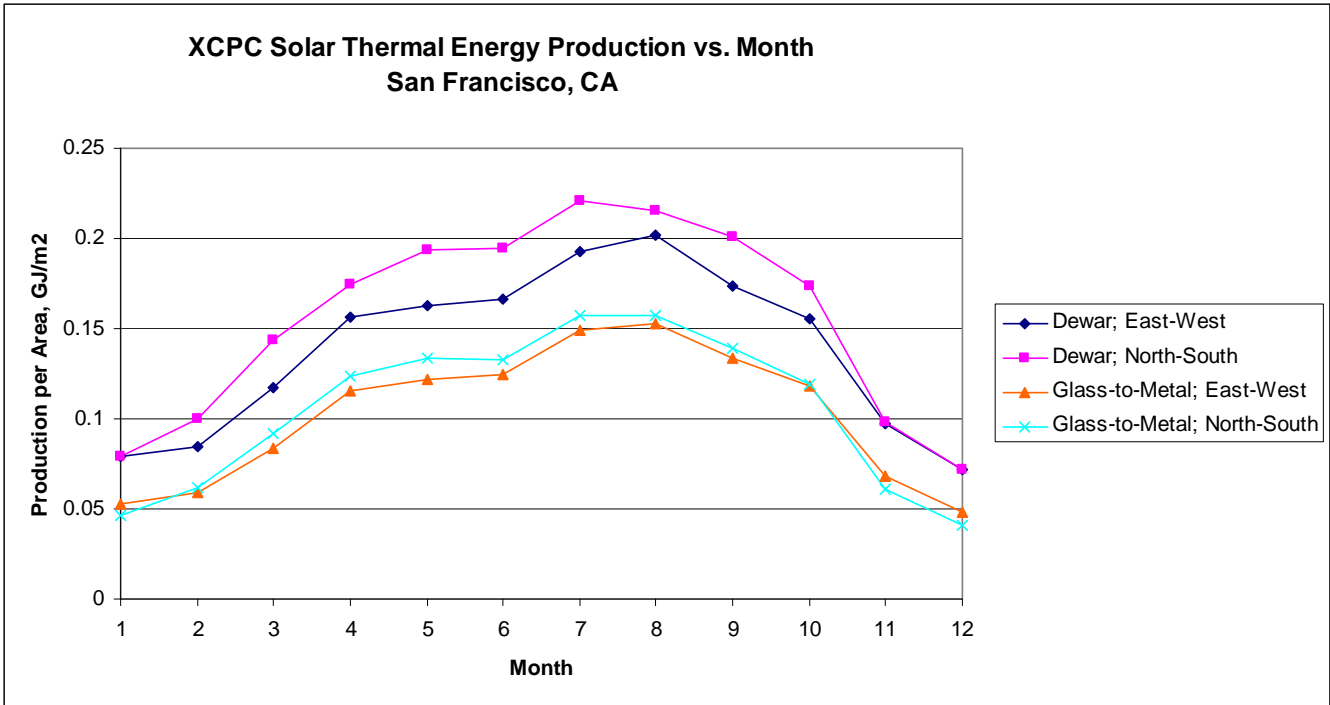


Figure 121. Annular Performance in a Diffused Environment

Source: The Regents of University of California

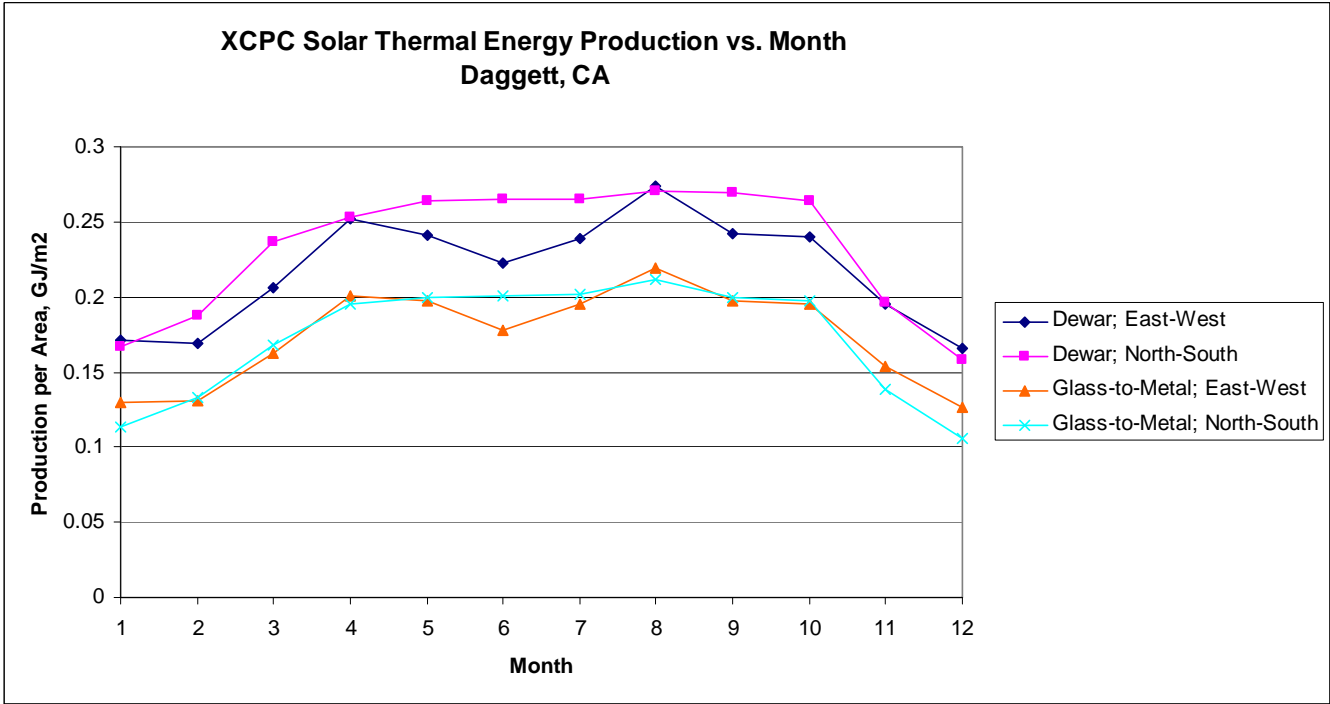


Figure 122. Annular Performance in a Direct Solar Environment

Source: The Regents of University of California

In agreement with the efficiency curves, the f-Chart results predict slightly better performance on the part of the all-glass, direct-flow dewar. Not predicted by the efficiency calculations, the f-Chart results predict an added performance benefit from the north-south orientation in locations with non-negligible diffuse solar radiation, such as in San Francisco. The enhanced

benefit of the north-south orientation in non-desert climate zones is believed to be a result of the acceptance angle. The acceptance half angle for the north-south reflector design is 60° and for the east-west reflector design, it is 35°. Under diffuse weather conditions (e.g. overcast, cloudy or humid) a more significant fraction of the solar resource is scattered and, therefore, a wider acceptance angle becomes more of a factor to enhancing the collector's performance.

Collector Cost Analysis

The Task 8 Draft XCPX Cost Comparison Report provides a bill of materials (BOM) analysis for each of the final design concepts and variations listed above. The results of this analysis are in Table 31.

XCPX concept	All-glass dewar: Direct Flow	All-glass dewar: Direct Flow	Metal absorber flow-through	Metal absorber flow-through	Metal absorber heat pipe
Orientation	East-West	North-South	East-West	North-South	North-South
Bill of Materials					
Absorber tube					
Tube type	Sunrain All-glass dewar with improved selective coating (TTY-MC)	Sunrain All-glass dewar with improved selective coating (TTY-MC)	Beijing Eurocon metal absorber tube with counterflow insert	Beijing Eurocon metal absorber tube with counterflow insert	Beijing Eurocon metal absorber tube with heat pipe
Length of tube	1800 mm	1800 mm	1800 mm	1800 mm	1800 mm
OD of tube	58 mm	58 mm	65 mm	65 mm	65 mm
Diameter of absorber	47 mm	47 mm	56 mm	56 mm	56 mm
Price of one tube	\$3.20	\$3.20	\$22.00	\$22.00	\$21.00
Price of tubes [per aperture of reflector (m2)]	\$6.40	\$9.94	\$37.19	\$58.27	\$55.62
Reflector					
Material	Alanod	Alanod	Alanod	Alanod	Alanod
Reflectivity	90%	90%	90%	90%	90%
Acceptance angle	± 34°	± 60°	± 34°	± 60°	± 60°
Truncation	20%	20%	20%	20%	20%
Length of reflector (mm)	1860	1860	1860	1860	1860
Width (mm) of reflector opening (incl 1mm spacing)	269	173	318	203	203
Depth (mm) of reflector	212	83	261	97	97
Arclength of reflector (mm)	562.6	278.8	685.6	327.8	327.8
Aperture of one reflector (m2)	0.50034	0.32178	0.59148	0.37758	0.37758
Reflector material needed per tube (m2)	1.046436	0.518568	1.275216	0.609708	0.609708
Price of reflector material (incl. support structure) per m2	\$15.00	\$15.00	\$15.00	\$15.00	\$15.00
Price of reflector per tube	\$15.70	\$7.78	\$19.13	\$9.15	\$9.15
Price of reflector [per aperture of reflector (m2)]	\$31.37	\$24.17	\$32.34	\$24.22	\$24.22
Manifold					
Length of manifold	~2.2m	~2.2m	~2m	~2.1m	~2.1m
Tubes per manifold	8	12	6	10	10
Price of manifold (Eurocon)	\$180.00	\$190.00	\$96.00	\$106.00	\$80.00
Estimated price of manifold in mass production	\$90.00	\$95.00	\$48.00	\$53.00	\$40.00
Price of manifold per tube	\$11.25	\$7.92	\$8.00	\$5.30	\$4.00
Price of manifold [per aperture of reflector (m2)]	\$22.48	\$24.60	\$13.53	\$14.04	\$10.59
Collector frame and rack					
Dimensions of one collector	~2.2m x 2m	~2.2m x 2m	~2m x 2m	~2.1m x 2m	~2.1m x 2m
Price of one frame including rack (Eurocon)	\$176.00	\$176.00	\$176.00	\$176.00	\$176.00
Estimated price of one frame including rack in mass production	\$88.00	\$88.00	\$88.00	\$88.00	\$88.00
Price of one frame including rack per tube	\$11.00	\$7.33	\$14.67	\$8.80	\$8.80
Price of frame and rack [per aperture of reflector (m2)]	\$21.99	\$22.79	\$24.80	\$23.31	\$23.31
Total BOM [per aperture of reflector (m2)]	\$82.24	\$81.51	\$107.86	\$119.83	\$113.74
Total BOM [per aperture of reflector (sf)]	\$7.64	\$7.58	\$10.02	\$11.14	\$10.57

Table 31. Cost Comparison of XCPX Design Concepts in High Volume Production (10,000 tubes)

Source: The Regents of University of California

The BOM cost analysis results favor the direct-flow all-glass dewar designs. The all-glass dewar collectors are estimated to be from 24% to 32% lower in cost than the metal absorber with glass-to-metal seal collectors. But it is notable that the metal absorber with glass-to-metal seal

collector is estimated to cost \$107.86/m² (\$10.02/ft²), which is right at our cost goal target, and the north-south version is within 11% of the cost target.

Further, although the BOM cost estimates point to the dewar designs, this cost calculation is only one component of the complete cost analysis that should be performed for the final, single collector down select. The Contractor recommends that, as part of the final selection, we perform analysis to determine the levelized cost of energy (LCOE, \$/kWh) and the installed cost per generation capacity (\$/kW) for each design concept and orientation variation.

Collector Down Select

Table 32 provides the down-select matrix for the XCPC collectors under consideration.

Collector	All Glass Dewar – Direct Flow	All Glass Dewar – Direct Flow	Metal Abs. with Glass-to-Metal Seal and Counter Flow-Through	Metal Abs. with Glass-to-Metal Seal and Counter Flow-Through	Metal Abs. with Glass-to-Metal Seal and Heat Pipe
Orientation	East-West	North-South	East-West	North-South	North-South
Cost, \$/m²	82.24	81.51	107.86	119.83	113.74
Annual Energy Production, GJ/m² (Daggett, CA)	2.617	2.798	2.086	2.066	Unknown
Cost, \$/GJ (Daggett, CA)	31.43	29.13	51.70	58.00	Unknown
Annual Energy Production, GJ/m² (San Francisco, CA)	1.659	1.868	1.228	1.265	Unknown
Cost, \$/GJ (San Francisco, CA)	49.57	43.63	87.83	94.73	Unknown
Collector Efficiency (@200°C, current properties)	50%	46%	47%	40%	Unknown
Collector Efficiency (@200°C, improved properties)	57%	52%	53%	46%	Unknown
Performance Profile (i.e. hourly load matching)	Unknown	Unknown	Unknown	Unknown	Unknown
O&M (cost and convenience)	Good	Good	Good	Good	Good
Manufacturability	Requires modest development	Requires modest development	Excellent	Excellent	Requires significant development
Robustness, Durability, Lifetime	Requires modest development	Requires modest development	Excellent	Excellent	Requires significant development

Risk: Technical/ Marketability	Moderate	Moderate	Low	Low	High
	Low- Moderate	Low- Moderate	Low- Moderate	Low- Moderate	High
Potential for Improvement	Excellent	Excellent	Low-Good	Low-Good	Unknown

Table 32. Down-Select Matrix

Source: The Regents of University of California

Conclusions

The down-select matrix in Table 32 shows that the first case under consideration – the direct-flow all-glass dewar – has the best predicted performance of all the collector designs under consideration. At 200°C, the project team’s heat transfer analysis, optical analysis, and the measured material properties show this collector’s efficiency projection leads the other projections by a range from 6% to 25%. Although this collector shows better performance capability and lower cost, the metal absorber with glass-to-metal seal design is closer to commercial readiness as well as showing an impressive projected performance. Readiness for commercialization is also a significant consideration for the collector of choice for this project. The glass-to-metal seal collector design currently has better manufacturability, and better durability/robustness and lower technical risk (i.e. lower risk in the event of glass tube breakage) than the all-glass dewar design. Because the all-glass dewar design uses the glass tube directly for containing the heat transfer fluid, it has a higher risk for:

- potential heat transfer fluid leaks between the glass dewar and the manifold,
- tube breakage resulting in a significant heat transfer fluid spill.

Although the required technical development effort necessary to overcome these risks is not viewed as significant, it is somewhat uncertain. Therefore, the design selected as the preferred design for consideration under this project is the metal absorber with glass-to-metal seal. This collector design is very close to commercialization in addition to showing excellent performance prospects. The project team’s heat transfer analysis shows the east-west orientation design has fairly significant efficiency benefits (47% vs. 40% at 200°C) but our f-Chart analysis results show that, because of the north-south concentrator’s wider acceptance angle, there may be benefits to the north-south orientation design. To determine which orientation results in the best performance, the project team recommends testing both orientation designs in multiple climates and more detailed modeling.

2.11. Task 12

This report describes the detailed design of the XCPC that was selected in Task 11. The selected design is called “Metal absorber with glass-to-metal seal and counter flow tube.”

This design uses an evacuated glass tube with a glass-to-metal seal at one end that maintains the vacuum to insulate the metal absorber (Figure 123 and 124). The metal absorber is a thin cylindrical metallic fin with a selective coating that enables high solar absorptance and reduces radiative heat loss. The fin is welded to a metal counter flow tube. The heat absorbed by the fin is transferred to the manifold by the circulating fluid within the metal tube.

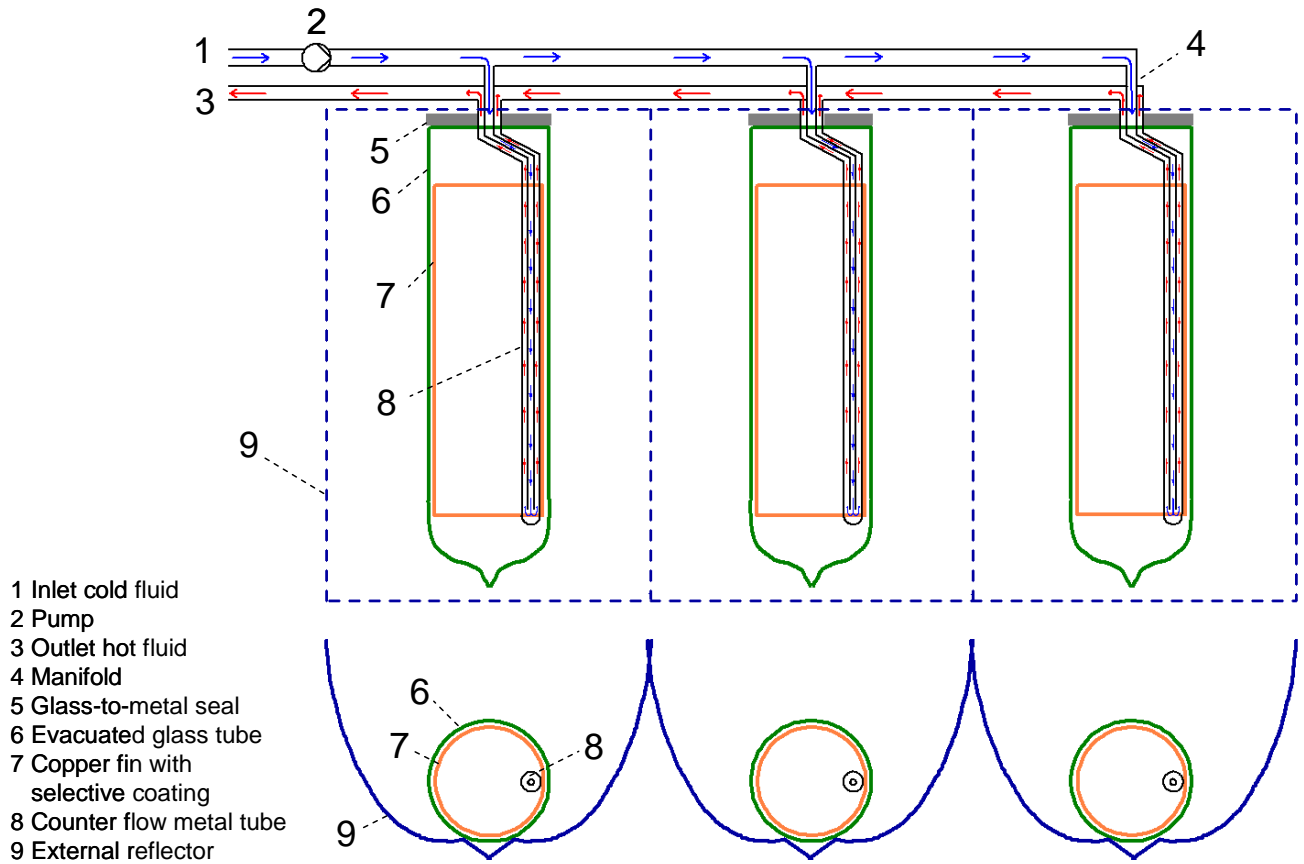


Figure 123. Schematic of XCPC Design
 Source: The Regents of University of California

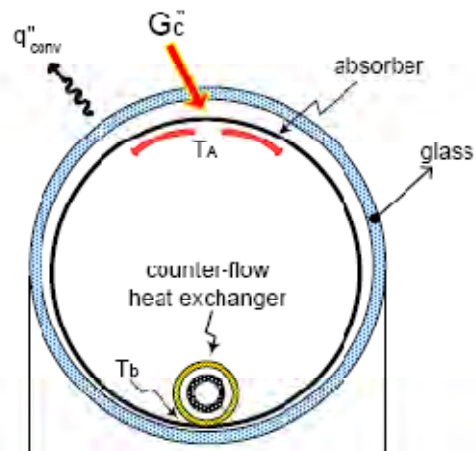


Figure 124. Cross section of absorber tube
 Source: The Regents of University of California

The XCPC design consists of the following elements:

- Evacuated glass tube with metal absorber
- Manifold
- Reflector

- Frame

Evacuated Glass Tube

The evacuated glass tube (including the metal absorber) is made by Beijing Eurocon Solar Energy Tech. Company in Beijing, China. The tube has the following dimensions:

Diameter of outer tube wall: 65 mm
Diameter of inner tube wall: 61.8 mm
Length: 1,800 mm

The metal absorber is a cylindrical aluminum fin of 1mm thickness, 56 mm in diameter and 1,720 mm long. It is coated with a selective coating that was developed by Beijing Eurocon Solar Energy Tech. Company.

The copper counter-flow tube conducts the heat transfer fluid from the manifold through the absorber tube back to the manifold. The counter-flow tube consists of an inner tube (I.D. 6 mm, O.D. 7 mm) and an outer tube (I.D. 10.5 mm, O.D. 12 mm). The counter-flow tube is welded onto the metal absorber.

The glass tube (including the metal absorber and counter-flow tube) is depicted in Figure 125.

The transmittance of the glass tube was measured at NREL. The solar-weighted transmittance was found to be 91.7%, which is a good result. We also measured the absorptance and emittance of the absorber. The absorptance was found to be 0.904, with an emittance of 0.050 at room temperature, and an emittance of 0.064 at 200°C.

Manifold

The copper manifold is made by Beijing Eurocon Solar Energy Tech. Company in Beijing, China. The manifold collects the fluid that is circulated through the parallel absorber tubes. A drawing of the manifold is depicted in Figure 126.

Reflector

The reflector material is a polished aluminum reflector made by Alanod, Germany. We use the Alanod MiroSun product. Its solar-weighted hemispherical reflectance is 91.9%.

The concentration ratio of the reflector is 1.15 (if the tubes are oriented in North-South direction) and 1.8 (in East-West orientation). The acceptance angle is $\pm 60^\circ$ (North-South) and $\pm 34^\circ$ (East-West). The truncation is 20% in both orientations.

The shape of the reflector for both directions is depicted in Figure 127.

Frame

The wooden frame is made by Great Spaces Inc. in Merced, California. It holds six absorber tubes, the reflector and the manifold. The frame contains seven wooden ribs for each tube that are mounted on a wooden ground plate. The ribs provide support for the reflector foil. The Alanod reflector foil is glued onto the wooden ribs. The ribs are cut to the shape that is necessary to achieve the optical concentration. The absorber tubes are then placed

perpendicular to the ribs. A drawing of the frame (for the North-South orientation) is depicted in Figure 128.

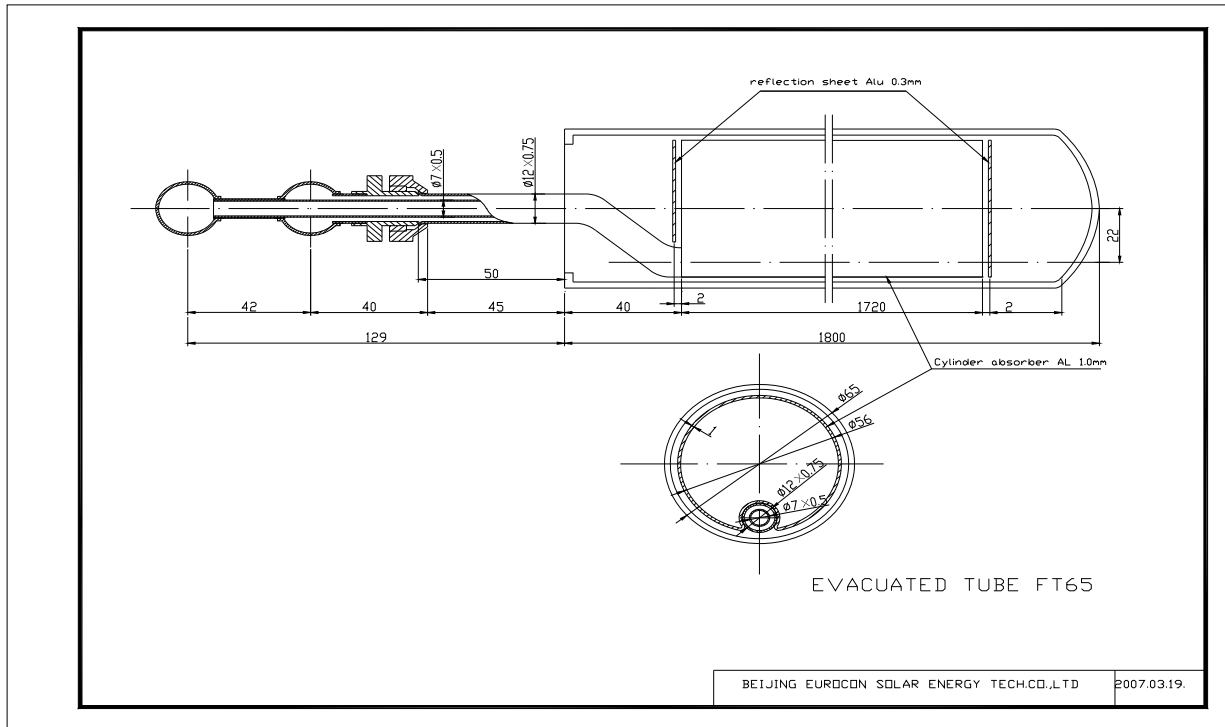


Figure 125. Evacuated glass tube with metal absorber (all units in mm)

Source: The Regents of University of California

List of possible vendors of the parts for the XCPC prototype:

Evacuated glass tube (including the metal absorber) and manifold

Beijing Eurocon Solar Energy Tech. Co. Ltd.
No. 30 Xueyuan Road
Haidian District
Beijing 10083
China

Reflector

Alanod
P.O. Box 3910
180 Leadville Ave. N
Ketchum, Idaho 83340

Frame

Great Spaces USA
360 Grogan Ave
Merced, CA 95340

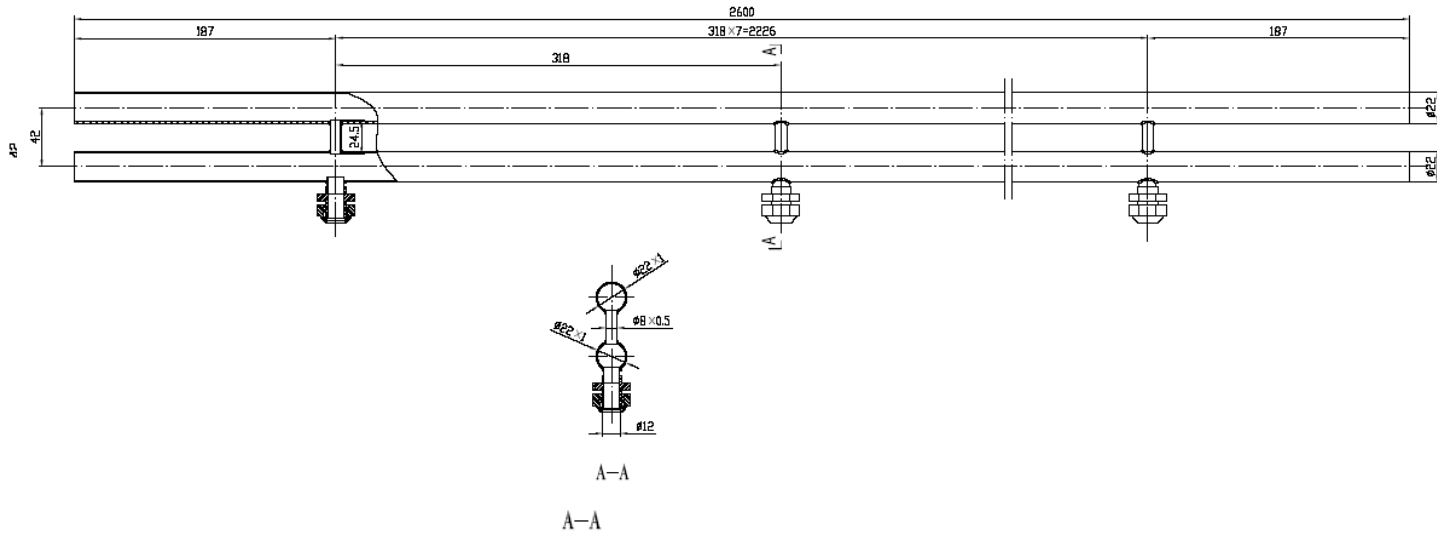


Figure 126. Manifold for North-South orientation [all units in mm]

Source: The Regents of University of California

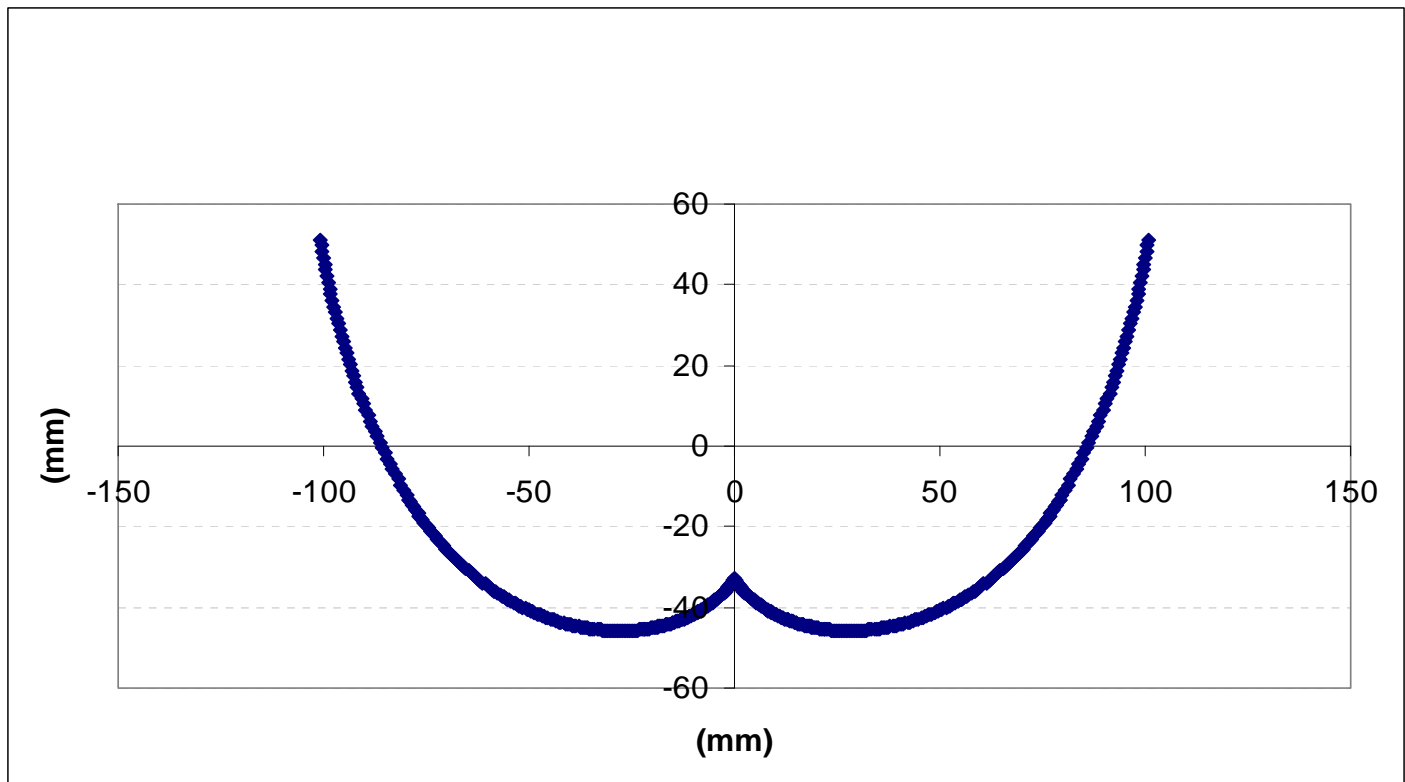


Figure 126b: Manifold for East-West orientation [all units in mm]

Source: The Regents of University of California

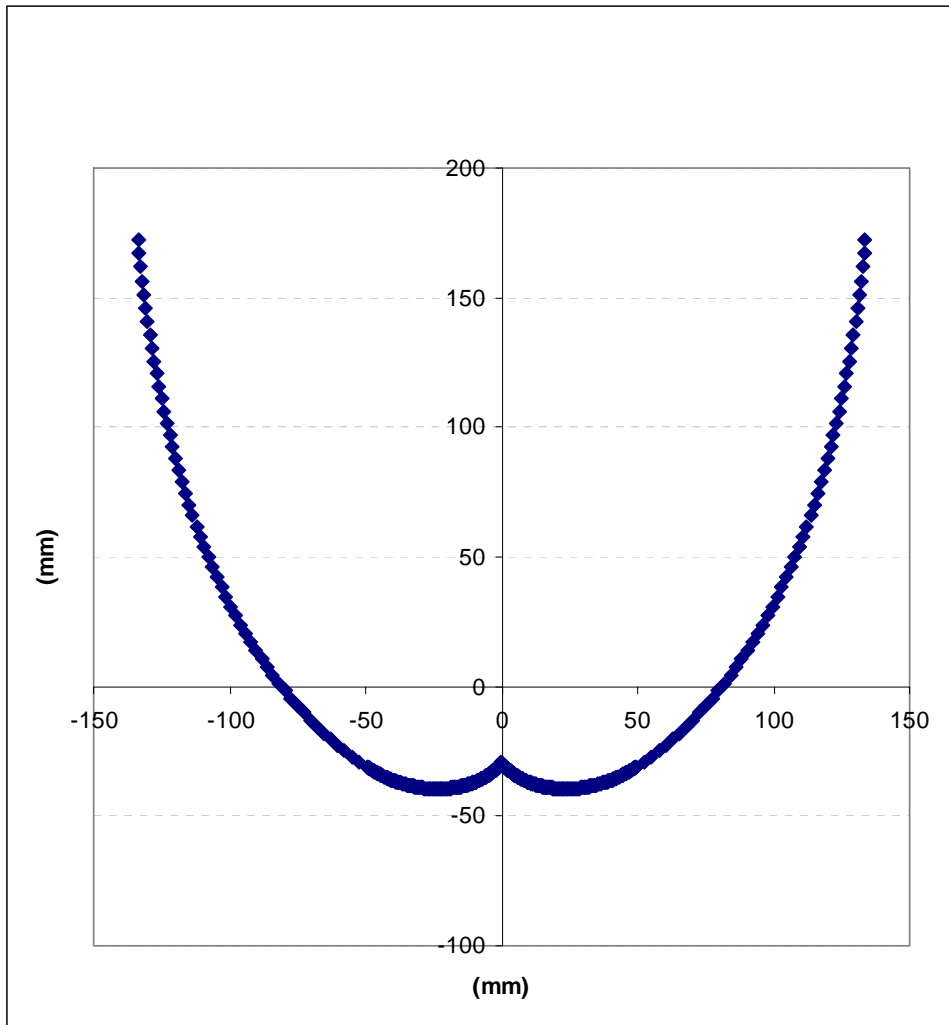


Figure 127a. Cross section of reflector for North-South orientation
 Source: The Regents of University of California

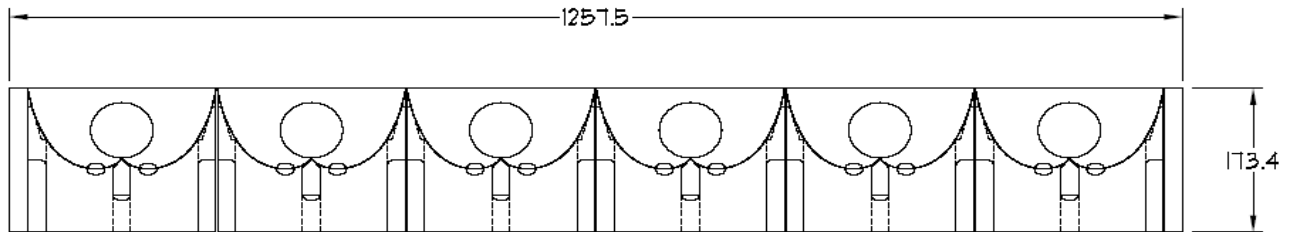


Figure 127b. Cross section of reflector for East-West orientation
 Source: The Regents of University of California

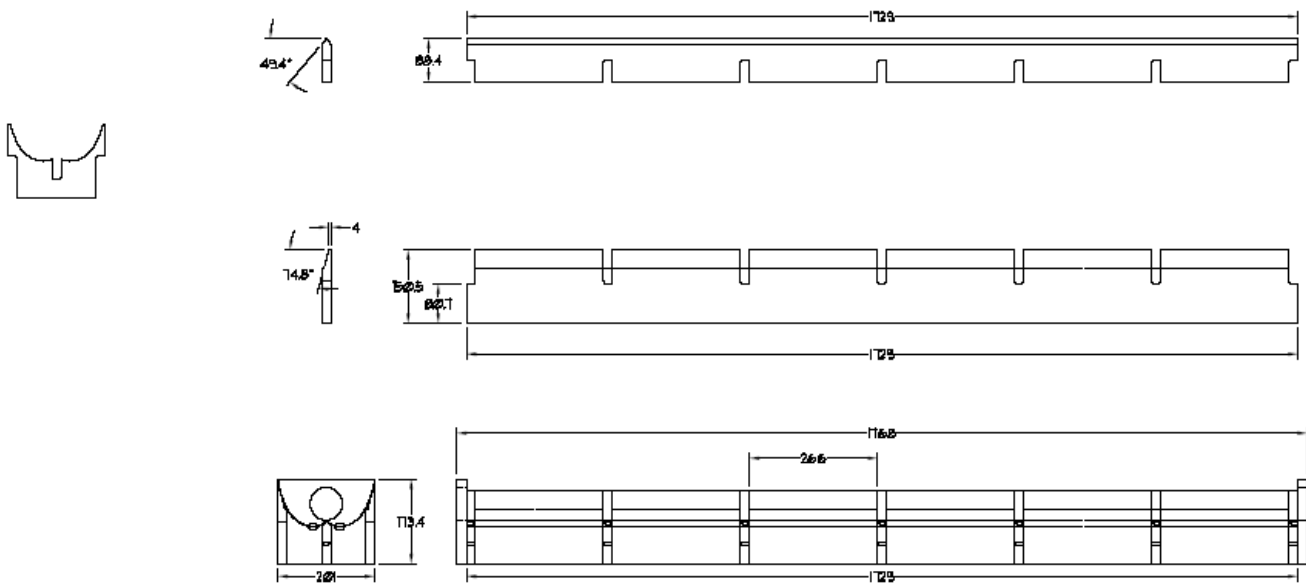


Figure 128. End view (upper drawing) and length view (three lower drawings) of frame for XPCP system in North-South orientation

Source: The Regents of University of California

2.12. Task 13

This report confirms that two prototype versions of the XPCP have been manufactured according to the drawings as described in the Task 12 report. One version includes the absorber tubes in North-South orientation, the other version in East-West orientation.

The picture below shows the North-South version.



2.13. Task 14

Expected optical efficiency and Incident Angular Modifier (IAM)

The expected optical efficiency for the XCPC in East-West orientation is 63.9% in normal incidence, and 67.5% averaged over all incidence angles between 0 degree and 34 degrees. The expected IAM curve is depicted in Figure 129.

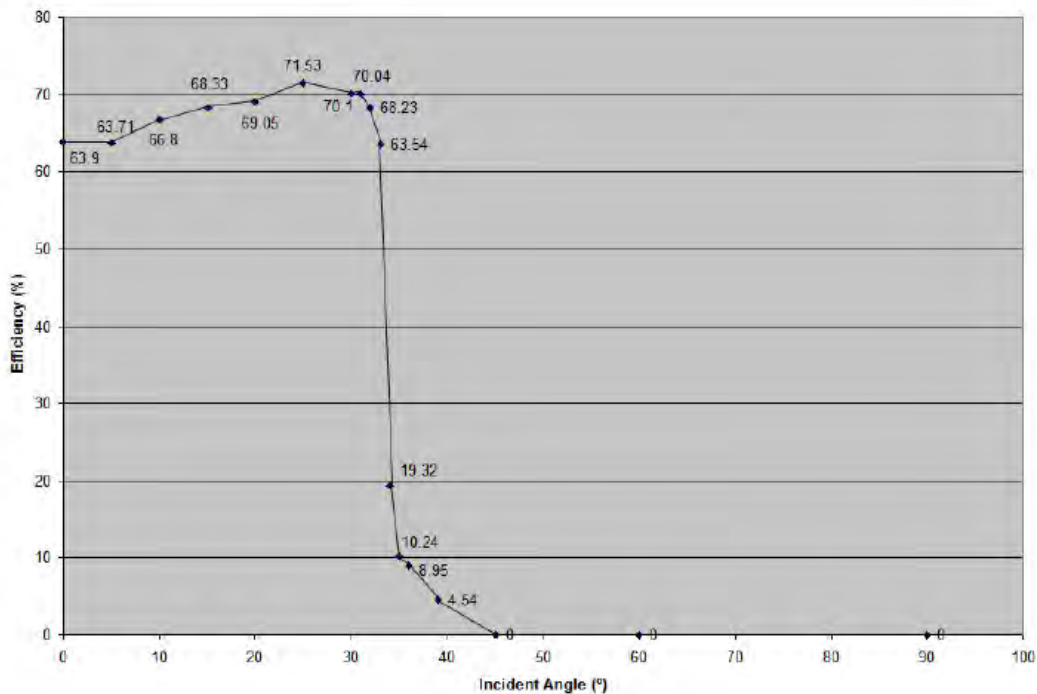


Figure 129. Expected Optical Efficiency and Incidence Angle Modifier for East-West orientation
Source: The Regents of University of California

Expected thermal efficiency

The expected thermal efficiency of the XCPC is depicted as the blue lines in Figure 130. The solid blue line (“Eurocon horizontal”) describes the expected thermal efficiency of the XCPC in East-West orientation, the dashed blue line (“Eurocon vertical”) in North-South orientation.

Glass-to-Metal Seal Tube

Orange: Alanod, alum, thickness = 0.8 mm
 Blue: Eurocon alum, thickness of 1.0 mm
 Red: TiNOX, copper thickness of 0.2 mm

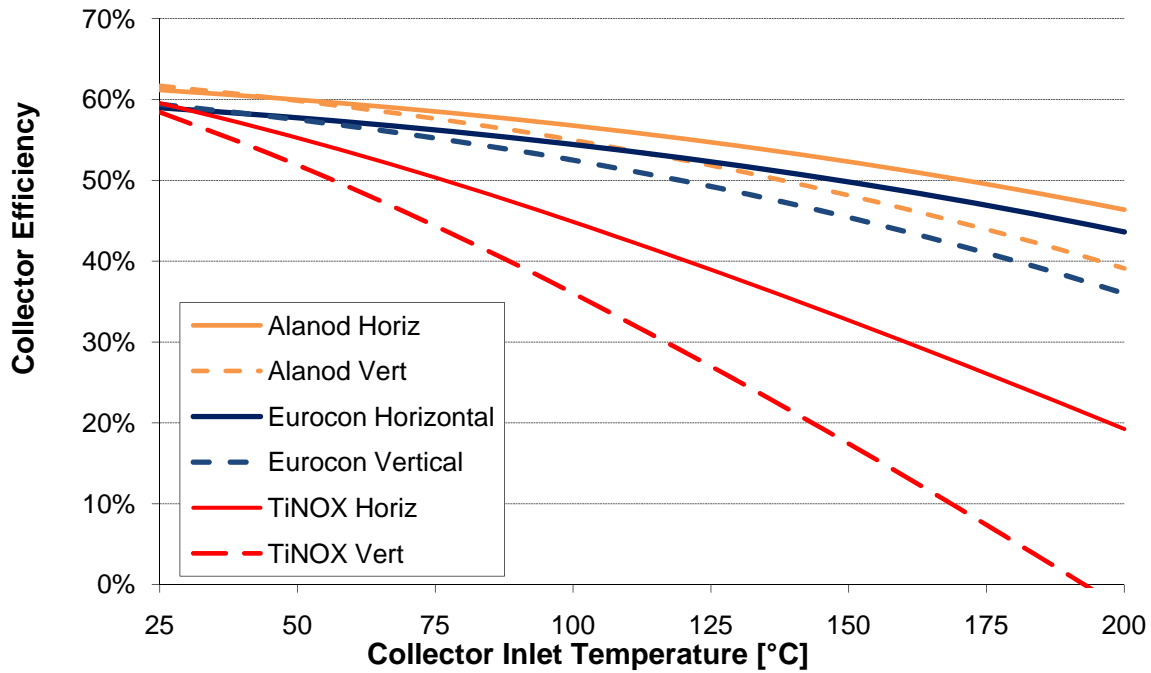


Figure 130. Expected thermal efficiency of XCPC

Source: The Regents of University of California

Table 33: Summary expectations table

Tube orientation	Optical efficiency at normal incidence	Collector efficiency at 200°C inlet temperature	Heat loss coefficient
East-West (horizontal)	64.1%	43%	1.172
North-South (vertical)	67.3%	36%	1.787

Source: The Regents of University of California

2.14. Task 15

Test plan to test the performance of the XCPC prototype

The following test plan is based on the international standard for solar thermal collector testing, ISO 9806-1 (Part 1). Some modifications have been made to account for the specific design, namely a stationary concentrating evacuated tube collector, and the temperature range of operation, which is up to 450°F.

The tests to be performed in Task 16 will include:

- Collector time constant
- Collector thermal efficiency
- Collector optical efficiency
- Collector incident angle modifier
- Pressure drop across the collector

Description of Test Loop

The test facility uses a closed loop system that includes a circulating oil temperature controller with integrated pump and expansion tank (see Figure 131). The circulating oil temperature controller provides a selectable constant temperature (up to 500°F) to the heat transfer fluid that is circulated through the collector. The loop further includes a flow meter, temperature sensors before and after the collector, and a calorimeter. The calorimeter is described in detail below. The solar collector is mounted on a dual axis tracker to allow the measurement of collector performance under controlled incidence angles.

The test facility further includes a meteorological station with a Precision Spectral Pyranometer that is mounted on the same tracker as the solar collector, a Normal Incidence Pyrheliometer mounted on a separate dual-axis tracker, a thermometer to measure the ambient temperature, and an anemometer.

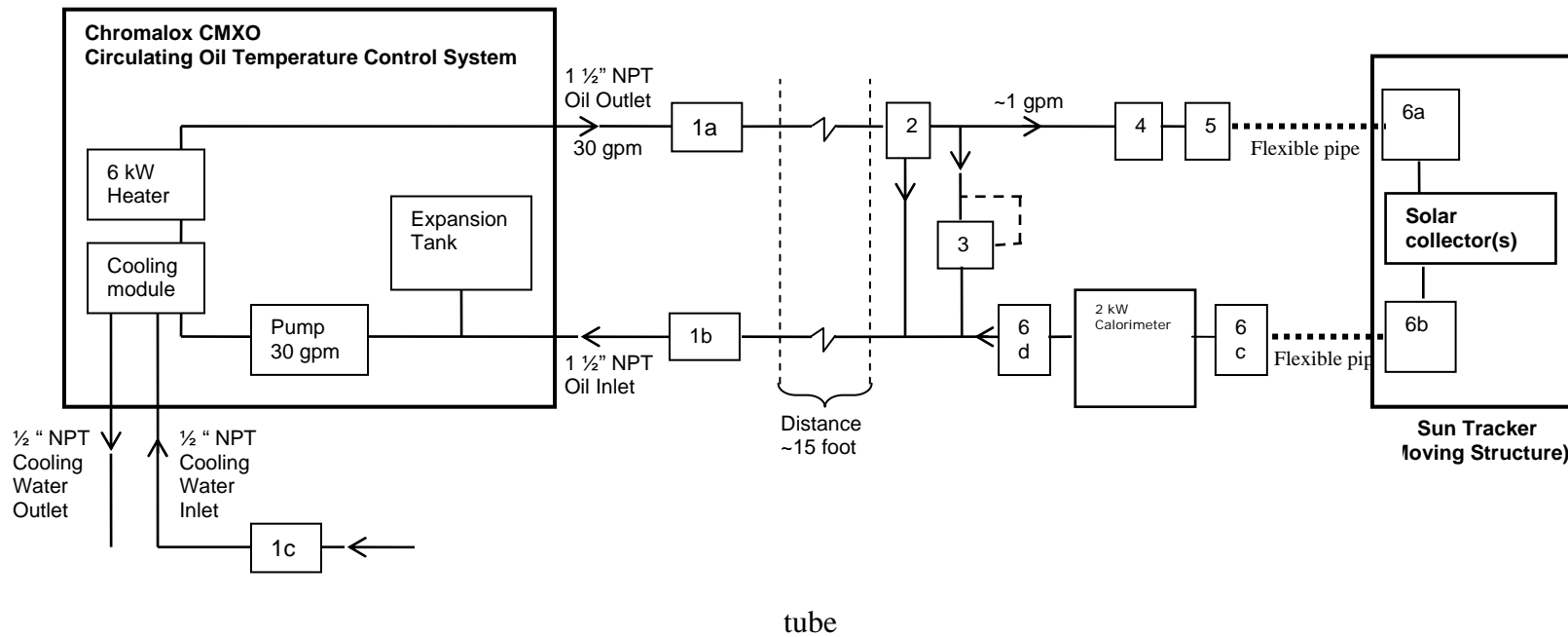


Figure 131. Schematic of Test Facility
 Source: The Regents of University of California

The data from the flow meter, the temperature sensors and the meteorological station are recorded through a data acquisition system.

Instrumentation

Circulating oil temperature controller:	Chromalox CMXO 6kW (with integrated pump and expansion tank)
Temperature sensors:	Type-K thermocouples from Omega
Flow meter:	Micro Motion Coriolis F-Series sensor
Flow control valve:	Valtek ½" Flow Top Control Valve
Back pressure regulating valve:	Jordan: 1" 50-100-S6-I5-S6-Y-8-21-S6-MD Pressure Control Valve
Sun tracker:	Wattsun AZ-125 dual axis tracker
Calorimeter:	Custom made by Valin Inc.
Pyranometer:	Eppley Precision Spectral Pyranometer
Pyrheliometer:	Eppley Normal Incidence Pyrheliometer
Amplifiers:	Agilent 34970A Data Acquisition/Switch Unit
Data logger:	Obvius A8811 and A8923

Test Procedure for Collector Time Constant

Testing will be performed outdoors with a solar irradiance on the plane of the collector aperture greater than 800 W/m². The heat transfer fluid will be circulated through the collector at the same flow rate as used during collector thermal efficiency testing.

Initially the collector's aperture will be shielded from solar radiation by means of a solar-reflecting cover, and the temperature of the heat transfer fluid at the collector inlet will be approximately equal to the ambient air temperature. When a steady state has been reached, the cover will be removed and measurements of the collector fluid inlet temperature (t_{in}), the collector fluid outlet temperature (t_e), and the surrounding air temperature (t_a) will be taken until steady-state conditions have been reached again. A steady state condition is assumed to exist when the outlet temperature of the fluid varies by less than 0.05°C per minute.

The difference between the temperature of the fluid at the collector outlet and that of the surrounding air ($t_e - t_a$) will be measured against time, beginning with the initial steady-state condition $(t_e - t_a)_0$ and continuing until the second steady state has been achieved at a higher temperature $(t_e - t_a)_2$ (see Fig. 2). The time constant τ_c of the collector is defined as the time taken for the collector outlet temperature to rise by 63.2% of the total increase from $(t_e - t_a)_0$ to $(t_e - t_a)_2$ following the step increase in solar irradiance at time zero.

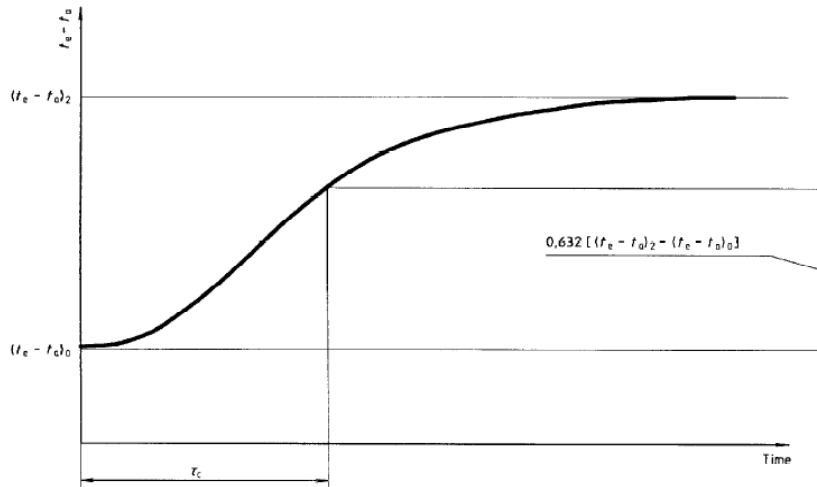


Figure 132. Collector time constant
 Source: The Regents of University of California

Collector Thermal Efficiency

The instantaneous collector efficiency η_{coll} is defined as

$$\eta_{coll} = \frac{\dot{Q}}{A_A G}$$

with

$$\begin{aligned} \dot{Q} &= \dot{m} c_f \Delta T_{coll} \\ G &= G_{direct} - \frac{G_{diffuse}}{c} \\ G_{diffuse} &= G_{hemi} - G_{direct} \end{aligned}$$

where

\dot{Q} : useful power extracted from collector,

\dot{m} : mass flow rate of heat transfer fluid,

c_f : specific heat capacity of the heat transfer fluid,

ΔT_{coll} : temperature difference between collector fluid at collector outlet and inlet,

A_A : aperture area of collector,

G : solar irradiance captured by concentrating collector,

G_{direct} : direct normal irradiance (measured with a pyrheliometer),

$G_{diffuse}$: diffuse sky irradiance,

G_{hemi} : hemispherical irradiance (measured with a pyranometer).

c : geometric concentration of collector

The determination of the instantaneous collector efficiency based on the formula above requires the measurement of the mass flow rate of heat transfer fluid, the temperature difference between the heat transfer fluid at the collector outlet and inlet, the aperture area of collector, the solar irradiance, and the knowledge of the specific heat capacity of the heat transfer fluid (at various temperatures).

Efficiency Measurement with Calorimeter

The instantaneous collector efficiency η_{coll} has been defined above as

$$\eta_{coll} = \frac{\dot{Q}}{A_A G} = \frac{\dot{m} c_f \Delta T_{coll}}{A_A G}$$

If one prefers not to rely on the measurement accuracy of \dot{m} and the accuracy of the tabulated values of the heat capacity c_f of the heat transfer medium, an alternative approach can be used to determine η_{coll} . This is by using a calorimeter, which is a perfectly insulated electric heater placed in series after the solar collector. In this case, the heat loss of the calorimeter is assumed to be zero, and the useful power extracted from the calorimeter $\dot{Q}_{calorimeter}$ is equal to the electric power consumption of the calorimeter, which can be measured very accurately.

With

$$\dot{Q}_{calorimeter} = \dot{m} \cdot c_f \cdot \Delta T_{calorimeter},$$

and assuming that the values of \dot{m} and c_f are approximately equal in the collector and in the calorimeter, the product $\dot{m} c_f$ can be replaced by:

$$\dot{m} \cdot c_f = \frac{\dot{Q}_{calorimeter}}{\Delta T_{calorimeter}},$$

where

$\dot{Q}_{calorimeter}$: useful power extracted from collector (= power consumption of calorimeter);

$\Delta T_{calorimeter}$: temperature difference of fluid between calorimeter outlet and inlet.

Thus, the instantaneous collector efficiency becomes:

$$\eta_{coll} = \frac{1}{A_{AG}} \cdot \dot{Q}_{calorimeter} \cdot \frac{\Delta T_{coll}}{\Delta T_{calorimeter}}.$$

The determination of the instantaneous collector efficiency based on the method using a calorimeter requires the measurement of the temperature difference of the heat transfer fluid at the collector outlet and inlet, the temperature difference of the heat transfer fluid at the calorimeter outlet and inlet, the aperture area of collector, and the solar irradiance. It is not necessary to measure the mass flow rate of heat transfer fluid and to know the specific heat capacity of the heat transfer fluid.

Temperature dependence of collector efficiency

The temperature dependence of the instantaneous efficiency η_{coll} can be represented graphically as a function of the reduced temperature difference T^* (see Fig. 3). The thermal performance of the collector can then be characterized by the two coefficients a_1 and a_2 , which are determined by a least square parabolic curve fit:

$$\eta_{coll} = \eta_0 - a_1 T^* - a_2 G (T^*)^2$$

with

η_0 : optical efficiency

T^* : reduced temperature difference

$$T^* = \frac{t_{in} - t_a}{G}$$

where

t_a : ambient temperature,

t_{in} : collector inlet temperature,

a_1 and a_2 : coefficients determined from least squares parabolic curve fit,

and the value of G in the formula above is assumed to be 800 W/m^2 .

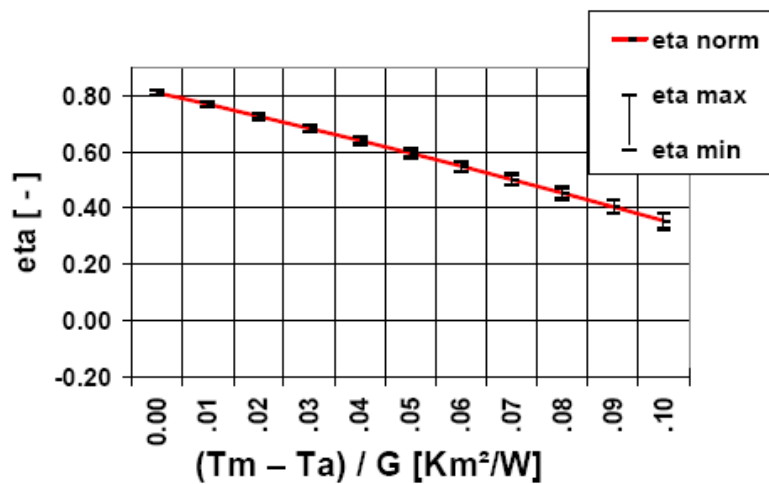


Figure 133. Example of a collector efficiency vs. temperature curve

Source: The Regents of University of California

Collector optical efficiency

The optical efficiency of the collector will be determined using the same test procedure as for the thermal efficiency tests (as described above), only that the temperature of the heat transfer fluid at the collector inlet will be kept equal to the ambient temperature. In this case the calculated thermal efficiency is equal to the optical efficiency (no heat loss).

Collector incident angle modifier

The collector incident angle modifier (IAM) will be determined by measuring the optical efficiency (as described above) under variation of the incidence angle between the sunlight and the collector plane.

Pressure drop across the collector

The pressure drop across the collector will be measured by comparing the difference in the pressure of the heat transfer fluid after and before the collector. The pressure drop measurements will be made for different temperatures between ambient and 400°F.

Schedule of Events

XCPC in North-South orientation

Collector time constant	9/17/07 – 9/19/07
Collector thermal efficiency	9/20/07 – 9/28/07
Collector optical efficiency	10/1/07 – 10/5/07
Collector incident angle modifier	10/1/07 – 10/5/07
Pressure drop across the collector	9/20/07 – 10/5/07

XCPC in East-West orientation

Collector time constant	10/8/07 – 10/10/07
Collector thermal efficiency	10/17/07 – 10/26/07
Collector optical efficiency	10/11/07 – 10/16/07
Collector incident angle modifier	10/11/07 – 10/16/07
Pressure drop across the collector	10/17/07 – 10/26/07

2.15. Task 16

The goal of this task was to test the XCPCs per the test plan outlined in Task 15. The tests include: instantaneous thermal efficiency, optical efficiency, incidence angle modifier, all-day performance, time constant, and pressure drop.

2.15.1. Tested Collectors

In this task the contractor tested the XCPC versions named “Metal absorber with glass-to-metal seal – North-South orientation” and “Metal absorber with glass-to-metal seal – East-West orientation.” The detailed design and the specifications of these XCPCs have been described in the Task 12 Report. Both tested collectors consisted of 6 counterflow absorber tubes each.

2.15.2. Test Protocol

The tests were conducted according to the following test plan:

Collector Thermal Efficiency

The instantaneous collector efficiency η_{coll} is defined as

$$\eta_{coll} = \frac{\dot{Q}}{A_A G}$$

with

$$\dot{Q} = \dot{m} c_p \Delta T_{coll},$$

$$G = G_{direct} + \frac{G_{diffuse}}{C_x},$$

$$G_{diffuse} = G_{hemi} - G_{direct}$$

Where

\dot{Q} : useful power extracted from collector,

\dot{m} : mass flow rate of heat transfer fluid,

c_p : specific heat capacity of the heat transfer fluid,

ΔT_{coll} : temperature difference between collector fluid at collector outlet and inlet,

A_A : effective aperture area of collector – we define this area as the length of the active area of the absorber tube (which is the area covered by the selective coating) times the width of the reflector

G : solar irradiance captured by concentrating collector,

G_{direct} : direct normal irradiance (measured with a pyrheliometer),

$G_{diffuse}$: diffuse sky irradiance,

G_{hemi} : hemispherical irradiance (measured with a pyranometer).

C_x : geometric concentration of collector

Temperature dependence of collector efficiency

The temperature dependence of the instantaneous efficiency η_{coll} can be represented graphically as a function of the reduced temperature T^* . The thermal performance of the collector can then be characterized by the two coefficients a_1 and a_2 , which are determined by a least square parabolic curve fit:

$$\eta_{coll} = \eta_o - a_1 T^* - a_2 G (T^*)^2$$

with

η_o : optical efficiency

T^* : reduced temperature

$$T^* = \frac{T_{in} - T_{amb}}{G}$$

where

T_{amb} : ambient temperature,

T_{in} : collector inlet temperature,

a_1 and a_2 : coefficients determined from least squares parabolic curve fit, and the value of G in the formula above is assumed to be 1000 W/m^2 .

2.15.3. Description of Test Loop

The test facility used is a closed loop system that includes a circulating oil temperature controller with integrated pump and expansion tank (see Fig. 1). The circulating oil temperature controller provides a selectable constant temperature (up to 500°F) to the heat transfer fluid that is circulated through the collector. The loop further includes a flow meter and temperature sensors before and after the collector. There are flow mixers introduced into the loop before each temperature sensor. The solar collector is mounted on a dual axis tracker to allow the measurement of collector performance under controlled incidence angles.

The test facility further includes a meteorological station with a Precision Spectral Pyranometer and a Normal Incidence Pyrheliometer that are both mounted on the same tracker as the solar collector, a thermometer to measure the ambient temperature, and an anemometer.

The data from the flow meter, the temperature sensors, and the meteorological stations were recorded through a data acquisition system.

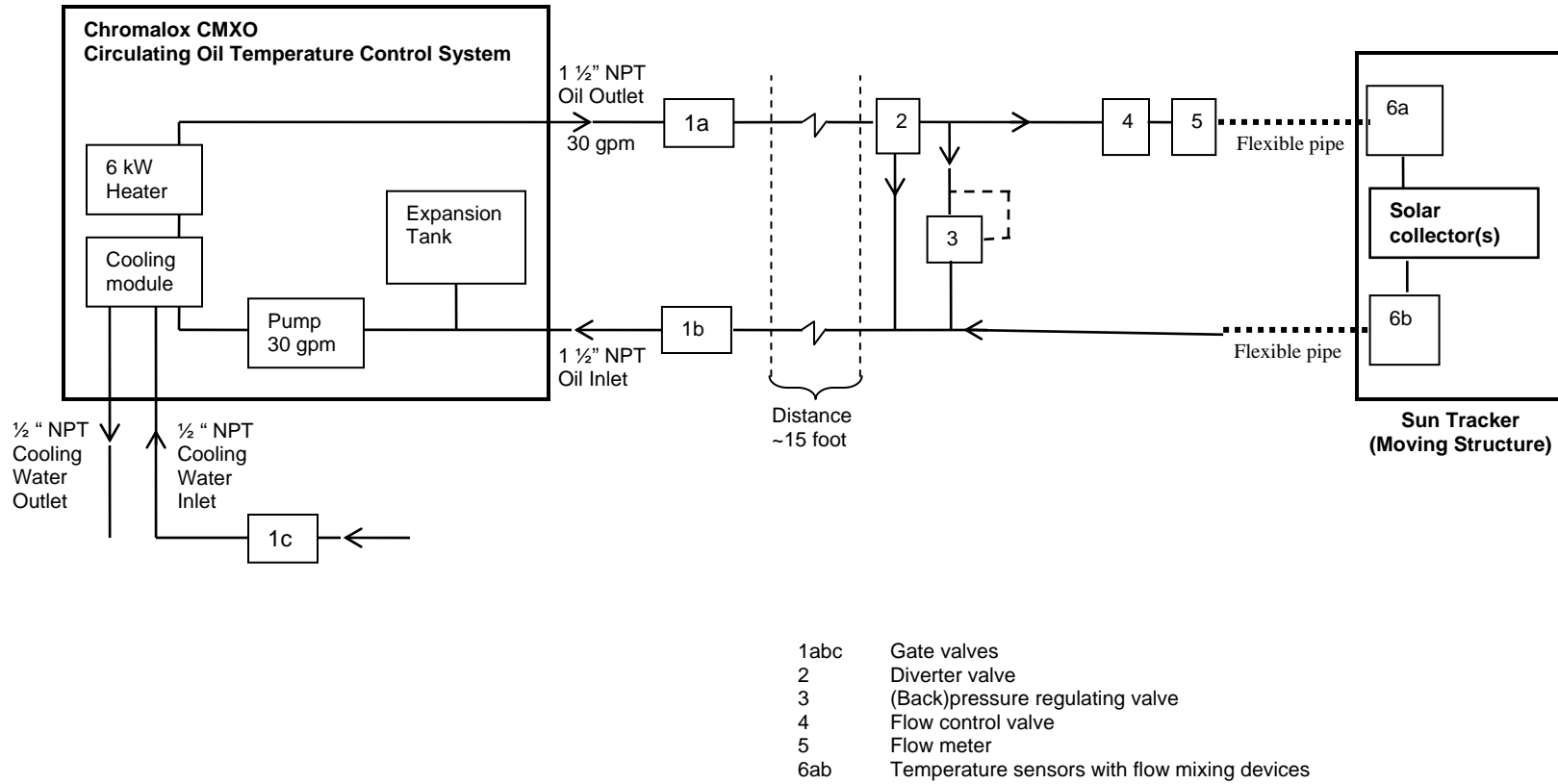


Figure 134. Schematic of Test Facility
Source: The Regents of University of California

2.15.4. Instrumentation

Circulating oil temperature controller: and expansion tank)	Chromalox CMXO 6kW (with integrated pump
Temperature sensors:	Type-K thermocouples from Omega
Flow meter:	Micro Motion Coriolis F-Series sensor
Flow control valve:	Valtek ½" Flow Top Control Valve
Back pressure regulating valve:	Jordan: 1" 50-100-S6-I5-S6-Y-8-21-S6-MD
Pressure Control Valve	
Sun tracker:	Wattsun AZ-125 dual axis tracker
Pyranometer:	Eppley Precision Spectral Pyranometer
Pyrheliometer:	Eppley Normal Incidence Pyrheliometer
Data Acquisition System:	Agilent 34970A Data Acquisition/Switch Unit

2.15.5. Test Results of "Metal absorber with glass-to-metal seal – North-South orientation"

Collector description

Table 34. Collector Description of North-South Counterflow with Alanod Collector

Orientation	North-South
Concentration C_x	1.15
Effective Collector Area A_A	2.0 m ²
Tube Type	Counterflow-Tube
Number of Tubes	6
Reflector	Alanod (90%)

Source: The Regents of University of California

Collector optical efficiency

The optical efficiency of the collector was measured with 21-23°C water. The heat capacity of the water was assumed to be 4.18 kJ/kg-K.

The optical efficiency based on an effective irradiance (according to Ari Rabl¹⁰: $G = G_{DNI} + G_{diffuse}/C_x$) was found to be 69.5%. The optical efficiency based on direct normal irradiance ($G = G_{DNI}$) was found to be 87.7%.

Collector thermal efficiency

The efficiency of the XCPC was measured at the following collector inlet temperatures: 80°C, 100°C, 120°C, 140°C, 160°C, 180°C, and 200°C; and at the following flow rates: 40-45 g/s, and 80 g/s of Duratherm 600 mineral oil.

The heat capacity of the oil was measured by Rose Consulting in November 2007. A linear approximation to the measurements was used to calculate the efficiency of the collector:

$$c_p = 0.002261 \cdot T_m + 1.896.$$

¹⁰ Ari Rabl, "Active Solar Collectors and Their Applications," Oxford University Press, 1985.

The performance characteristics are tabulated in Table and the collector efficiencies are depicted in

Figure through Figure. Figure 3 and Figure 5 are derived from Figure 2 and Figure 4 respectively by assuming an ambient temperature of 25°C and an effective insolation of 1,000 W/m² that is captured by the XCPC. Figures 2 and 3 display the efficiencies based on the effective irradiance G_E while figures 4 and 5 display the efficiencies based on the direct normal irradiance (DNI) G_{DNI} .

Table 35. Performance Characteristics of North-South Counterflow with Alanod Collector

	G=G_E	G=G_{DNI}
Optical Efficiency η_o	69.5%	87.7%
Efficiency at 100 °C	57.2%	72.2%
Efficiency at 200 °C	36.3%	45.2%
Loss coefficient (1) a_1	1.445 W/m ² -K	1.793 W/m ² -K
Loss coefficient (2) a_2	.00285 W/m ² -K ²	.00363 W/m ² -K ²
Overall heat loss coefficient U	1.910 W/m ² -K	1.973 W/m ² -K

Source: The Regents of University of California

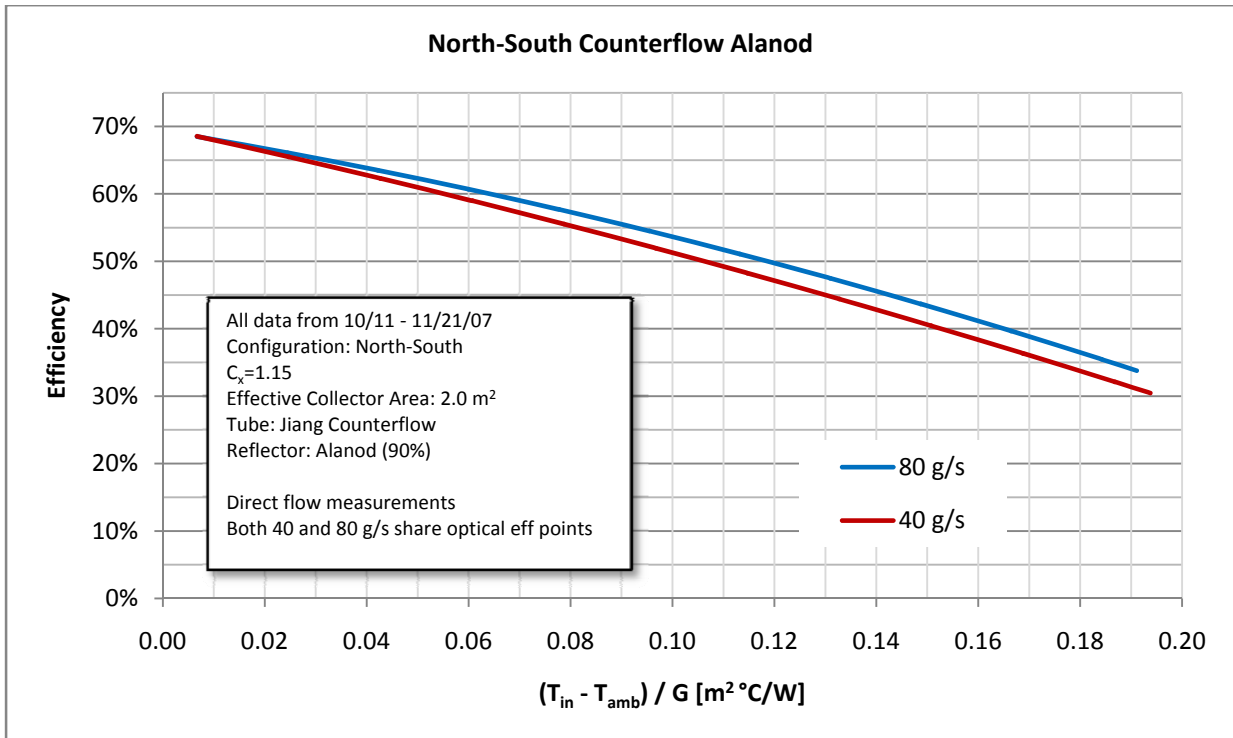


Figure 135. North-South Counterflow with Alanod Effective Reduced Efficiency Curve
 Source: The Regents of University of California

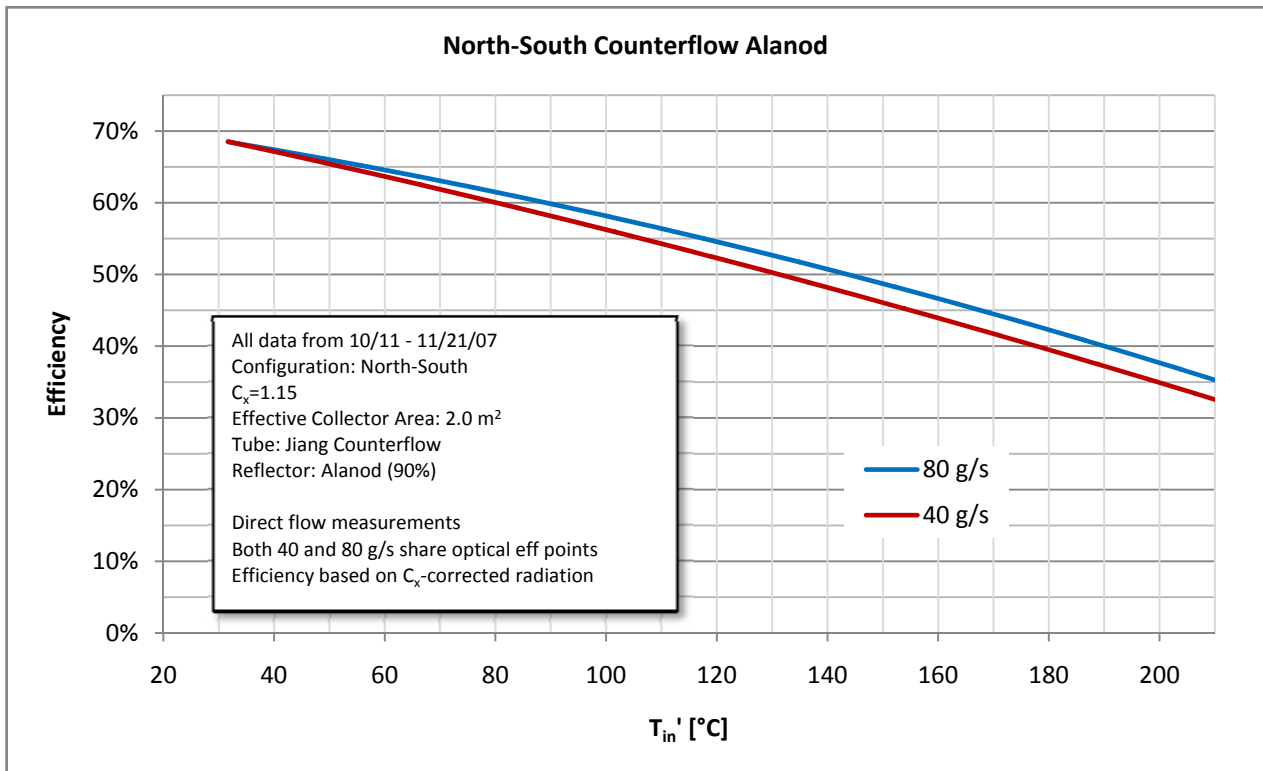


Figure 136. North-South Counterflow with Alanod Effective Standardized Efficiency Curve

Source: The Regents of University of California

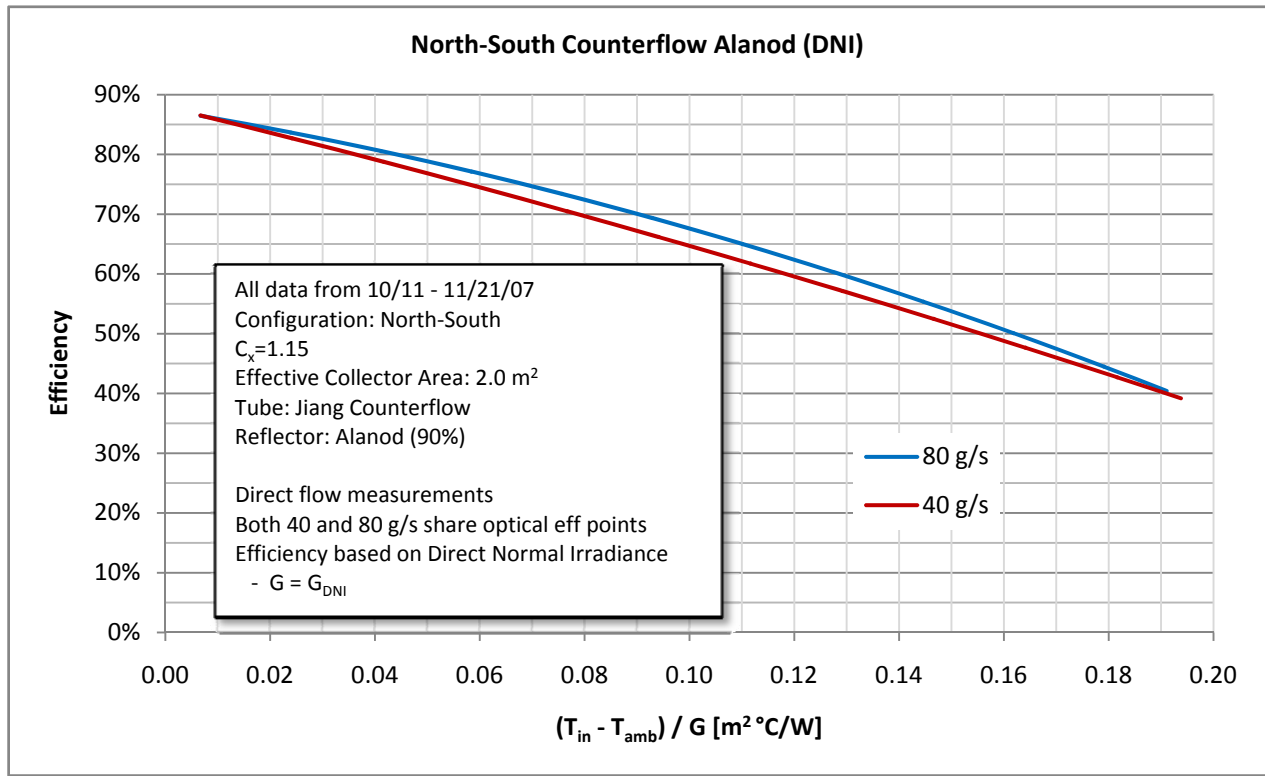


Figure137. North-South Counterflow with Alanod Direct Reduced Efficiency Curve

Source: The Regents of University of California

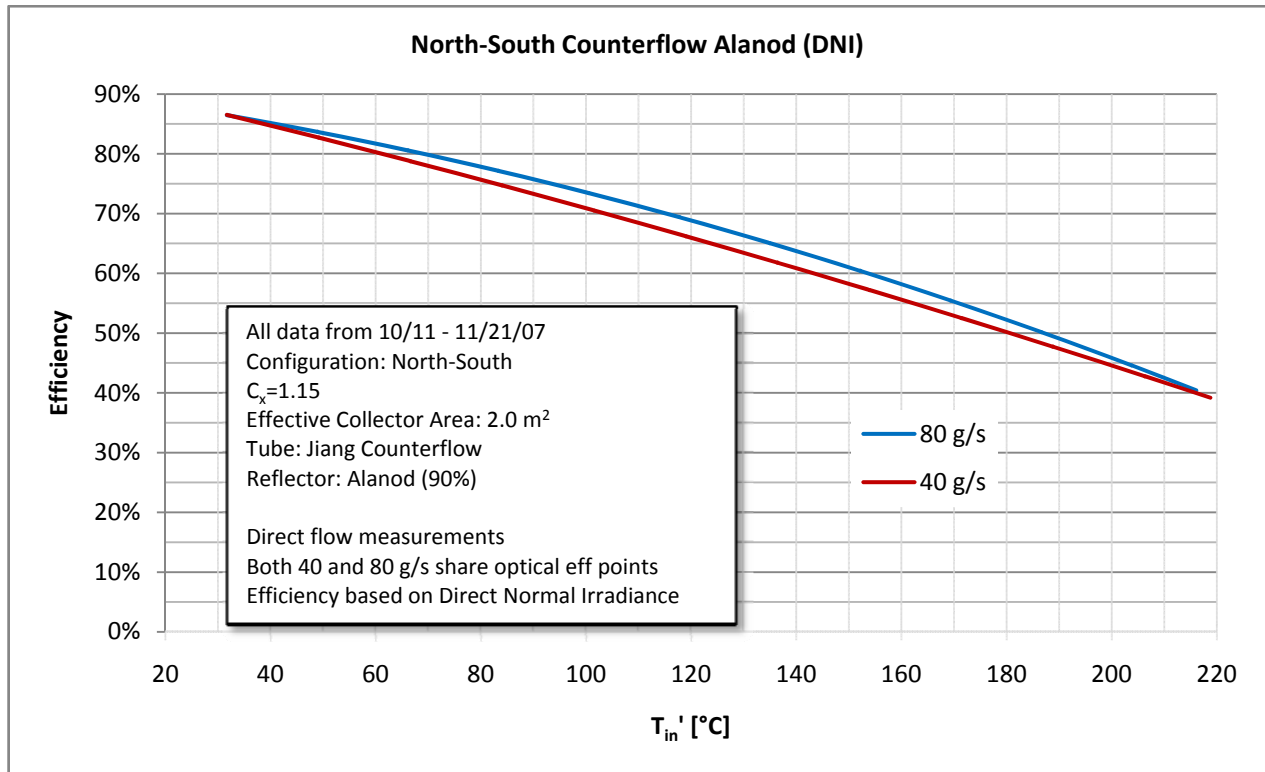


Figure138. North-South Counterflow with Alanod Direct Standardized Efficiency Curve

Source: The Regents of University of California

Collector Incident Angle Modifier (IAM) and All-Day Performance

The IAM was measured by positioning the collector due south and tilted to be normal to the sun at solar noon (not tracking) and recording the instantaneous thermal collector efficiency at a collector inlet temperature of 140 °C over the course of the day. In this measurement the instantaneous efficiency was based on the direct normal insolation only that was measured with a Normal Incidence Pyrheliometer on a separate tracker. Figure 6 shows the relative drop in efficiency during the day as the sun angle varies between -51° and $+59^\circ$ at 90% relative to normal incidence. The acceptance angle was measured as $\pm 55^\circ$.

The test used to determine the IAM chart and the acceptance angle can also be used to understand the collector's all-day performance. During the test, the collector performed within 90% of the nominal efficiency for roughly 7.3 hours.

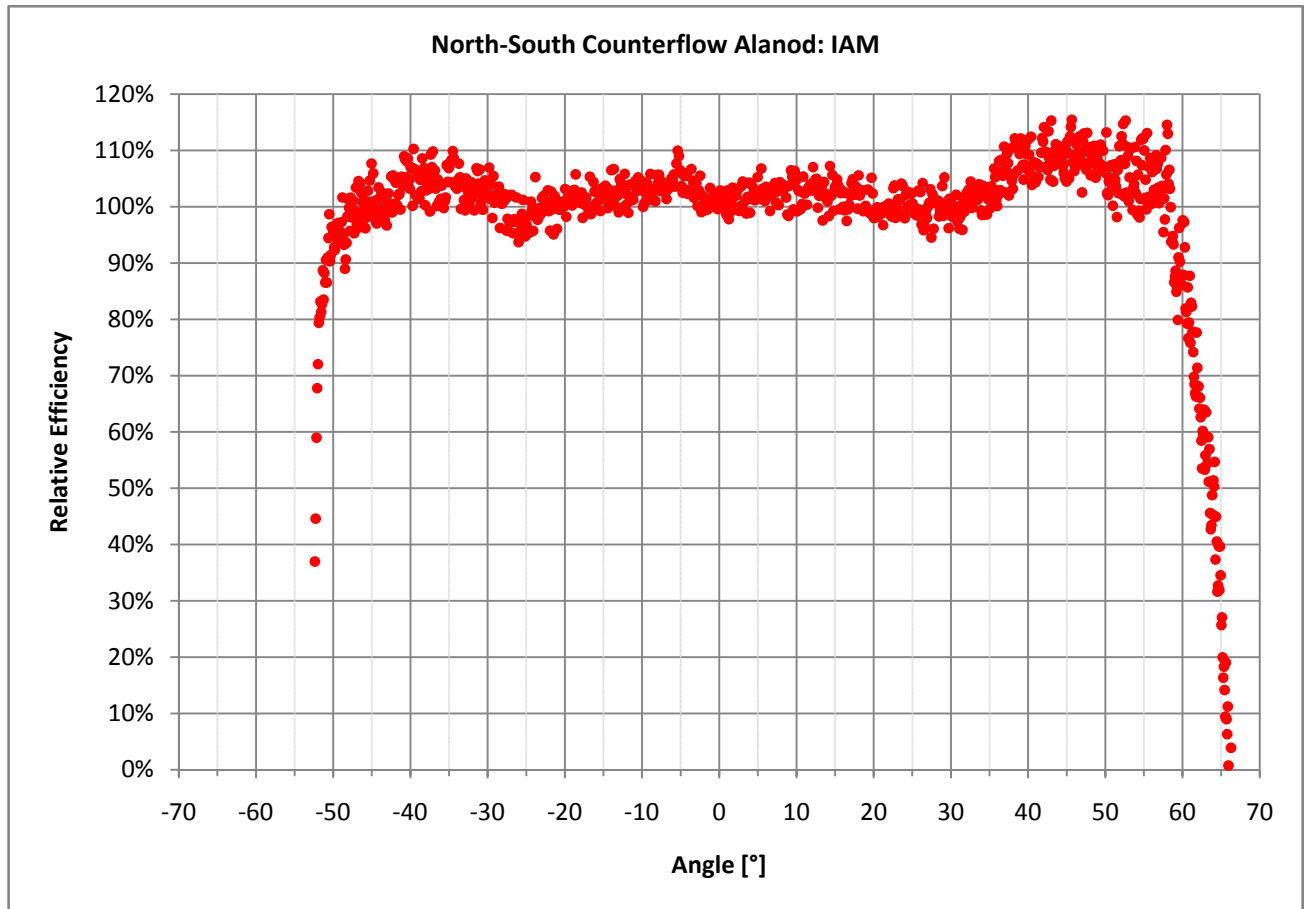


Figure 139. North-South Counterflow with Alanod: IAM Chart

Source: The Regents of University of California

Time Constant

The time constant was measured as described in Task 15 at 100°C and 35 g/s on 10/18/07. Measurements were taken for roughly twenty minutes after the collector cover was removed. Figure 140 shows the results of the test where the time constant τ_c was found to be 100 seconds.

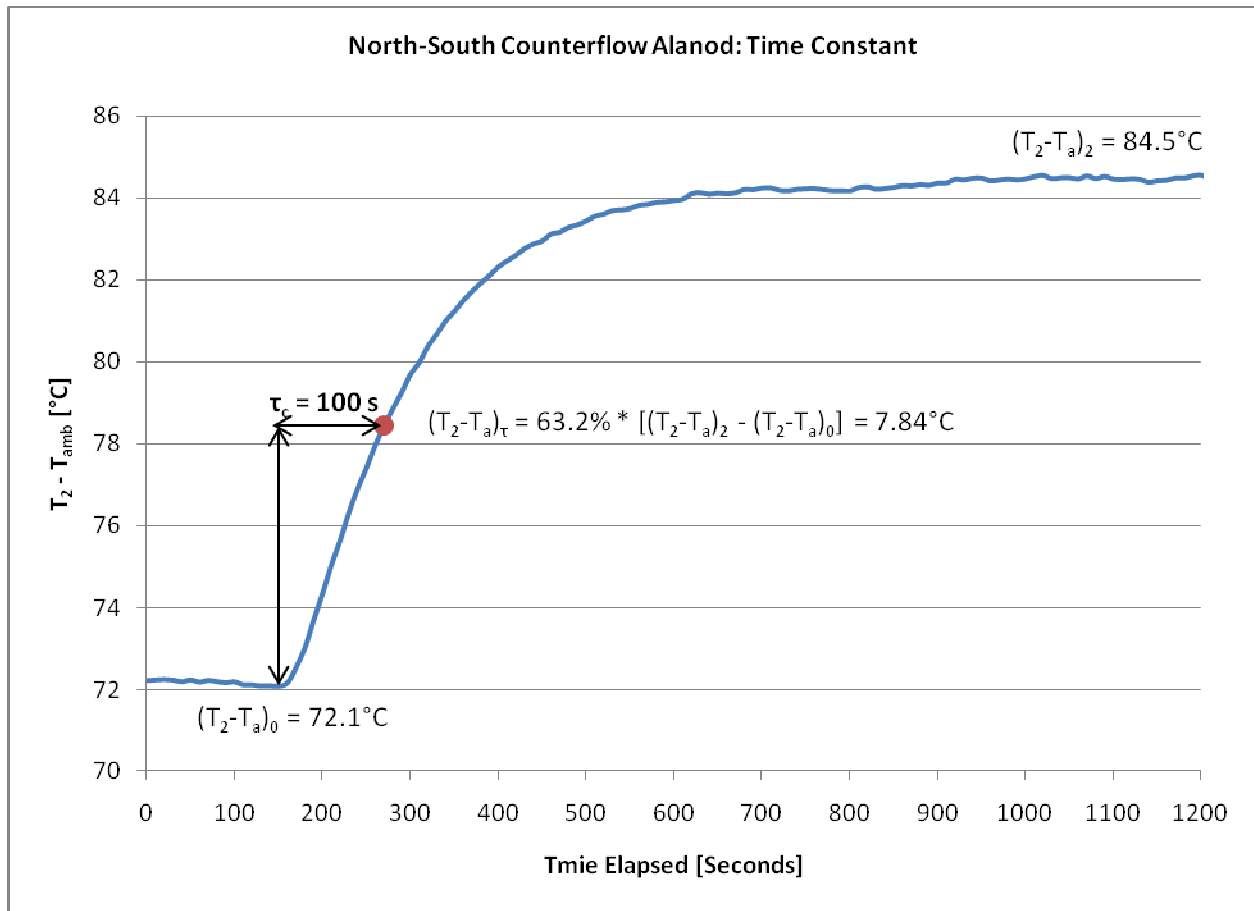


Figure 140. North-South Counterflow Time Constant Plot

Source: The Regents of University of California

Pressure drop across the collector

The pressure drop across the collector (6 absorber tubes) was measured to be between 1 psi (at an oil temperature of 200°C) and 14 psi (at an oil temperature of 8°C) at a flowrate of 80 g/s. The pressure drop measurements were done with the flow mixing devices inserted into the loop before the temperature sensors. It should be noted that the flow mixers increase the flow resistance.

2.15.6. Test Results of “Metal absorber with glass-to-metal seal – East-West orientation”

Collector description

Table 36. Description of East-West Counterflow with Alanod Collector

Orientation	East-West
Concentration	1.80
Effective Collector Area	3.1 m ²
Tube Type	Counterflow-Tube
Number of Tubes	6
Reflector	Alanod (90%)

Source: The Regents of University of California

Collector optical efficiency

The optical efficiency was not measured directly for this collector. The optical efficiency used in the analysis of this collector was assumed to be the average of a linear extrapolation of the thermal efficiency and the modeled optical efficiency.

The optical efficiency based on an effective irradiance ($G = G_{DNI} + G_{diffuse}/C_x$) was assumed to be 64.4%. The optical efficiency based on direct normal irradiance ($G = G_{DNI}$) was assumed to be 69.3%.

Collector thermal efficiency

The efficiency of the XCPC was measured at the following collector inlet temperatures: 120°C, 140°C, 160°C, 180°C, and 200°C; and at the following flow rates: 80 g/s and 120 g/s of Duratherm 600 mineral oil.

The heat capacity of the oil was assumed to be consistent with the data tables provided by Duratherm. A linear approximation to the table was used to calculate the efficiency of the collector: $c_p = 0.0032266 \cdot T_m + 1.84$.

The performance characteristics are summarized in Table 4 and the collector efficiencies are depicted in Figure 8 through Figure 11. Figure 9 and Figure 11 are derived from Figure 8 and Figure 10 respectively by assuming an ambient temperature of 25°C and an effective insolation of 1,000 W/m² that is captured by the XCPC. Figures 8 and 9 display the efficiencies based on the effective irradiance G_E while figures 10 and 11 display the efficiencies based on the direct normal irradiance (DNI) G_{DNI} .

Table 37. Performance Characteristics of East-West Counterflow with Alanod Collector

Source: The Regents of University of California

	G=G_{Rabl}	G=G_{DNI}
Optical Efficiency η_o	64.6%	69.3%
Efficiency at 100 °C	54.6%	59.9%
Efficiency at 200 °C	40.3%	44.3%
Loss coefficient (1) a_1	1.293 W/m ² -K	1.139 W/m ² -K
Loss coefficient (2) a_2	0.0007 W/m ² -K ²	0.00207 W/m ² -K ²
Overall heat loss coefficient U	1.393 W/m ² -K	1.436 W/m ² -K

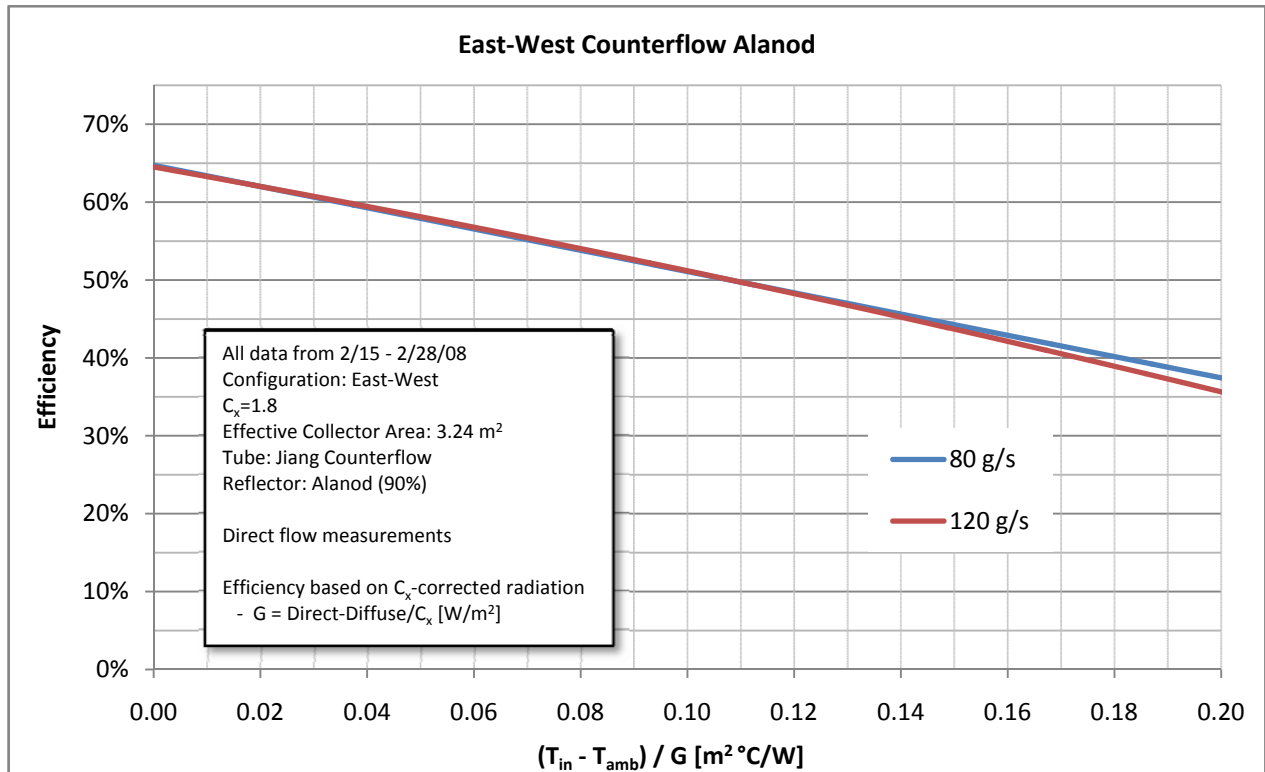


Figure 141. East-West Counterflow with Alanod Effective Reduced Efficiency Curve

Source: The Regents of University of California

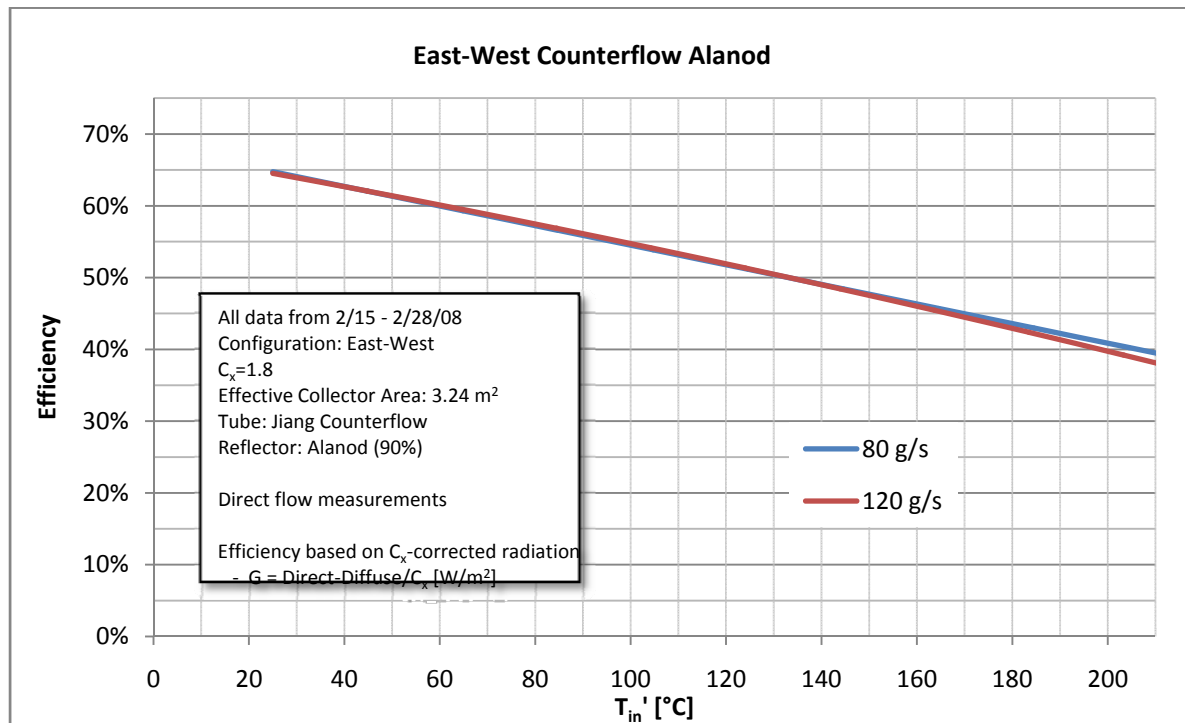


Figure 142. East-West Counterflow with Alanod Effective Standardized Efficiency Curve

Source: The Regents of University of California

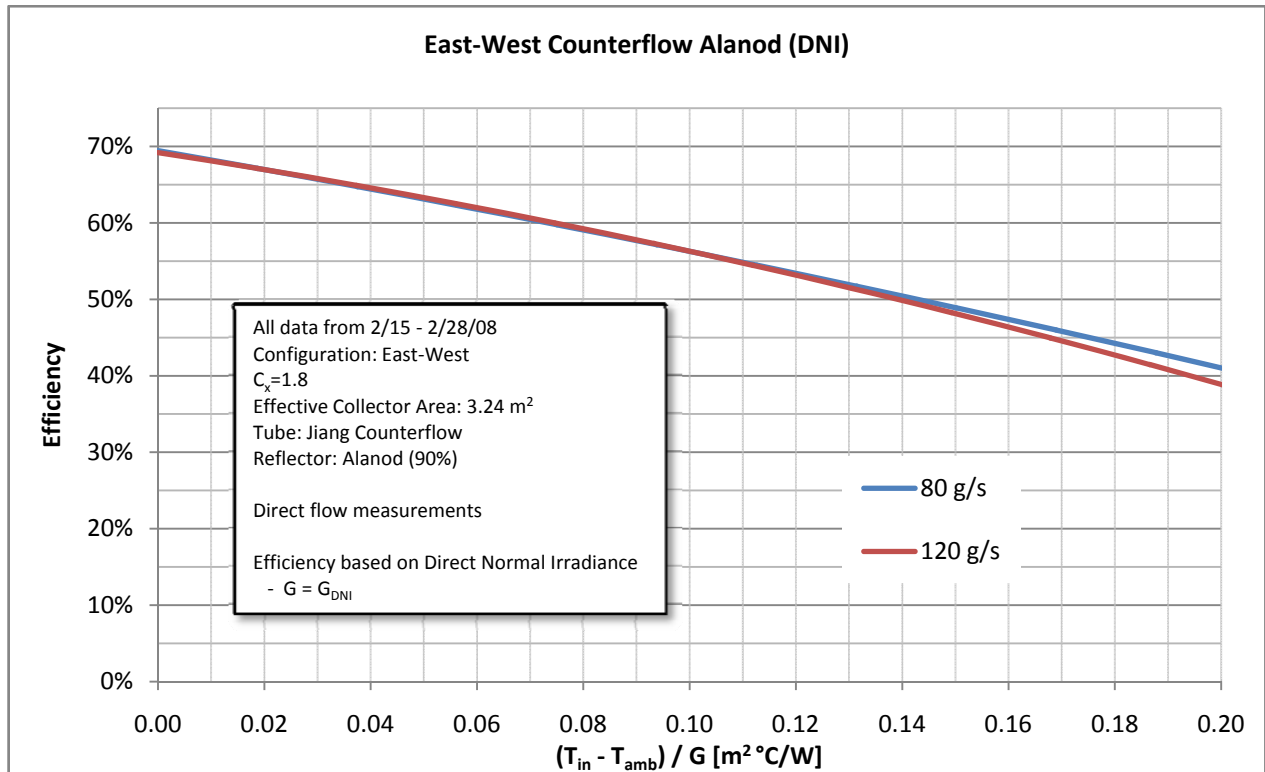


Figure 143. East-West Counterflow with Alanod Direct Reduced Efficiency Curve

Source: The Regents of University of California

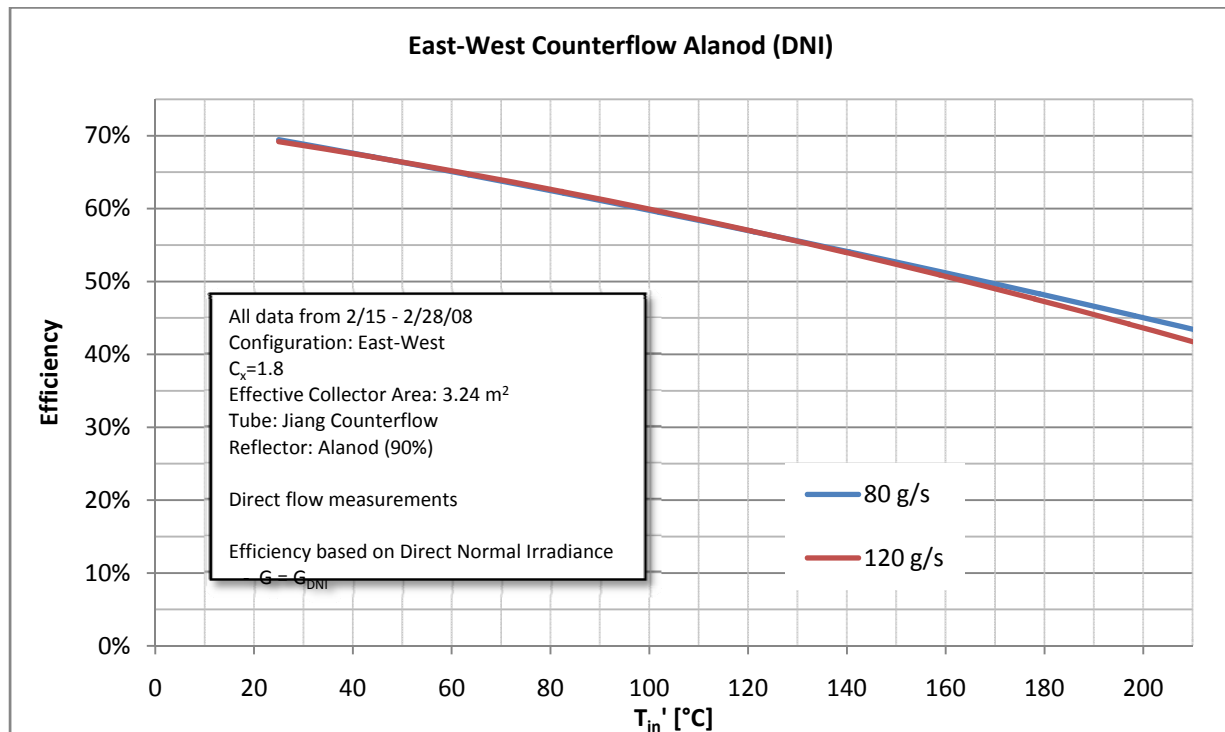


Figure 144. East-West Counterflow with Alanod Direct Standardized Efficiency Curve

Source: The Regents of University of California

Collector Incident Angle Modifier (IAM)

The IAM was not measured for this specific configuration. The IAM was measured for the East-West U-Tube with Reflectech collector with virtually identical geometrical optics and can be used to describe the East-West Counterflow with Alanod collector. Refer to Task 19 for the IAM chart.

2.15.7. Discussion

North-South Counterflow with Alanod

Figure 12 compares the measured efficiency with the modeled efficiency of the North-South Counterflow with Alanod collector assuming 1000 W/m² effective irradiance and an ambient temperature of 25°C. The “Measured” values in Figure 12 and in this discussion were measured at a flowrate of 80 g/s. The efficiencies referenced in Figure 145 compare the useful power out of the collector to the effective irradiance over the collector’s effective area: —.

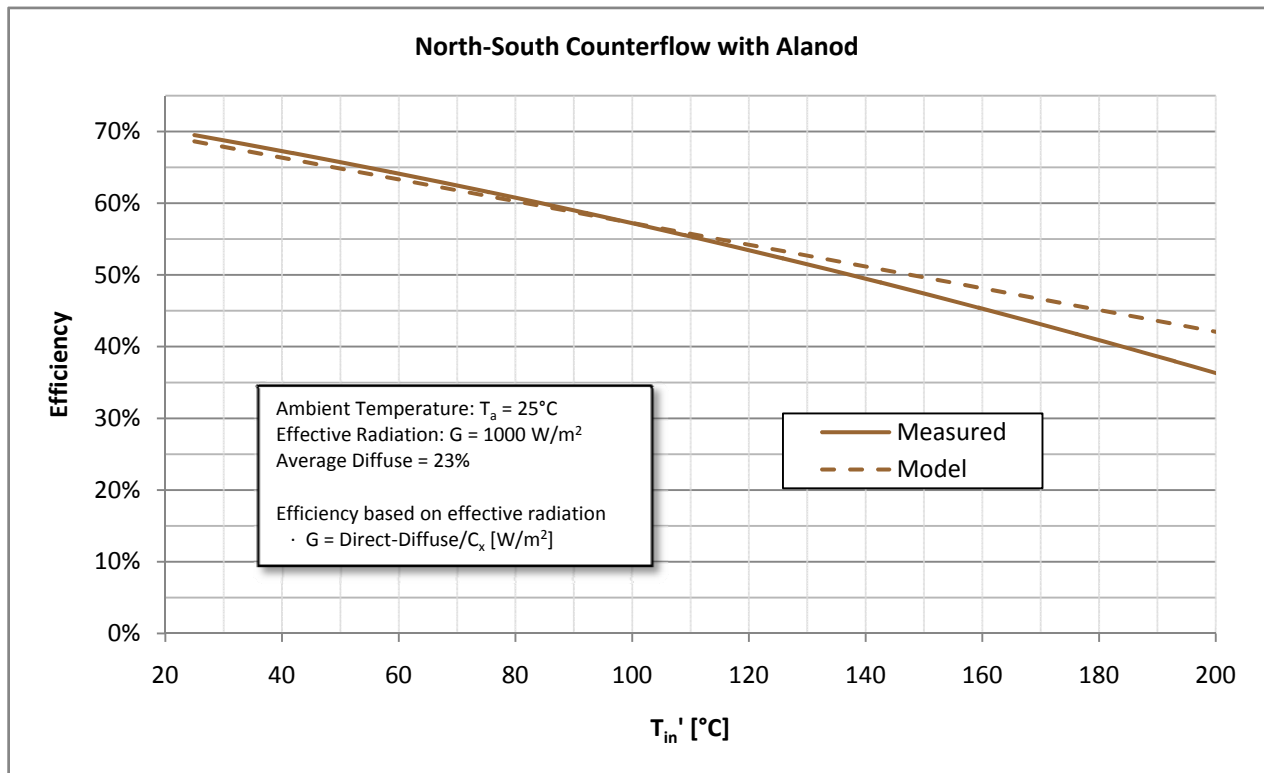


Figure 145. North-South Counterflow with Alanod: Measured vs. Model

Source: The Regents of University of California

The measured optical efficiency at 69.5% was slightly higher than the expected modeled optical efficiency (67.3%). The efficiency of this collector measured at 200°C (37.2%) is roughly three percentage points less than what the model predicted at 40.0%. The overall heat transfer coefficient measured for the North-South Counterflow with Alanod collector is 1.91 W/m²-K compared to 1.79 W/m²-K. These indicate that the performance of the prototype appears to be

slightly less than what the model predicted. Overall, the measurements of the optical and thermal efficiency appear to have a very good agreement with the model.

As seen in Figure 6, the acceptance angle of the North-South Counterflow with Alanod collector was found to be +/- 55 degrees as opposed to the designed +/- 60 degrees which suggests that the optics of the system are not exactly as designed. One possible defect is the shape of the reflector is not accurate. A more likely reason for the lowered acceptance angle is that the placement of the absorber may not have been in the designed position. If the absorber is lower than the designed position then the acceptance angle will be lowered while also increasing the optical efficiency at normal incidence which may also explain the higher than expected optical efficiency. This could happen if either the glass tubes' placement in the frame's holes were off or the absorber in the glass tube was not exactly concentric.

In addition to a lower than predicted acceptance angle, the IAM chart seems to be off center. The fact that the measurements were done continuously throughout the day, the shift in the chart is likely due to a thermal constant.

Efficiencies based on DNI in Figures 4 and 5 appear very high. These high efficiencies are due to the fact that this collector was tested when there was a relatively large percentage of diffuse light. During the testing of this collector, the percent diffuse ranged between 15% and 30% with an average of 23%.

East-West Counterflow with Alanod

Figure 13 compares the measured efficiency with the modeled efficiency of the North-South Counterflow with Alanod collector assuming 1000 W/m² effective irradiance and an ambient temperature of 25°C. The "Measured" values in Figure 13 and in this discussion were measured at a flowrate of 80 g/s. The efficiencies referenced in Figure 13 compare the useful power out of the collector to the effective irradiance over the collector's effective area: $\eta = \frac{P_{out}}{G_{EA}}$. The optical efficiency value used for the measured chart was an assumed value of 64.6%. Since the least squared quadratic curve has a natural shape, the assumed optical efficiency appears to fit the rest of the data.

The measured efficiency at 200°C in Figure 13 is 40% compared to the model efficiency of 47.4%. The overall heat transfer coefficient measured for the collector and the model were 1.39 W/m²-K and 1.17 W/m²-K respectively. The thermal efficiency of the East-West Counterflow with Alanod collector appears to suffer from more heat loss than what was expected from the model. This lower efficiency is likely, in part, due to a high thermal resistance in the counterflow tubes. This high resistance and the higher concentration ratio of the East-West collector would allow the absorber temperature to be much higher than the oil temperature resulting in a large radiative loss from the absorber. In addition, the efficiency curve in Figure 13 is nearly linear which suggests that there is a large portion of the heat loss that is not due to radiation and can be assumed to be from losses in the manifold insulation.

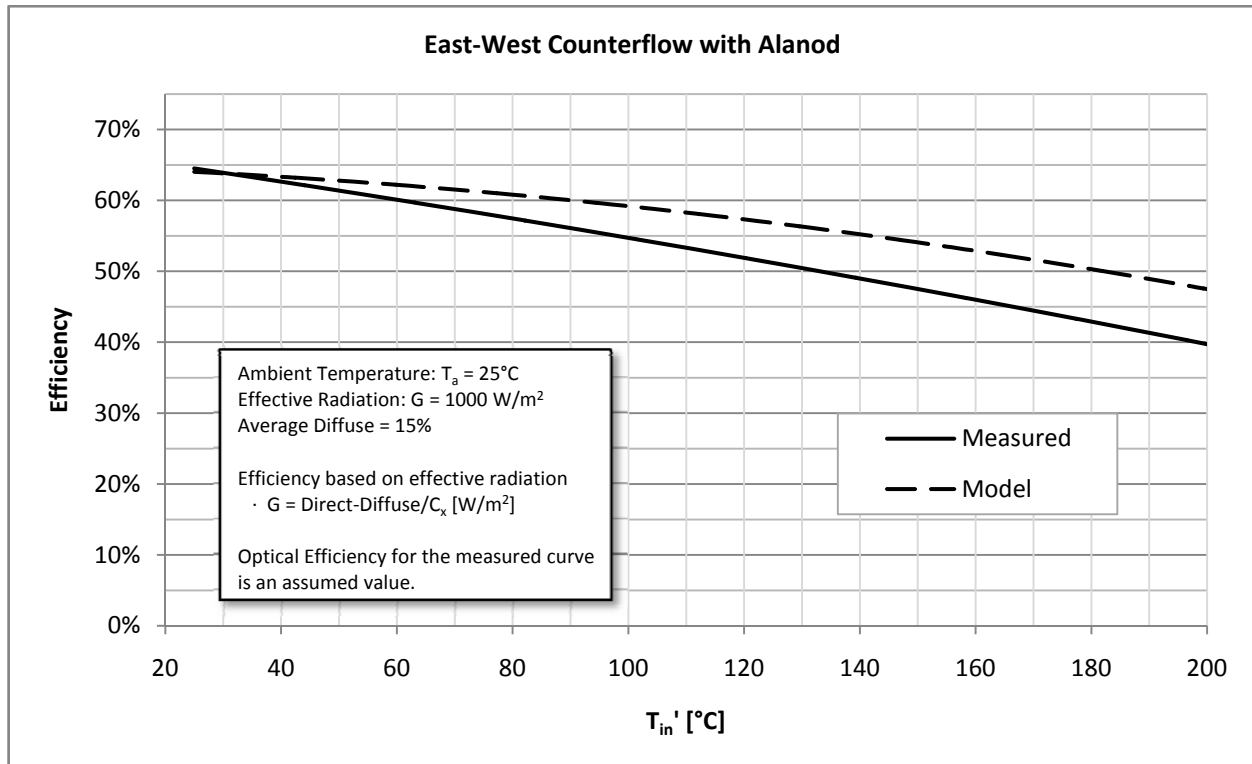


Figure 146 East-West Counterflow with Alanod: Measured vs. Model

Source: The Regents of University of California

Efficiencies based on effective irradiance in Figure 8 are roughly 9% lower than the efficiencies based on DNI in Figure 10 for this East-West collector. With an average diffuse of 15% during testing and a concentration of 1.8, one would expect an 8% difference in the efficiency between DNI and effective irradiance. The amount of diffuse accepted by the collector appears to agree with factor in the effective irradiance calculations.

Comparison

Figure 14 and Table compares the efficiencies of the North-South and the East-West Counterflow with Alanod collectors. As expected, the North-South version has a higher optical efficiency. The North-South collector outperformed the East-West collector from temperatures up to 150°C while the model suggests that the East-West collector should have a higher efficiency starting at about 85°C. As stated earlier, the East-West collector likely suffered from a large thermal resistance in the absorber and manifold heat losses which contributed to its lowered efficiency.

Table 38: Comparison of the North-South and East-West Counterflow with Alanod collectors

	$G=G_{Rabl}$		$G=G_{DNI}$	
	North-South	East-West	North-South	East-West
Optical Efficiency	69.5%	64.6%	87.7%	69.3%
Efficiency at 100 °C	57.2%	54.6%	73.7%	59.9%
Efficiency at 200 °C	36.3%	40.3%	53.3%	44.3%
Loss coefficient (1)	1.445 W/m ² -K	1.293 W/m ² -K	1.793 W/m ² -	1.139 W/m ² -

	$G=G_{Rabl}$		$G=G_{DNI}$	
	North-South	East-West	North-South	East-West
			K	K
Loss coefficient (2)	$.00323 \text{ W/m}^2\text{-K}^2$	$0.0007 \text{ W/m}^2\text{-K}^2$	$.0045 \text{ W/m}^2\text{-K}^2$	$.0021 \text{ W/m}^2\text{-K}^2$
Overall heat loss coefficient	$1.910 \text{ W/m}^2\text{-K}$	$1.393 \text{ W/m}^2\text{-K}$	$1.973 \text{ W/m}^2\text{-K}$	$1.436 \text{ W/m}^2\text{-K}$
Acceptance angle ¹¹	$\pm 55^\circ$	$\pm 32.5^\circ$	$\pm 55^\circ$	$\pm 32.5^\circ$

Source: The Regents of University of California

Another possible source of error is the fact that two different methods of assuming the heat capacity of the oil were employed. The measurements used to determine the heat capacity of the oil that were used for the North-South calculations were lower than the table values from the oil manufacturer that were used for the East-West calculations. If the same values for the heat capacity were used, it is likely that the East-West collector would look additionally worse compared to the North-South collector.

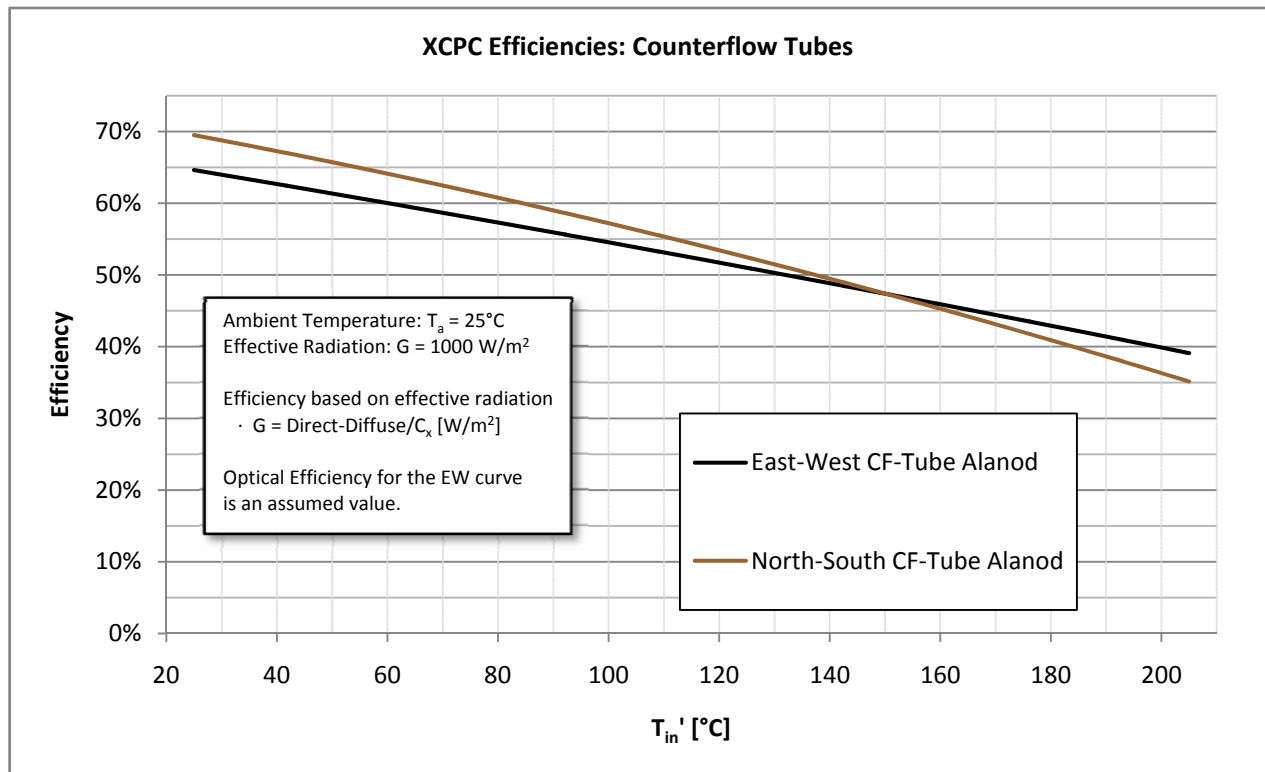


Figure 147. Counterflow Efficiencies: North-South vs. East-West

Source: The Regents of University of California

¹¹ The acceptance angle of the East-West Counterflow Alanod collector can be assumed to be the same as the U-Tube Reflectech version as presented in the table.

Possible errors

Errors in the data may come from any of the following: instrumental errors, measurement errors, assumed values, tolerance errors, environmental effects, ground reflection, and errors in theory.

Although calibrated, instruments such as pyranometers, pyrhemometers, thermocouples and other temperature sensors, the flowmeter, and data acquisition systems may have non-trivial errors associated with them. While steps were taken to minimize these sources of error, it is impossible to avoid them completely. Errors in any of these instruments would affect the efficiency measurements and/or the temperature scale.

The effective area of the collector is a possible source of error due to it being measured manually but this error should be less than a fraction of a percent. Any error in the area of the collector would directly affect the calculated efficiency values.

Material properties of the oil, absorber, glass, and reflector may differ from the model. The heat capacity values used for the heat transfer oil (Duratherm 600) were measured by an outside source (Rose Consulting) with their own set of possible errors. The lab that measured the heat capacity of the oil estimated the error to be as high as 2%. Any error in the heat capacity would directly affect the calculated efficiency values. Any differences in the properties of the reflector, glass, or absorber would create an error in estimating the optical and thermal efficiencies.

The shape of the reflector and the position of the holes in the frame are subject to tolerance errors that would affect the optical efficiency and the acceptance angle.

Soiling of the reflectors and the glass tubes can have a negative effect on the optical efficiency.

Ground reflection is inevitable when testing solar thermal collectors outdoors. The amount of ground reflection available to the collector depends on the optics and orientation of the collector, the time of day and the position of the tracker. While the pyranometer mounted on the tracker should be able to detect all or most of the ground reflection, the angle of incidence may be too severe to be accepted by the collector. Collectors with lower concentrations and collectors oriented in a vertical position like the North-South collectors will be able to accept more of this reflected radiation. The ground reflection will be treated as diffuse light. Ground reflection can cause variation in data and cause East-West collectors to have an apparent lower than expected performance.

Much of the data presented in this report uses an effective irradiance to represent the amount of available power to the collector. The effective irradiance adjustment attempts to take into account that a concentrating optical system cannot accept all of the diffuse and is therefore not considered in the efficiency. Using this method will favor collectors with larger concentration ratios

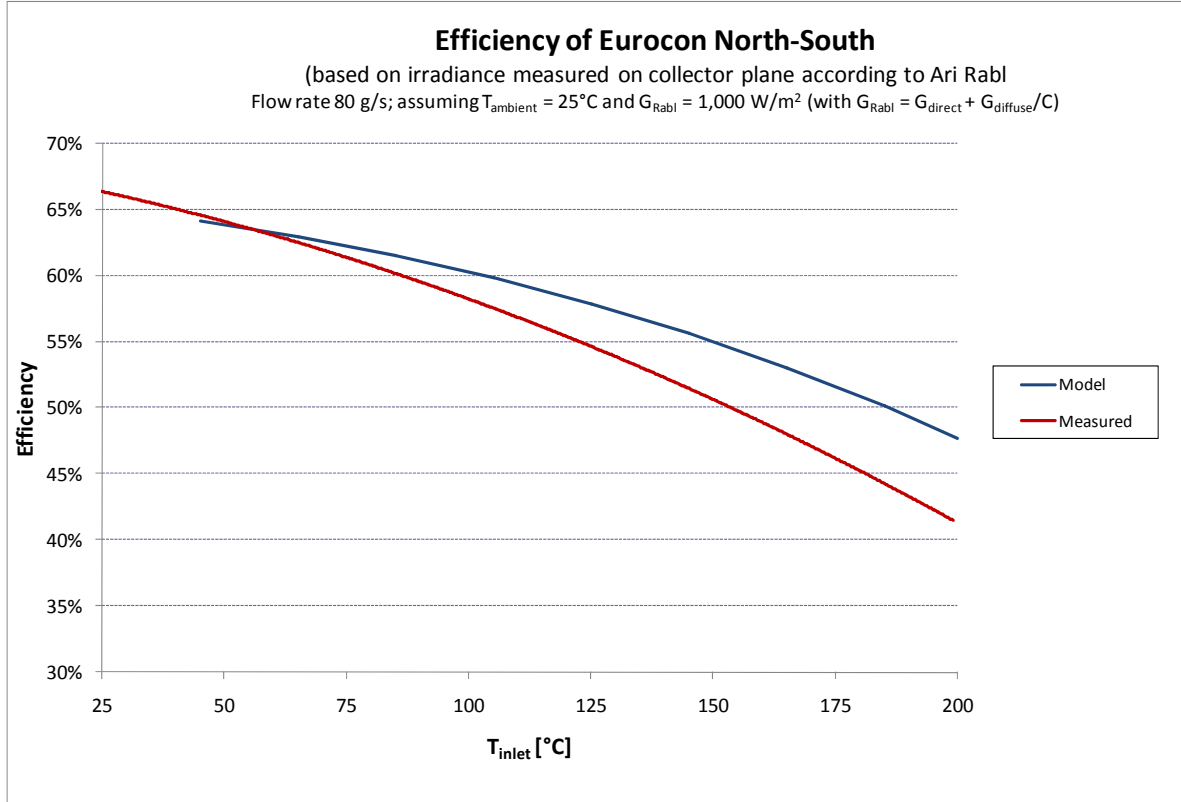
Other data is presented in this report uses the direct normal irradiance (DNI) to represent the incoming radiation. This method completely ignores diffuse radiation which favors collectors with low concentrations. Using this method with data having a large percent of the irradiance as diffuse can create apparently high efficiencies.

Since the testing was done outdoors, it is virtually impossible to test with a constant or consistent ambient temperature. The charts and the data presented in this report attempt to minimize the effect of the differences in the ambient temperature by presenting data with the reduced temperature. Unfortunately, these evacuated tube collectors primarily lose heat through radiation which is non-linear. In addition, the emissivity of the absorber is a function of the absorber temperature only and not of the ambient temperature. This creates a less than perfect correction for the ambient temperature which is most apparent when a collector was tested during very different outdoor temperatures or when comparing two different collectors that were tested in different seasons.

2.16. Task 17

In this task the contractor compared the test results for optical and thermal collector efficiency obtained in Task 16 with the expected optical and thermal efficiency predicted by models that were originally developed in Task 5 and further improved in the course of this Task. The comparison applies to the XCPC collector named “Metal absorber with glass-to-metal seal – North-South orientation.” The detailed design and the specifications of this XCPC have been described in the Task 12 Report. The tested collector consisted of 6 absorber tubes.

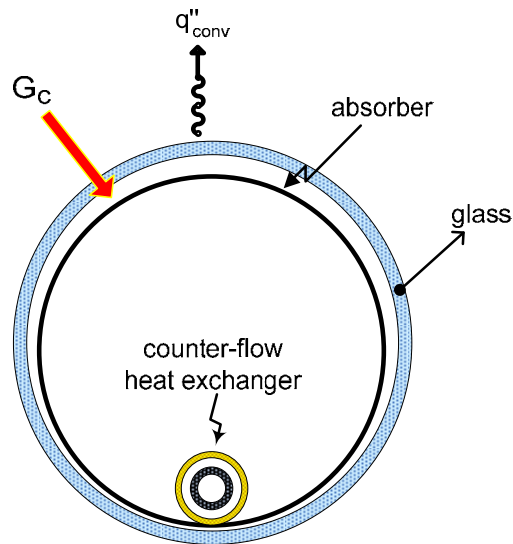
Figure 148. Shows the comparison between expectations from modeling with achieved test results.



Source: The Regents of University of California

Figure 149. Comparison of measured and modeled collector efficiency

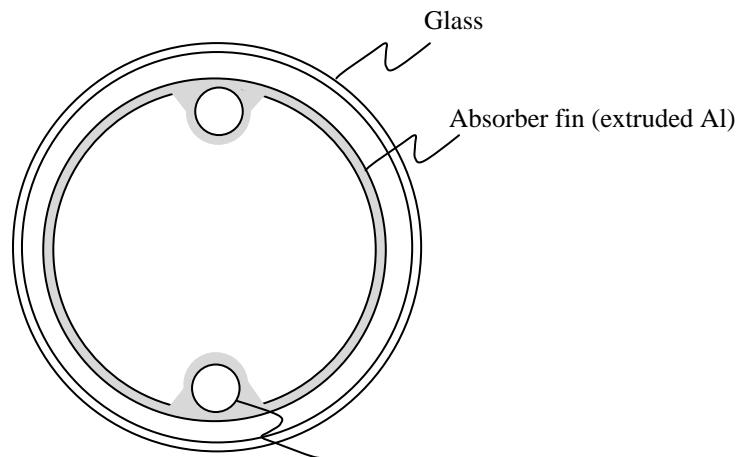
Source: The Regents of University of California



The comparison shows that the measured optical efficiency is very close to expectations, namely around 65%. This indicates that the manufacturing of the external reflectors and the alignment of the absorber tubes relative to the reflectors are well done.

There is a shortfall of measured thermal efficiency relative to the model at higher temperatures. The contractor has two explanations for that: First, the model does not consider the heat losses in the manifold. The manifold has been insulated well, but such insulation can never be perfect. Secondly, the absorber tube uses a cylindrical metal fin absorber that is welded just along one fine line onto the counter-flow heat exchanger that carries the heat transfer fluid (Figure 149). The thermal contact between the cylindrical metal fin absorber and the counter-flow tube is believed to constitute the limiting factor in heat transfer and thus the thermal performance of the absorber tube.

Figure150. Schematic of absorber tube used in tested XCPC



Source: The Regents of University of California

An improved version of the XCPC with a U-tube heat exchanger instead of the counter-flow heat exchanger will be manufactured and tested in the next project tasks. This U-tube version is expected to have better heat transfer and thus thermal efficiency than the version with the counter-flow tube, because there will be two connection lines between absorber fin and metal tube instead of one. An additional advantage of the new version will be that the aluminum absorber fin will be made out of extruded aluminum instead of using an aluminum foil. The extruded absorber fin will have better mechanical stability than the foil. A schematic drawing of the improved version of the XCPC is shown in Figure 150.

2.17. Task 18

Test plan to test the performance of the XCPC prototype

The following test plan is based on the international standard for solar thermal collector testing, ISO 9806-1 (Part 1). Some modifications have been made to account for the specific design, namely a stationary concentrating evacuated tube collector, and the temperature range of operation, which is up to 450°F.

The tests to be performed in Task 19 will include:

- Collector time constant
- Collector thermal efficiency
- Collector optical efficiency
- Collector incident angle modifier
- Pressure drop across the collector

Description of Test Loop

The test facility uses a closed loop system that includes a circulating oil temperature controller with integrated pump and expansion tank (see Figure 151). The circulating oil temperature controller provides a selectable constant temperature (up to 500°F) to the heat transfer fluid that is circulated through the collector. The loop further includes a flow meter, temperature sensors before and after the collector, and a calorimeter. The calorimeter is described in detail below. The solar collector is mounted on a dual axis tracker to allow the measurement of collector performance under controlled incidence angles.

The test facility further includes a meteorological station with a Precision Spectral Pyranometer that is mounted on the same tracker as the solar collector, a Normal Incidence Pyrheliometer mounted on a separate dual-axis tracker, a thermometer to measure the ambient temperature, and an anemometer.

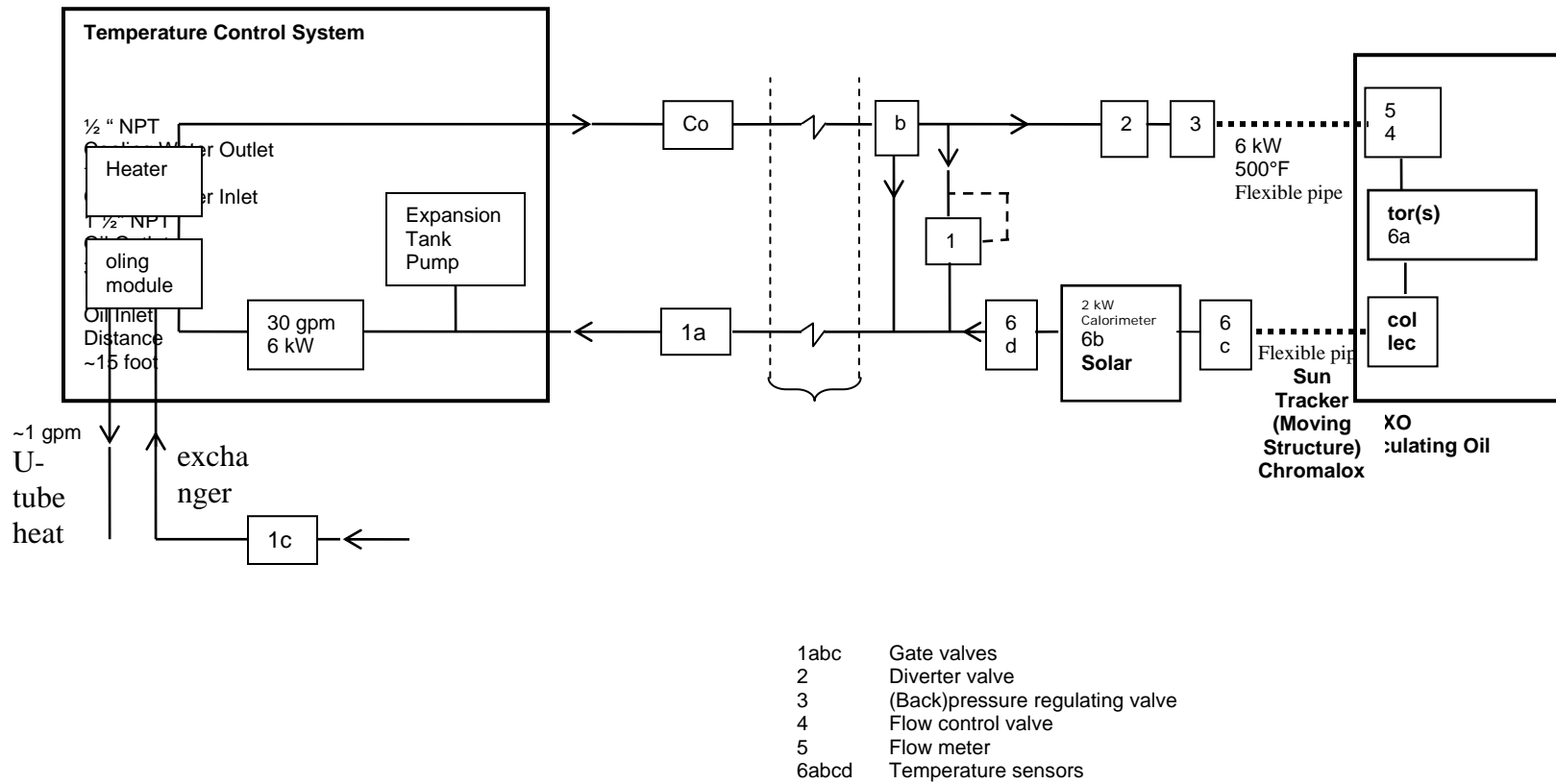


Figure 151. Schematic of Test Facility
 Source: The Regents of University of California

The data from the flow meter, the temperature sensors and the meteorological station are recorded through a data acquisition system.

Instrumentation

Circulating oil temperature controller:	Chromalox CMXO 6kW (with integrated pump and expansion tank)
Temperature sensors:	Type-K thermocouples from Omega
Flow meter:	Micro Motion Coriolis F-Series sensor
Flow control valve:	Valtek ½" Flow Top Control Valve
Back pressure regulating valve:	Jordan: 1" 50-100-S6-I5-S6-Y-8-21-S6-MD Pressure Control Valve
Sun tracker:	Wattsun AZ-125 dual axis tracker
Calorimeter:	Custom made by Valin Inc.
Pyranometer:	Eppley Precision Spectral Pyranometer
Pyrheliometer:	Eppley Normal Incidence Pyrheliometer
Amplifiers:	Agilent 34970A Data Acquisition/Switch Unit
Data logger:	Obvius A8811 and A8923

Test Procedure for Collector Time Constant

Testing will be performed outdoors with a solar irradiance on the plane of the collector aperture greater than 800 W/m². The heat transfer fluid will be circulated through the collector at the same flow rate as used during collector thermal efficiency testing.

Initially the collector's aperture will be shielded from solar radiation by means of a solar-reflecting cover, and the temperature of the heat transfer fluid at the collector inlet will be approximately equal to the ambient air temperature. When a steady state has been reached, the cover will be removed and measurements of the collector fluid inlet temperature (t_{in}), the collector fluid outlet temperature (t_e), and the surrounding air temperature (t_a) will be taken until steady-state conditions have been reached again. A steady state condition is assumed to exist when the outlet temperature of the fluid varies by less than 0.05°C per minute.

The difference between the temperature of the fluid at the collector outlet and that of the surrounding air ($t_e - t_a$) will be measured against time, beginning with the initial steady-state condition $(t_e - t_a)_0$ and continuing until the second steady state has been achieved at a higher temperature $(t_e - t_a)_2$ (see Figure 152). The time constant τ_c of the collector is defined as the time taken for the collector outlet temperature to rise by 63.2% of the total increase from $(t_e - t_a)_0$ to $(t_e - t_a)_2$ following the step increase in solar irradiance at time zero.

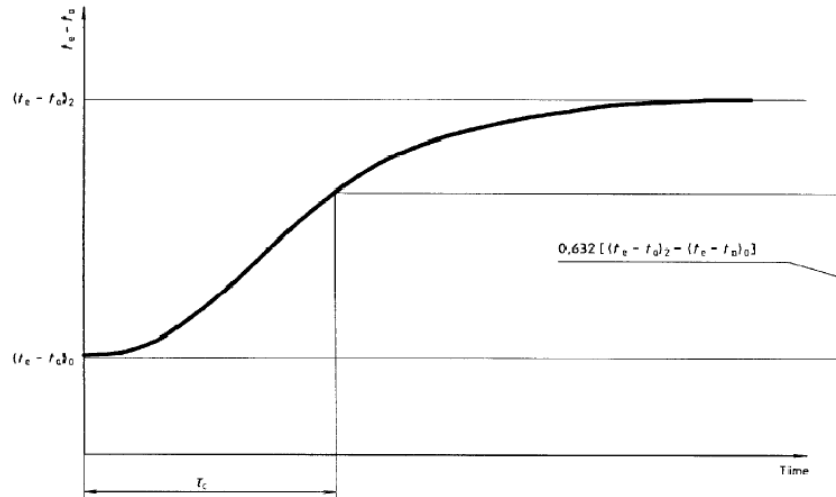


Figure 152. Collector time constant
 Source: The Regents of University of California

Collector Thermal Efficiency

The instantaneous collector efficiency η_{coll} is defined as

$$\eta_{coll} = \frac{\dot{Q}}{A_A G}$$

with

$$\begin{aligned} \dot{Q} &= \dot{m} c_f \Delta T_{coll} \\ G &= G_{direct} - \frac{G_{diffuse}}{c} \\ G_{diffuse} &= G_{hemi} - G_{direct} \end{aligned}$$

where

- \dot{Q} : useful power extracted from collector,
- \dot{m} : mass flow rate of heat transfer fluid,
- c_f : specific heat capacity of the heat transfer fluid,
- ΔT_{coll} : temperature difference between collector fluid at collector outlet and inlet,
- A_A : aperture area of collector,
- G : solar irradiance captured by concentrating collector,

G_{direct} : direct normal irradiance (measured with a pyrheliometer),
 $G_{diffuse}$: diffuse sky irradiance,
 G_{hemi} : hemispherical irradiance (measured with a pyranometer).
 c : geometric concentration of collector

The determination of the instantaneous collector efficiency based on the formula above requires the measurement of the mass flow rate of heat transfer fluid, the temperature difference between the heat transfer fluid at the collector outlet and inlet, the aperture area of collector, the solar irradiance, and the knowledge of the specific heat capacity of the heat transfer fluid (at various temperatures).

Efficiency Measurement with Calorimeter

The instantaneous collector efficiency η_{coll} has been defined above as

$$\eta_{coll} = \frac{\dot{Q}}{A_A G} = \frac{\dot{m} c_f \Delta T_{coll}}{A_A G}$$

If one prefers not to rely on the measurement accuracy of \dot{m} and the accuracy of the tabulated values of the heat capacity c_f of the heat transfer medium, an alternative approach can be used to determine η_{coll} . This is by using a calorimeter, which is a perfectly insulated electric heater placed in series after the solar collector. In this case, the heat loss of the calorimeter is assumed to be zero, and the useful power extracted from the calorimeter $\dot{Q}_{calorimeter}$ is equal to the electric power consumption of the calorimeter, which can be measured very accurately.

With

$$\dot{Q}_{calorimeter} = \dot{m} \cdot c_f \cdot \Delta T_{calorimeter},$$

and assuming that the values of \dot{m} and c_f are approximately equal in the collector and in the calorimeter, the product $\dot{m} c_f$ can be replaced by:

$$\dot{m} \cdot c_f = \frac{\dot{Q}_{calorimeter}}{\Delta T_{calorimeter}},$$

where

$\dot{Q}_{calorimeter}$: useful power extracted from collector (= power consumption of calorimeter);
 $\Delta T_{calorimeter}$: temperature difference of fluid between calorimeter outlet and inlet.

Thus, the instantaneous collector efficiency becomes:

$$\eta_{coll} = \frac{1}{A_A G} \cdot \dot{Q}_{calorimeter} \cdot \frac{\Delta T_{coll}}{\Delta T_{calorimeter}}$$

The determination of the instantaneous collector efficiency based on the method using a calorimeter requires the measurement of the temperature difference of the heat transfer fluid at the collector outlet and inlet, the temperature difference of the heat transfer fluid at the calorimeter outlet and inlet, the aperture area of collector, and the solar irradiance. It is not necessary to measure the mass flow rate of heat transfer fluid and to know the specific heat capacity of the heat transfer fluid.

Temperature dependence of collector efficiency

The temperature dependence of the instantaneous efficiency η_{coll} can be represented graphically as a function of the reduced temperature difference T^* (see Figure 153). The thermal performance of the collector can then be characterized by the two coefficients a_1 and a_2 , which are determined by a least square parabolic curve fit:

$$\eta_{coll} = \eta_0 - a_1 T^* - a_2 G (T^*)^2$$

with

η_0 : optical efficiency

T^* : reduced temperature difference

$$T^* = \frac{t_{in} - t_a}{G}$$

where

t_a : ambient temperature,

t_{in} : collector inlet temperature,

a_1 and a_2 : coefficients determined from least squares parabolic curve fit, and the value of G in the formula above is assumed to be 800 W/m^2 .

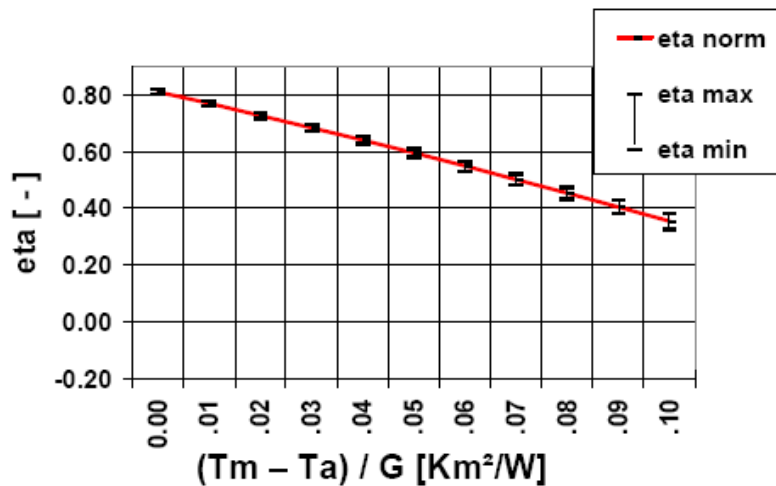


Figure 153. Example of a collector efficiency vs. temperature curve

Source: The Regents of University of California

Collector optical efficiency

The optical efficiency of the collector will be determined using the same test procedure as for the thermal efficiency tests (as described above), only that the temperature of the heat transfer fluid at the collector inlet will be kept equal to the ambient temperature. In this case the calculated thermal efficiency is equal to the optical efficiency (no heat loss).

Collector incident angle modifier

The collector incident angle modifier (IAM) will be determined by measuring the optical efficiency (as described above) under variation of the incidence angle between the sunlight and the collector plane.

Pressure drop across the collector

The pressure drop across the collector will be measured by comparing the difference in the pressure of the heat transfer fluid after and before the collector. The pressure drop measurements will be made for different temperatures between ambient and 400°F.

2.18. Task 19

The goal of this task was to test the improved XCPCs per the test plan outlined in Task 18. The tests include: instantaneous thermal efficiency, optical efficiency, incidence angle modifier, and stagnation.

2.18.1. Tested Collectors

In this task the contractor tested the following XCPC versions:

U-Tube with Alanod Reflectors in North-South orientation

U-Tube with Alanod Reflectors in East-West orientation

X-Tube with Alanod Reflectors in East-West orientation

U-Tube with Reflectech Reflectors in North-South orientation

U-Tube with Reflectech Reflectors in East-West orientation

The detailed design and the specifications of these XCPCs have been described in the Task 17 Report. Both tested collectors consisted of 6 absorber tubes each.

2.18.2. Collector Thermal Efficiency: Method 1

The instantaneous collector efficiency η_{coll} is defined as

$$\eta_{coll} = \frac{\dot{Q}}{A_A G}$$

with

$$\dot{Q} = \dot{m} c_p \Delta T_{coll},$$

$$G = G_{direct} + \frac{G_{diffuse}}{c_x},$$

$$G_{diffuse} = G_{hemi} - G_{direct}$$

Where

\dot{Q} : useful power extracted from collector,

\dot{m} : mass flow rate of heat transfer fluid,

c_p : specific heat capacity of the heat transfer fluid,

ΔT_{coll} : temperature difference between collector fluid at collector outlet and inlet,

A_A : effective aperture area of collector – we define this area as the length of the active area of the absorber tube (which is the area covered by the selective coating) times the width of the reflector

G : solar irradiance captured by concentrating collector,

G_{direct} : direct normal irradiance (measured with a pyrliometer),

$G_{diffuse}$: diffuse sky irradiance,

G_{hemi} : hemispherical irradiance (measured with a pyranometer).

C_x : geometric concentration of collector

2.18.3. Collector Thermal Efficiency: Method 2

The instantaneous collector efficiency η_{coll} can be defined as

$$\eta_{coll} = \frac{\dot{Q}_{coll}}{A_A G}$$

with

$$\dot{Q}_{coll} = \frac{\dot{Q}_{cal} \cdot \Delta T_{coll}}{\Delta T_{cal}},$$

$$G = G_{direct} + \frac{G_{diffuse}}{C_x},$$

$$G_{diffuse} = G_{hemi} - G_{direct}$$

Where

\dot{Q}_{coll} : useful power extracted from collector,

\dot{Q}_{cal} : calorimeter power,

ΔT_{coll} : temperature difference between collector fluid at collector outlet and inlet,

ΔT_{cal} : temperature difference between the fluid at the calorimeter outlet and inlet,

A_A : effective aperture area of collector – we define this area as the length of the active area of the absorber tube (which is the area covered by the selective coating) times the width of the reflector

G : solar irradiance captured by concentrating collector,

G_{direct} : direct normal irradiance (measured with a pyrheliometer),

$G_{diffuse}$: diffuse sky irradiance,

G_{hemi} : hemispherical irradiance (measured with a pyranometer).

C_x : geometric concentration of collector

2.18.4. Temperature dependence of collector efficiency

The temperature dependence of the instantaneous efficiency η_{coll} can be represented graphically as a function of the reduced temperature T^* . The thermal performance of the collector can then be characterized by the two coefficients a_1 and a_2 , which are determined by a least square parabolic curve fit:

$$\eta_{coll} = \eta_o - a_1 T^* - a_2 G (T^*)^2$$

with

η_o : optical efficiency

T^* : reduced temperature

$$T^* = \frac{T_{in} - T_{amb}}{G}$$

where

T_{amb} : ambient temperature,

T_{in} : collector inlet temperature,

a_1 and a_2 : coefficients determined from least squares parabolic curve fit, and the value of G in the formula above is assumed to be 1000 W/m^2 .

2.18.5. Description of Test Loop

The test facility used is a closed loop system that includes a circulating oil temperature controller with integrated pump and expansion tank (see Fig. 1). The circulating oil temperature controller provides a selectable constant temperature (up to 500°F) to the heat transfer fluid that is circulated through the collector. The loop further includes a flow meter and temperature sensors before and after the collector. There are flow mixers introduced into the loop before each temperature sensor. The solar collector is mounted on a dual axis tracker to allow the measurement of collector performance under controlled incidence angles.

The test facility further includes a meteorological station with a Precision Spectral Pyranometer and a Normal Incidence Pyrhemometer that are both mounted on the same tracker as the solar collector, a thermometer to measure the ambient temperature, and an anemometer.

In addition, a calorimeter was used as an improved method of determining the instantaneous thermal efficiency without depending on knowing the heat capacity of the oil¹². XXX

¹² The U-Tube with Alanod Reflectors in North-South configuration collector was not tested using this method.

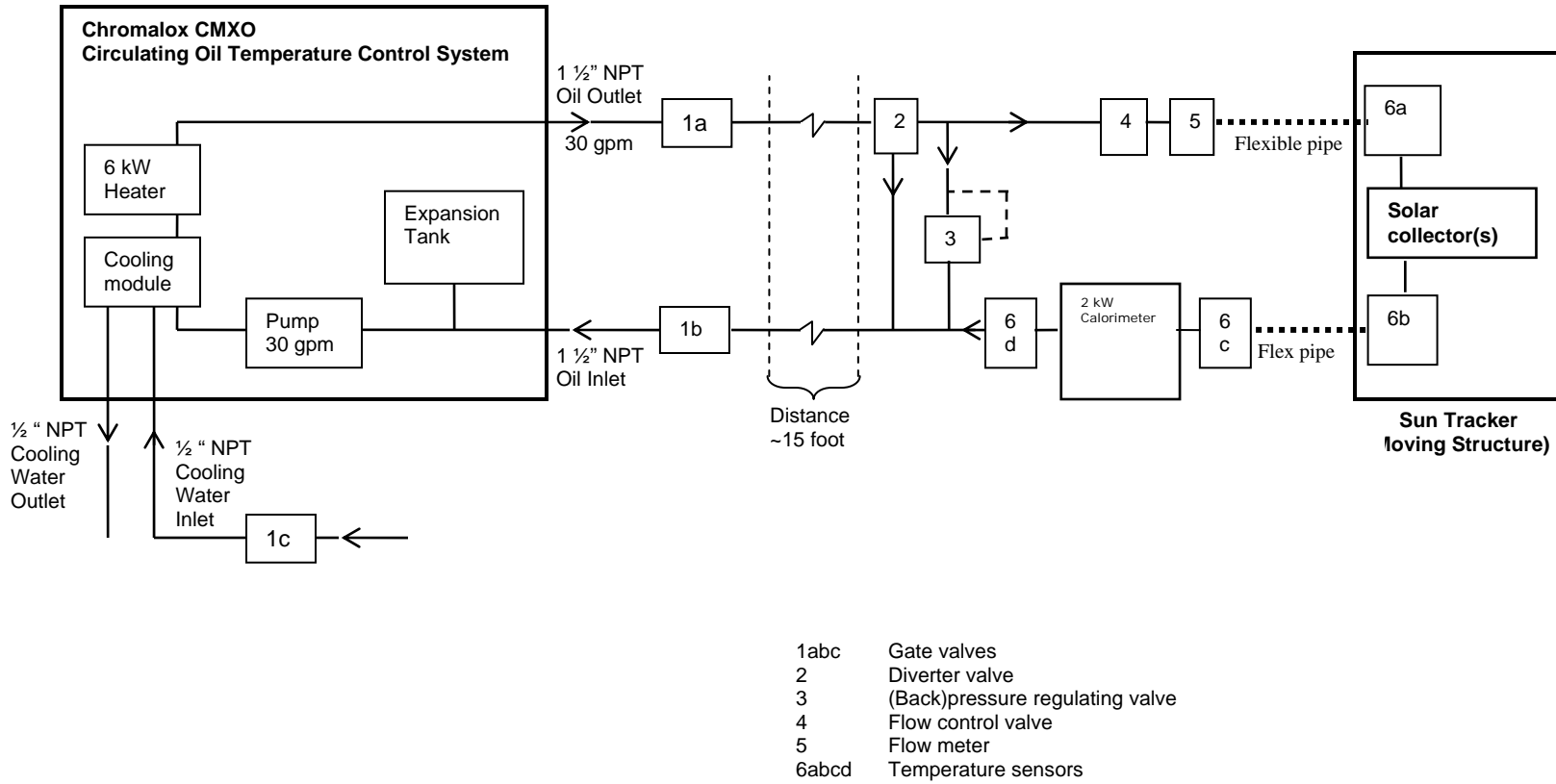


Figure 154. Schematic of Test Facility
Source: The Regents of University of California

The data from the flow meter, the temperature sensors and the meteorological station were recorded through a data acquisition system.

2.18.6. Instrumentation

- Circulating oil temperature controller: Chromalox CMXO 6kW (with integrated pump and expansion tank)
- Temperature sensors: Type-K thermocouples from Omega
- Flow meter: Micro Motion Coriolis F-Series sensor
- Flow control valve: Valtek ½" Flow Top Control Valve
- Back pressure regulating valve: Jordan: 1" 50-100-S6-I5-S6-Y-8-21-S6-MD Pressure Control Valve
- Sun tracker: Wattsun AZ-125 dual axis tracker
- Calorimeter: Custom made by Valin Inc.
- Pyranometer: Eppley Precision Spectral Pyranometer
- Pyrheliometer: Eppley Normal Incidence Pyrliometer
- Data Acquisition System 1: Agilent 34970A Data Acquisition/Switch Unit
- Data Acquisition System 2: Acquisuite Data Acquisition System

2.18.7. Test Results of “U-Tube with Alanod Reflectors in North-South orientation”

Collector description

Table 39. Collector Description of North-South U-Tube with Alanod Collector

Orientation	North-South
Concentration C_x	1.15
Effective Collector Area A_A	2.076 m ²
Tube Type	U-Tube
Number of Tubes	6
Reflector	Alanod (90%)

Source: The Regents of University of California

Collector optical efficiency

The optical efficiency of the North-South Counterflow with Alanod collector was used as an assumed value of the optical efficiency of the North-South U-Tube with Alanod since the geometry and optical properties of the system were assumed to be unchanged.

The optical efficiency based on an effective irradiance ($G = G_{DNI} + G_{diffuse}/C_x$) was assumed to be 69.1%. The optical efficiency based on direct normal irradiance ($G = G_{DNI}$) was assumed to be 79.3%.

Collector thermal efficiency

The efficiency of the XCPC was measured from 6/30 - 7/3/08 using “Method 1” at the following collector inlet temperatures: 80°C, 100°C, 120°C, 140°C, 160°C, 180°C, and 200°C; and at the following flow rates: 80 g/s, 100 g/s, 120 g/s, and 140 g/s.

The heat capacity of the oil was measured in August 2008 using the calorimeter during the East-West U-Tube with Alanod tests. A linear approximation to the measurements was used to calculate the efficiency of the collector: $c_p = 0.00489 \cdot T_m + 1.815$.

The performance characteristics are tabulated in Table 2 and the collector efficiencies are depicted in

Figure 1 through Figure 158. Figure 3 and Figure 7 are derived from Figure 2 and Figure 4 respectively by assuming an ambient temperature of 25°C and an effective insolation of 1,000 W/m² that is captured by the XCPC. Figures 2 and 3 display the efficiencies based on the effective irradiance G_E while Figures 4 and 5 display the efficiencies based on the direct normal irradiance (DNI) G_{DNI} .

Table 40. Performance Characteristics of North-South U-Tube with Alanod Collector

	G=G_E	G=G_{DNI}
Optical Efficiency η_o	69.1%	79.3%
Efficiency at 100 °C	58.5%	69.3%
Efficiency at 200 °C	36.4%	36.4%
Loss coefficient (1) a_1	1.080 W/m ² -K	0.595 W/m ² -K
Loss coefficient (2) a_2	0.00351 W/m ² -K ²	0.00993 W/m ² -K ²
Overall heat loss coefficient U	1.891 W/m ² -K	2.382 W/m ² -K

Source: The Regents of University of California

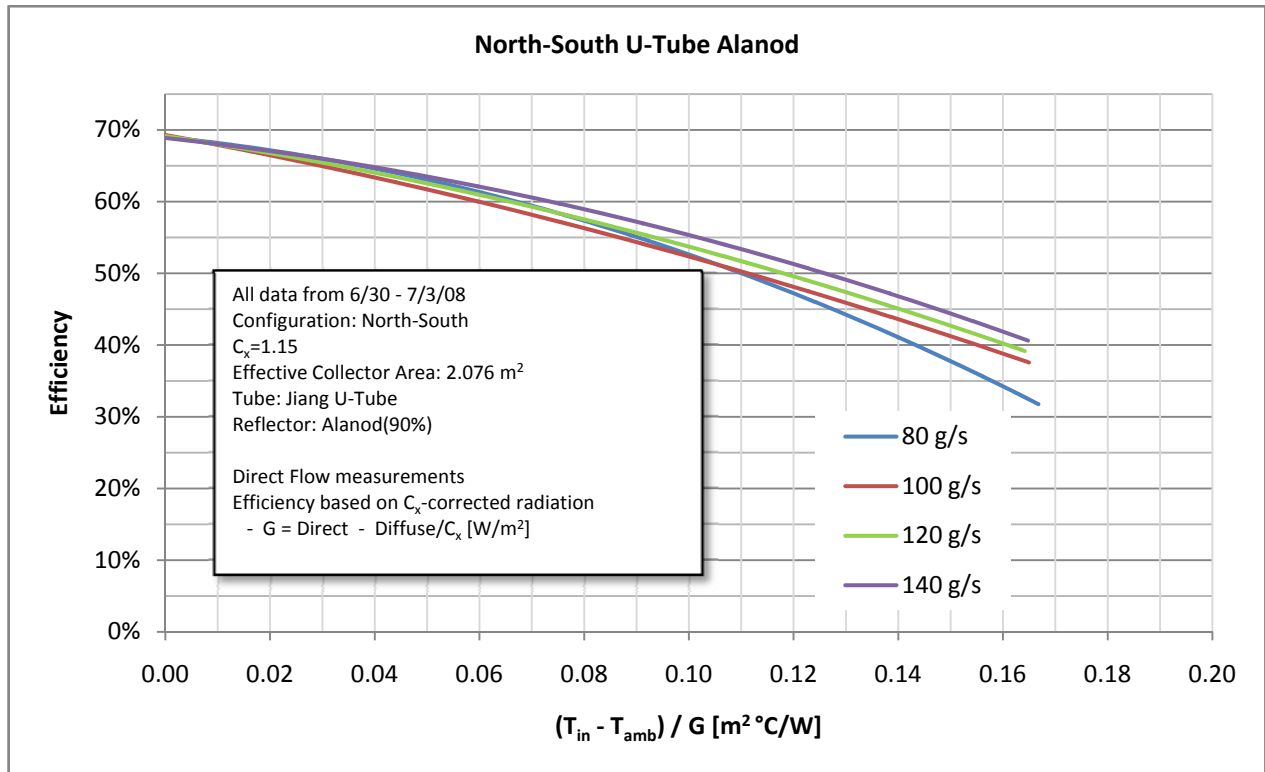


Figure 155. North-South U-Tube with Alanod Effective Reduced Efficiency Curve

Source: The Regents of University of California

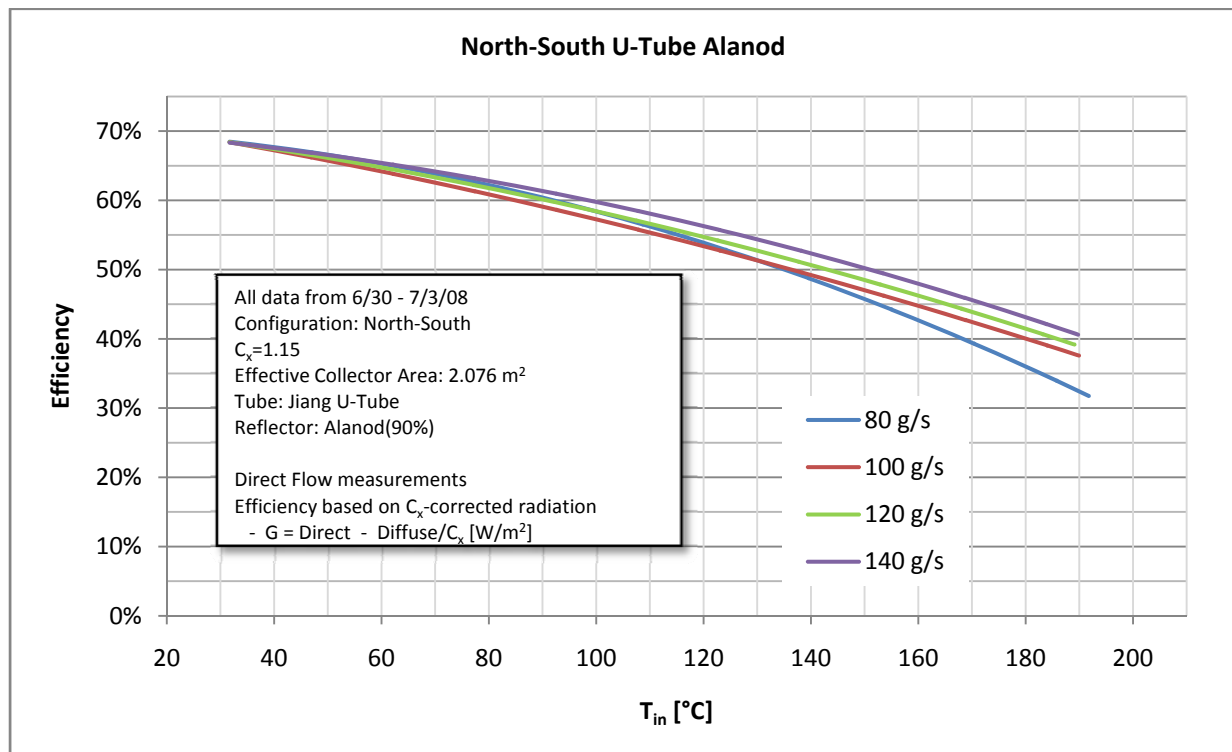


Figure 156. North-South U-Tube with Alanod Effective Standardized Efficiency Curve

Source: The Regents of University of California

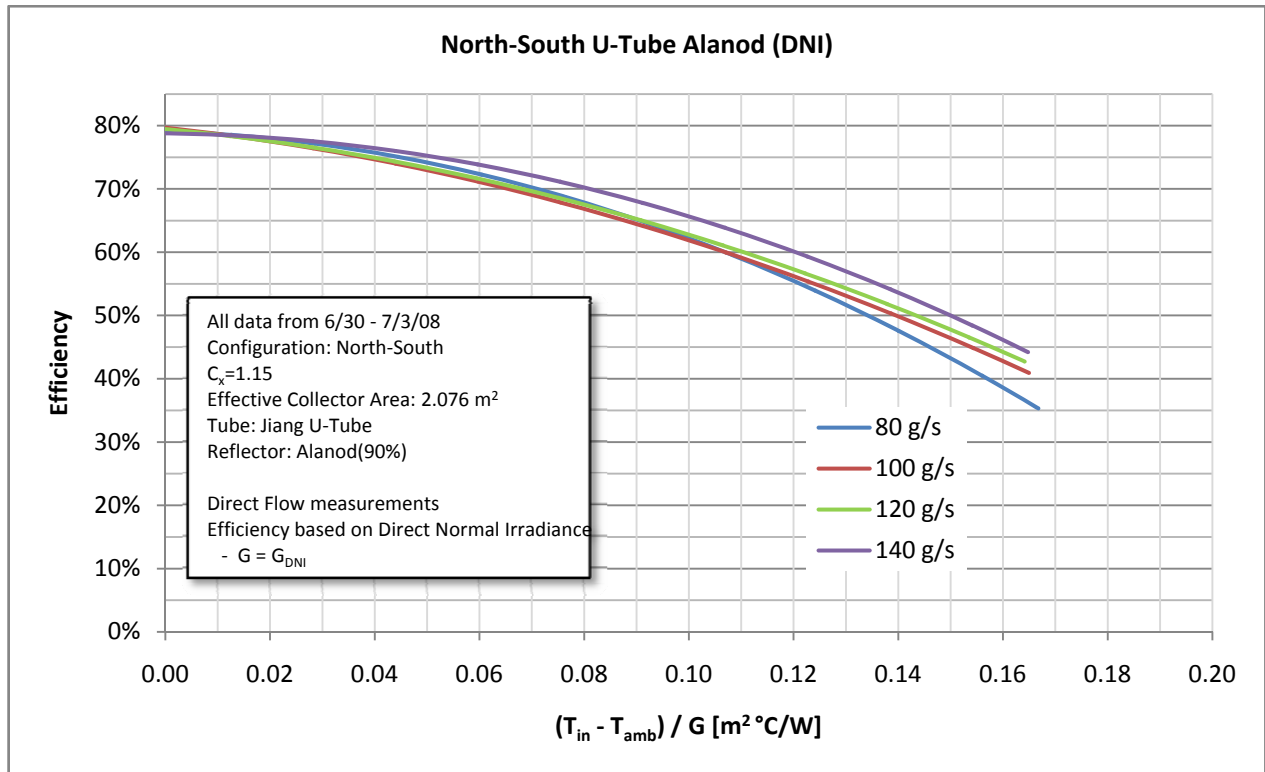


Figure 157. North-South U-Tube with Alanod Direct Reduced Efficiency Curve

Source: The Regents of University of California

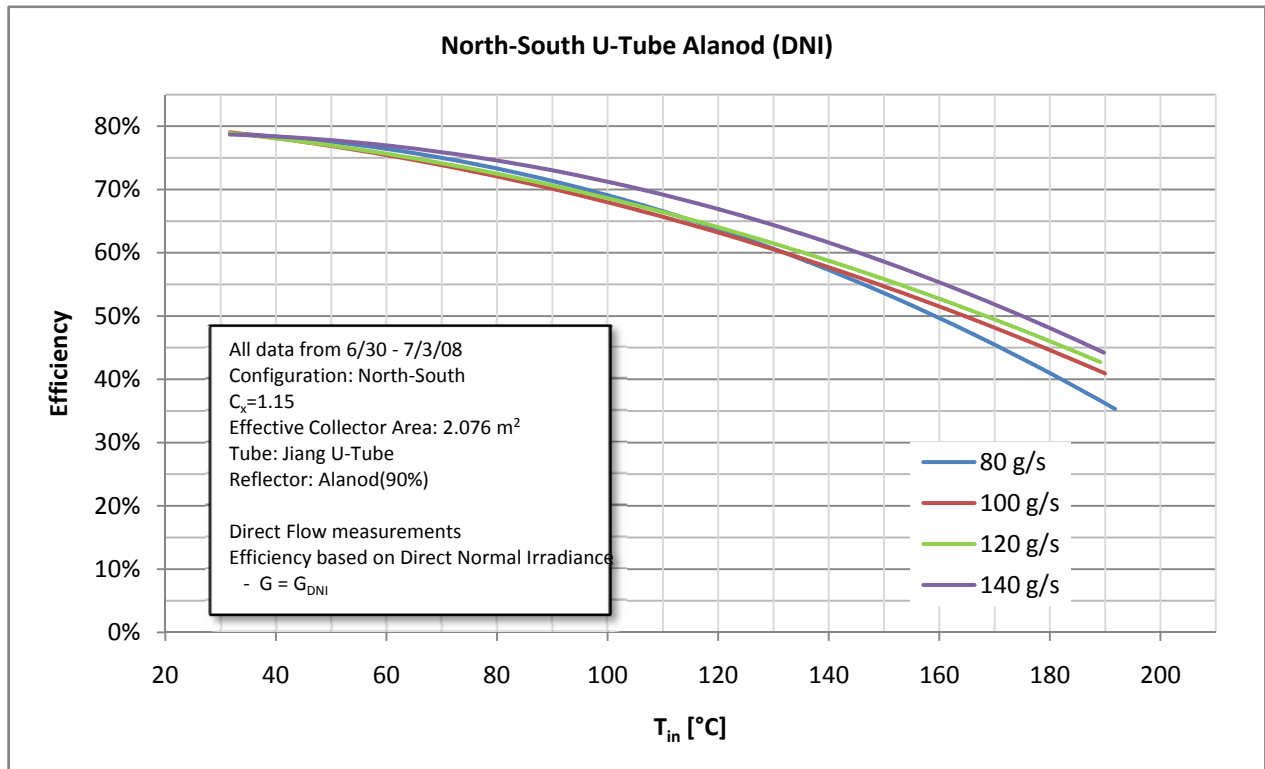


Figure 158. North-South U-Tube with Alanod Direct Standardized Efficiency Curve

Source: The Regents of University of California

Collector Incident Angle Modifier (IAM)

The incident angle modifier (IAM) was not measured for this specific configuration. Since IAM is almost completely dependent on the geometric shape of the reflector and the placement of the tubes, it is reasonable to use the previously measured IAM to describe this collector.

2.18.8. Test Results of “U-Tube with Alanod Reflectors in East-West orientation”

Collector description

Table 41. Description of East-West U-Tube with Alanod Collector

Orientation	East-West
Concentration C_x	1.80
Effective Collector Area A_A	3.24 m ²
Tube Type	U-Tube
Number of Tubes	6
Reflector	Alanod (90%)

Source: The Regents of University of California

Collector optical efficiency

The optical efficiency of the East-West U-Tube with Alanod collector was assumed to be the value taken from a linear extrapolation.

The optical efficiency based on an effective irradiance ($G = G_{DNI} + G_{diffuse}/C_x$) was assumed to be 66.4%. The optical efficiency based on direct normal irradiance ($G = G_{DNI}$) was assumed to be 71.5%.

Collector thermal efficiency

The efficiency of the XCPC was measured from 8/13 – 8/27/08 using “Method 1” and “Method 2” at the following collector inlet temperatures: 80°C, 100°C, 120°C, 140°C, 160°C, 180°C, and 200°C; and at the following flow rates: 80 g/s, 100 g/s, 120 g/s, 140 g/s, and 160 g/s. All efficiencies reported are based on “Method 2.”

The performance characteristics are tabulated in Table 4 and the collector efficiencies are depicted in Figure 6 through Figure 9. Figure 7 and Figure 9 are derived from Figure 6 and Figure 8 respectively by assuming an ambient temperature of 25°C and an effective insolation of 1,000 W/m² that is captured by the XCPC. Figures 6 and 7 display the efficiencies based on the effective irradiance G_E while Figures 8 and 9 display the efficiencies based on the direct normal irradiance (DNI) G_{DNI} .

Table 42. Performance Characteristics of East-West U-Tube with Alanod Collector

Source: The Regents of University of California

	$G=G_E$	$G=G_{DNI}$
Optical Efficiency	66.4%	71.5%
Efficiency at 100 °C	58.3%	63.1%
Efficiency at 200 °C	43.2%	45.2% %
Loss coefficient (1)	0.908 W/m ² -K	0.822 W/m ² -K
Loss coefficient (2)	0.00239 W/m ² -K ²	0.00387 W/m ² -K ²
Overall heat loss coefficient	1.339 W/m ² -K	1.519 W/m ² -K

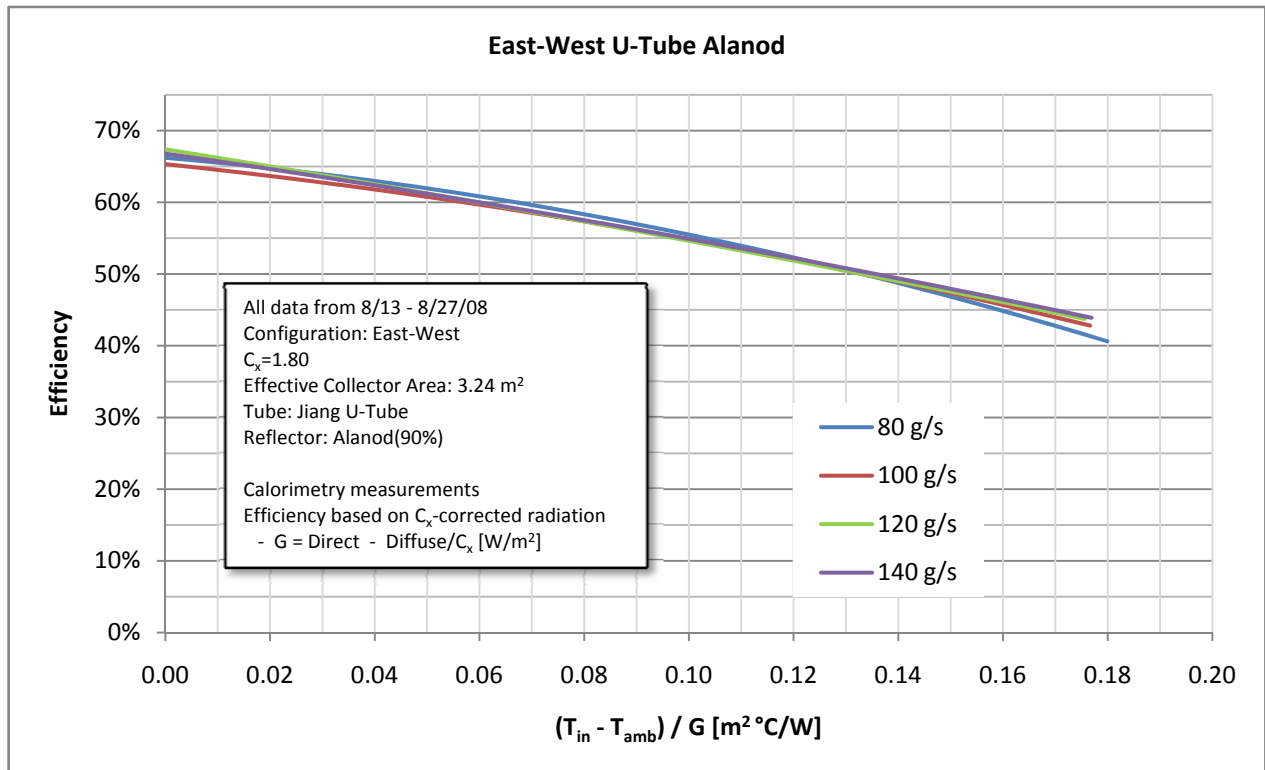


Figure 159. East-West U-Tube with Alanod Effective Reduced Efficiency Curve

Source: The Regents of University of California

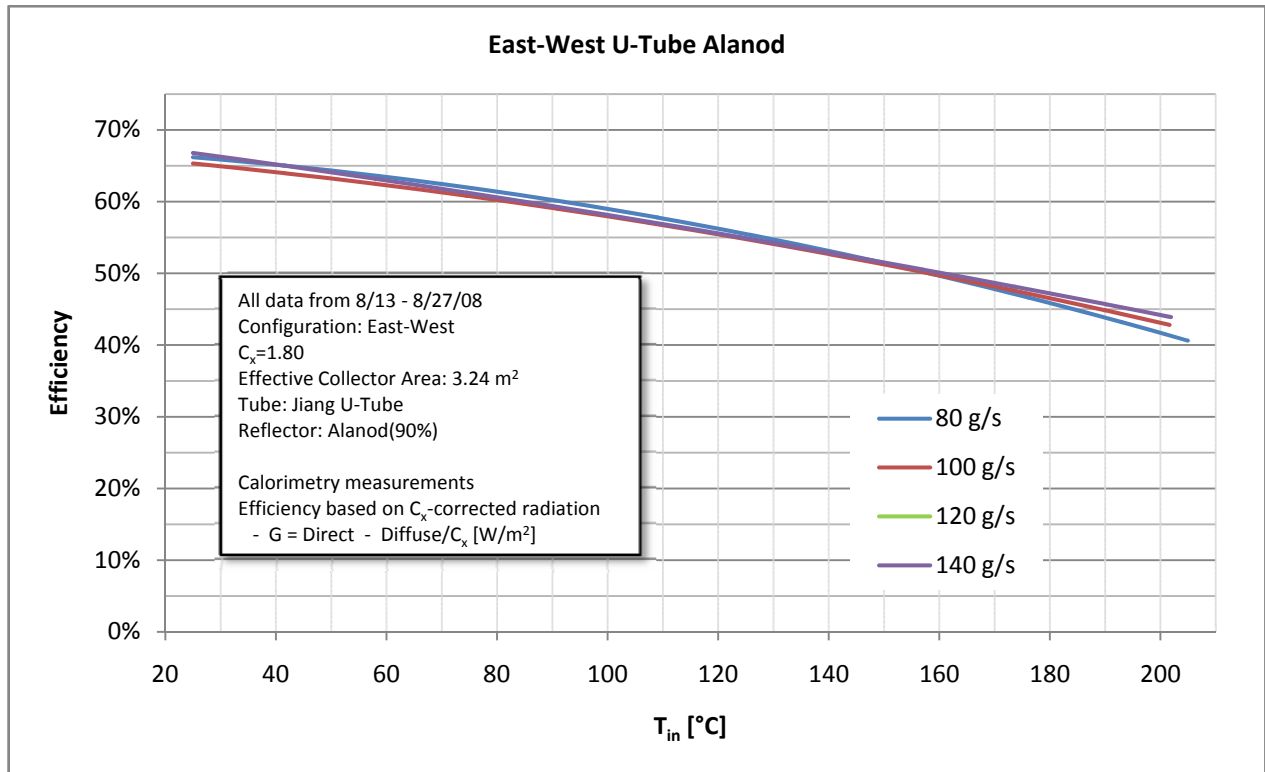


Figure 160. East-West U-Tube with Alanod Effective Standardized Efficiency Curve

Source: The Regents of University of California

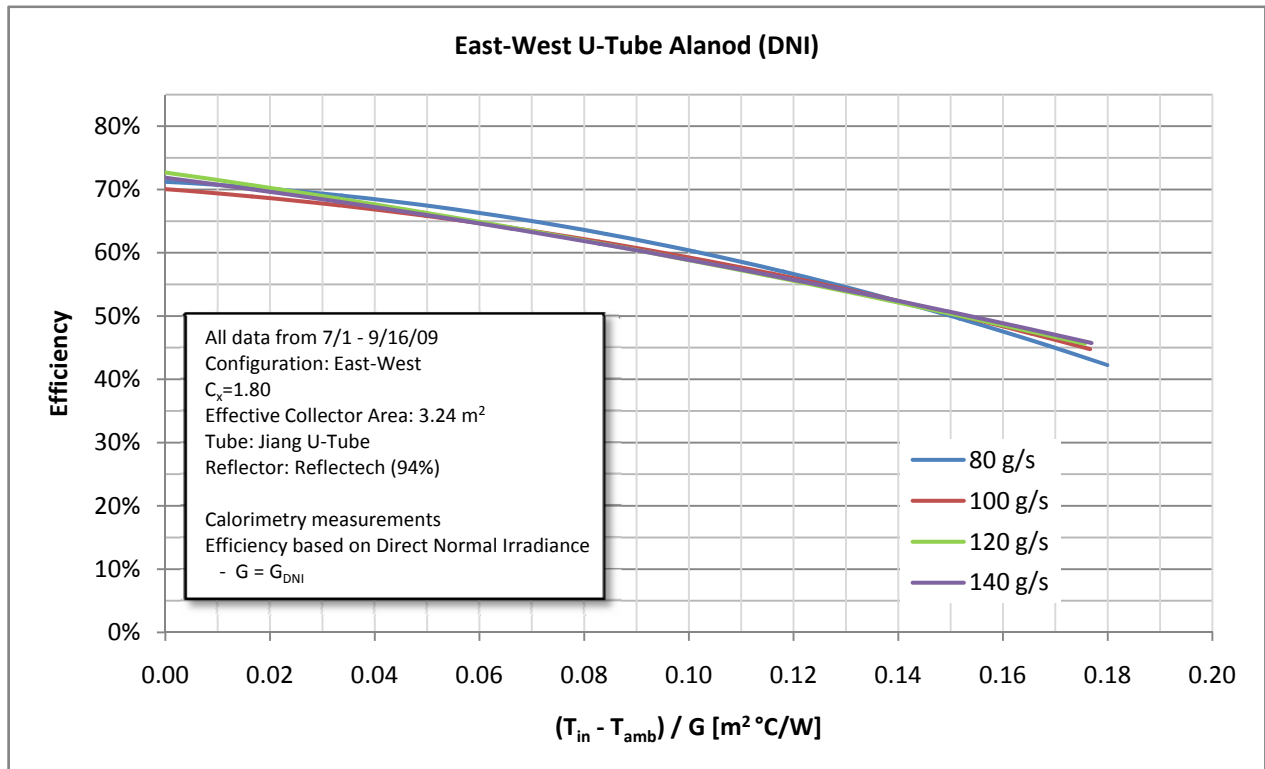


Figure 161. East-West U-Tube with Alanod Direct Reduced Efficiency Curve

Source: The Regents of University of California

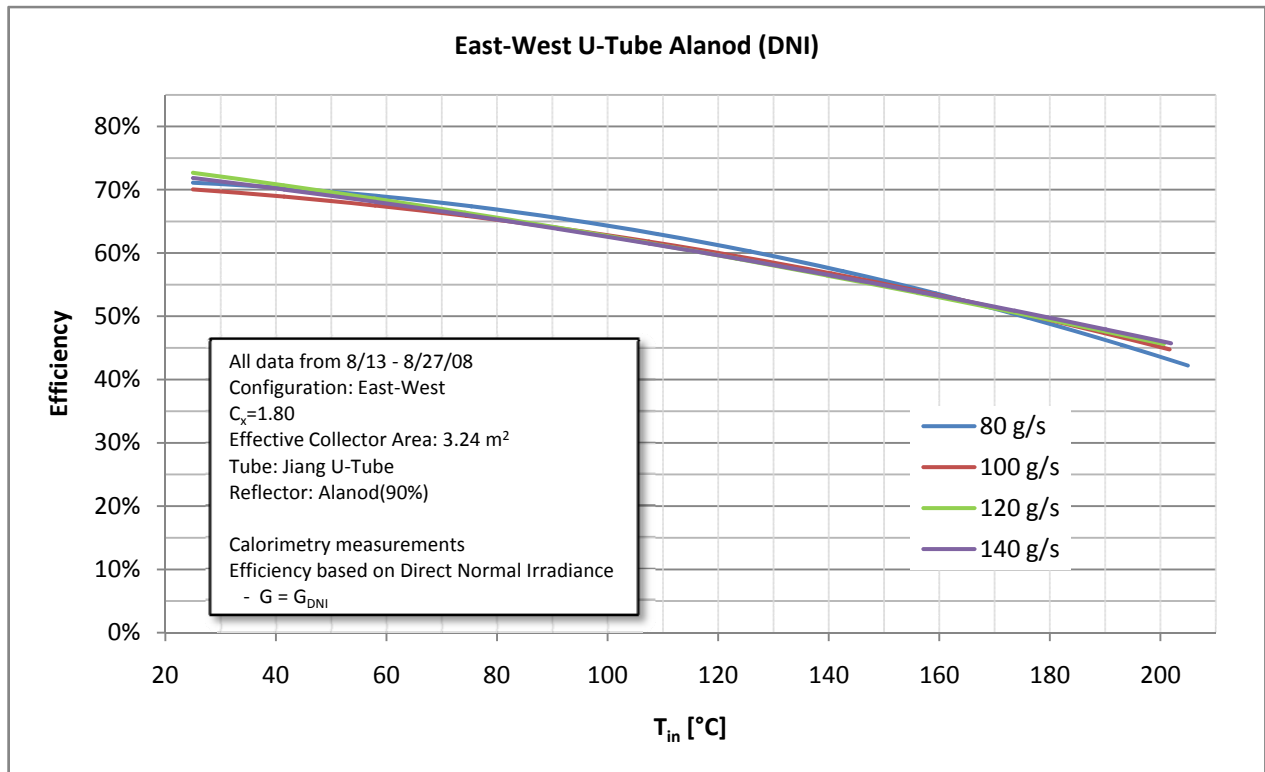


Figure 162. East-West U-Tube with Alanod Direct Standardized Efficiency Curve

Source: The Regents of University of California

Collector Incident Angle Modifier (IAM)

The incident angle modifier (IAM) was not measured for this specific configuration. Since IAM is almost completely dependent on the geometric shape of the reflector and the placement of the tubes, it is reasonable to use the measured IAM from the U-Tube with Reflectech Reflectors in East-West collector to describe this collector.

2.18.9. Test Results of “X-Tube with Alanod Reflectors in East-West orientation”

Collector description

Table 43. Description of East-West Counterflow with Alanod Collector

Orientation	East-West
Concentration	1.80
Effective Collector Area	3.1 m ²
Tube Type	X-Tube
Number of Tubes	6
Reflector	Alanod (90%)

Source: The Regents of University of California

Collector optical efficiency

The optical efficiency of the East-West X-Tube with Alanod collector was assumed to be the value taken from a linear extrapolation.

The optical efficiency based on an effective irradiance ($G = G_{DNI} + G_{diffuse}/C_x$) was assumed to be 68.6%. The optical efficiency based on direct normal irradiance ($G = G_{DNI}$) was assumed to be 75.0%.

Collector thermal efficiency

The efficiency of the XCPC was measured from 9/18 – 10/13/08 using “Method 1” and “Method 2” at the following collector inlet temperatures: 80°C, 100°C, 120°C, 140°C, 160°C, 180°C, and 200°C; and at the following flow rates: 80 g/s, 100 g/s, 120 g/s, 140 g/s, and 160 g/s. All efficiencies reported are based on “Method 2.”

The performance characteristics are tabulated in Table 6 and the collector efficiencies are depicted in Figure 10 through Figure 13. Figure 11 and Figure 13 are derived from Figure 10 and Figure 12 respectively by assuming an ambient temperature of 25°C and an effective insolation of 1,000 W/m² that is captured by the XCPC. Figures 10 and 11 display the efficiencies based on the effective irradiance G_E while Figures 12 and 13 display the efficiencies based on the direct normal irradiance (DNI) G_{DNI} .

Table 44. Performance Characteristics of East-West X-Tube with Alanod Collector

	G=G_E	G=G_{DNI}
Optical Efficiency η_o	68.6%	75.0%
Efficiency at 100 °C	59.9%	65.9%
Efficiency at 200 °C	39.9%	43.4%
Loss coefficient (1) a_1	0.799 W/m ² -K	0.799 W/m ² -K
Loss coefficient (2) a_2	0.00481 W/m ² -K ²	0.00481 W/m ² -K ²
Overall heat loss coefficient U	1.664 W/m ² -K	1.838 W/m ² -K

Source: The Regents of University of California

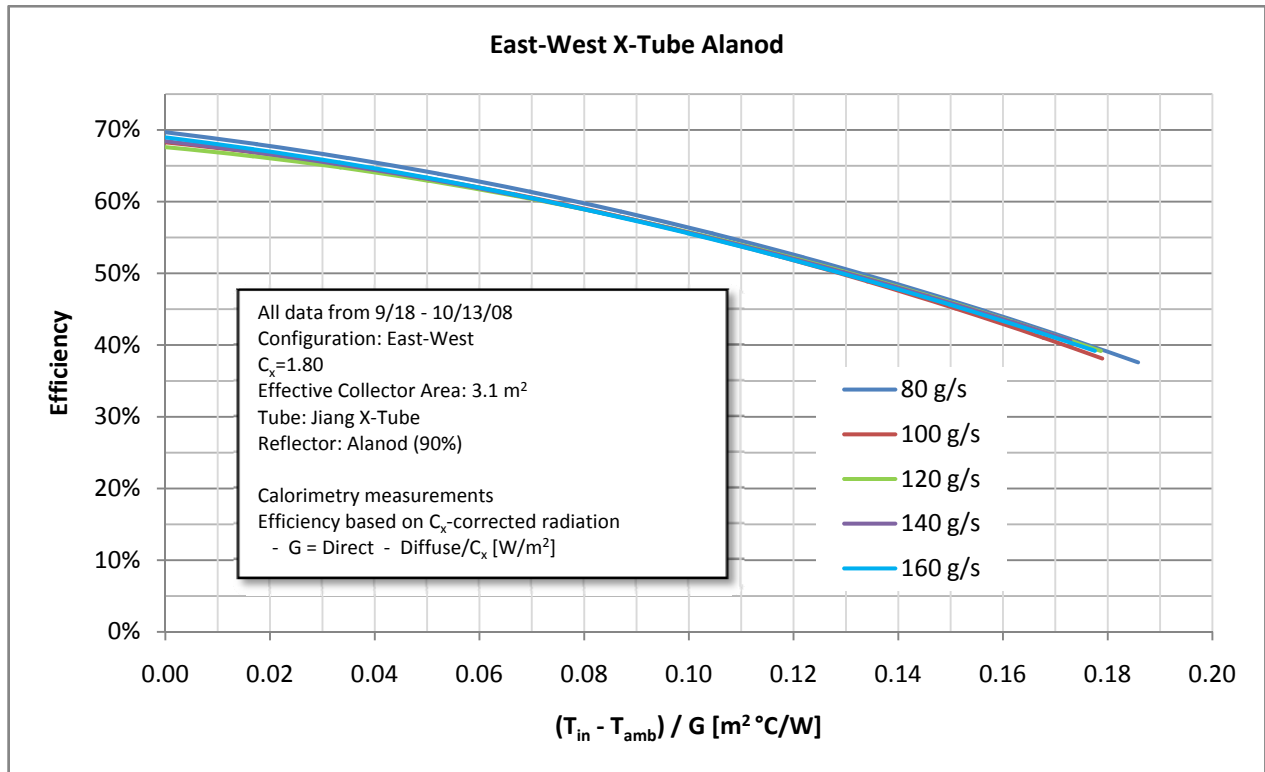


Figure 163. East-West X-Tube with Alanod Effective Reduced Efficiency Curve

Source: The Regents of University of California

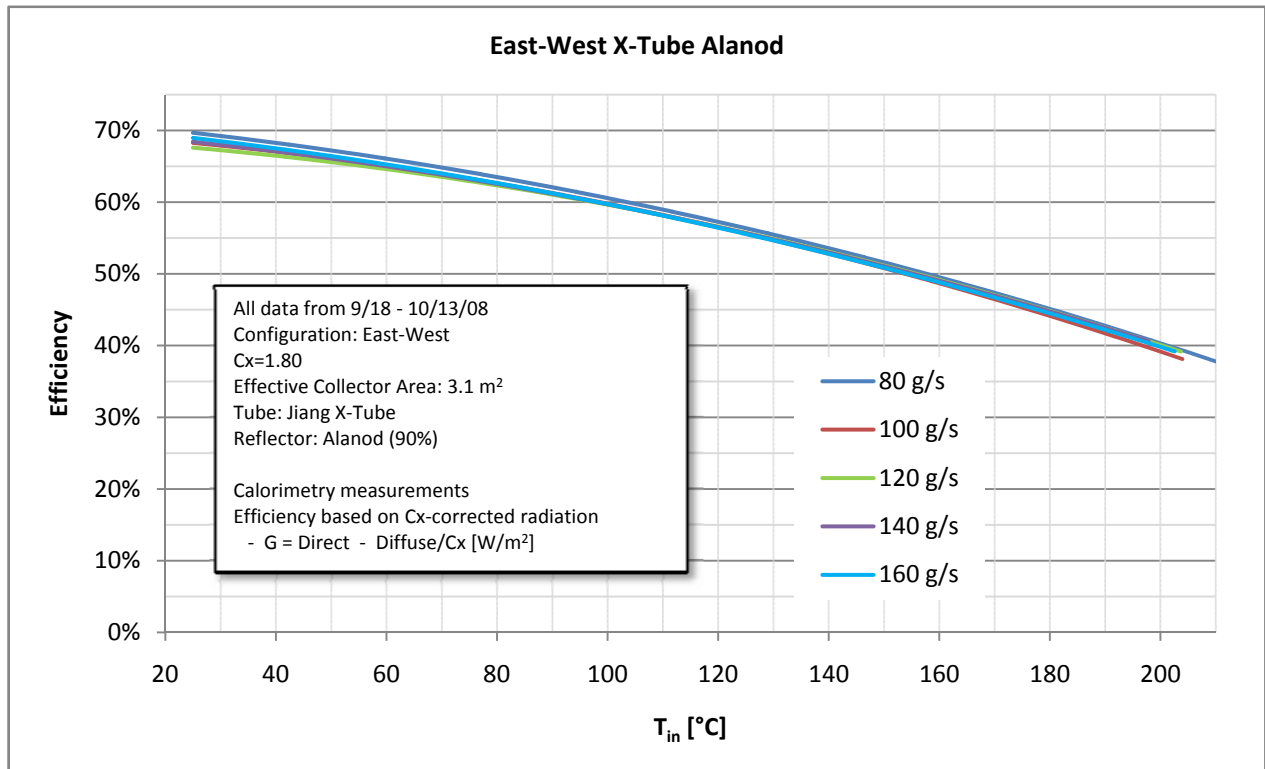


Figure 164 East-West X-Tube with Alanod Effective Standardized Efficiency Curve

Source: The Regents of University of California

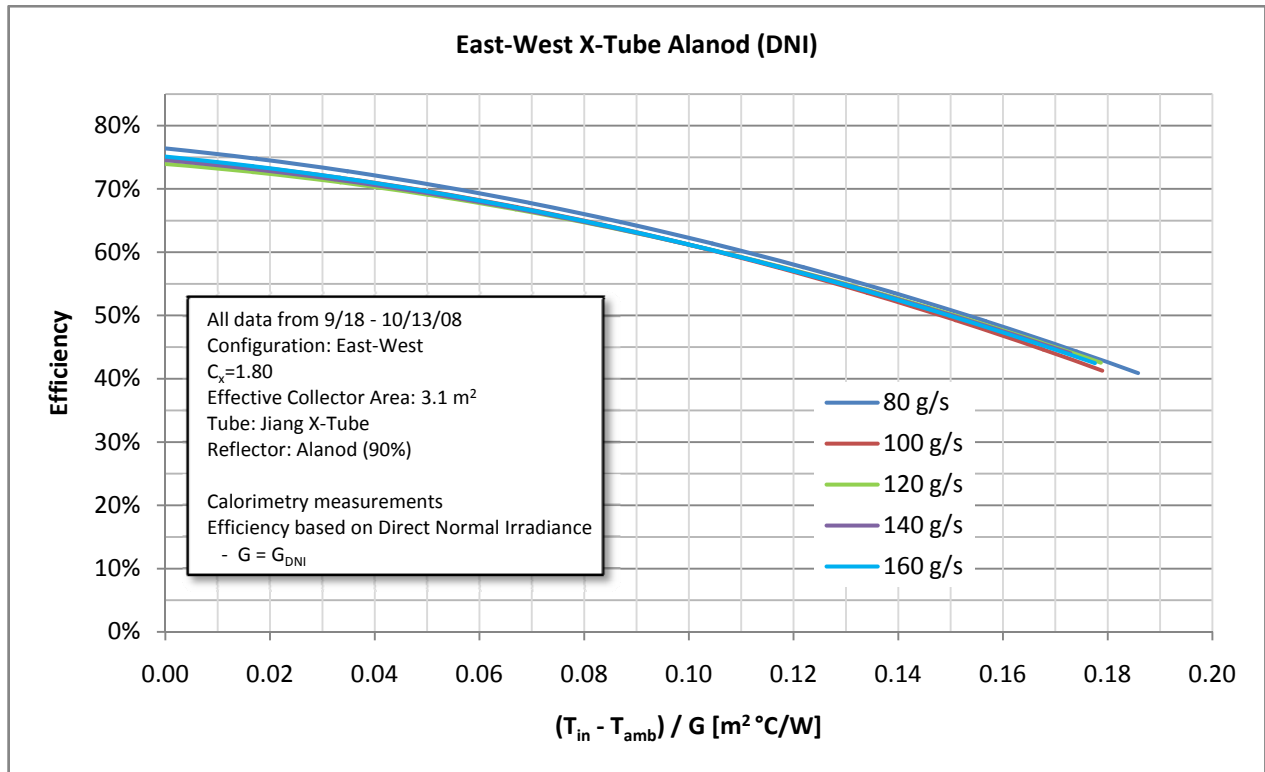


Figure 165. East-West X-Tube with Alanod Direct Reduced Efficiency Curve

Source: The Regents of University of California

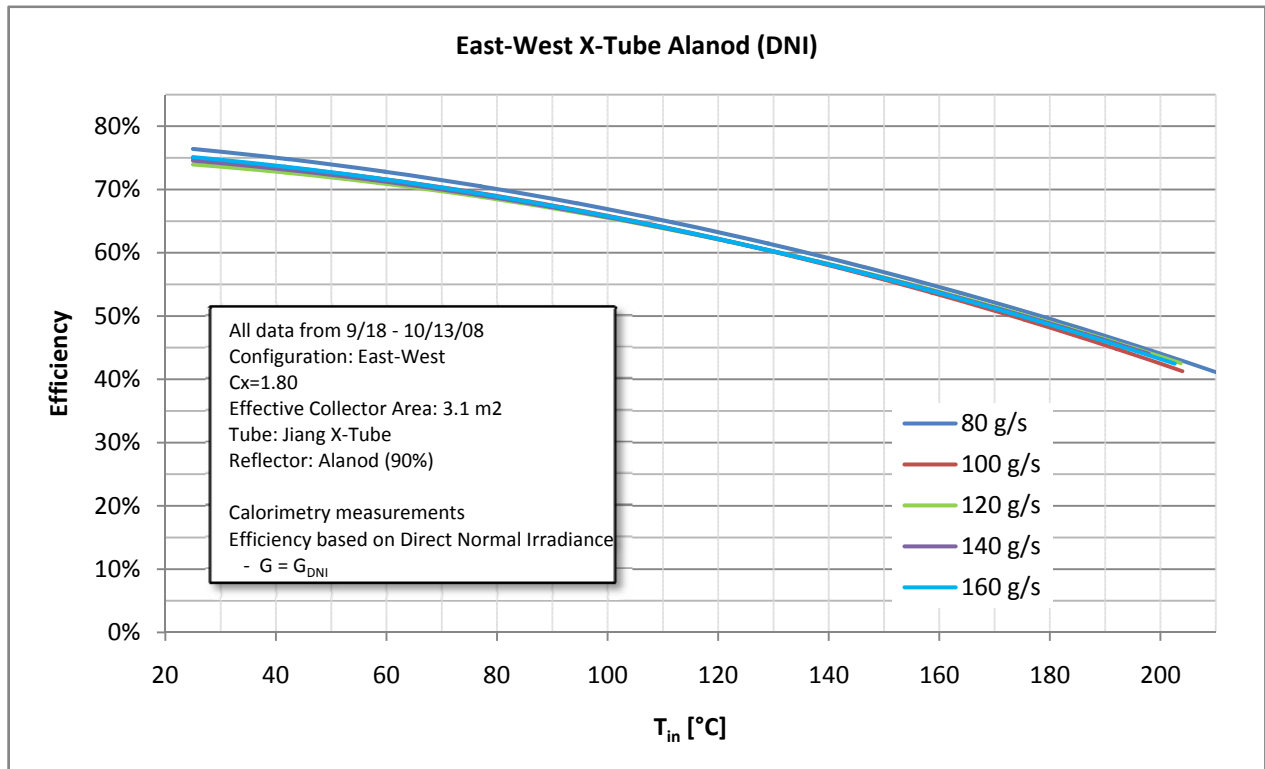


Figure 166. East-West X-Tube with Alanod Direct Standardized Efficiency Curve

Source: The Regents of University of California

Collector Incident Angle Modifier (IAM)

The incident angle modifier (IAM) was not measured for this specific configuration. Since IAM is almost completely dependent on the geometric shape of the reflector and the placement of the tubes, it is reasonable to use the measured IAM from the U-Tube with Reflectech Reflectors in East-West collector to describe this collector.

2.18.10. Test Results of “U-Tube with Reflectech Reflectors in North-South orientation”

Collector description

Table 45. Description of North-South U-Tube with Reflectech Collector

Orientation	North-South
Concentration C_x	1.15
Effective Collector Area A_A	2.076 m ²
Tube Type	U-Tube
Number of Tubes	6
Reflector	Reflectech (95%)

Source: The Regents of University of California

Collector optical efficiency

The optical efficiency of the North-South U-Tube with Reflectech collector was measured on 10/23/08 with an average inlet temperature of 30°C and an average ambient temperature of 21°C.

The optical efficiency based on an effective irradiance ($G = G_{DNI} + G_{diffuse}/C_x$) was found to be 71.3%. The optical efficiency based on direct normal irradiance ($G = G_{DNI}$) was found to be 88.5%.

Collector thermal efficiency

The efficiency of the XCPC was measured from 10/23/08 – 3/19/09 using “Method 1” and “Method 2” at the following collector inlet temperatures: 80°C, 100°C, 120°C, 140°C, 160°C, 180°C, and 200°C; and at the following flow rates: 80 g/s, 100 g/s, 120 g/s, 140 g/s, and 160 g/s. All efficiencies reported are based on “Method 2.”

The performance characteristics are tabulated in Table 8 and the collector efficiencies are depicted in Figure 14 through Figure 17. Figure 15 and Figure 17 are derived from Figure 14 and Figure 16 respectively by assuming an ambient temperature of 25°C and an effective insolation of 1,000 W/m² that is captured by the XCPC. Figures 14 and 15 display the efficiencies based on the effective irradiance G_E while Figures 16 and 17 display the efficiencies based on the direct normal irradiance (DNI) G_{DNI} .

Table 46. Performance Characteristics of North-South U-Tube with Reflectech Collector

	$G=G_E$	$G=G_{DNI}$
Optical Efficiency	71.3%	88.5%
Efficiency at 100 °C	61.9%	71.7%
Efficiency at 200 °C	35.8%	43.3%
Loss coefficient (1)	0.664 W/m ² -K	1.975 W/m ² -K
Loss coefficient (2)	0.00780 W/m ² -K ²	0.00348 W/m ² -K ²
Overall heat loss coefficient	2.068 W/m ² -K	2.602 W/m ² -K

Source: The Regents of University of California

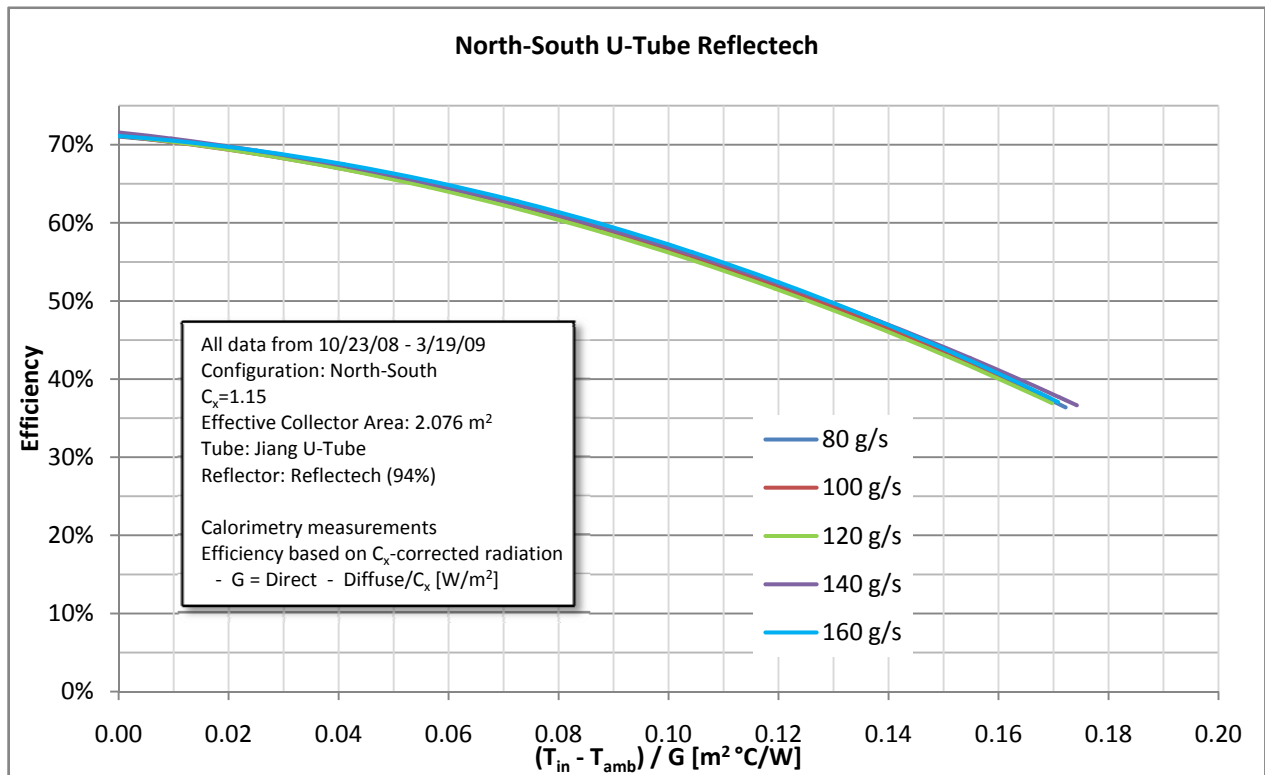


Figure 167. North-South U-Tube with Reflectech Effective Reduced Efficiency Curve

Source: The Regents of University of California

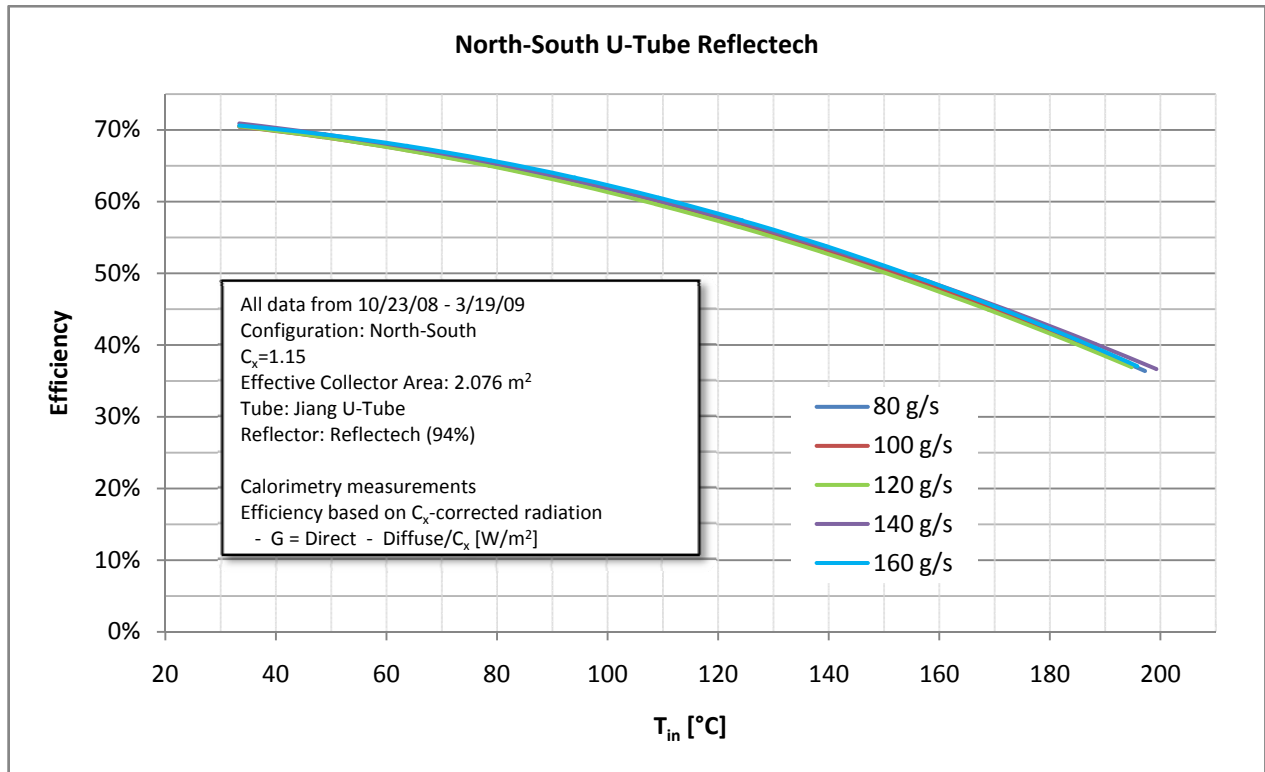


Figure 168 North-South U-Tube with Reflectech Effective Standardized Efficiency Curve

Source: The Regents of University of California

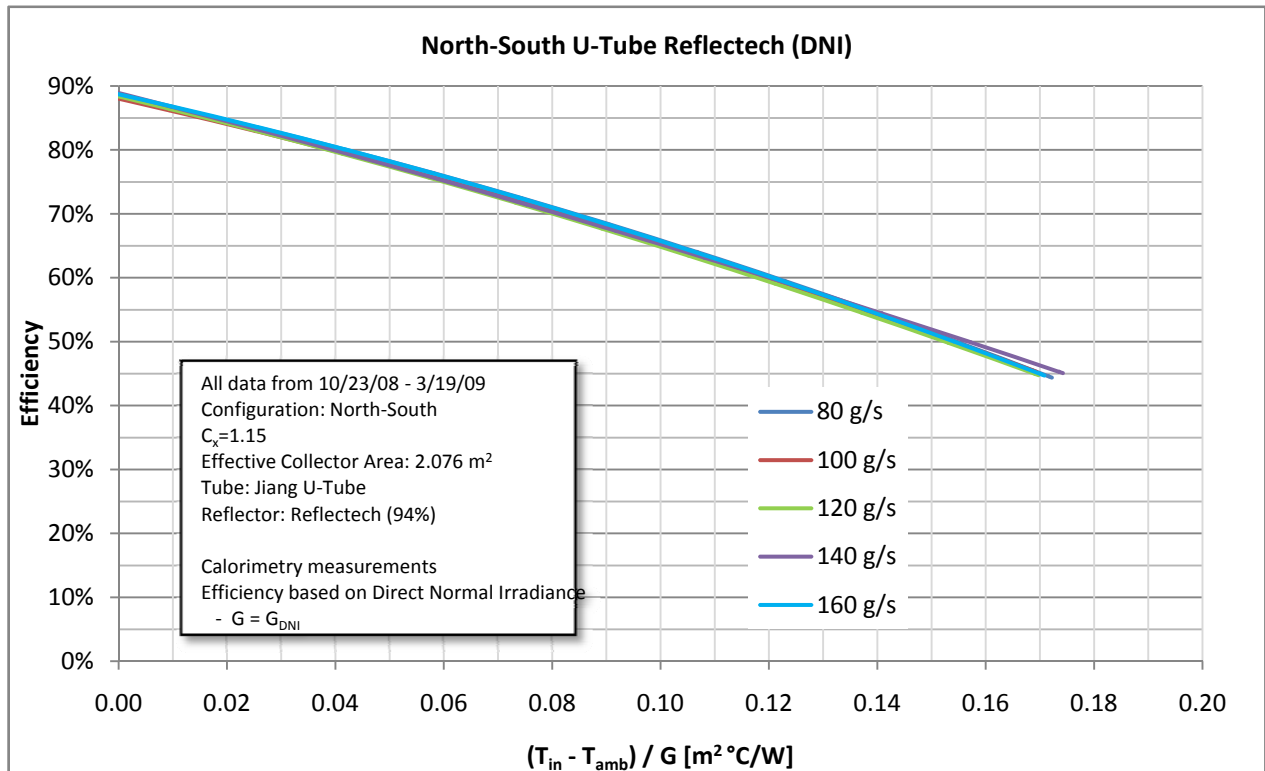


Figure 169. North-South U-Tube with Reflectech Direct Reduced Efficiency Curve

Source: The Regents of University of California

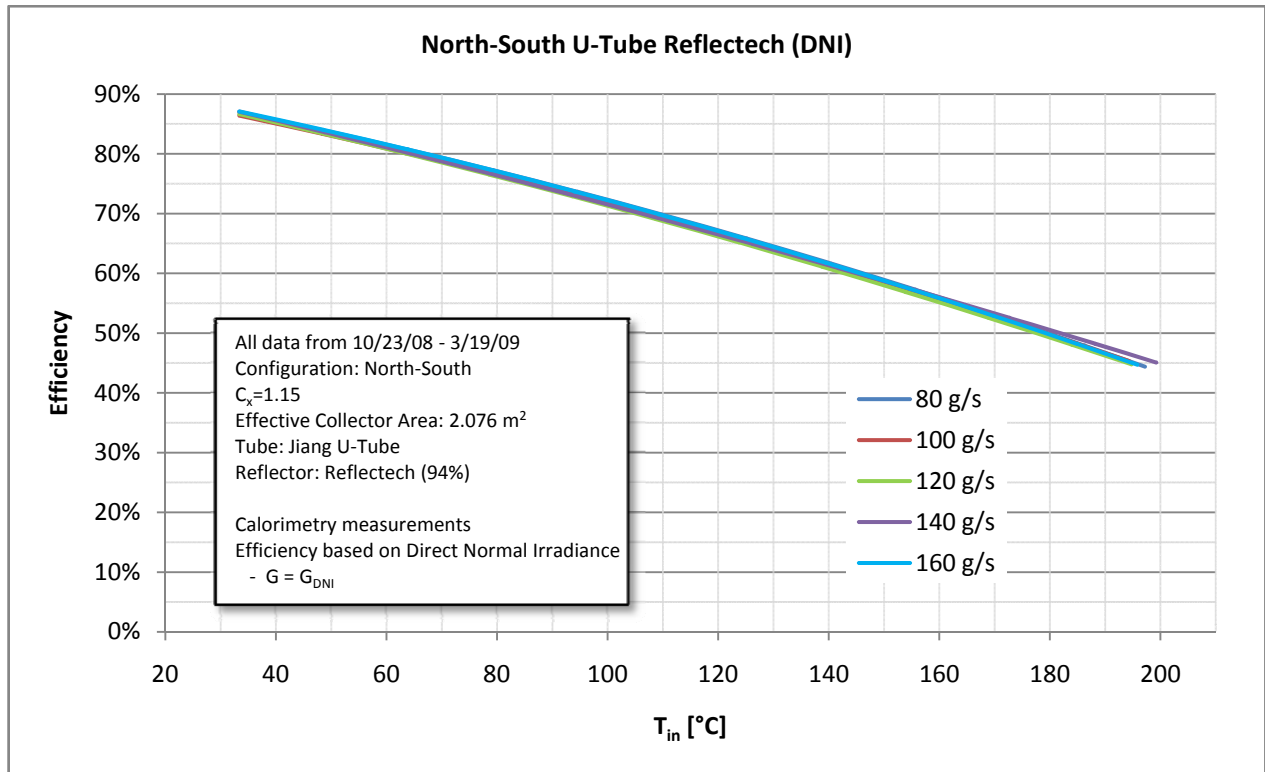


Figure 170. North-South U-Tube with Reflectech Direct Standardized Efficiency Curve

Source: The Regents of University of California

Stagnation Test

A u-tube filled with oil was mounted in an individual collector on a separate tracker to test for stagnation. Temperatures were measured on the tube’s glass , on the outside of the pipe-to-manifold connection , and roughly two feet into the oil-filled inlet pipe . Ambient temperature, PSP, NIP, wind speed and direction measurements were also taken. The test conditions are described in Table 47.

Table 47. Stagnation test conditions for North-South U-Tube with Reflectech

Average	25°C
Average	823 W/m ²
Average	1030 W/m ²
Average %Diffuse	20%
Average wind speed	3.5 Mph

Source: The Regents of University of California

The maximum temperature measured inside the tube was 289°C. The inside temperature reached 283°C 60 minutes after the tube was exposed to sunlight. No apparent damage to the tube was reported after the test was completed.

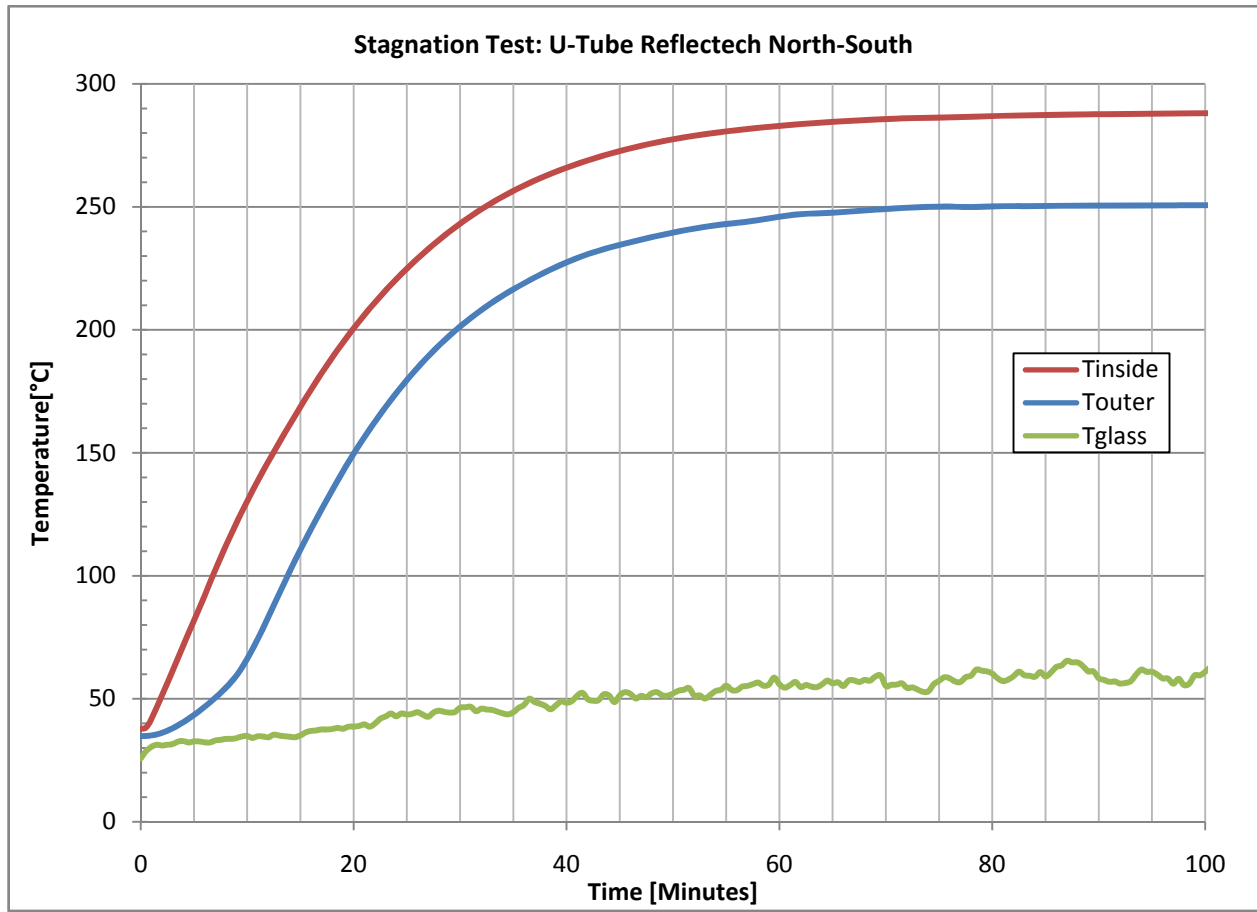


Figure 171. North-South U-Tube with Reflectech stagnation test results

Source: The Regents of University of California

Collector Incident Angle Modifier (IAM)

The incident angle modifier (IAM) was not measured for this specific configuration. Since IAM is almost completely dependent on the geometric shape of the reflector and the placement of the tubes, it is reasonable to use the measured IAM from the Counterflow-Tube with Alanod Reflectors in North-South orientation collector to describe this collector.

2.18.11. Test Results of “U-Tube with Reflectech Reflectors in East-West orientation”

Collector description

Table 48. Description of East-West U-Tube with Reflectech Collector

Orientation	East-West
Concentration C_x	1.15
Effective Collector Area A_A	3.24 m ²
Tube Type	U-Tube
Number of Tubes	6
Reflector	Reflectech (95%)

Source: The Regents of University of California

Collector optical efficiency

The optical efficiency of the East-West U-Tube with Alanod collector was assumed to be the value taken from a linear extrapolation.

The optical efficiency based on an effective irradiance ($G = G_{DNI} + G_{diffuse}/C_x$) was assumed to be 64.4%. The optical efficiency based on direct normal irradiance ($G = G_{DNI}$) was assumed to be 69.7%.

Collector thermal efficiency

The efficiency of the XCPC was measured from 7/1 – 9/16/08 using “Method 1” and “Method 2” at the following collector inlet temperatures: 80°C, 100°C, 120°C, 140°C, 160°C, 180°C, and 200°C; and at the following flow rates: 80 g/s, 100 g/s, 120 g/s, 140 g/s, and 160 g/s. All efficiencies reported are based on “Method 2.”

The performance characteristics are tabulated in Table 11 and the collector efficiencies are depicted in Figure 19 through Figure 22. Figure 20 and Figure 22 are derived from Figure 19 and Figure 21 respectively by assuming an ambient temperature of 25°C and an effective insolation of 1,000 W/m² that is captured by the XCPC. Figures 19 and 20 display the efficiencies based on the effective irradiance G_E while Figures 21 and 22 display the efficiencies based on the direct normal irradiance (DNI) G_{DNI} .

Table 49. Performance Characteristics of East-West U-Tube with Reflectech Collector

	G=G_E	G=G_{DNI}
Optical Efficiency η_o	64.4%	69.7%
Efficiency at 100 °C	58.1%	62.6%
Efficiency at 200 °C	41.7%	46.0%
Loss coefficient (1) a_1	0.488 W/m ² -K	0.633 W/m ² -K
Loss coefficient (2) a_2	0.00463 W/m ² -K ²	0.00411 W/m ² -K ²
Overall heat loss coefficient U	1.321 W/m ² -K	1.373 W/m ² -K

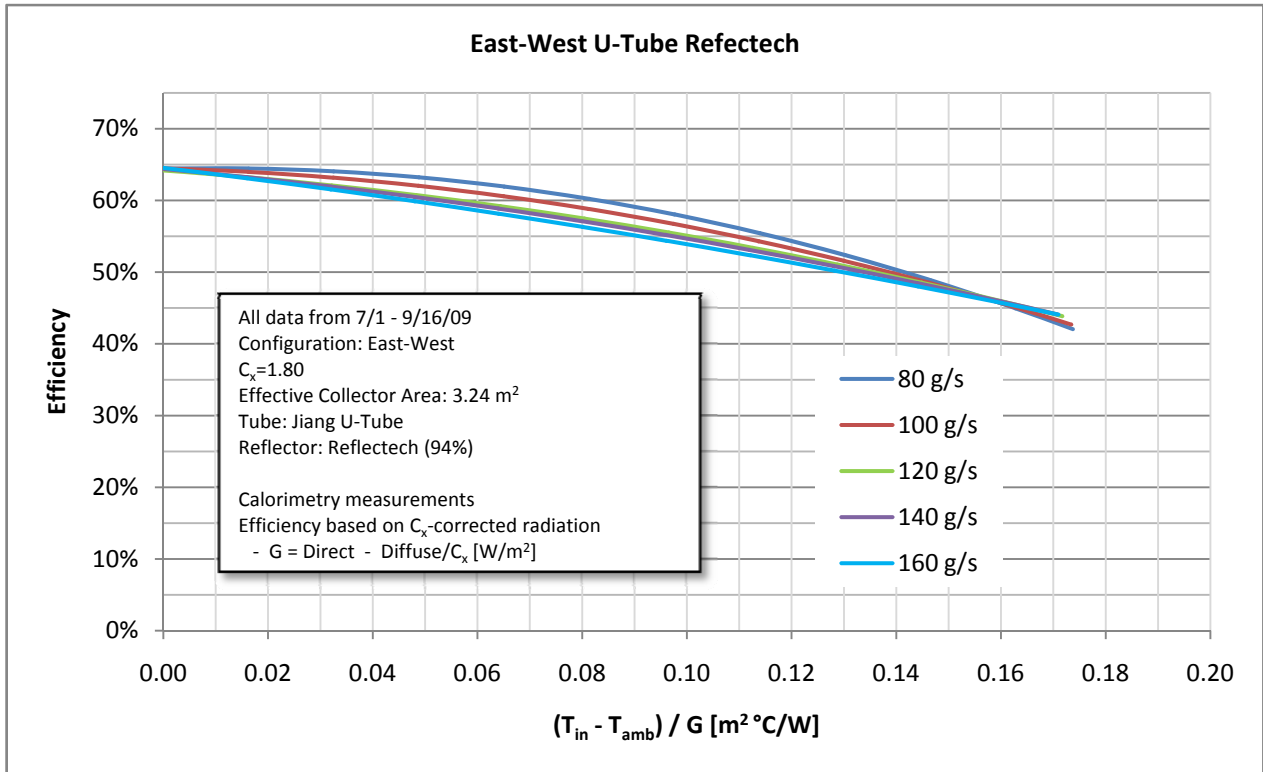


Figure 172. East-West U-Tube with Reflectech Effective Reduced Efficiency Curve

Source: The Regents of University of California

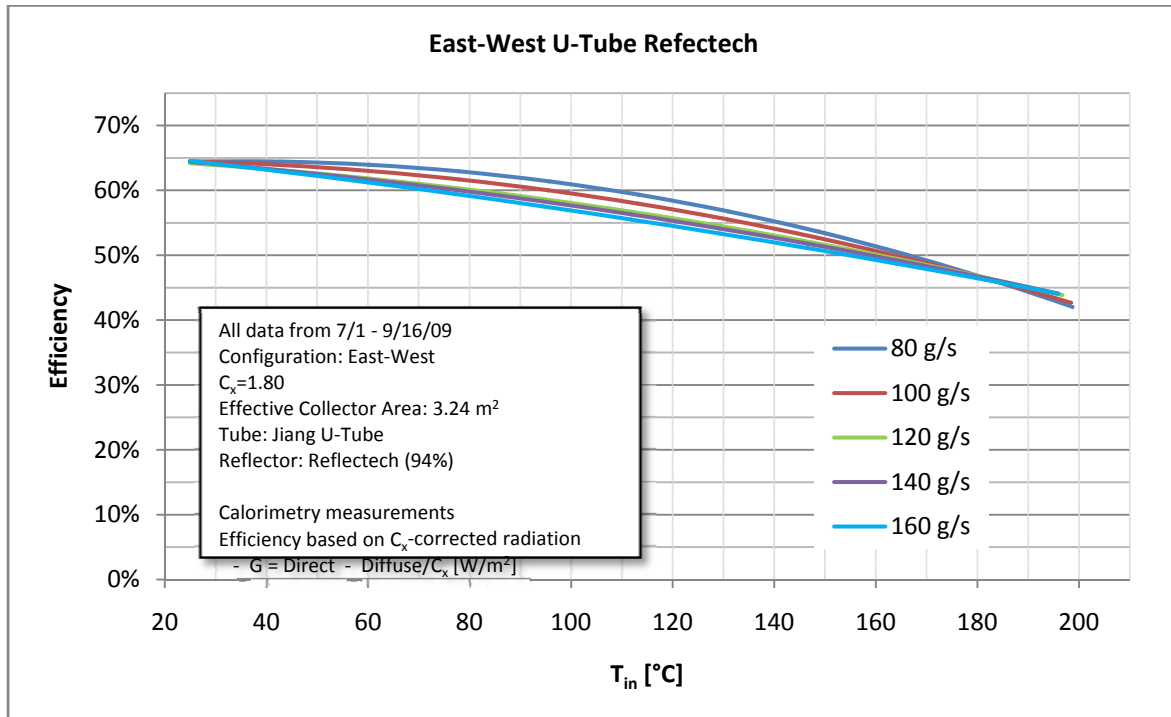


Figure 173 East-West U-Tube with Reflectech Effective Standardized Efficiency Curve

Source: The Regents of University of California

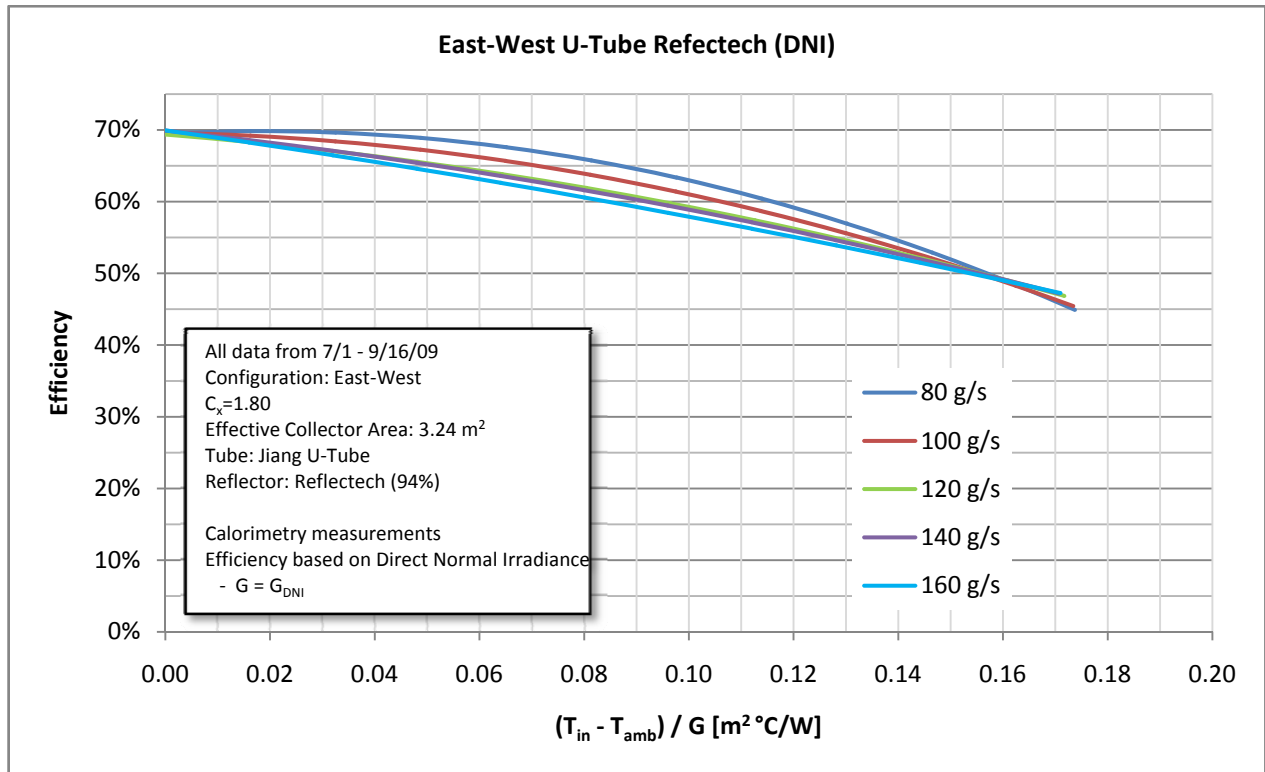


Figure 175. East-West U-Tube with Reflectech Direct Reduced Efficiency Curve
 Source: The Regents of University of California

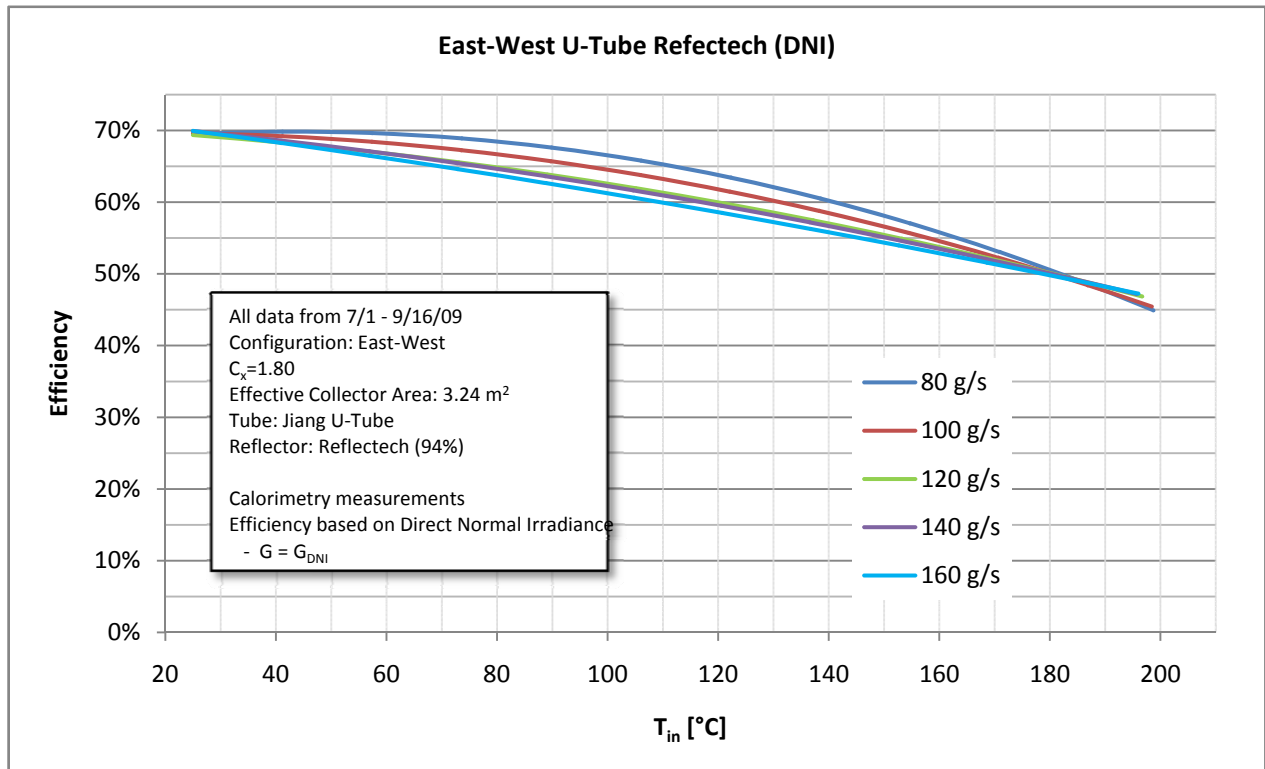


Figure 175 East-West U-Tube with Reflectech Direct Standardized Efficiency Curve
 Source: The Regents of University of California

Collector Incident Angle Modifier (IAM)

The IAM was measured at an inlet temperature of 120 °C. In this measurement the instantaneous efficiency was based on the direct normal insolation only that was measured with a Normal Incidence Pyrheliometer on a separate tracker. Figure 23 shows the relative drop in efficiency during the test as the sun angle varies between 0° and 45° relative to normal incidence. At roughly 32.5°, the collector performs at 90% of the nominal efficiency.

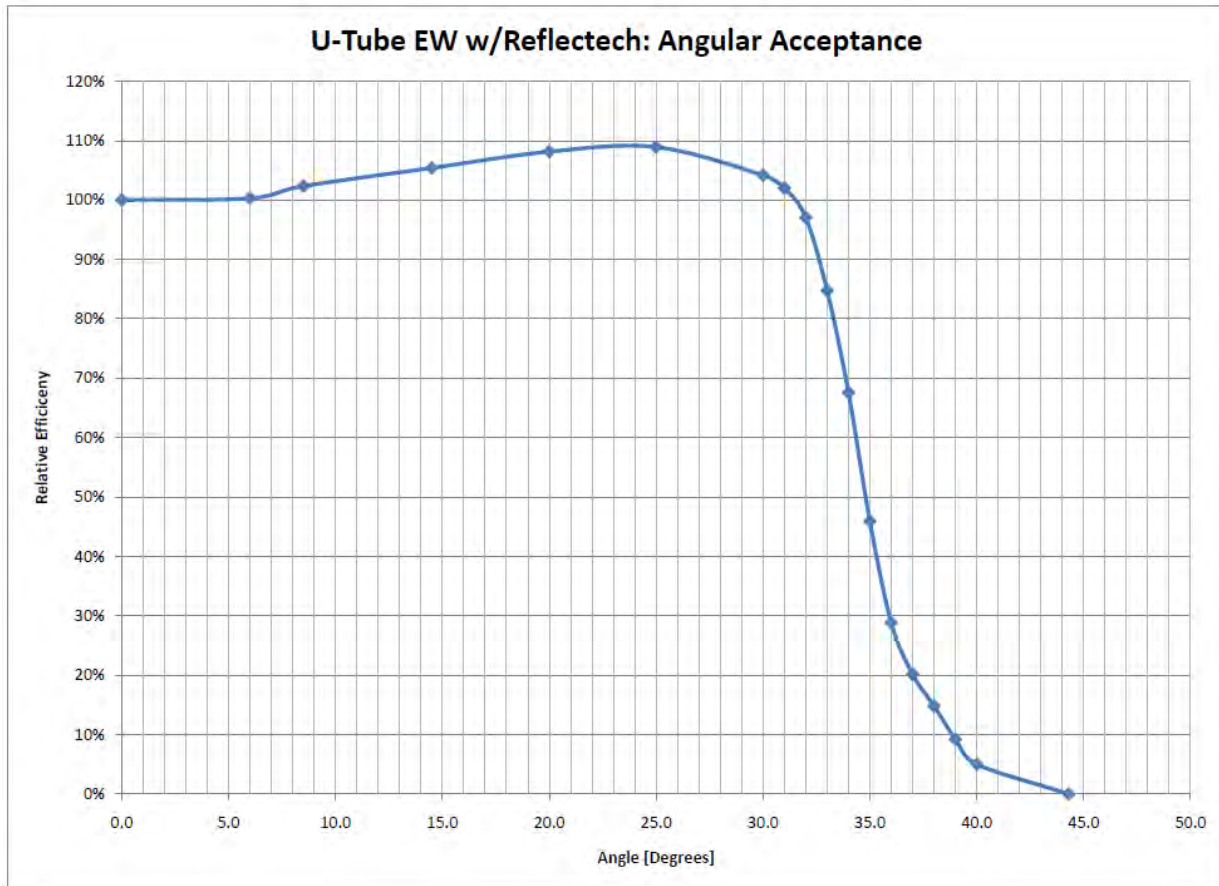


Figure 176. East-West U-Tube with Reflectech: IAM Chart

Source: The Regents of University of California

2.18.12. Summary of Results

Tables 50 and 51 are a summary of the efficiencies of all of the collectors tested based on the effective irradiance and DNI respectively.

Table 50. Performance Summary of All Collectors Based on Effective Irradiation

	NS AL CF	EW AL CF	NS AL UT	EW AL UT	EW AL XT	NS RT UT	EW RT UT
η_o	69.5%	64.62%	69.1%	66.4%	68.6%	71.3%	64.4%
$\eta(100^\circ\text{C})$	57.2%	54.61%	58.5%	58.3%	59.9%	61.9%	58.1%
$\eta(200^\circ\text{C})$	36.3%	40.29%	36.4%	43.2%	39.9%	35.8%	41.7%
a_1	1.445	1.293	1.080	0.908	0.799	0.664	0.488
a_2	0.00258	0.00070	0.00351	0.00239	0.00481	0.00780	0.00463
U	1.910	1.393	1.891	1.339	1.664	2.068	1.321

Source: The Regents of University of California

Table 51. Performance Summary of All Collectors Based on Direct Normal Irradiation

	NS AL CF	EW AL CF	NS AL UT	EW AL UT	EW AL XT	NS RT UT	EW RT UT
η_o	87.7%	69.33%	79.3%	71.5%	75.0%	88.5%	69.7%
$\eta(100^\circ\text{C})$	72.2%	59.85%	69.3%	63.1%	65.9%	71.7%	62.6%
$\eta(200^\circ\text{C})$	45.2%	44.33%	36.4%	45.2%	43.4%	43.3%	46.0%
a_1	1.793	1.139	0.595	0.822	0.756	1.975	0.633
a_2	0.00363	0.00207	0.00993	0.00387	0.00601	0.00348	0.00411
U	2.447	1.436	2.382	1.519	1.838	2.602	1.373
%Diffus e	23%	15%	15%	11%	15%	17%	11%

Source: The Regents of University of California

2.18.13. Discussion

Improvements to North-South Collector (U-Tube and Reflectech)

Figures 24 and 25 compare the improved North-South collectors with the original design, North-South Counterflow with Alanod collector. The charts assume that the ambient temperature is 25°C and the effective irradiance is 1000 W/m². The efficiencies shown in Figure 24 and Figure 25 are based on effective irradiance and DNI respectively.

The U-tube with Alanod version was designed to improve the performance of the collector by reducing the thermal resistance inside of the tube. In Figure 24 and Table 12, one can see that by simply replacing the counterflow tube with a U-tube virtually had no effect. This is likely due to the fact that the counterflow tube version performed very well and therefore the thermal resistance in the counterflow tube was reasonable.

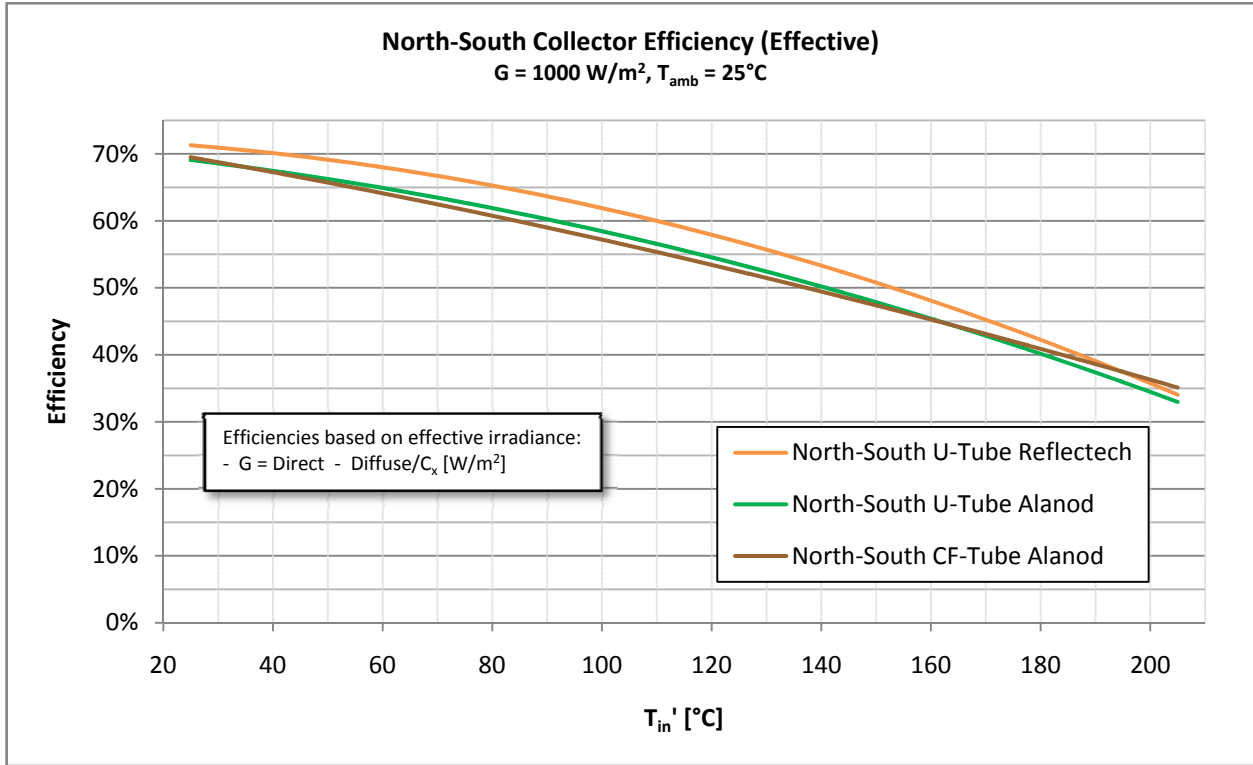


Figure 177. North-South Collector Efficiency (Effective)

Source: The Regents of University of California

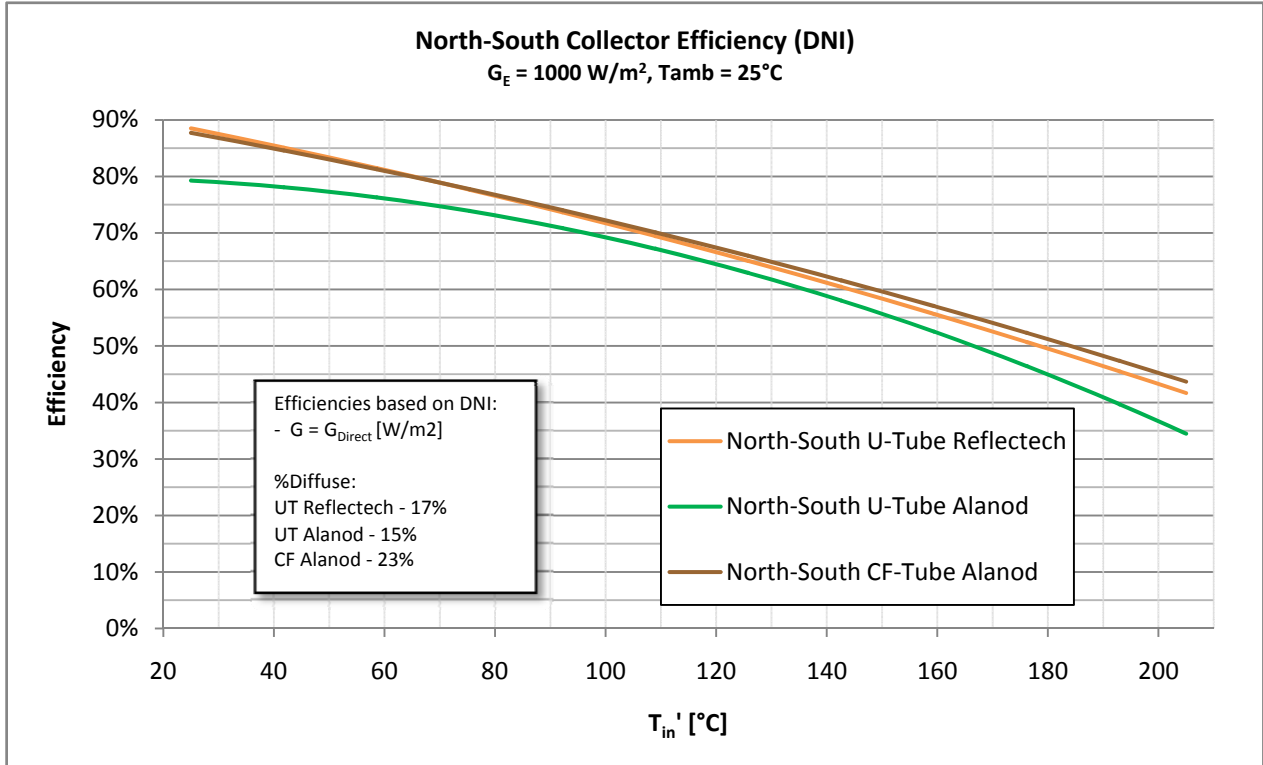


Figure 178. North-South Collector Efficiency (DNI)

Source: The Regents of University of California

The Reflectech design was intended to improve the optical efficiency of the collector. The measured optical efficiency gain from applying Reflectech was roughly 2.5% as opposed to the expected 4%. One possible reason for the optical efficiency gain not being as expected is that the Reflectech film was difficult to apply to the Alanod reflectors and this resulted in bubbles under the film and scratches on the surface of the film.

The overall performance of the Reflectech version, as seen in Figure 24, was better than the Alanod versions for most temperatures. At temperatures higher than 180°C, the efficiency of the Reflectech version appears to converge with the Alanod version. This poor performance at higher temperatures is likely due to the differences in the ambient temperatures that the collectors were tested. The U-Tube Reflectech version was tested with an average ambient temperature of 2°C and 9°C below the U-Tube Alanod version tests during optical efficiency and 200°C measurements respectively.

In Figure 25 and Table 13 the performance values are reported based on DNI. As one could see, this chart is very different from Figure 24. The main reason for the difference is that the amount of diffuse radiation measured during the tests ranged from 15% to 23%.

Improvements to East-West Collector (X-Tube, U-Tube, and Reflectech)

The proposed improvements to the East-West Counterflow with Alanod were to change to the U-Tube and the X-Tube (extruded tube) and to add Reflectech film to the reflectors. Figures 26 and 27 compare these improved designs to the original counterflow with Alanod design. The charts assume that the ambient temperature is 25°C and the effective irradiance is 1000 W/m². The efficiencies shown in Figure 26 and Figure 27 are based on effective irradiance and DNI respectively.

As seen in Figure 26 and 27, the use of the X-tube over the counterflow tube appears to have improved the performance at lower temperatures while having little effect at higher temperatures. The ambient temperature and the percent of the irradiance being diffuse during the tests for the East-West Counterflow and the X-Tube were not much different. These small differences are unlikely to have contributed to any error in comparing these two collectors.

The assumed optical efficiency of the X-Tube collector looks higher than one would expect by about two percentage points. This error is likely due to the nature of using a linear extrapolation to estimate the optical efficiency.

Employing the U-tube in place of the counterflow tube in the Alanod collector seems to have also improved the efficiency. The increase in the efficiency seems to be consistent through all temperatures tested. At lower temperatures, the U-tube with Alanod collector does not appear to perform as well as the X-tube collector and this may be due to the additional diffuse radiation during the X-tube testing.

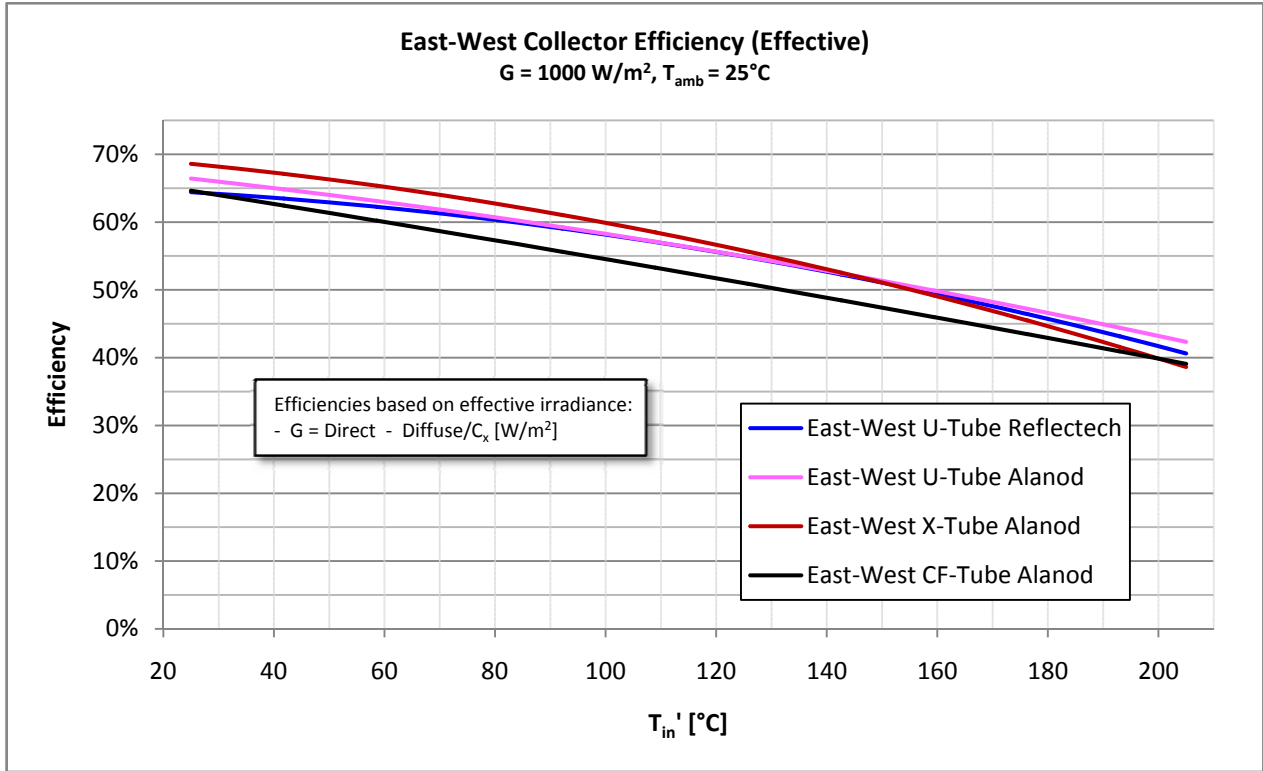


Figure 179. East-West Collector Efficiency (Effective)

Source: The Regents of University of California

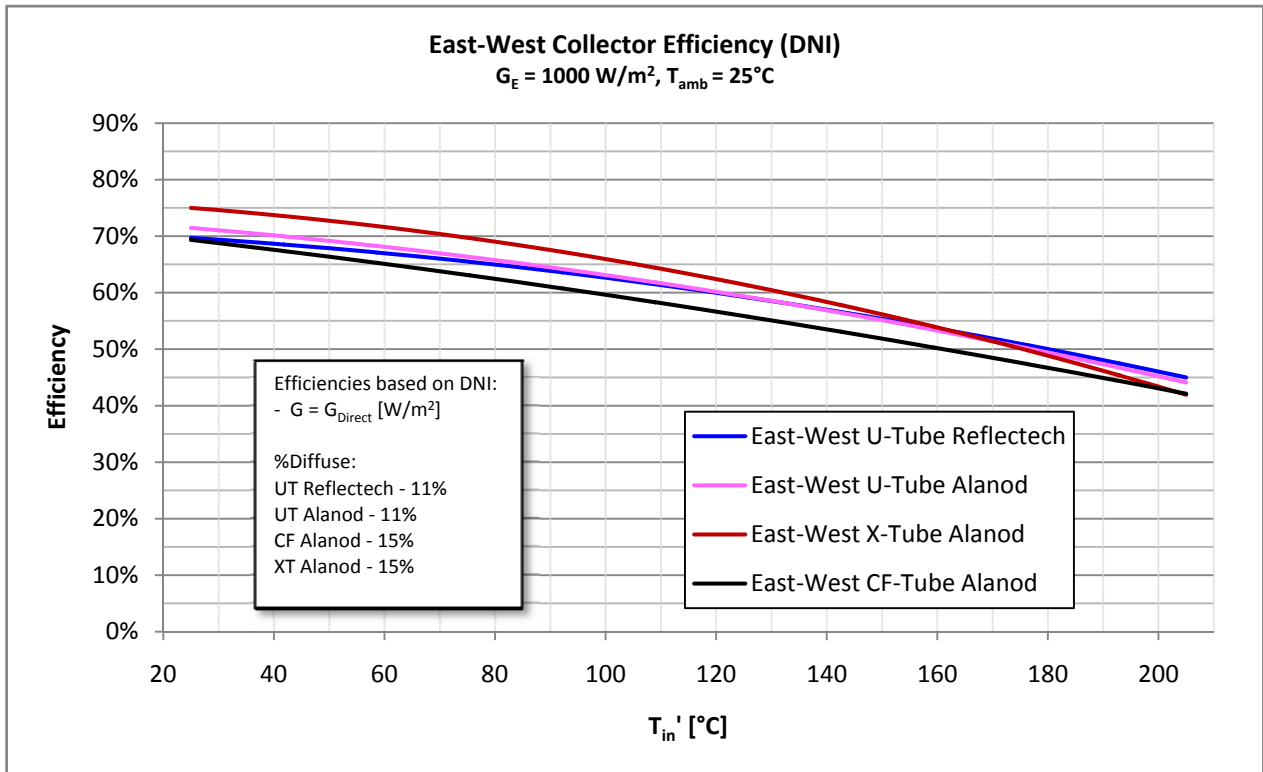


Figure 180. East-West Collector Efficiency (DNI)

Source: The Regents of University of California

Applying Reflectech film over the Alanod reflectors was expected to improve the optical efficiency of the collector in addition to adding to the efficiencies at all temperatures. This anticipated increase in efficiency cannot be seen in the data at any temperature. The most likely reason for this lack of improvement is that applying the Reflectech film was difficult and resulted in bubbles and blemishes. Both the North-South and the East-West versions with Reflectech had many imperfections yet only the North-South version seems to have improved the performance as can be seen in Figures 28 and 29. The fact that the East-West collector has a higher concentration and a lower acceptance angle makes it more sensitive to imperfections in the optics in the system than the North-South version.

When comparing the charts in Figures 26 and 27, there seems to be little difference in the shape of the curves. In addition, the efficiencies based on the direct irradiance only show about five percentage points higher than the efficiencies based on the effective irradiance. This implies that the East-West collector is only able to collect about half of the diffuse irradiance as expected with a concentration of 1.8.

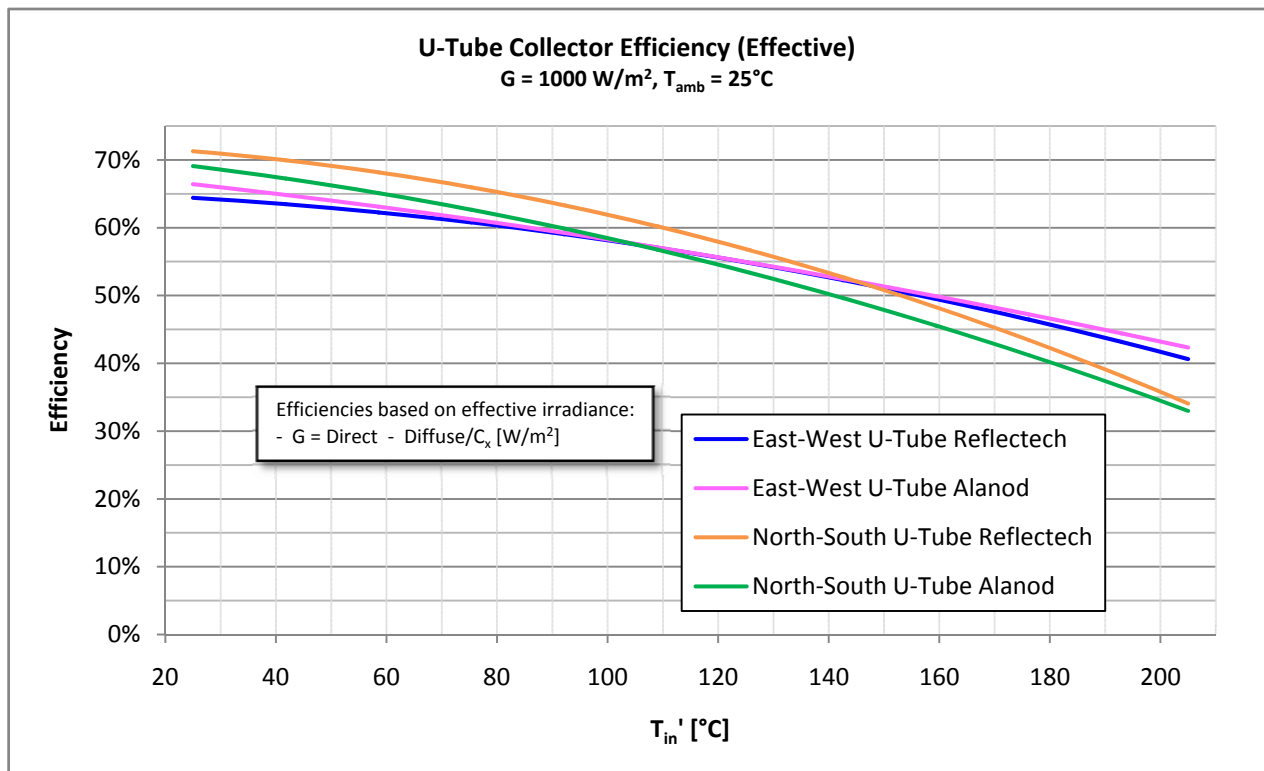


Figure 181 U-Tube Collector Efficiency (Effective)

Source: The Regents of University of California

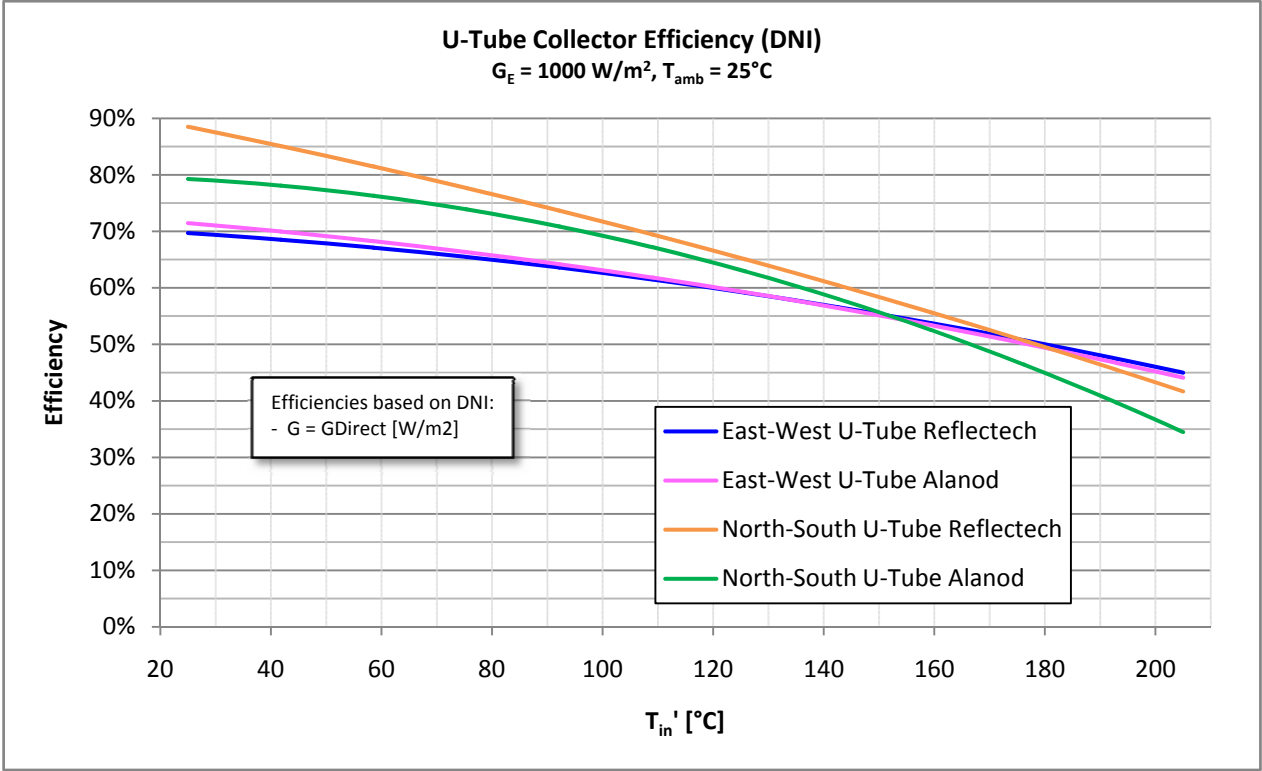


Figure 182. East-West Collector Efficiency (DNI)

Source: The Regents of University of California

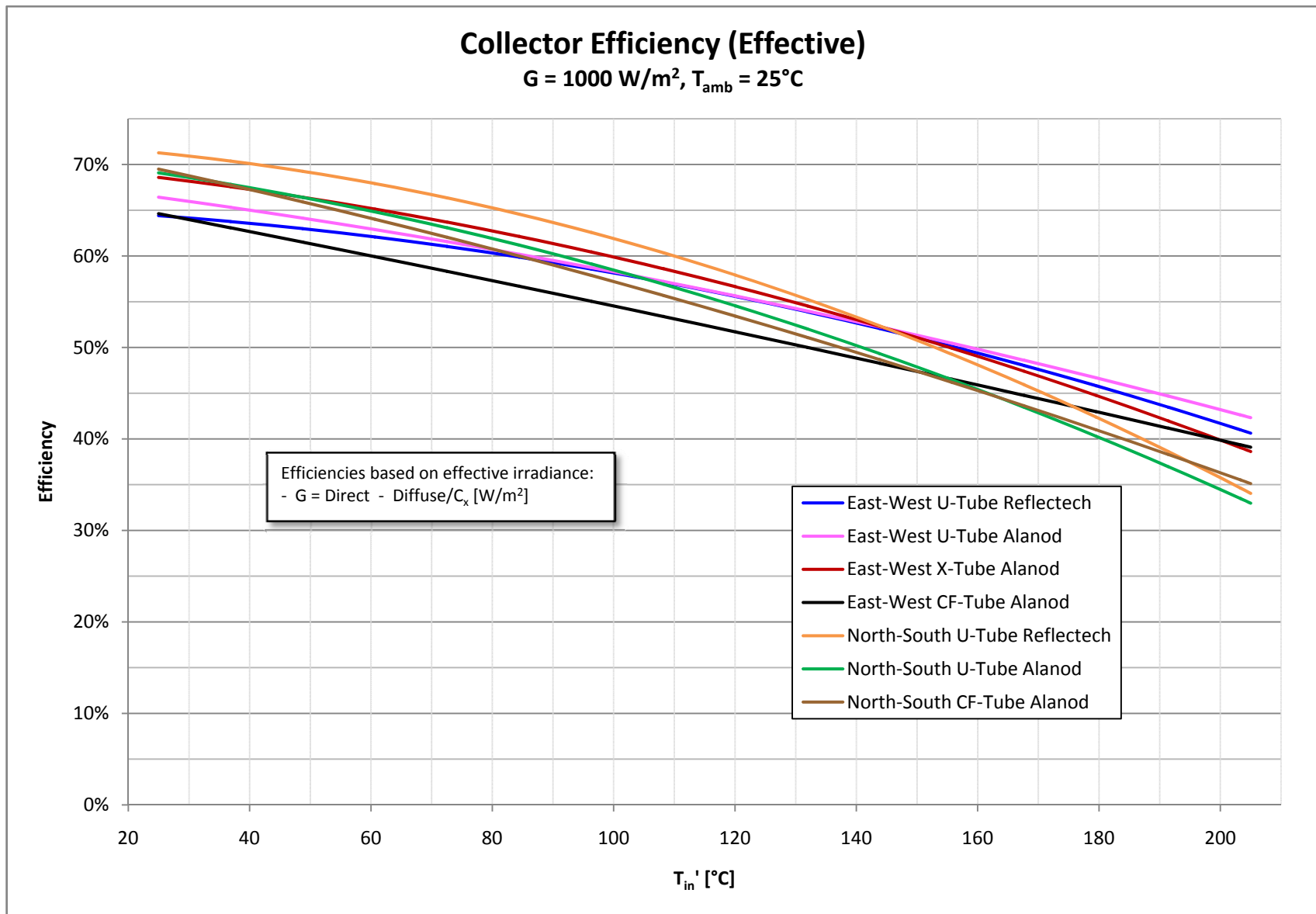


Figure 183 Collector Efficiency (Effective)

Source: The Regents of University of California

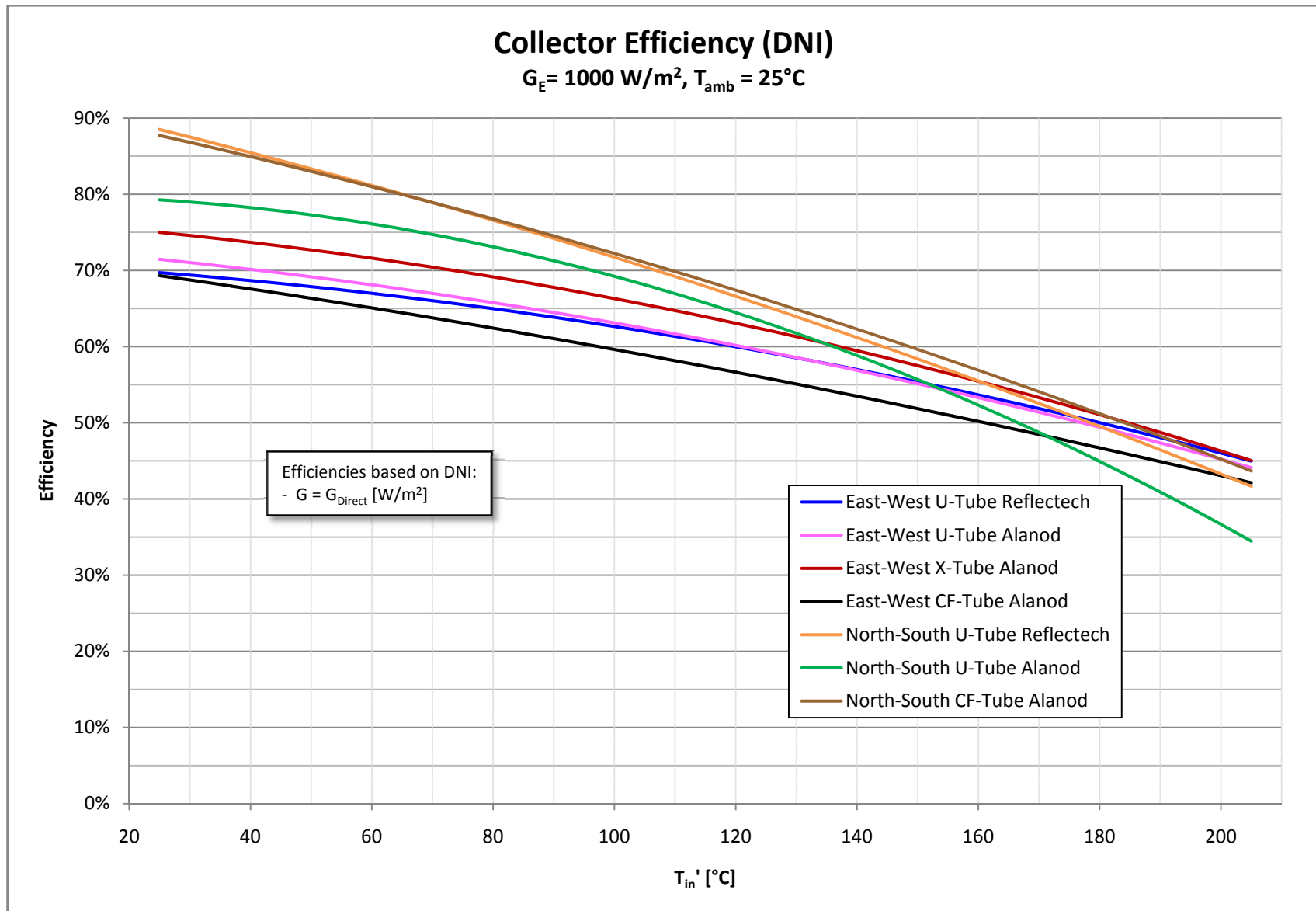


Figure 184. Collector Efficiency (DNI)

Source: The Regents of University of California

Possible errors

Errors in the data may come from any of the following: instrumental errors, measurement errors, assumed values, tolerance errors, environmental effects, ground reflection, and errors in theory.

Although calibrated, instruments such as pyranometers, pyrhemometers, thermocouples and other temperature sensors, the flowmeter, and data acquisition systems may have non-trivial errors associated with them. While steps were taken to minimize these sources of error, it is impossible to avoid them completely. Errors in any of these instruments would affect the efficiency measurements and/or the temperature scale.

The effective area of the collector is a possible source of error due to it being measured manually but this error should be less than a fraction of a percent. Any error in the area of the collector would directly affect the calculated efficiency values.

The heat capacity of the oil seems to change over time. Since both of the counterflow and the North-South U-Tube with Alanod collectors' test did not use a calorimeter, the assumed values have an unknown error. An outside source, Rose Consulting, measured the heat capacity of the oil in November 2007 and in September 2009. The measurements in 2007 found the heat capacity of the oil to be less than the table values provided by the oil's manufacturer while the measurements in 2009 found that the heat capacity was higher than the table values. The September 2009 measurements from Rose Consulting agree well with the heat capacity measured during the East-West U-Tube with Alanod tests.

The shape of the reflector and the position of the holes in the frame are subject to tolerance errors that would affect the optical efficiency and the acceptance angle. In addition, the surface quality of the reflector surface will affect the results.

Soiling of the reflectors and the glass tubes can have a negative effect on the optical efficiency. Ground reflection is inevitable when testing solar thermal collectors outdoors. The amount of ground reflection available to the collector depends on the optics and orientation of the collector, the time of day and the position of the tracker. While the pyranometer mounted on the tracker should be able to detect all or most of the ground reflection, the angle of incidence may be too severe to be accepted by the collector. Collectors with lower concentrations and collectors oriented in a vertical position like the North-South collectors will be able to accept more of this reflected radiation. The ground reflection will be treated as diffuse light. Ground reflection can cause variation in data and cause East-West collectors to have an apparent lower than expected performance.

Much of the data presented in this report uses an effective irradiance to represent the amount of available power to the collector. The effective irradiance adjustment attempts to take into account that a concentrating optical system cannot accept all of the diffuse and is therefore not considered in the efficiency. Using this method will favor collectors with larger concentration ratios.

Other data is presented in this report uses the direct normal irradiance (DNI) to represent the incoming radiation. This method completely ignores diffuse radiation which favors collectors with low concentrations. Using this method with data having a large percent of the irradiance as diffuse can create apparently high efficiencies.

Since the testing was done outdoors, it is virtually impossible to test with a constant or consistent ambient temperature. The charts and the data presented in this report attempt to minimize the effect of the differences in the ambient temperature by presenting data with the reduced temperature. Unfortunately, these evacuated tube collectors primarily lose heat through radiation which is non-linear. In addition, the emissivity of the absorber is a function of the absorber temperature only and not of the ambient temperature. This creates a less than perfect correction for the ambient temperature which is most apparent when a collector was tested during very different outdoor temperatures or when comparing two different collectors that were tested in different seasons.

Introduction

The history of this public-private partnership with the XCPC solar thermal project may be instructive to The California Energy Commission as an example how such private-public partnerships become success stories. When Gary Conley was approached by UC Merced to partner and provide the dominant match, he agreed for H₂Go, Inc., his IP development and holding company which spawned SolFocus, the CPV company. However, the SolFocus A-series had just closed and as he was the co-founder and CEO, the board asked the thermal grant work be done within SolFocus. Some years later, when the SolFocus "XCPC Concept Loop" had been proved successful, thermal work at SolFocus was acquired back by H₂Go to be spun out into B2U Solar, specifically to commercialize the technology. B2U is in the late stages in closing an A-series round of financing.

SolFocus participated in the UC Merced solar thermal project at a rather significant level of cost share because of the promise of cost-effective heat generation by solar energy. The novel non-imaging optics technology developed at UC Merced was already well-known to us from a previous small-grants Energy Commission project in concentrating photovoltaic. With non-imaging concentration, fixed solar collectors are capable of generating high temperature in the 200 degree Centigrade range. Moreover, because of the wide angular acceptance (the non-imaging collectors "see" most of the sky) even diffuse solar radiation is utilized, in contrast to tracking concentrators that "see" only direct insolation. This is particularly important for areas of the world with high diffuse radiation. More importantly, it provides a distinct advantage over solar trough and other concentrator solar thermal designs which turn on or off with each passing cloud, making key applications such as double-effect chillers difficult if not impossible. The majority of industrial and commercial thermal needs are within the temperature realm provided by this design.

As the project developed and we started to see positive results from prototype testing at UC Merced, the company made a significant financial commitment to take the next step and build a

“concept loop” of approximately 20 KW Thermal solar energy collectors which would be on the path toward eventual commercialization.

Following successful operation of the concept loop at the NASA AMES laboratory in Mountain View California, H₂Go decided to take the next critical step on the path to commercialization. A company devoted totally to solar thermal systems and applications, B2U Solar, is being spun out as an independent entity. The solar collector was redesigned with new manufacturing techniques, benefiting from the concept loop experience. In the process, a thorough cost study was performed to indentify the economics of our solar thermal technology as an alternative to natural gas fuel. The company has already delivered product to its first customer, the Gas Technology Institute in Chicago (GTI). GTI will integrate the B2U Solar system to drive the de-aeration stage of a large industrial boiler in order to demonstrate to the utilities and large corporate customers the viability of the technology.

Industrial engineering and pilot production is performed in San Jose and advanced industrial design will be contracted to a major design-to-manufacturing firm once funding is completed. Initial series manufacturing is starting in China as our tube manufacturer and early volume customers are also in China. A unique environment exists in China in as they have moved from steam, as used in the US, to oil as the process heat transfer medium, for a number of factors including much higher efficiency and the elimination of high pressure found with steam. Further, the Chinese government is driving renewables through curtailment. That is, a factory owner is capped on the amount of fuel he receives, or the amount of coal he can burn. If he wishes to increase production, an alternative form of fuel must be found. As such, a large appetite for renewable sources has developed. While initial production ramp and installations are made in China, H₂Go will install a large variety of demonstrations projections throughout the United States and particularly, in California. These will be conducted in concert with GTI and several major industrial partners, from HVAC to boiler industries. As market development is matured in the US, production sites will be established throughout the country based upon a range of selection criteria.

Finally, an advanced version of the collector was designed and built to be even more efficient and cost effective. We are well on the way to a successful solar thermal business.

All these steps are documented in the material to follow. This is with images of actual hardware, real-life data and economic spread sheets.

We believe these developments extend well-beyond the typical R&D project that is partially funded by state or federal agencies with industry participation. It represents in our view, the emergence of a new, disruptive technology in solar thermal utilization.

THE CONCEPT LOOP

In 2008, UC Merced and SolFocus requested from The Commission that Tasks 21-29 be directed toward commercialization efforts with SolFocus as the lead. This was formally approved. SolFocus hired a project manager, Mary Jane Hale with extensive solar experience and a distinguished record at NREL in managing solar thermal programs.

SolFocus designed and build a concept thermal loop consisting of 10 North-South CPC's modeled after the prototypes at UC Merced, but with a view toward eventual manufacturing and production. The prototype for this concept loop was built at the SolFocus Mt. View, CA facility. Note this was done entirely with SolFocus funds at significant expense. It represents an outstanding commitment of the company which goes well above and beyond typical industry participation in a research project, and is testimony to how seriously the company perceives the promise of high temperature, non-tracking solar thermal technology. We had the benefit of the UC Merced test loop experience and the UC Merced prototypes which had been fabricated in a furniture factory in Merced.

The frame is aluminum and the reflecting material is Alanod, which is a protected silver on aluminum substrate with good solar reflecting properties. Eventually, we expect the Alanod sheet to provide structural stability without need for extensive framing and support. A cost reduction effort using a proprietary reflective structure on different substrates is already underway at H₂Go, Inc.

The evacuated tube receivers were extruded aluminum with selective coating. The heat transfer characteristics were considered sufficient for the low-concentration North-South design.

- North-South: Concentration Factor = 1.15, acceptance angle ~ +/- 60 deg
An image of the first prototype is shown on the following page.

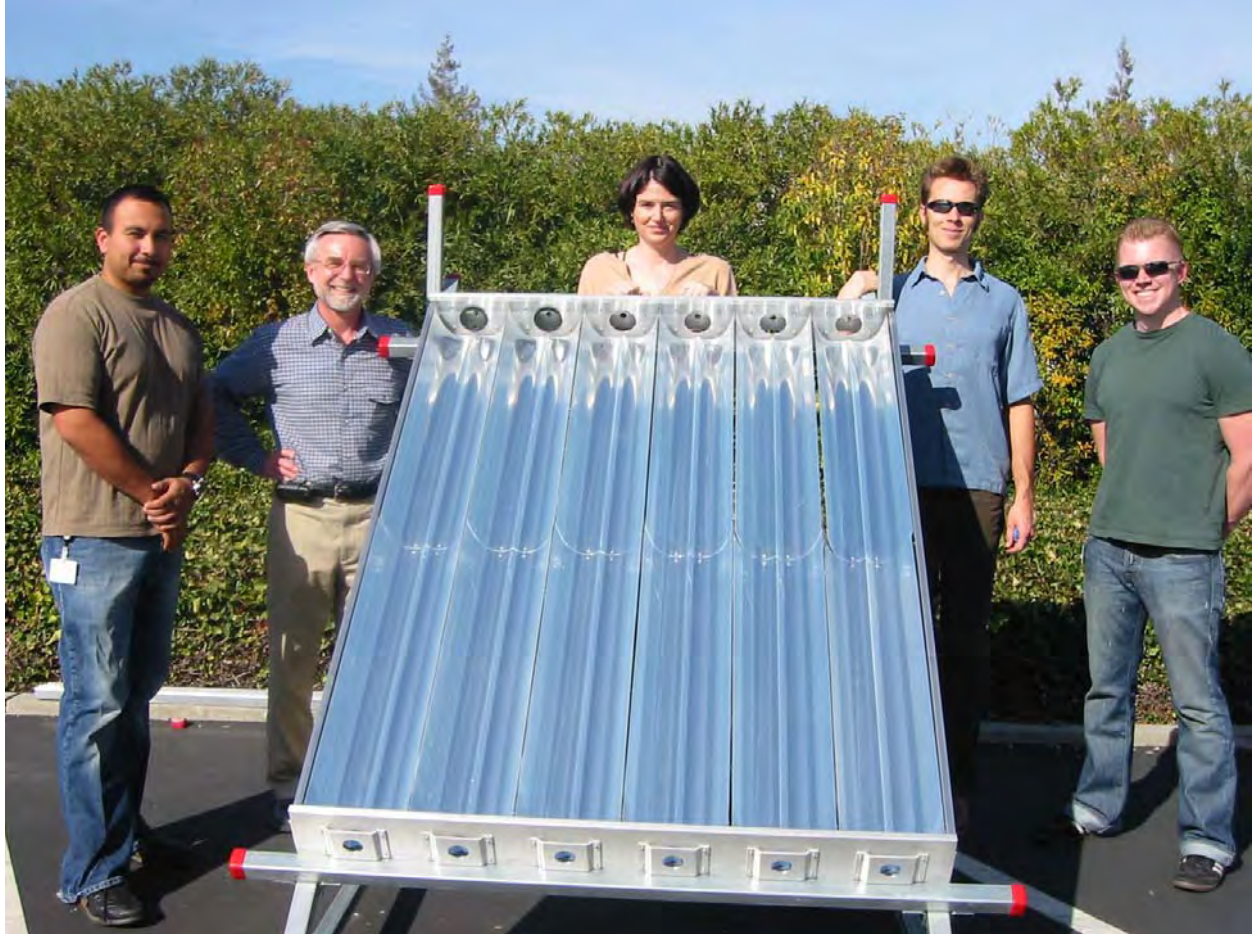


Figure 185. The team leader, Mary Jane Hale is accompanied by members of the SolFocus solar thermal engineering team.

Photo Credit: The Regents of University of California

The prototype collector was operated with water at the Mountain View facility. The results were deemed sufficient to proceed to a **concept loop of 10 collectors**

To be deployed at NASA-Ames which is a NASA laboratory situated close to the company in Mountain View.

CONCEPT LOOP at NASA AMES

Considerable effort was expended in finding a suitable site at NASA AMES with both access and security. We required both electric power for instruments, pumps, etc. as well as a water supply. We decided our initial heat transfer fluid would be water before switching to the DuraTherm 600 heat transfer oil used at UC Merced. The ground had to be prepared and leveled. An enclosure was procured to serve as a command and control center for the concept loop.

The concept loop benefited from our experience of the UC Merced test loop, which in our opinion is world-class. No university campus we know of has a thermal collector testing loop with the sophistication and reliability of the UC Merced facility. We are aware of a solar thermal

test facility at SANDIA Laboratory in Albuquerque , New Mexico. That facility cost millions to build yet the UC Merced facility is superior because, in addition to incorporating a state-of-the-art Coriolis Force flow meter, it also incorporates a self-calibrating CALORIMETER. The self-calibrating calorimeter provides a measurement of heat flow from the solar collector which is independent of heat capacity of the oil and the flow rate. It is well-know that the heat capacity properties of heat transfer oils change significantly with temperature and time. In our opinion, results with an oil loop which does not incorporate a calorimeter are not credible. For practical and debugging purposes, we selected to use water as the heat transfer fluid. Water has stable properties which do not change with time or operation and any spillage would be harmless. We did however, choose to incorporate a Coriolis Force flow meter.



Figure 186. NASA-AMES Concept loop with Professor Roland Winston

Photo Credit: The Regents of University of California



Another view of the NASA-AMES Concept loop with project manager Mary Jane Hale and Roland Winston.

Photo Credit: The Regents of University of California



The concept loop with Solar Engineer Francis Truntzer and Roland Winston.



An overall view of the Concept Loop.

Photo Credit: The Regents of University of California



A close-up of the Concept loop collectors.



A close-up of the Concept loop from the side.

Photo Credit: The Regents of University of California

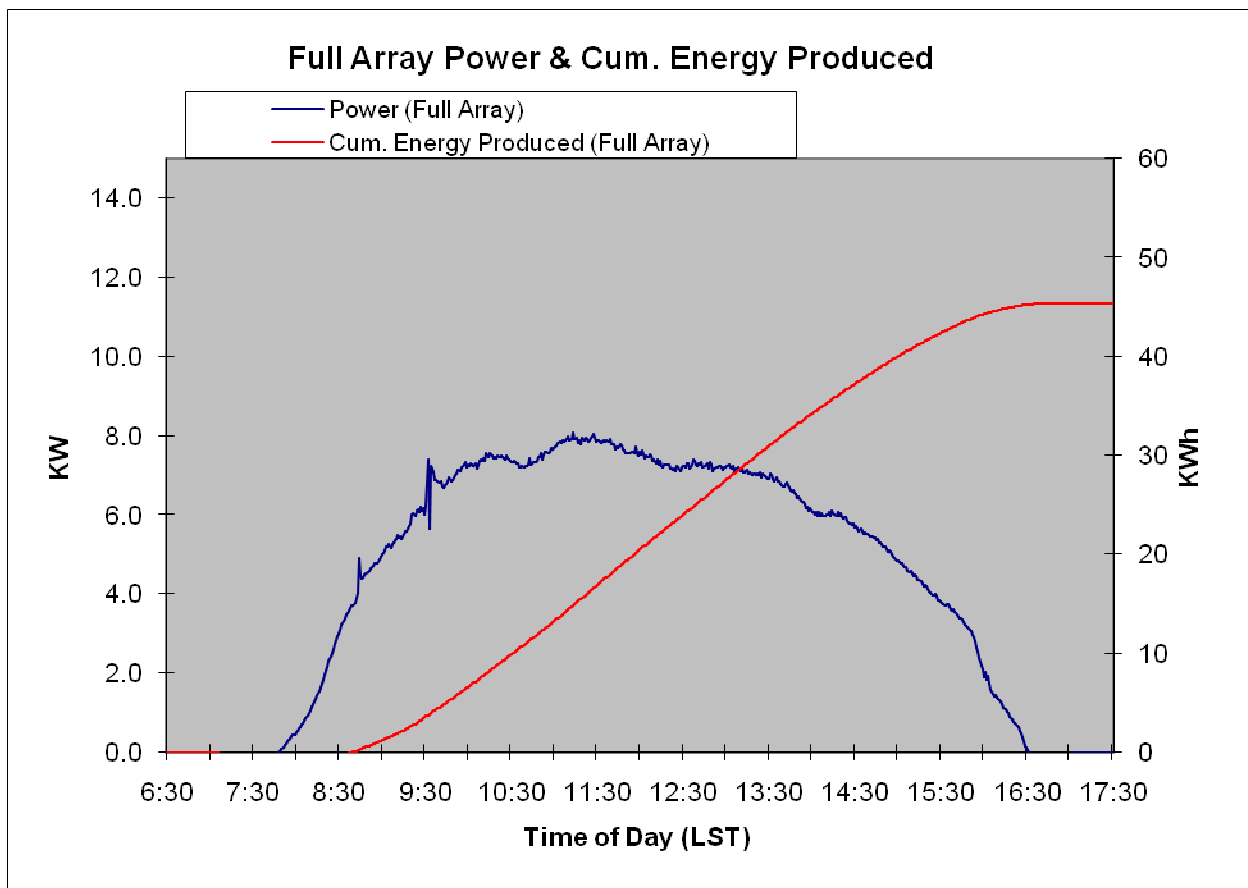


The SolFocus team with the NASA-AMES Concept loop. In the center are Gary Conley, CEO, Mary Jane Hale and Nancy Hartsoch.

Photo Credit: The Regents of University of California

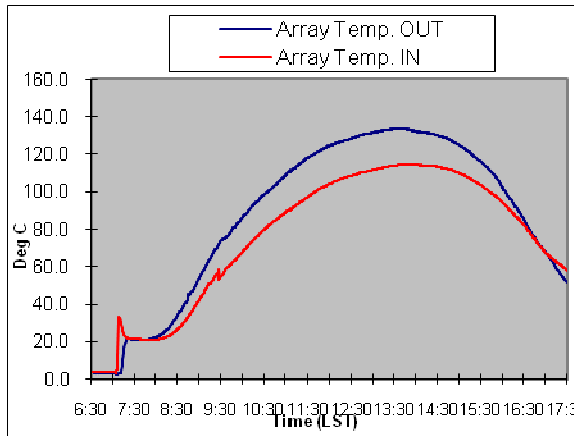
TESTING of CONCEPT LOOP

The instrumentation for the concept loop was selected for long-term performance testing in contrast to the instantaneous performance testing done at the UC Merced test loop. Our collectors have fixed orientation, as appropriate to actual use rather than being deployed on tracking stands. The total ground insolation was motored by horizontal EPPLY pyranometers, while a shadow band detector gave information on direct versus diffuse solar radiation. The heat transfer fluid was water, obviating the need for a precision calorimeter such as was used at UC Merced. In some respects we emulated the UC Merced test system. The flow was measure by a Coriolis Force flow meter and the temperatures with thermocouples (not platinum resistance thermometers). There was use of in-line mixers to ensure the flow stream is well-mixed before the temperature is measured.

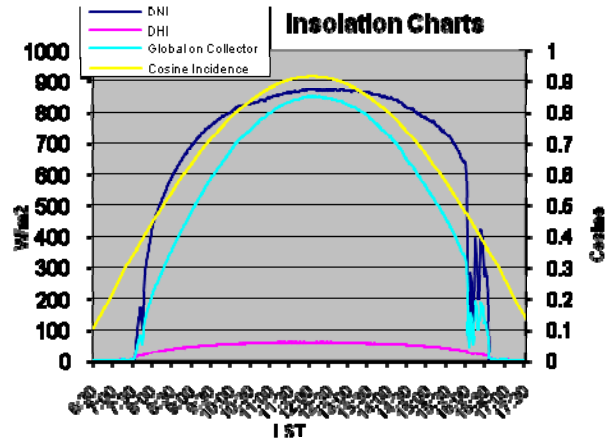


Graph of all day power output performance on December 17, 2008

Source: The Regents of University of California



Graph of temperature achieved

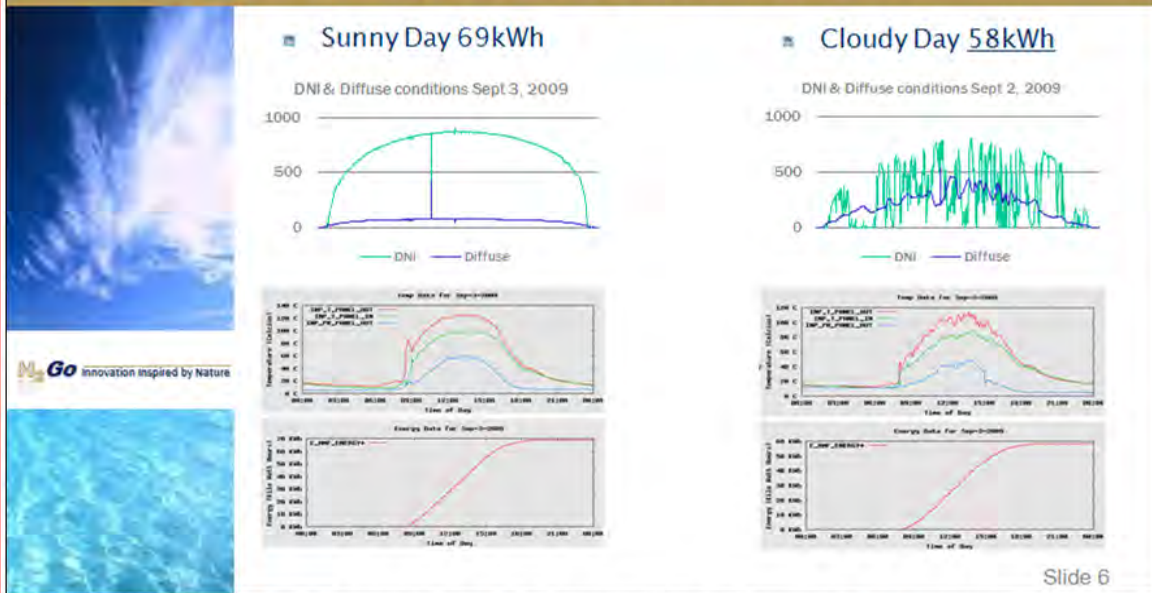


We achieved over 45 kWh of output power over 120° C*

Source: The Regents of University of California

*Note that the temperatures in the above graphs correlate to 200°C when using oil. We had to keep the output low to prevent our cooling water from boiling. We employed an evaporative chiller to keep the temperature artificially low.

Strong Diffuse Performance



The left graphs show a bright sunny day, with the green line on the upper chart representing direct normal insolation and the blue one the diffuse light. Below it, the temperatures for the cooling, inlet, and outlet pints are given and below that the total power production for that day.

The right series represent the same data set but for a rather cloudy day before the last one. Note that while the percentage of direct sunlight dropped almost to half of the prior day, the system still produced considerable power, and only 15% less than on the sunny day. Also note the linearity of the power produced, smooth and not spiky as a linear Fresnel or trough design would give.

The test loop is purposely operated at lower temperatures. It runs unattended and the cooling system water will boil off if not kept under 100C.

ABOUT

H₂Go NICC Solar Thermal Technology

The H₂Go NICC (Non-imaging Concentrator Collector) technology is an evacuated tube collector with a non-imaging reflector. The system design allows heating fluid for applications up to 200°C. The NICC approach provides higher efficiency and temperature than other collectors, now targeting over 50% efficiency at 250°C.

The system will be lower cost than other approaches and able to achieve higher temperatures without tracking. Existing non-tracking systems have historically been limited to low temperatures of 90°C or less, while higher temperature tracking systems are complex and expensive compared to stationary designs. Lack of performance in diffuse conditions of tracking systems have also been an issue of concern. With the proprietary design of the H₂Go NICC system, medium-range temperatures can now be achieved without tracking, combining the cost and reliability benefits of stationary systems with the performance of tracking systems.

Performance and feasibility testing as well as preliminary analysis predict cost and performance goals are achievable with the design. The H₂Go NICC technology is well-suited to many mid-temperature commercial and industrial processes, including drying, cooling, and refrigeration.

This project was completed by SolFocus in collaboration with the University of California, Merced and the California Energy Commission. H₂Go, Inc. is developing further IP and a new company, **B2U Solar**, is now being formed to commercialize this technology.



H₂Go Innovations Inspired by Nature



An Overview of H₂Go Medium Temperature Non-Tracking Solar Thermal Technology

Non-Imaging Concentrator Collector

October 2, 2009

Coming soon...

B2U Solar

H₂Go, Inc.

Phone: (408) 888-0544

H₂Go Innovations Inspired by Nature

INTRODUCTION

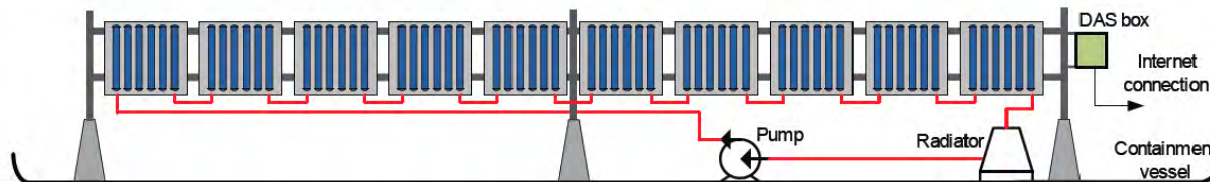
The NICC Solar Thermal Test Site

H₂Go is collaborating with NASA to test its prototype solar thermal collector, the NICC (Non-imaging Concentrator Collector), at a test site provided by NASA. This pre-prototype test loop is the next step of the NICC technology development program which aims to test this new technology in a system layout similar to what will be utilized in actual applications.

Through this project, H₂Go hopes to achieve several goals.

- Measure and monitor NICC system-level performance
- Track technology reliability and failure modes
- Optimize assembly layout
- Build a foundation for the first demonstration systems
- Demonstrate the technology to potential customers

H₂Go has been testing for the past 12 months and will continue (covering two summer seasons) while preparing to install a significant design enhancement. The collector array has ten collector modules totaling 20m² which are connected in series. An evaporative cooler dissipates the collected energy, and a return pump and expansion (drain-back) tank completes the system. The solar thermal system is completely closed-loop



and operates autonomously with remote monitoring and control.



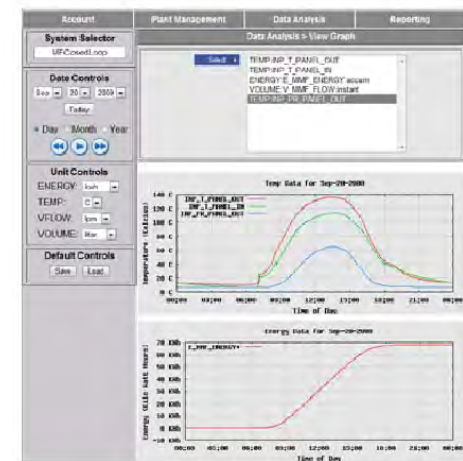
Above: Roland Winston and colleague at solar thermal test site.

This development test is a necessary step to precede commercial installation of full-scale systems where this technology can be used for commercial and industrial processes. The purpose of this test is to measure the technology's performance relative to expectations both from mechanical and thermal perspectives. To determine this, H₂Go closely monitors such areas as solar resource, temperatures between collectors and system inlet/outlet, heat transfer fluid flow rate, and maintenance requirements, as well as other factors. This NASA test site will be used to characterize the collectors, gathering performance data over a variety of ambient and operating conditions.

An Emerging Market Opportunity

As natural gas prices continues to increase, and with the ongoing pressure on green-house gas reductions, solar thermal continues to gain traction for having tremendous potential in key market segments. These commercial and industrial applications include HVAC, industrial process, and desalination projects, among others. A key element for the success of solar thermal technology in these markets is its manufacturability at low cost and high volume, while remaining highly reliable. The most important of these factors for achieving superior market penetration is to exceed cost targets with an aim for a levelized cost of energy (LCOE) *less expensive* than fossil fuels.

H₂Go has developed a base design which it believes can meet all of these criteria. With the installation of its new system test platform at NASA, the company is creating B2U Solar to further develop the technology and to commercialize product offerings and applications to leverage this strong market opportunity.



Loop Output for One Day, 68kWh.

The Gas Technology Institute (GTI) Project

The first commercial project for B2U Solar is with the Gas Technology Institute in Chicago. GTI ordered an initial 10kWt system composed of 10 B2U NICC panels. These will be integrated with the de-aeration stage of a large industrial boiler to reduce the overall natural gas consumption. The de-aeration stage was selected as it easily accommodated a heat-transfer medium. This stage is where feed water is initially heated to remove dissolved oxygen and where chemicals are added before being fed into the boiler chamber. It consumes up to 20% of the total energy use of an industrial boiler.

Following are a series of photographs of the installation:

Photo Credit: The Regents of University of California

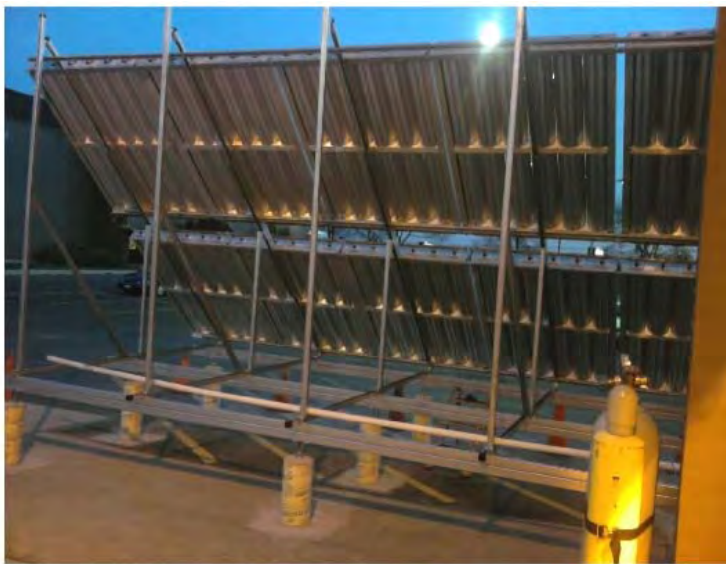


Photo Credit: The Regents of University of California



A levelized cost of energy (LCOE) analysis has been developed for several versions of the NICC collector. The results range from ~ 2 cents - ~ 4 cents per kWh depending on collector design, making this an attractive option for displacing natural gas.

		BOM Scenario					
		N-S Utube conservative	N-S Utube mid-range	N-S Utube aggressive	E-W Utube conservative	E-W Utube mid-range	E-W Utube aggressive
		A	B	C	D	E	F
LCOE (c/kWh)		2.33	1.97	1.59	2.23	1.85	1.49
LCOE (\$/million btu)		6.83	5.76	4.67	6.54	5.41	4.37
Model Inputs		A	B	C	D	E	F
Location (pull down menu)		PhoenixAZ	PhoenixAZ	PhoenixAZ	PhoenixAZ	PhoenixAZ	PhoenixAZ
System Performance Ratio		1	1	1	1	1	1
Material Costs							
Area of Assembly (m ²)		m ² /SCA	2037	2037	2037	2037	2037
Collector Cost Variables:		Units	A	B	C	D	F
Area of SCA Module (m ²)		m ² /module	2.34	2.34	2.34	2.50	2.50
Collector Tubes (evac glass tubes)		\$/module	132.00	114.00	91.20	120.00	80.00
Reflector		\$/module	100.00	80.00	64.00	150.00	96.00
Manifold (copper tubing)		\$/module	40.00	30.00	24.00	40.00	30.00
Aluminum Frame		\$/module	80.00	70.00	56.00	80.00	56.00
Collector Cost per m ² SCA		\$/m ²	150.43	125.64	100.51	156.00	102.40
Fluid Cost Variables:							
Linear meters of interconnecting pipe per m ² SCA		m/m ²	0.31	0.31	0.31	0.31	0.31
BOS Pipe Length (collector to heat exchanger)		m	6.10	6.1	6.1	6.1	6.10
Volume of fluid per meter of interconnecting pipe		gallon/m	0.09	0.09	0.09	0.09	0.09
Volume of fluid per collector (3 tubes and half manifold)		gallon/m ²	0.196	0.196	0.196	0.196	0.20
Fluid Cost		\$/gallon	14.2	14.2	14.2	14.2	14.2
Fluid Cost per m ² SCA		\$/m ²	3.19	3.18	3.18	3.18	3.18
Pump Cost Variables:							
Pumps per SCA			3	3	3	3	3
Pump Cost		\$/pump	800	800	640	800	800
Pump Cost per m ² SCA		\$/m ²	1.18	1.18	0.94	1.18	0.94
BOS Pipe Cost Variables:							
BOS Pipe Cost (3/4" NOM x SCH 40 x SRL)		\$/m	10.0	10.0	10.0	10.0	10.0
Insulation Cost		\$/m	2.50	2.5	2.5	2.5	2.5
BOS Pipe Cost per m ² SCA		\$/m ²	0.04	0.030	0.030	0.030	0.030
Heat Exchanger Cost Variables:							
Heat Exchanger Cost each		\$/exchanger	0.0	0.0	0.0	0.0	0.0
Number of Heat Exchangers per SCA			0	0	0	0	0
Heat Exchanger Cost per m ² of SCA		\$/m ²	0.00	0.00	0.00	0.00	0.00
Total Material BOM per m² SCA		\$/m²	154.83	130.03	104.67	160.39	132.39
Overhead Costs							
Additional Costs as % of Material BOM							
O&M		Annual %	3.0%	3.0%	3.0%	3.0%	3.0%
Insurance		Annual %	0.5%	0.5%	0.5%	0.5%	0.5%
Warranty		Annual %	5.0%	5.0%	5.0%	5.0%	5.0%
Project Management		One-time %	2.0%	2.0%	2.0%	2.0%	2.0%
Shipping		One-time %	10.0%	10.0%	10.0%	10.0%	10.0%
Additional Fixed Costs							
Land		\$/m ²	0.0	0.0	0.0	0.0	0.0
Installation Labor (use this or % above)		\$/m ²	15.0	15.0	15.0	15.0	15.0
Engineering		\$/m ²	10.0	10.0	10.0	10.0	10.0
Permitting		\$/m ²	10.0	10.0	10.0	10.0	10.0
NICC Full Assembly per m² of SCA							
		Units	A	B	C	D	F
Materials BOM		\$/m ²	154.83	130.03	104.67	160.39	132.39
Project Management		\$/m ²	3.10	2.60	2.09	3.21	2.65
Shipping		\$/m ²	15.48	13.00	10.47	16.04	13.24
Land		\$/m ²	0.00	0.00	0.00	0.00	0.00
Installation		\$/m ²	15.00	15.00	15.00	15.00	15.00
Engineering		\$/m ²	10.00	10.00	10.00	10.00	10.00
Permitting		\$/m ²	10.00	10.00	10.00	10.00	10.00
Total One-Time Costs		\$/m²	208.41	180.64	152.23	214.64	183.28
O&M		\$/m ²	4.64	3.90	3.14	4.81	3.97
Insurance		\$/m ²	0.77	0.65	0.52	0.80	0.66
Total Annual Costs		\$/m²	5.42	4.55	3.66	5.61	4.63

B2U Solar LCOE model excerpt - PHX scenario

LCOE Scenario Summary (Cost Only)													
(In cents/kWh)	N-S Utube conservative	N-S Utube mid-range	N-S Utube aggressive	E-W Utube conservative	E-W Utube mid-range	E-W Utube aggressive	(In USD/MMBTU)	N-S Utube conservative	N-S Utube mid-range	N-S Utube aggressive	E-W Utube conservative	E-W Utube mid-range	E-W Utube aggressive
San Francisco CA	2.97	2.51	2.05	2.90	2.42	1.97	San Francisco CA	8.69	7.36	6.00	8.51	7.08	5.77
Phoenix AZ	2.33	1.97	1.59	2.23	1.85	1.49	Phoenix AZ	6.83	5.76	4.67	6.54	5.41	4.37
Houston TX	3.32	2.82	2.30	3.49	2.92	2.38	Houston TX	9.74	8.26	6.75	10.24	8.54	6.98
New York NY	3.71	3.16	2.59	3.77	3.15	2.58	New York NY	10.89	9.25	7.58	11.05	9.23	7.56
Beijing China	3.56	3.02	2.47	3.75	3.13	2.57	Beijing China	10.43	8.86	7.25	11.00	9.19	7.52
Mumbai India	2.89	2.45	2.00	2.97	2.48	2.02	Mumbai India	8.48	7.18	5.85	8.72	7.26	5.91
Paris France	4.82	4.11	3.38	5.04	4.23	3.48	Paris France	14.13	12.04	9.91	14.78	12.40	10.20

LCOE Scenario Summary (with 30% Gross Profit)													
(In cents/kWh)	N-S Utube conservative	N-S Utube mid-range	N-S Utube aggressive	E-W Utube conservative	E-W Utube mid-range	E-W Utube aggressive	(In USD/MMBTU)	N-S Utube conservative	N-S Utube mid-range	N-S Utube aggressive	E-W Utube conservative	E-W Utube mid-range	E-W Utube aggressive
San Francisco CA	3.85	3.27	2.66	3.78	3.14	2.56	San Francisco CA	11.30	9.57	7.80	11.07	9.21	7.50
Phoenix AZ	3.03	2.55	2.07	2.90	2.40	1.94	Phoenix AZ	8.88	7.49	6.07	8.50	7.03	5.68
Houston TX	4.32	3.66	3.00	4.54	3.79	3.10	Houston TX	12.66	10.74	8.78	13.31	11.11	9.08
New York NY	4.83	4.10	3.36	4.90	4.10	3.35	New York NY	14.15	12.03	9.85	14.36	12.01	9.83
Beijing China	4.62	3.93	3.21	4.88	4.08	3.34	Beijing China	13.55	11.51	9.42	14.29	11.95	9.78
Mumbai India	3.76	3.19	2.60	3.87	3.22	2.62	Mumbai India	11.03	9.34	7.61	11.34	9.44	7.69
Paris France	6.26	5.34	4.39	6.56	5.50	4.52	Paris France	18.36	15.65	12.88	19.22	16.12	13.26

Cost of Natural Gas in US

http://tonto.eia.doe.gov/dnav/ng/ng_pri_sum_dcu_nus_m.htm

Year 2009	cents/kWh	cents/ft ³
Pipeline Price	1.14	0.34
US City Gate Price	1.84	0.55
US Industrial	1.67	0.50
US Commercial	3.11	0.93
US Residential	4.35	1.30

Year 2008	cents/kWh	cents/ft ³
Pipeline Price	2.87	0.86
US City Gate Price	3.08	0.92
US Industrial	3.21	0.96
US Commercial	4.01	1.20
US Residential	4.58	1.37

Year 2007 (Benchmark)	cents/kWh	cents/ft ³
Pipeline Price	2.28	0.68
US City Gate Price	2.71	0.81
US Industrial	2.58	0.77
US Commercial	3.78	1.13
US Residential	4.38	1.31

NG Future Pipeline Prices (cents/kWh, Dec. 09)

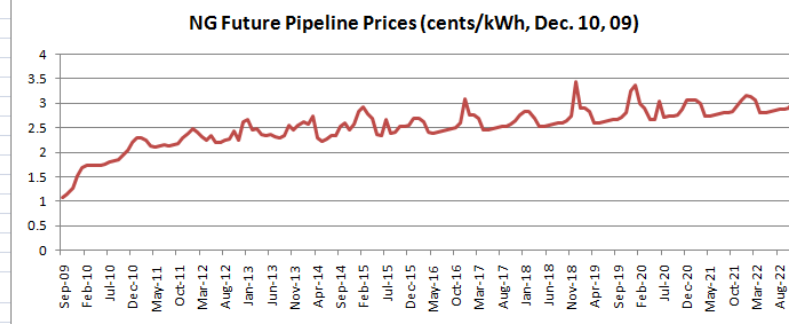
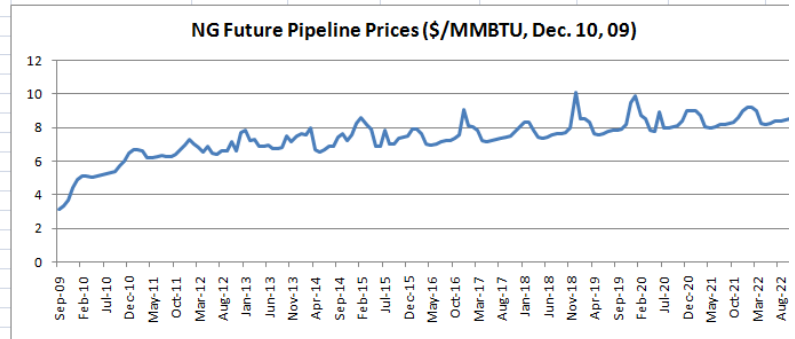
http://quotes.ino.com/exchanges/?r=NYMEX_NG

	USD/MMBTU	Cent/kWh (divide 293)
Sep-09	3.132	1.06894198
Oct-09	3.345	1.14163823
Nov-09	3.675	1.25426621
Dec-09	4.425	1.51023891
Jan-10	4.915	1.6774744
Feb-10	5.095	1.73890785
Mar-10	5.11	1.7440273
Apr-10	5.06	1.72696246
May-10	5.1	1.74061433
Jun-10	5.175	1.7662116
Jul-10	5.255	1.79351536
Aug-10	5.33	1.81911263
Sep-10	5.41	1.84641638
Oct-10	5.705	1.94709898
Nov-10	5.985	2.04266212
Dec-10	6.46	2.20477816
Jan-11	6.695	2.28498294
Feb-11	6.705	2.2883959
Mar-11	6.6	2.25255973
Apr-11	6.22	2.12286689
May-11	6.205	2.11774744
Jun-11	6.265	2.13822526
Jul-11	6.33	2.16040956
Aug-11	6.26	2.13651877
Sep-11	6.28	2.14334471
Oct-11	6.4	2.18430034
Nov-11	6.7	2.28668942
Dec-11	6.99	2.38566553
Jan-12	7.3	2.49146758
Feb-12	7.045	2.40443686
Mar-12	6.82	2.32764505
Apr-12	6.58	2.24573379
May-12	6.86	2.34129693
Jun-12	6.47	2.20819113
Jul-12	6.435	2.19624573
Aug-12	6.595	2.25085324
Sep-12	6.625	2.26109215
Oct-12	7.15	2.44027304
Nov-12	6.6	2.25255973
Dec-12	7.205	2.42699999

Conversions

<http://www.energy.rochester.edu/units/conversions.pdf>

1kWh = 3412 btu = 860 Kcal
1ft ³ natural gas = 1020 btu
1.055kJ = 1 btu
1 kJ = 0.239 kCal



World Natural Gas Prices (2007 Benchmark)

<http://www.eia.doe.gov/emeu/international/gasprice.html>

Year 2007	cents/kWh	cents/kCal
Spain - Household	7.46	0.00867
Spain - Industrial	3.27	0.00380
Taiwan - Industrial	4.09	0.00476
France - Industrial	3.56	0.00414
South Korea - Industrial	4.74	0.00551
Mexico - Industrial	2.99	0.00347
China - Household	4.22	0.00490
China - Industry	4.04	0.00470

-- for compar
-- for compar

CO2 emissions of Natural Gas Combustion

<http://www.naturalgas.org/> Carbon taxes have been suggested (5 to 100

0.18	kg CO2/kWh
0.000181239	tons CO2/kWh

H2Go, Inc. CONFIDENTIAL

B2U Solar multi-location vs. gas futures Source: The Regents of University of California

NEXT GENERATION XCPC SOLAR COLLECTOR

To further improve cost effectiveness and performance efficiency, B2U has begun investigating a next generation. The current embodiment for series production is shown below:

ITEM NO.	PART NUMBER	DESCRIPTION	QTY.
1	400-000545-001	REFLECTOR, SOLAR THERMAL	12
2	400-000550-000	END FLATE - COLLECTOR FRAME - SOLAR THERMAL	2
3	400-000554-000	SIDE RAIL - COLLECTOR FRAME - SOLAR THERMAL	2
4	400-000555-000	MID SUPPORT - COLLECTOR FRAME - SOLAR THERMAL	1
5	GMTG3945 (MAPCO)	GROMMET, RUBBER 3.5" ID	12
6	2588A155 (McMASTER)	RIVET-C/SINK 1/8" DIA	48
7	400-000556-000	TUBE TOP BRACKET, COLLECTOR BOX, SOLAR THERMAL	6
8	CA652-2 (AllyrBoardElectronics)	#6-32 AL PEM NUT	48
9	400-000557-000	TUBE BOTTOM BRACKET, COLLECTOR FRAME, SOLAR THERMAL	6
10	92185A145 (McMASTER)	SCREW, #6-32x5/16"L, SOCKET HD CAP, S16SS	48
11	25778A501	5/16x.413"L RIVET-HIGH STRENGTH, AL	32

REVISIONS

REV	DESCRIPTION	DATE	APPROVED
01	ENGINEERING RELEASE	2/7/08	N/A

NOTES: UNLESS OTHERWISE SPECIFIED:
1. REMOVE ALL BURRS AND SHARP EDGES.

PROPERTY OF HUGO, INC. ALL RIGHTS RESERVED. THIS DRAWING IS UNCLASSIFIED UNLESS INDICATED OTHERWISE. ANY REPRODUCTION OR DISTRIBUTION OF THIS DRAWING WITHOUT THE WRITTEN PERMISSION OF HUGO, INC. IS PROHIBITED. HUGO, INC. IS NOT RESPONSIBLE FOR ANY DAMAGE TO PROPERTY OR PERSONS ARISING FROM THE USE OF THIS DRAWING.

HUGO, INC. PROPRIETARY AND CONFIDENTIAL

400-000545-001-002
REV: 002
DATE: 2/7/08
SCALE: 1:1
SHEET: 1 OF 2

H₂Go Innovations Powered by Astute

COLLECTOR BOX ASSY, SOLAR THERMAL

SCALE: 1:1

400-000547-000-002

DO NOT SCALE DRAWING

3/25/11 CJS

Source: The Regents of University of California

H₂Go Innovations Powered by Astute

TITLE: FULL ASSY - EAST/WEST

SIZE	DWG. NO.	REV
SCALE: 1:30	WEIGHT:	SHEET 1 OF 2

Configuration where the manifold is shared between two banks of receiver tubes.

Source: The Regents of University of California



Next generation B2U Solar NICC prototype with shared manifold

Photo Credit: The Regents of University of California



Photo Credit: The Regents of University of California



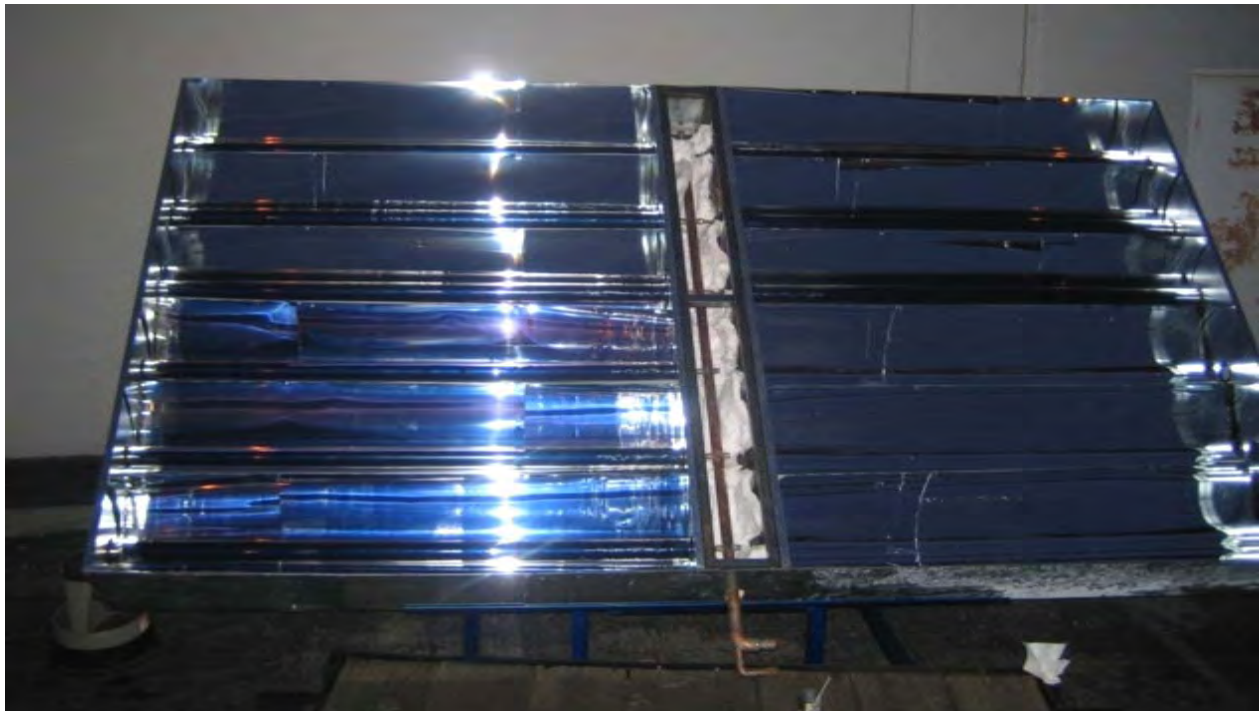
Photo Credit: The Regents of University of California



Photo Credit: The Regents of University of California



Photo Credit: The Regents of University of California



Front view of next generation XCPC. Notice the spectacular “non-imaging optics effect” The entire aperture is dark because all the light is reflected onto the absorber.

Photo Credit: The Regents of University of California

Conclusion

We have traced the evolution of this California Energy Commission project from proof of concept in a university laboratory (UC Merced) to proof of concept in a quasi industrial setting (NASA-AMES Concept Loop) to commercialization in a start-up company (B2U Solar).

We believe this is an exemplary success story of progress from public-private partnership (academia to industry) aided by public support.

3.0 Conclusions and Recommendations

Conclusions

This project met its stated objectives and was completed on time and within budget. The XCPC design is both thermally efficient and affordable to manufacture. So much so that project partner SolFocus has already spun off a new company called B2U to commercialize this technology in numerous high-impact areas.

- The initial designs performed well from 25 to 200C (roughly 75 to 400F).
 - North-South version (counterflow tube with alanod) performed as predicted by models while the East-West version (counterflow tube with alanod) fell short due to high thermal resistance in the counterflow tube under the higher concentration.
 - The NS version had an optical efficiency of 70% and an efficiency of 36% at 200C based on effective irradiance (or 45% at 200C based on DNI)
 - The EW version had an optical efficiency of 66% and an efficiency of 40% at 200C based on effective irradiance (or 44% at 200C based on DNI)
 - Efficiencies reported are based on an ambient temperature of 25C and an effective solar flux of 1000 W/m².
- The improved designs also performed well from 25 to 200C (roughly 75 to 400F).
 - The North-South version improved with the addition of the Reflectech film but the addition of the U-Tube over the counterflow tube seems to have not improved the efficiency.
 - The East-West version appears to have improved by using the X-Tube and the U-Tube almost equally over the counterflow tube. The addition of the Reflectech films did not improve the performance of the collector and this may be due to imperfections in the application of the film.
- The best North-South version was the U-Tube with Reflectech:
- The best East-West version (and arguably the best overall version) was the U-Tube with Alanod.
 - Optical efficiency: 66%
 - Efficiency at 200C (based on effective irradiance): 43%
 - Efficiency at 200C (based on DNI): 46%
- An East-West U-Tube with Reflectech would likely have higher efficiencies if the application of the film were done better (and not by hand)

Using private funding, UC Merced researchers are now building a “solar cooling” prototype at UC Merced to showcase this technology, and new applications for this technology are being explored.

Recommendations

- The XCPC designs are best used between 100 and 200C (or possibly a little higher).
 - This is well suited for absorption chillers, desal, etc.
- The East-West version is best suited in lower diffuse areas and/or temperatures in the range of 150 to 200C
- The North-South version is better suited for higher diffuse and/or temperatures in the range of 100 to 160C
- The manifolds should be considered when deciding on the best design to use for a particular application

- North-South manifolds are easily connected in series due to the fact that they are parallel to the ground.
- East-West manifolds are more difficult to connect one to another
- East-West manifolds also limit the energy density of the solar field due to spaces between collectors
- Higher R-Value (per inch) insulation could be used on the manifolds to reduce heat loss. Surface area of the insulation should be minimized to reduce heat loss.
- Higher flowrates will provide a slight increase in efficiency due to lower absorber temperatures but higher flowrates generally require more power to pump. This trade off should be considered
- Both versions could have improved more from the Reflectech film if the application was better.

References

- <http://www.solarpanelsplus.com/images/yazaki-chiller-diagram.jpg>
http://www.eere.energy.gov/de/thermally_activated/tech_basics.html
<http://www.unity.com.ph/images/faq2.jpg>
http://www.barber-nichols.com/images/rankine_cycle.jpg
http://www.eere.energy.gov/de/thermally_activated/
http://www.eere.energy.gov/de/thermally_activated/tech_basics.html
<http://www.adsorptionchiller.bigstep.com/>
http://www.energy.ca.gov/pier/iaw/presentations/FIER_LOWE.PDF
<http://www.malteser-krankenhaus-kamenz.de/englisch/install/adschill/adschill.htm>
Frost and Sullivan Report #7501-19, 2000
Brasz, J.; Biederman, B. O.; Holdmann, G.; GRC Annual Meeting, 2005⁸
<http://www.energylan.sandia.gov/sunlab/Snapshot/solartres.htm>
<http://www.xpedio.carrier.com/idc/groups/public/documents/marketing/05-810-003-25.pdf>
http://www.wastechengineering.com/papers/vacuum_distillation.htm
<http://www2.hawaii.edu/~nabil/solar.htm>
http://www.sc.doe.gov/bes/reports/files/SEU_rpt.pdf
http://www.utcpower.com/fs/com/bin/fs_com_Page/0,11491,0104,00.html
http://www.eere.energy.gov/de/pdfs/absorption_future.pdf
Thyrum, Geoffrey, "Critical Aspects of Modeling Heat Pipe Assisted Heat Sinks",
http://www.hhmz.net/news/62/2006-3-24_6302344477.html, 2006.